Imperial College London

The dysregulation of lipid metabolism caused by hepatitis C virus

by

Charles Burch

Thesis submitted for the degree of

Doctor of Philosophy

Imperial College London

2017

Faculty of Medicine, Department of Virology,

St Mary's Campus, Norfolk Place, Imperial College London

Dedication

This Ph.D. thesis and the accomplished works presented herein are dedicated with the utmost love and respect to my late father, Charles Walter Taylor Burch (03/11/1919 – 28/08/2008). My father gave support throughout my life, fostered my creativity, and inspired me to work arduously to realise my potential while instilling an appreciation of technology and nature along with a fascination of the intricacies of the world we live in.

I hope you are proud of the man you encouraged me to be and the scientist I am becoming.

Abstract

The life cycle of HCV involves a dysregulation in host lipid metabolism that may precede metabolic complications such as insulin resistance (IR), type 2 diabetes mellitus (T2DM), and hepatic steatosis which are often associated with chronic infection. Thioredoxin-Interacting Protein (TXNIP), a host factor that is induced by oxidative stress, and associated with disturbances in host lipid and glucose metabolism, has been reported to be overexpressed during HCV infection where its siRNA-mediated knockdown resulted in a significant impairment of virus replication. This study investigated the mechanisms by which HCV may bring about the overexpression of TXNIP by examining the unfolded protein response (UPR) and mitochondrial dysfunction in HCV gt2a infection models. These pathways were tested in HCV SGR- and JFH-1 infected Huh7 cells by targeting inositol-requiring enzyme 1α (IRE-1α) activity and mitochondrial voltage-dependent anion channel (VDAC) oscillation, and the effects on TXNIP expression, lipid metabolism, and virus replication were measured. The data from this work indicate that the UPR is more relevant to HCV SGR replication, whilst ameliorating mitochondrial dysfunction appears to restore glucose metabolism, downregulate lipogenic gene transcription, inhibit lipid droplet (LD) biogenesis, and reduce JFH-1 RNA replication.

Table of Contents

Abstract 4
Table of Figures 13
Abbreviations 16
Presentations 26
Acknowledgments 27
Copyright Declaration 28
Declaration of Originality 29
Chapter 1: Introduction 30
1.1. Overview of Hepatitis C virus (HCV) 31
1.2. The Molecular biology of HCV 32
1.2.1. HCV Structural (S) proteins 36
1.2.1.1. Core (C) 36
1.2.1.2. Envelope glycoproteins (E1, E2) 39
1.2.2. HCV Nonstructural (NS) proteins 41
1.2.2.1. p7 41
1.2.2.2. NS2 42
1.2.2.3. NS3 44
1.2.2.4. NS4A 47
1.2.2.5. NS4B 48
1.2.2.6. NS5A 51
1.2.2.7. NS5B 54
1.3. *In vitro* HCV infection systems 56
1.3.1. HCV pseudoparticles (HCVpp) 57
1.3.2. HCV subgenomic replicons (HCV SGR) 58
1.3.3. Infectious HCV models 59
1.4. The HCV life cycle and Host Lipid Metabolism 62
1.4.1. HCV and Lipid Species 64
1.5. HCV, Innate Immunity, and Lipid Metabolism 69

1.5.1. HCV and Innate Immune Sensing 71
1.5.1.1. HCV and Retinoic Acid Inducible Gene-like Receptors (RLRs)..... 71
1.5.1.2. HCV and Toll-like Receptors (TLRs) 72
1.6. Diversity and Geographical distribution of HCV 76
1.6.1. Evolution of HCV Genotypes 78
1.7. Homeostatic Glucose Metabolism..... 80
1.7.1. Glucose Uptake 80
1.7.2. Glucose Storage..... 81
1.7.3. Glucose Metabolism 84
1.7.3.1. Glycolysis 84
1.7.3.2. The Tricarboxylic Acid (TCA) cycle 89
1.7.3.3. Regulation of The TCA Cycle..... 92
1.8. Metabolic Disorders associated with HCV infection 99
1.8.1. Insulin Resistance (IR)..... 99
1.8.2. Type 2 Diabetes Mellitus (T2DM) 101
1.8.2.1. Insulin Signaling in T2DM..... 102
1.8.3. Hepatic steatosis 103
1.9. Treatment for HCV infection 105
1.9.1. Ribavirin (RBA)..... 106
1.9.2. Interferon-based therapies..... 107
1.9.2.1. Interferon (peg-IFN α, λ)..... 107
1.9.3. 1st generation direct acting antivirals (DAAs) 108
1.9.4. 2nd generation direct acting antivirals (DAAs) 109
1.9.4.1. Simeprevir 109
1.9.4.2. Daclatasvir (DCV)..... 110
1.9.4.3. Sofosbuvir 111
1.9.5. Host-Factor Therapeutics 112
1.9.5.1. Cyclophilin Inhibitors 112
1.9.5.2. Miravirsen..... 114
1.10. Study of Host Factors in HCV Infection 118

1.10.1. RNA Microarray 118
1.10.2. Microarray in HCV 119
1.10.3. Functional genomics 122
1.10.4. Thioredoxin-interacting protein (TXNIP) 124
1.10.4.1. TXNIP Transcriptional induction 125
1.10.4.2. TXNIP mRNA Regulation 127
1.10.4.2.1. TXNIP mRNA Regulation by the Unfolded Protein Response (UPR) 128
1.10.4.2.2. TXNIP mRNA Regulation by Histone Deactylases (HDACs) and Histone Acetyltransferases (HATs) 129
1.10.5. TXNIP Function 130
1.10.5.1. TXNIP and Glucose Metabolism 131
1.10.5.2. TXNIP and Lipid Metabolism 132
Hypothesis & Aims 134
Chapter 2: Materials & Methods 136
2.1. Materials 137
2.1.1. Reagents 137
2.1.2. Consumables 138
2.1.3. Enzymes 139
2.1.4. Kits 139
2.1.5. Markers 139
2.1.6. Buffers 140
2.1.7. Antibodies 141
2.1.8. siRNA sequences (simplex) – Sigma-Aldrich 141
2.1.9. Primer Sequences – Invitrogen 142
2.1.9.1. Reference 142
2.1.9.2. ER stress markers 142
2.1.9.3. Mitochondrial DNA (mtDNA) 142
2.1.9.4. Glucose metabolism 143
2.1.9.5. Lipid metabolism 143
2.1.10. Cells 144

2.1.11. Plasmids 144
2.2. Methods 145
2.2.1. Re-evaluation of Microarray Data 145
2.2.2. Cell culture 145
2.2.3. Isolation and Purification of Nucleic Acids 147
a) Cell Lysis using TRIzol® Reagent 147
b) Isolation of Total Cellular RNA 148
c) Isolation of Extracellular viral RNA 148
d) Isolation of Total Cellular DNA 149
2.2.4. PCR Primer Design 150
2.2.5. Quantitative Reverse-Transcription Polymerase Chain Reaction (qRT-PCR) 150
2.2.6. Isolation of JFH-1 Plasmid DNA (pJFH-1) from bacterial stocks 151
2.2.7. Preparation of pJFH-1 Plasmid DNA 152
2.2.8. *In vitro* transcription of JFH-1 RNA 153
2.2.9. Production of infectious Hepatitis C virus (JFH-1) 153
2.2.10. Production of JFH-1 virus stocks via serial passage 154
2.2.11. Preparation of JFH-1 virus stocks 154
2.2.12. Immunostaining of HCV Antigens 155
2.2.13. Titration of JFH-1 infectivity 156
2.2.14. cDNA synthesis (Two-step PCR) 156
2.2.15. Absolute Quantitation of Intracellular/Extracellular HCV 157
2.2.16. Preparation of Total Cellular Protein 158
a) Cell Lysis 158
b) Bradford Assay 158
c) Concentration of Total Cellular Protein Lysates 159
2.2.17. miR-17 Expression (miScript PCR) 159
2.2.18. 2% TBE Agarose Gel Electrophoresis 160
2.2.19. Measurement of Intracellular Calcium 160
2.2.20. Measurement of Reactive Oxygen Species (ROS) 161

2.2.21. Determination of Mitochondria-Associated Apoptotsis Activity (Mitochondrial ToxGlo™) 162
2.2.22. Assessment of Mitochondrial Membrane Potential 162
2.2.23. Long PCR of Mitochondrial DNA (mtDNA) 163
2.2.24. Staining of Intracellular Lipid Droplets (LDs) 163
2.2.25. Determination of Intracellular [glucose] 164
2.2.26. Determination of Intracellular glycogen content 165
2.2.27. Quantification of Intracellular [triglyceride] 165
2.2.28. Western Blotting of Host and Viral Protein expression 166
2.2.29. siRNA-Mediated Knockdown of Host Genes 167
2.2.30. Statistical Analysis 167
Chapter 3: ER stress and Dysregulated Lipid Metabolism in HCV Infection 168
3.1. Overview: 169
3.2. Results & Discussion 170
3.2.1. Gene Ontology pathway analysis of re-evaluated Microarray data (PUFA Biosynthesis) 170
3.2.2. Lipogenic Gene Transcription in HCV SGR cells +/- glucose (24, 48 Hours) 173
3.2.3. Gene Transcription of STC2 and Mlx in HCV SGR cells +/- glucose (24, 48 Hours) 176
3.2.4. Intracellular glucose concentration in Huh7 and HCV SGR cells +/- glucose (24, 48 Hours) 178
3.2.5. Intracellular HCV SGR genome copy number in HCV SGR cells +/- glucose (24, 48 Hours) 180
3.2.6. Gene Ontology pathway analysis of re-evaluated microarray data (UPR induction) 182
3.2.7. Gene Transcription of STC2 and HSPA5 in HCV gt2a Infection Models 184
3.2.8. Cytosolic Ca^{2+} in HCV gt2a Infection Models (24, 48 Hours) 186
3.2.9. miR-17 expression in HCV gt2a Infection Models (24, 48 Hours) 188
3.2.10. Lipogenic Gene Transcription in HCV gt2a Infection Models Treated with STF-083010 (24, 48 Hours) 191

3.2.11. HCV genome copy number in HCV gt2a Infection Models Treated with STF-083010 (24, 48 Hours) 196
3.2.12. Host and Viral Protein Expression in HCV SGR cells Treated with STF-083010 (24, 48 Hours) 200
3.3. Conclusion 203
Chapter 4: Mitochondrial Dysfunction and dysregulated Lipid Metabolism in HCV infection 205
4.1. Overview 206
4.2. Results & Discussion 207
4.2.1. Mitochondrial Ca^{2+} in HCV gt2a Infection Models (24, 48 Hours) 208
4.2.2. Mitochondrial DNA (mtDNA) in JFH-1 infected Huh7 cells (24, 48 Hours) 211
4.2.3. Inhibition of Mitochondrial Ca^{2+} Uptake in HCV gt2a Infection Models (24, 48 Hours) 213
4.2.4. Mitochondrial Membrane Potential (mt$\Delta\Psi$m) in HCV gt2a Infection Models (24, 48 Hours) 216
4.2.5. Mitochondrial-Associated Apoptosis in HCV SGR cells (24, 48 Hours) 219
4.2.6. Oxidative Phosphorylation Gene Transcription in HCV gt2a Infection Models +/- L-glutamate (24, 48 Hours) 221
4.2.7. Intracellular [Glucose] in HCV gt2a Infection Models +/- L-glutamate (24, 48 Hours) 228
4.2.8. Intracellular Glycogen Content in HCV gt2a Infection Models +/- L-glutamate (24, 48 Hours) 230
4.2.9. Lipogenic Gene Transcription in HCV gt2a Infection Models +/- L-glutamate (24, 48 Hours) 233
4.2.10. Intracellular [triglyceride] in HCV gt2a Infection Models +/- L-glutamate (24, 48 Hours) 240
4.2.11. Intracellular Lipid Droplets (LDs) in HCV gt2a Infection Models +/- L-glutamate (24, 48 Hours) 244
4.2.12. HCV genome copy number in HCV gt2a Infection Models +/- L-glutamate (24, 48 Hours) 251
4.2.13. Host and Viral Protein Expression in HCV gt2a Infection Models +/- L-glutamate (24, 48 Hours) 255

4.2.14. Intracellular reactive oxygen species (ROS) in JFH-1 infected Huh7 cells +/- L-glutamate (24, 48 Hours) 258
4.3. Conclusion 260
Chapter 5: The Role of Host Genes in HCV Replication 263
5.1. Overview 264
5.2. Results and Discussion 265
5.2.2. Effects of TXNIP Silencing in HCV SGR Cells (24, 48 Hours) 266
5.2.3. Effects of Mlx Silencing in HCV SGR Cells (24, 48 Hours) 268
5.3 Conclusion 273
Chapter 6: General Discussion & Conclusion 274
6. General Discussion 275
6.1. ER stress and Dysregulated Lipid Metabolism during HCV infection 277
6.2. Mitochondrial Dysfunction and Dysregulated Lipid Metabolism during HCV infection 281
6.3. The Role of Host Genes in HCV Replication 293
6.4. Conclusion 294
Bibliography 297
Appendix 342
Appendix A1 – ΔC_T Graphs for qRT-PCR Data (Chapter 3) 343
A1.1. – ΔC_T for Lipogenic gene transcription in HCV SGR cells +/- glucose [25 mM] (24, 48 Hours) 343
A1.2. – ΔC_T for STC2 and Mlx transcripton in HCV SGR cells +/- glucose [25 mM] (24, 48 Hours) 344
A1.3. - ΔC_T for STC2 and HSPA5 transcripton in HCV gt2a infection models (24, 48 hours) 345
A1.4. - ΔC_T for miR-17 expression levels in HCV gt2a infection models treated with STF-083010 (24, 48 hours) 346
A1.5. - ΔC_T for Lipogenic gene transcription in HCV SGR cells treated with STF-083010 (24, 48 Hours) 347
A1.6 - ΔC_T for Lipogenic gene transcription in JFH-1 infected Huh7 cells treated with STF-083010 (24, 48 Hours) 348

Appendix A2 – ΔC_T Graphs for qRT-PCR Data (Chapter 4) 349

A2.1. – ΔC_T for Oxidative Phosphorylation gene transcription in Huh7 and HCV SGR cells +/- L-glutamate (24, 48 hours) 349

A2.2. – ΔC_T for Oxidative phosphorylation gene transcription in Mock- and JFH-1 infected Huh7 cells (MOI – 7.5) +/- L-glutamate (24, 48 hours) 350

A2.3. – ΔC_T for Lipogenic gene transcription in Huh7 and HCV SGR cells +/- L-glutamate (24, 48 hours) 351

A2.4. - ΔC_T for Lipogenic gene transcription in Mock- and JFH-1 infected Huh7 cells (MOI – 7.5) +/- L-glutamate (24, 48 hours) 352

Appendix A3 – ΔCT Graphs for qRT-PCR Data (Chapter 5) 353

A3.1. – ΔC_T for TXNIP transcription in HCV SGR cells transfected with siRNA targeting TXNIP (siTXNIP) (24, 48 Hours) 353

A3.2. – ΔC_T for Mlx transcription in HCV SGR cells transfected with siRNA targeting Mlx (siMlx) (24, 48 Hours) 353

A3.3. – ΔC_T for TXNIP transcription in HCV SGR cells transfected with siRNA targeting Mlx (siMlx) (24, 48 Hours) 354

Table of Figures

Figure 1 - The Genomic Organisation of hepatitis C virus 33
Figure 2 - The secondary structure of HCV 5'- and 3' UTRs 35
Figure 3 – The genomic organisation of HCV subgenomic replicons 59
Figure 4 – The HCV life cycle 62
Figure 5 - HCV induced lipogenesis via IKKα 70
Figure 6 - Innate immune sensing of HCV to induce the interferon response 74
Figure 7 - Mechanisms of Innate Immune Evasion by HCV 75
Figure 8 - The worldwide distribution and prevalence of HCV (gt 1- 6) 77
Figure 9 - The Chemical Structure of a Glycogen Short Chain 82
Figure 10 - Glycogen Metabolic Pathways 83
Figure 11 - The Glycolytic Pathway 86
Figure 12 - The Network of Glucose Metabolic Pathways 88
Figure 13 - The Tricarboxylic Acid (TCA) Cycle 89
Figure 14 - Mitochondrial Ca^{2+} Import from the Endoplasmic Reticulum 96
Figure 15 - Anaplerosis and Cataplerosis in the Tricarboxylic Acid (TCA) Cycle 98
Figure 16 - TXNIP mRNA regulation by activated IRE-1α following ER stress 129
Figure 17 - GeneGO™ Metacore™ pathway analysis from re-evaluated microarray data (PUFA Biosynthesis) 171
Figure 18 (A, B) – Lipogenic gene transcription in HCV SGR cells +/- glucose [25 mM] (24, 48 Hours) 173
Figure 19 (A, B) - Gene transcription of STC2 and Mlx in HCV SGR cells +/- glucose [25 mM] (24, 48 Hours) 176
Figure 20 (A, B) - Average intracellular [glucose] (μM) in Huh7 and HCV SGR cells +/- glucose [25 mM] (24, 48 hours) 178
Figure 21 - Intracellular HCV SGR replication in HCV SGR cells +/- glucose [25 mM] (24, 48 hours) 180
Figure 22 – GeneGO™ Metacore™ pathway analysis from re-evaluated microarray data (UPR induction) 182
Figure 23 (A, B) – Gene Transcription of STC2 and HSPA5 in HCV gt2a infection models (24, 48 hours) 184
Figure 24 - Cytosolic Ca^{2+} in HCV gt2a Infection Models (24, 48 hours) 186
Figure 25 (A, B) - miR-17 expression levels in HCV gt2a infection models treated with STF-083010 (24, 48 hours) 188
Figure 26 (A, B) - Lipogenic gene transcription in HCV SGR cells treated with STF-083010 (24, 48 Hours) 191
Figure 27 (A, B) - Lipogenic gene transcription in JFH-1 infected Huh7 cells treated with STF-083010 (24, 48 Hours) 194

Figure 28 - Intracellular HCV SGR replication in HCV SGR cells +/- STF-083010 (24, 48 hours) 196
Figure 29 - Intracellular HCV replication in JFH-1 infected Huh7 cells (MOI – 7.5) +/- STF-083010 (24, 48 hours) 197
Figure 30 - Extracellular HCV secretion in JFH-1 infected Huh7 cells (MOI – 7.5) +/- STF-083010 (24, 48 hours) 198
Figure 31 - Protein quantification in Huh7 and HCV SGR cells +/- STF-083010 (24, 48 hours) 200
Figure 32 – Densitometry analysis of TXNIP protein expression in Huh7 and HCV SGR cells +/- STF-083010 (24, 48 hours) 201
Figure 33 – Densitometry analysis of HCV NS3 protein expression in HCV SGR cells +/- STF-083010 (24, 48 hours) 202
Figure 34 - ER Stress Induced Mechanism of TXNIP Overexpression 204
Figure 35 (A - C) - Mitochondrial Ca^{2+} in HCV gt2a Infection Models (24, 48 hours) 208
Figure 36 - PCR Amplification of Mitochondrial DNA (mtDNA) in Mock- and JFH-1 infected Huh7 cells (MOI – 7.5) (24, 48 Hours) 211
Figure 37 (A - C) - Mitochondrial Ca^{2+} ions in HCV gt2a infection models +/- L-glutamate (24, 48 hours) 213
Figure 38 (A, B) – Mitochondrial Membrane Potential (mt$\Delta\Psi$m) in HCV gt2a Infection Models +/- L-glutamate (24, 48 hours) 216
Figure 39 (A, B) – Induction of Mitochondria-Associated Apoptosis in HCV SGR cells (24, 48 Hours) 219
Figure 40 (A, B) – Oxidative Phosphorylation gene transcription in HCV SGR cells +/- L-glutamate (24, 48 hours) 221
Figure 41 (A, B) – Oxidative phosphorylation gene transcription in JFH-1 infected Huh7 cells (MOI – 7.5) +/- L-glutamate (24, 48 hours) 225
Figure 42 (A – C) - Average intracellular [glucose] (µM) in HCV gt2a Infection Models +/- L-glutamate (24, 48 hours) 228
Figure 43 (A - C) - Intracellular Glycogen Content (µg μl^{-1}) in HCV gt2a Infection Models +/- L-glutamate (24, 48 Hours) 231
Figure 44 (A, B) – Lipogenic gene transcription in HCV SGR cells +/- L-glutamate (24, 48 hours) 234
Figure 45 (A, B) – Lipogenic gene transcription in JFH-1 infected Huh7 cells (MOI – 7.5) +/- L-glutamate (24, 48 hours) 237
Figure 46 (A - C) - Intracellular [triglyceride] (µM) in HCV gt2a Infection Models +/- L-glutamate (24, 48 Hours) 240
Figure 47 (A – L) - Oil-Red-O stained Huh7 and HCV SGR cells (24, 48 hours) 244
Figure 48 (A – L) - Oil- Red-O stained Huh7 and HCV SGR cells + L-glutamate (24, 48 hours) 245

Figure 49 (A – L) - Oil-Red-O (ORO) staining of intracellular lipid droplets in Mock- and JFH-1 infected Huh7 cells (MOI – 7.5) (24, 48 Hours)..... 246
Figure 50 (A – L) - Oil-Red-O (ORO) staining of intracellular lipid droplets in Mock- and JFH-1 infected Huh7 cells (MOI – 7.5) + L-glutamate (24, 48 Hours)... 247
Figure 51 (A, B) - Quantification of ORO stained intracellular LDs in HCV gt2a infection models +/- L-glutamate (24, 48 Hours) 248
Figure 52 - Intracellular HCV SGR replication in HCV SGR cells +/- L-glutamate (24, 48 Hours) 251
Figure 53 - Intracellular HCV replication in JFH-1 infected Huh7 cells (MOI – 7.5) +/- L-glutamate (24, 48 Hours) 252
Figure 54 - Extracellular HCV secretion in JFH-1 infected Huh7 cells (MOI – 7.5) +/- L-glutamate (24, 48 Hours) 253
Figure 55 - Protein quantification (HCV NS3, TXNIP, Actin) in Huh7 and HCV SGR cells +/- L-glutamate (24, 48 hours)..... 255
Figure 56 - Densitometry analysis of TXNIP protein expression in Huh7 and HCV SGR cells +/- L-glutamate (48 Hours) 255
Figure 57 - Densitometry analysis of HCV NS3 protein expression in HCV SGR cells +/- L-glutamate (48 Hours) 256
Figure 58 (A, B) - Fluorometric analysis of reactive oxygen species (ROS) in Mock- and JFH-1 infected Huh7 cells +/- L-glutamate [0.5 mM] (24, 48 Hours)..... 258
Figure 59 – TXNIP upregulation through mitochondrial dysfunction induced by calcium ion overload following ER stress 262
Figure 60 - TXNIP transcription in HCV SGR cells transfected with siRNA targeting TXNIP (siTXNIP) (24, 48 Hours) 266
Figure 61 - Intracellular HCV SGR replication in HCV SGR cells transfected with siRNA targeting TXNIP (siTXNIP) (24, 48 Hours) 267
Figure 62 - Mlx transcription in HCV SGR cells transfected with siRNA targeting Mlx (siMlx) (24, 48 Hours)..... 268
Figure 63 - TXNIP transcription in HCV SGR cells transfected with siRNA targeting Mlx (siMlx) (24, 48 Hours) 269
Figure 64 - Intracellular HCV SGR replication in HCV SGR cells transfected with siRNA targeting Mlx (siMlx) (24, 48 Hours) 270
Figure 65 - GeneGO™ Metacore™ pathway analysis from re-evaluated microarray data (Hexokinase 2 (HXK2) Transcription)..... 272

Abbreviations

(-) sense	Antisense
(+) sense	Sense
A	Adenosine
aa	Amino acid
ABCA1	ATP-binding cassette transporter 1
ABLIM3	Actin binding LIM protein family member 3
ACC2	Acetyl-CoA carboxylase 2
ACLY	ATP citrate lyase
Acox1	Acyl CoA oxidase 1
ACSL	Acyl-CoA synthetase long-chain
ACSL3	Acyl-CoA synthetase long-chain family member 3
ADR	Adverse drug reaction
Ago	Argonaute
AH	Amphipathic helix
AIF	Apoptosis inducing factor
AKG	α-ketoglutarate
Akt	Protein kinase B
Alv	Alisporivir
AMP	Adenosine monophosphate
ANT	Adenine nucleotide translocator
AOX	Acyl CoA oxidase
Apo	Apolipoprotein
ARF1	ADP-ribosylation factor 1
ARFGAP1	ADP-ribosylation factor GTPase activating protein 1
Arg	Arginine
ARRDC4	Arrestin domain containing 4
ASK1	Apoptosis signal-regulating kinase 1
ASO	Antisense oligonucleotides
Asp	Asparagine
ATF6	Activating transcription factor 6
ATP	Adenosine triphosphate
ATP5L	ATP Synthase, Subunit G
Bcl-2	B-cell lymphoma 2 protein
BE	Branching enzyme
BiP	Binding Immunoglobulin Protein
BLAST	Basic Local Alignment Search Tool

BMI	Body-Mass Index
BVDV	Bovine Virus Diarrhoea Virus
C	Cytosine
Ca^{2+}	Calcium
CBP	Cyclic adenosine monophosphate response element binding protein
CCNE1	Cyclin E1
CDKN1B	Cyclin dependent kinase 1B
CERT	Ceramide transfer protein
CHC	Chronic hepatitis C
CHOP	CCAAT-enhancer binding protein (C/EBP) homologous protein
CIPMR	Cation independent mannose-6-phosphate receptor
CLDN1	Claudin-1
CNS	Central nervous system
CO_2	Carbon dioxide
Con1	Consensus genome 1
COPI	Coatomer protein I
CPT1a	Carnitine palmitoyl acyl-CoA transferase 1a
CRE	*Cis*-acting replication elements
Cs	Cyclosporin
C-Terminus	Carboxy-Terminus
CUTL1	Cutlike homeobox1
CYCS	Cytochrome C
Cyp	Cyclophilin
CYP4A	Cytochrome P450 4A
Cys	Cysteine
DAA	Direct acting antiviral
DBE	Debranching enzyme
DCV	Daclatasvir
DDX3X	DEAD box polypeptide, 3 X-linked
DENV	Dengue Virus
DGAT1	Diacylglycerol O-acyltransferase 1
DGAT1	Diacylglycerol acyl transferse-1
dH_20	Distilled water
DIDS	4,4′-diisothiocyanatostilbene-2,2′-disulfonic acid
DMEM	Dulbecco's modified essential medium
DNA	Deoxyribonucleic acid
DNL	*De novo* lipogenesis
DNS	3',5'-Dinitrosalicylic acid
dsRNA	Double stranded ribonucleic acid

E3BP	E3 binding protein
ECH1	Enoyl CoA hydratase 1
EGP	Endogenous Glucose Production
eIF	Eukaryotic Initiation Factor
ELOVL4	ELOVL fatty acid elongase 4
ELOVL7	ELOVL fatty acid elongase 7
EMCV	Encephalomyocarditis virus
EndoG	Endonuclease G
ER	Endoplasmic reticulum
ERK	Extracellular signaling related kinase
ESCRT	Endosomal sorting complex required for transport
ETC	Electron transport chain
EXPO	Exportin
FA	Fatty acid
FABP3	Fatty acid binding protein 3
FAD	Flavin adenine dinucleotide
FADH2	Flavin adenine dinucleotide (reduced)
FAPP2	Four phosphate adapter protein 2
FASN	Fatty Acid Synthase
FCCP	Carbonyl cyanide-4-(trifluoromethoxy)phenylhydrazone
FoxO1	Forkhead box 1
G	Guanosine
G1P	Glucose-1-phosphate
G418	Geneticin
G6P	Glucose-6-phosphate
G6Pase	Glucose-6-phosphatase
GAA	α-glucosidase
Gab1	Grb2-associated binder 1
GAPDH	Glyceraldehyde-3'-phosphate dehydrogenase
GBF1	Golgi-specific Brefeldin A resistance factor 1
GBV-B	GB virus-B
GCK	Glucokinase
GCKR	Glucokinase regulatory protein
GFP	Green fluorescent protein
GKRP	Glucokinase regulatory protein
Glc_{in}	Intracellular glucose
Glc_{out}	Extracellular glucose
Gln	Glutamine
Glu	Glutamate
GLUT	Glucose transporter

Gly	Glycine
GN	Glycogenin
GNG	Gluconeogenesis
GO	Gene ontology
GOLPH3	Golgi phosphoprotein 3
Grb2	Growth-factor-receptor-bound protein 2
GS	Glycogen synthase
GSK3	Glycogen synthase kinase 3
Gt	Genotype
H	Helical region
H2DCFDA	2',7'-dihydrofluoroscein diacetate
HAT	Histone Acetyltransferase
HBE	HNF-4 binding element
HBV	Hepatitis B virus
HCC	Hepatocellular carcinoma
HCV	Hepatitis C virus
HCV SGR	Hepatitis C virus subgenomic replicon
HCVcc	Cell-culture derived hepatitis C virus
HCVpp	Hepatitis C virus pseudo-particles
HCVser	Serum-derived HCV
HDAC	Histone deacetylase
HDL	High density lipoprotein
HEK	Human embryo kidney
HepG2	Human epithelial G2
HIF1α	Hypoxia-inducible factor 1α
His	Histidine
HIV-1	Human Immunodeficiency virus-1
HK	Hexokinase
HNF-4	Hepatocyte nuclear factor-4
HSP47	Heat shock protein 47
HSP90	Heat shock 90kDa protein
HSPA5	Heat shock 70kDa protein 5 (GRP78)
Huh7	Human hepatoma 7
h-VAP-33	33kDa human vesicle-associated membrane protein associated protein
HVR	Hypervariable Region
HXK1	Hexokinase I
HXK2	Hexokinase 2
IF	Immunofluorescence
IFN	Interferon

IKI	Iodine-Potassium Iodide
IKK	IκB kinase
IL	Interleukin
Ile	Isoleucine
IMM	Inner mitochondrial membrane
IMPDH	Inosine monophosphate dehydrogenase
IMS	Intermembrane space
Insig	Insulin induced gene
IP3R	Inositol-1,4,5-triphosphate
IPO	Importin
IPS-1	Interferon-β promoter stimulator-1
IR	Insulin resistance
IRE-1α	Inositol requiring enzyme-1α
IRES	Internal ribosomal entry site
IRF	Interferon regulatory factor
IRS	Insulin receptor substrate
ISDR	Interferon sensitivity determining region
ISG	Interferon stimulated gene
IVDAs	Intravenous drug abusers
JEV	Japanese encephalitis virus
JFH-1	Japanese Fulminant Hepatitis 1
JNK	c-Jun N-Terminal kinase
KB	Ketone Body
KDa	Kilodalton
KGDHC	α-ketoglutarate dehydrogenase complex
LCAD	long chain-specific CoA dehydrogenase
LCFAs	long-chain fatty acids
LD	Lipid Droplet
LDL	Low density lipoprotein
LDLR	Low density lipoprotein receptor
Leu	Leucine
LNA	Locked nucleic acid
LPA	Lysophosphatidic acid
L-PBE	L-peroxisomal bifunctional enzyme
LTB	Lymphotoxin B
LVP	Lipoviral particle
LXRE	Liver X receptor-elements
Lys	Lysine
MAb	Monoclonal antibody
MAMs	Mitochondrial associated membranes

MAPK	Mitogen activated protein kinases
MAVS	Mitochondrial antiviral signaling protein
MBD	Membrane binding domain
MCU	Mitochondrial calcium uniporter
Met-tRNA	Methionine transfer RNA
Mg^{2+}	Magnesium
MICA	MHC class I polypeptide-related sequence A
MiRISC	MicroRNA-containing-RNA-induced silencing complex
MiRs	MicroRNA
Mlx	Max like protein
MlxIP	Max like protein-interacting protein
MlxIPL	Mlx interacting protein-like protein
MoA	Mechanism of action
MOI	Multiplicity of infection
MPT	Mitochondrial Permeability Transition
mPTP	Mitochondrial permeability transition pore
mRNA	Messenger RNA
MS	Metabolic syndrome
mt$\Delta\Psi$m	(Change in) Mitochondrial membrane potential
mTOR	Mammalian target of rapamycin
MTP	Microsomal triglyceride transfer protein
MUFAs	Monounsaturated fatty acids
MW	Membranous web
nAb	Neutralising antibody
NaCaE	Sodium-calcium exchanger
NAD	Nicotinamide adenine dinucleotide
NADH	Nicotinamide adenine dinucleotide (reduced)
NADPH	Nicotinamide adenine dinucleotide phosphate
NBM	Nucleotide binding motif
NDUFAF	NADH dehydrogenase (Ubiquinone) complex I assembly factor
NEMO, IKKγ	NFκB essential modifier
Neo	Neomycin
NES	Nuclear export signal
NF-AT	Nuclear factor of activated T-cells
NFκB	Nuclear factor kappa B
NK	Natural killer
NLRP3	Nod-like receptor family, pyrin domain containing 3
NLS	Nuclear Localisation Signal
NPC	Nucleopore Complex
NPC1L1	Niemann-Pick C1 Like 1

NS	Non-Structural
N-terminus	Amino-terminus
NTR	Non-translated region
NUAK2	NUAK family kinase 2
OAS	2'-5'-oligoadenylate synthase
OCDN	Occludin
OGDH	Oxoglutarate (α-ketoglutarate) dehydrogenase
OMM	Outer mitochondrial membrane
ORF	Open reading frame
ORO	Oil-Red-O
OSBP	Oxysterol binding protein
OXPHOS	Oxidative phosphorylation
p.i.	Post-infection
PA28-γ	Proteasome Activator 28-γ
PAMP	Pathogen-associated molecular pattern
PAZ	Piwi-Argonaute-Zwille
PBS	Phosphate buffered saline
PCK2	Phosphoenolpyruvate carboxykinase 2
PCR	Polymerase chain reaction
PDH	Pyruvate dehydrogenase
PDHc	Pyruvate dehydrogenase complex
PDK4	Pyruvate dehydrogenase kinase 4
PEG	Polyethylene glycol
Peg-IFN	Pegylated-Interferon
PFK	Phosphofructokinase
PGM	Phosphoglucomutase
PH	Glycogen phosphorylase
Phe	Phenylalanine
PHH	Primary human hepatocytes
PI	Protease Inhibitor
PI(4)P	Phosphatidylinositol 4-phosphate
PI[4,5]P2	Phosphatidylinositol (4,5)-bisphophate
PI3K	Phosphatidylinositol 3-kinase
PI3P-5K	1-phosphatidylinositol 3-phosphate 5-kinase
PI4K	Phosphatidylinositol 4-kinase
PiC	Mitochondrial phosphate carrier
PIK	Phosphatidylinositol kinase
PIP	Phosphatidylinositol phosphate phosphatase
PIWI	P element-induced wimpy testes
PK	Pyruvate Kinase

PKA	Protein kinase A
PKC	Protein kinase C
PKR	Protein kinase R
Polβ	Polymerase β
Polγ	Polymerase γ
PPARGC1A	Peroxisome Proliferator Activated Receptor-γ coactivator 1a
PPAR-REs	Peroxisome proliferator activated receptor response elements
PPARα	Peroxisome proliferator activated-receptor α
PPARγ	Peroxisome proliferator activated receptor-γ
PPIase	Peptidyl-prolyl *cis-trans* isomerase
PPP	Pentose phosphate pathway
PRKAA2	5' AMP-activated protein kinase (AMPK)
PSME3	Proteasome Activator Subunit 3
PTL	3-ketoacyl-CoA thiolase
PTP	Protein tyrosine phosphatase
PTP1b	Protein-tyrosine phosphatase 1b
PUFAs	Polyunsaturated fatty acids
PYGL	Glycogen phosphorylase
qRT-PCR	Quantitative reverse transcription polymerase chain reaction
RAV	Resistance-associated variant
RBA	Ribavirin
RCs	Replication complexes
RdRp	RNA-dependent RNA polymerase
RELA	RELA proto-oncogene NFκB subunit
RIG-I	Retinoic acid-Inducible Gene 1
RMM	Relative molecular mass
RNA	Ribonucleic acid
RNAi	RNA Interference
ROS	Reactive oxygen species
RPLP0	Large ribosomal protein
rTCA cycle	Reverse Tricarboxylic acid cycle
RTN3	Reticulon 3
RTP	Ribavirin triphosphate
RXRα	Retinoid X receptor-α
S	Structural
S1P, S2P	Site 1 protease, Site 2 protease
S6K1	mTOR substrate p70 ribosomal S6 Kinase
Sac1	Sac1 phosphoinositide phosphatase
SBD	Sphingomyelin binding domain
SCAP	SREBP-cleavage activated protein

SCD1	Stearoyl co-enzyme A desaturase 1
SD	Standard deviation
SDH	Succinate dehydrogenase
SEC14L2	SEC14 like lipid binding 2
Ser	Serine
SERCA	Sarco-endoplasmic reticulum Calcium ATPase
SH3	Src homology 3
SHIP2	SH2-containing 5'-inositol phosphatase
shRNA	Short-hairpin RNA
siRNA	Small Interfering RNA
SL	Stem-Loop
SLC27A2	Fatty acid transport protein 2
Smac	Second mitochondria-derived activator of caspase
SNP	Single Nucleotide Polymorphisms
SOC	Standard of care
SOCE	Store operated calcium entry
SOCS	Suppressors of cytokine signaling
SOD1	Superoxide dismutase 1
SPP	Signal peptide peptidase
SR- β1	Scavenger receptor-β1
SRE	Sterol regulatory element
SREBP	Sterol regulatory element binding protein
ssRNA	Single stranded ribonucleic acid
STC2	Stanniocalcin 2
STING	Stimulator of interferon genes
SVR	Sustained virological response
T2DM	Type 2 diabetes mellitus
TBK1	TANK binding kinase 1
TCA cycle	Tricarboxylic acid cycle
TG	Triglyceride
TGN	*Trans* golgi network
TIP47	Tail-interacting protein 47
TIR	Toll-IL1 receptor
TLR	Toll-like receptor
TMD	Transmembrane domain
TMRE	Tetramethylrhodamine ethyl ester
TNFα	Tumour necrosis factor α
TRIB3	Tribbles pseudokinase 3
TRIF	Toll/IL-1 receptor domain-containing adaptor inducing IFN-β
Trp	Tryptophan

Trx	Thioredoxin
TU	Transducing units
TXNIP	Thioredoxin-interacting protein
Tyr	Tyrosine
U	Uridine
UDP	Uridine diphosphate
UDP-Glc	Uridine diphosphate-Glucose
UGGPase	UDP-glucose pyrophosphorylase
UP	Uridine phosphorylase
UPR	Unfolded protein response
UTP	Uridine triphosphate
UTR	Untranslated region
Val	Valine
VDAC	Voltage dependent anion channel
VDUP1	Vitamin D upregulated protein 1
VLCFA	Very long chain fatty acid
VLDL	Very low density lipoprotein
VLDLR	Very low density lipoprotein receptor
XBP-1	X-box binding protein 1

Presentations

The works featured in this thesis have been presented at the following conferences:

- **13th Annual HCV UK meeting (oral), Rydal Hall, Cumbria– 22/05/2015**
- **Annual SGM conference (oral), Birmingham ICC – 01/04/2015**
- **Annual SGM conference (poster), Liverpool ACC – 15/04/2014**

Acknowledgments

I would like to thank my friend, mentor, and supervisor, Dr. Michael J McGarvey for his patience, help, and guidance throughout my Ph.D.

I would like to acknowledge the Hepatology, Respiratory Medicine, and Virology departments as well associated staff and Ph.D. students at Imperial College including Dr. Stathis Giotis, Professor Peter O' Hare, Dr. Fouzia Sadiq, Dr. Marcus Dorner, Dr. Anna Ettorre, and Liyana Ahmad for all their help, feedback, and resources I received during my project.

I thank my mother and my friends for supporting me throughout my studies, and the MSc., BSc., and MRes students including Katharine Fox, Kanyada Koysombat, Kiran Jaswell, Philip Lau, and Mehrin Hossain, who I've taught and advised during their projects and who, in turn, helped me to find myself.

Copyright Declaration

The copyright of this thesis rests with the author and is made available under a Creative Commons Attribution Non-Commercial No Derivatives licence. Researchers are free to copy, distribute or transmit the thesis on the condition that they attribute it, that they do not use it for commercial purposes and that they do not alter, transform or build upon it. For any reuse or redistribution, researchers must make clear to others the licence terms of this work.

Declaration of Originality

The work contained in this thesis, submitted for the award of Doctor of Philosophy, is of my own efforts carried out in the Department of Virology at Imperial College, and has not been plagiarised. Cited works by other parties has been properly referenced where appropriate.

Chapter 1: Introduction

1.1. Overview of Hepatitis C virus (HCV)

HCV is an ongoing prevalent health issue and a major cause of liver disease across the world affecting between 130 - 185 million people [1]. Initially described as non-A, non-B hepatitis in 1989, according to estimates made by the World Health Organisation (WHO), it is possible that up to 3% of the world's population may be infected with this pathogen [1,2]. Furthermore, it is believed that up to 3 to 4 million cases of infection are diagnosed every year [1,3]. Around 20 - 30% of carriers with an acute infection, which is largely asymptomatic, are thought to spontaneously clear the virus [4]. The remaining 70 - 80% of infected individuals, however, may develop viral persistence and chronic disease, in which secondary pathologies such as cirrhosis, fibrosis, insulin resistance (IR), type 2 diabetes mellitus (T2DM), and hepatic steatosis are common [3–5]. HCV is a leading cause of liver failure and liver cancer (hepatocellular carcinoma) thereby necessitating a demand for liver transplantation [3].

HCV is a blood-borne virus that is mainly transmitted through contact with contaminated instruments, such as hypodermic needles as in the case of intravenous drug abusers (IVDAs), surgical instruments, or infectious donated organs and blood products [6]. However, in addition to these possible sources of infection, there is evidence that suggests the virus may have limited horizontal transmission through sexual practices [7].

1.2. The Molecular biology of HCV

Hepatitis C virus is a species of the *hepacivirus* genus that belongs to the *Flaviviridae* family which includes many other arthropod-borne viruses belonging to the *Flavivirus, Pestivirus,* and *Pegivirus* genera [8]. HCV shares attributes, in terms of both polyprotein structure and genomic organisation, with other flaviviruses such as Japanese encephalitis virus (JEV), Yellow Fever virus, and Dengue virus [9].

Hepatitis C virus is the aetiological agent of HCV infection and has been characterised as a comparatively small virus of spherical morphology that is estimated to be between 55 and 65nm in diameter [10]. HCV is primarily hepatotropic, though the proportion of infected liver cells *in vivo* may vary between 1 and 5% but has also been reported to be as high as 4.8 – 87% [11,12]. However, it has been reported that genetically distinct HCV RNA has also been isolated from neurological tissue [13]. The virus is enveloped by a membrane that is derived from the host cell which is decorated with virally encoded glycoproteins (E1, E2) that mediate viral entry into naive cells [14,15]. The envelope surrounds a capsid comprised of the viral core protein which contains a (+)-sense RNA genome of approximately 9.6kb that encodes a polyprotein of around 3,010 amino acids in length (**Figure 1**) [3,16].

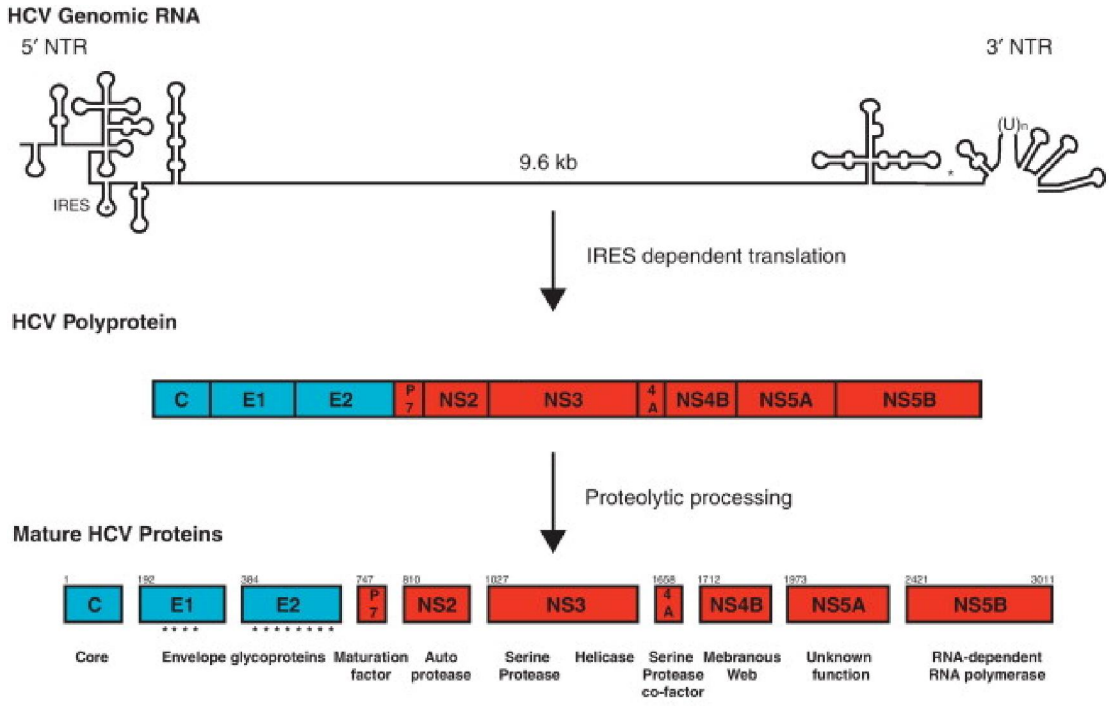


Figure 1 - The Genomic Organisation of hepatitis C virus

HCV Genomic RNA: The genome of HCV consists of (+)-sense RNA that is 9.6kb in length that is flanked by 5'- and 3'-nontranslated regions (NTRs/UTRs) which adopt secondary structures such as stem loops (SLs) and panhandles. **HCV Polyprotein:** Host cell ribosomes translate the HCV genome in an IRES dependent manner into a single polyprotein. **Mature HCV proteins:** The HCV polyprotein is proteolytically processed by host- and virally encoded proteases to yield 10 functional proteins that serve either a structural- or nonstructural role in virus replication [17].

The viral polyprotein is subject to proteolytically cleavage into functional subunits by host cell and virally encoded proteases both co- and post-translationally at the Endoplasmic Reticulum (ER) [18]. HCV has a single open-reading frame (ORF) and is flanked by 5'- and 3' nontranslated regions (NTRs) that are also referred to as untranslated regions (UTRs) [15]. The UTRs of the viral genome fold into highly conserved intramolecular secondary structures known as *cis*-acting replication elements (CREs) which rely on the interaction of co-factors to enhance the translation and transcription of viral genomes [19,20].

Both the structure and functions of the 5'-UTR of HCV are highly conserved among genotypes, indicating that these regions have an important role in viral fitness [21]. The HCV 5'-UTR, which spans approximately 340 nucleotides in length, has an internal ribosomal entry site (IRES) that initiates translation in a cap-independent manner and consists of 4 structural domains (Stem Loops (SL) I – IV) [19,22,23]. This region of the HCV genome facilitates translation of the viral polyprotein through the recruitment of the 40S subunit of host cell ribosomes and translation initiation factors, eIF2 (Met-tRNA) and eIF3 [19,21]. Additionally, stem loops III and IV of the 5'-UTR have been found to activate protein kinase R (PKR), an inhibitor of protein translation in response to the recognition of pathogen associated molecular patterns (PAMPs) such as dsRNA, which has no effect on translation of the HCV genome [24]. The 3'-UTR of HCV is around 220nt in length that comprise 3 domains, i.e. a variable region of around 40 nucleotides, a poly (U/UC) tract of variable size, both of which differ greatly between genotypes but are highly conserved within a given HCV genotype, and a highly conserved 98-base region termed the X-tail [25].

The 3'-UTR of HCV regulates the transcription of viral RNA genomes through the binding of glyceraldehyde-3-phosphate dehydrogenase (GAPDH), which is primarily involved in glycolysis and known to interact with cytoskeletal proteins (actin, tubulin), to the poly (U/UC) tract [26].

The X-tail is formed by 3 stem loop structures (SLI – III), the integrity of which is critical for virus replication [27]. A key feature of the HCV 3'-UTR is its ability to aid in the localisation of translation initiation factors, e.g. eIF2 and eIF3, to the 5'-UTR via so-called "long range" interactions [27]. The delivery of translation initiation factors and association of both the 5'- and 3'-UTRs has been shown to stimulate the cap-independent translation of the viral genome as well as stabilise the formation of 40S ribosomal subunits for subsequent rounds of IRES-mediated translation (ribosome recycling) following termination [25,27]. Additionally, the interactions which occur between the 5'- and 3'-UTRs of HCV also act as a molecular switch that may allow alternation between replication and translation of the HCV genome (**Figure 2**) [28,29].

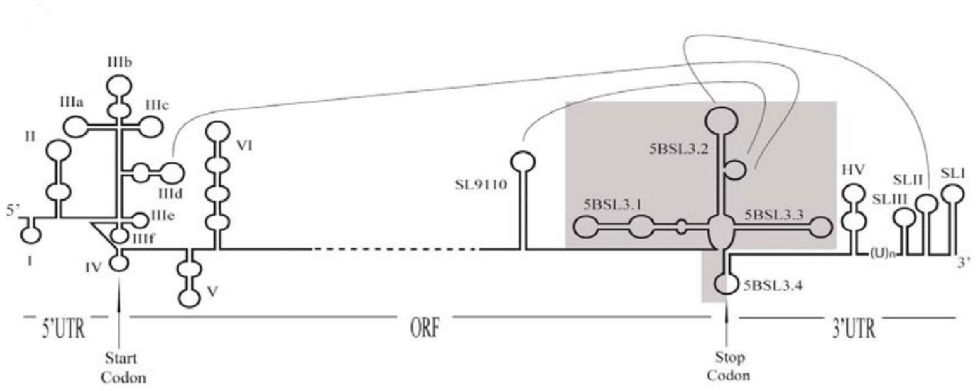


Figure 2 - The secondary structure of HCV 5'- and 3' UTRs

The genome of HCV encodes a single open-reading frame (ORF) that is flanked by 5'- and 3' untranslated regions (UTRs) which feature start- and stop codons, respectively. The 5' UTR adopts several secondary structure domains identified by roman numerals, with subdomains denoted by lower case letters. The 3' UTR features 3 stem loops (SL), a poly-U tract ($(U)_n$) a hypervariable region (HV), and CRE domain that encompasses subdomains (5BSL3.1 – 5BSL3.4). Curved lines between secondary structure domains indicate long-range interactions within the HCV genome [30].

Between the 5'- and 3'-UTRs of the HCV genome is a single ORF encoding a polyprotein which is subsequently cleaved into 10 proteins that have either a structural (S) (core, E1, E2) or non-structural (NS) (p7/NS1, NS2, NS3, NS4A, NS4B, NS5A, and NS5B) function [3].

1.2.1. HCV Structural (S) proteins

The core, and envelope glycoproteins (E1 and E2) of HCV, are mainly concerned with the assembly of particles that package the viral genome [31].

1.2.1.1. Core (C)

The core protein of HCV has a molecular weight of 19 - 21kDa, consists of 191 amino acids, and is the main constituent of the viral nucleocapsid that is involved in the binding of newly synthesised viral genomes and their encapsidation [17,32]. Cleavage of core protein from the HCV polyprotein occurs at its C-terminus by a host cell signal peptidase situated at the endoplasmic reticulum (ER) and results in an immature core protein (p23) that is associated to the ER membrane by a signal peptide [33]. This precursor is further cleaved by an intramembrane presenilin-type aspartic protease signal peptide peptidase (SPP) at the ER which causes the maturation and release of the core protein from the ER membrane [33].

The structure of HCV core is comprised of two amphipathic helices (HI and HII) that flank a hydrophobic loop which are features essential to the interaction with intracellular lipid droplets (LDs) [34]. Furthermore, the core protein has 3 domains (I - III) that vary in hydrophobicity [3].

Domain I is comprised of the first 117 amino acids of the protein and despite the presence of two short hydrophobic regions, is largely hydrophilic due to an abundance of basic residues which give rise to its RNA binding properties as well as ability to mediate assembly of the viral capsid [35,36]. Domain II, which spans from aa 118 – 174, is hydrophobic and important to the folding and stability of HCV core where it interacts with LDs, a key determinant of virion assembly, in addition to the ER membrane [34,36,37]. However, Domain III (aa 175 – 191) has the greatest hydrophobicity and serves as a signal sequence for targeting the E1 glycoprotein to the ER besides serving as a cleavage site to produce the mature form of the core protein (p21) [33,38]. Upon release from the HCV polypeptide, core protein may exist as dimeric forms in the cytosol or as a multimer [39]. The distribution of HCV core protein is widespread throughout an infected cell, where it can be found free in the cytoplasm and/or associated with various membrane structures such as lipid droplets (LDs,) the ER, mitochondria, and the nucleus [33,34,37,40–42].

The involvement of HCV core in the interplay of the ER and mitochondria might be explained by a study that found expression of this protein in liver cells resulted in a depletion of calcium ions stored within the ER lumen via decreased activity of sarco-endoplasmic reticulum calcium ATPase (SERCA) channels, which otherwise regulate the influx of calcium ions to the ER. [43]. The localisation of Ca^{2+} ions at the mitochondria may result in the bioenergetic dysfunction of this organelle to metabolise nutrients such as glucose, as well as induce cell death by the mitochondrial pathway of apoptosis [44,45].

Expression of the core protein during HCV infection has also been found to strongly associate with the manifestation of hepatic steatosis and HCC [46,47]. Furthermore, the expression of HCV core has been found to correlate with an increase in size and cholesteryl ester content of LDs [48].

HCV core may interact with both viral and host proteins, which may lead to the dysregulation of lipid metabolism. For example, core may co-localise with the HCV NS5A and facilitate the association of HCV NS5A with Apolipoprotein A1 (ApoA1), a constituent of high density lipoproteins (HDLs) [49]. Additionally, the expression of core protein leads to an inhibition of microsomal triglyceride transfer protein (MTP), a carrier of neutral lipids between membrane vesicles, that ultimately results in the reduced production and export of very-low density lipoproteins (VLDLs) [50,51].

Interestingly, core in addition to HCV NS proteins, i.e. NS3, NS5A, has been reported to have putative nuclear localisation signals (NLS) which facilitates localisation to the nucleus [42,52,53]. This may result in their interaction with nucleopore complexes (NPCs) and nuclear transport factors (NTFs), e.g. importin α5 (IPOA5) and importin β3 (IPO5), and conversely Nuclear Export Signals (NES) via exportin 1 (EXPO1/CRM1) which give rise to their nuclear entry and export [54]. It has also been suggested that NTFs may be involved in guiding viral proteins to the membranous web for viral replication [55].

1.2.1.2. Envelope glycoproteins (E1, E2)

The two envelope proteins of HCV, E1 and E2, have approximate molecular weights of 31kDa and 70Da, respectively, and are heavily glycosylated though this varies among HCV genotypes [56,57]. These glycosylated motifs are highly conserved and mainly consist of complex mannose side chains [58]. The glycans of HCV envelope proteins have important roles in antigenic variation, cell entry by receptor-mediated endocytosis, and protein folding to form noncovalent E1/E2 heterodimers linked by disulfide bridges [57,59–61]. The E1E2 heterodimers of HCV fulfil a role in cell entry, the primary stage of virus infection. E2 may bind to scavenger receptor-β type 1 (SR-β1), a high affinity receptor that is a requirement for the infection of cells that express co-receptors such as low-density lipoprotein receptor (LDLR), and CD81 [60].

Following this, the E1 glycoprotein is activated and serves as a fusogenic subunit, triggering the fusion and pH-dependent receptor mediated endocytosis of the virus particle with the phospholipid bilayer of the plasma membrane [62,63].

E2 may be targeted by neutralising antibodies (nAb) though this is complicated by high selection pressure and, therefore, the frequency of mutation in domains known as hypervariable regions, e.g. HVR1, *in vitro* [64]. Additionally, the ability of neutralising antibodies to bind to E2 is further impaired by the association and apparent "masking effect" of E2 with serum lipoproteins e.g. low-density lipoprotein (LDL) [65,66]. Both envelope proteins feature transmembrane domains (TMDs) that are made up of two short hydrophobic regions, separated by a sequence of charged amino acids, which enables them to reside on the cytosolic side of ER membrane following cleavage in the ER lumen [67]. The E1 and E2 glycoproteins interact with different ER-chaperone proteins such as calreticulin, GRP78 (BiP), and calnexin to form tertiary structure [68]. Furthermore, the expression of HCV envelope proteins has been reported to result in the induction of the CCAAT-enhancer binding protein homologous protein (CHOP) and induce the splicing of X-box binding protein 1 (XBP1), both of which are indicative of unfolded protein response (UPR) induction [69].

1.2.2. HCV Nonstructural (NS) proteins

The non-structural (NS) proteins are mainly involved in replication of the HCV genome and alteration of the host cell environment and immune responses to facilitate the synthesis of progeny virus.

1.2.2.1. p7

p7 is flanked at its N- and C termini by the E2 glycoprotein and nonstructural protein, NS2, respectively, in the HCV polyprotein [70]. The sequences preceding these termini are conserved, hydrophobic, and characteristic of signal peptides which direct the translocation of E2/p7 and p7/NS2 polyprotein to the ER where cleavage by host SPPs can occur [71]. p7 is a hydrophobic protein, comprised of approximately 63 amino acids, which can form either hexameric or heptameric structures within lipid bilayers to function as cation selective channels and facilitate ion flux [72].

p7 is a membrane spanning protein with two transmembrane alpha helices (TM1 and TM2) that face the ER lumen which are joined by a cytoplasmic loop [73]. It has been shown that the integrity of this cytoplasmic loop is crucial to the ion channel activity of p7 [74]. This is important to HCV replication as the ability of p7 to regulate the flux of H^+ ions may affect the intravesicular pH of compartments such as the lysosome, as well as the production of infectious virions [75].

Furthermore, p7 co-localises at the ER, in a strain-specific manner, with NS2 in the recruitment of viral core protein from LDs to the ER [76]. This finding is supported by a study that found p7 function to be crucial to the unloading of core protein from LDs in order for the encapsidation of viral RNA and envelopment of the nucleocapsid to occur [77]. Thus, it is considered that both the proton channel and core recruitment properties of p7 are critical for the virion assembly and egress stages of the HCV life cycle [78].

1.2.2.2. NS2

HCV NS2 is a transmembrane protein that is approximately 217 amino acids in length and has a molecular weight of 23 kDa [56,79,80]. The N-terminus of the NS2 is a highly hydrophobic membrane-binding domain (MBD) which associates with the ER [3]. The C-terminus, meanwhile, is exposed to the cytoplasm where NS2 may form a cysteine protease dimer with composite active sites [81]. The activity of this subdomain releases NS2 from the N-terminal third of NS3 via conformation-dependent autocatalysis that is stimulated by exogenous zinc [81,82]. Furthermore, this phenomenon is a requisite for active NS3 to accumulate so HCV RNA replication can occur [83]. The complication of hepatic steatosis during HCV infection has, in part, been attributed to the expression of NS2 [84]. Oem *et al*., found that NS2 is capable of increasing expression and processing of the transcription factor, sterol regulatory element-binding protein-1c (SREBP-1c) [84].

The authors found that NS2 can upregulate the transcription of SREBP-1c through binding to sterol regulatory elements (SREs) and liver X receptor elements (LXREs) within the SREBP-1c promoter, and may induce the transcription of a downstream lipogenic genes, e.g. Fatty Acid Synthase (FASN) [84]. Furthermore, SREBP-1c is a host factor that belongs to the helix-loop-helix leucine zipper family of transcription factors, associated with fatty acid biosynthesis, and is normally bound to SREBP-cleavage activating protein (SCAP) and tethered to the ER by Insig (insulin induced gene) protein [85].

In the context of oxidative stress during HCV infection, the SREBP-SCAP complex is released from Insig and translocates to the Golgi compartment to be processed by site 1- and 2 proteases (s1p, s2p) [85]. Following proteolytic cleavage of the N-termini, SREBPs are imported to the nucleus where they can transcriptionally induce genes such as fatty acid synthase (FASN) [84,85]. However, Oem *et al*., did not elaborate on how NS2 could transcriptionally activate SREBP-1c in the nucleus as NS2 is thought to be localised to the ER during virus assembly [84,86]. However, a nuclear localisation signal (NLS) in HCV NS2 was identified to complex with the nuclear importin, IPOA5 [55]. Similar to the NLS found in the core protein by the same research group, this was tested in a JFH-1 model using synthetic peptides to compete for association with cellular nuclear transport machinery, i.e. IPOA5 [55]. With the mechanism for the nuclear import of NS2 reduced, it was found that intra- and extracellular replication of HCV was suppressed 1- and 2-fold, respectively [55].

Similarly, comparable effects on virus replication were also observed when the nuclear export signal (NES) of NS2 was antagonised using synthetic peptides to compete for the exportin, Xpo1/CRM1 [55].

1.2.2.3. NS3

NS3 is a large, hydrophobic viral protein composed of 631 amino acids with a molecular weight of approximately 70kDa [56,87]. The N-terminus of NS3 is a trypsin-like serine protease whilst the C-terminus has helicase and ATPase properties which are required for the replication of viral RNA [88,89]. Upon synthesis of the viral polyprotein, NS3/NS4A undergo autocatalysis in *cis*, where the N-Terminus of NS3 may perform downstream proteolytic cleavage of NS proteins, i.e. NS4B – NS5B, in *trans* [90]. The serine-protease activity has been mapped to a triad of three residues namely His57, Asp81, and Ser139 [91,92]. Mutation studies involving substitution of His57 or Ser139 resulted in a loss of *trans* protease activity, demonstrating the importance of these residues in processing the replicase region of the HCV polyprotein [93]. Furthermore, the catalytic triad of NS3 is adjacent to a zinc binding motif which does not affect catalysis, but maintains the tertiary structure of the β-barrel domains of the protein and, by proxy, the NS3 active site [94–96]. In addition, it has been found that the viral RNA dependent RNA polymerase (RdRp) of HCV, i.e. NS5B, may enhance the helicase activity of NS3 up to 7-fold [97].

Thus, the NS3 protease is a desirable therapeutic target as in the case of Boceprevir and Telaprevir [98]. However, it has been shown that drug resistance, owing to reduced binding affinity of Boceprevir to the NS3 active site through acquired point mutations remains problematic in the development of antiviral treatments (**section 1.9.3.**) [98–101].

The helicase domain of NS3 is involved in the unwinding of dsRNA intermediates in an ATP-dependent manner [102,103]. Further to this, helicase activity is able to remove secondary structures and nucleic acid binding proteins within template ssRNA which may otherwise interfere with replication of the viral genome [19,104]. The unwinding activity has been found to occur sequentially at 18bp intervals and relies on the NS4A protein for optimal positioning of NS3 with substrate RNA [105,106]. A report also suggests that the protease activity of NS3 is dependent on its complex with heat shock protein 90 (HSP90), a molecular chaperone that is involved in the folding and stabilisation of proteins following cellular stress [107].

Additionally, NS3 may have other roles besides RNA helicase and protease functions. For example, Errington *et al*., found HCV NS3 to have both a cytoplasmic and nuclear localisation when human liver biopsies from donors infected with HCV were probed using anti-HCV NS3 antibodies and considered this an indication that NS3 may be involved in viral persistence [52].

This finding is supported by the work of Levin *et al*., who identified an IPOA5 binding peptide sequence in NS3 which led to a decrease in intra- and extracellular RNA synthesis when peptide constructs competed for this nuclear importin [(55)].

HCV NS3 may also interact with the catalytic subunit of protein kinase A (PKA) via a peptide with similarity to the general consensus sequence of PKA [(108)]. This association leads to the exclusion of PKA from the nucleus and its retention in the cytoplasm which results in the reduced phosphorylation of nuclear histones and, therefore, the transcription of genes, as well as affecting many cytoplasmic processes such as cytoskeletal motility, secretion, and ion channel function [(108)].

In addition to the disruption of cellular functions, NS3 may also circumvent innate immune responses (**section 1.5.1.1.**) e.g. disable the induction of interferon by retinoic acid inducible gene I (RIG-I) and toll-like receptor 3 (TLR3) pathways via cleavage of signalling molecules such as mitochondrial antiviral signaling protein (MAVS) and Toll/IL-1 receptor domain-containing adaptor inducing IFN-β (TRIF) [(109)].

1.2.2.4. NS4A

NS4A is a small protein (8kDa) comprised of 54 amino acids that is recognised as an essential co-factor of the HCV NS3 serine protease [56,110]. The hydrophobic N-terminus of NS4A features an alpha-helical, single-pass transmembrane domain which undergoes homotypic dimerisation and is essential to RNA replication and virus assembly due to its association with the ER [111]. Moreover, this association enables the targeting of the NS3 serine protease to the ER membrane in close proximity to the mitochondria which may affect calcium ion concentrations at the mitochondria and thus the metabolic function of this organelle [112,113].

Besides playing a role in the localisation of NS3 serine protease, NS4A also functions as a co-factor which involves the association of 9 residues (aa 22 – 31) in its C-terminus with 22 amino acids of the NS3 N-terminus [114,115]. This stabilises HCV NS3 and enhances its protease activity at downstream cleavage sites of the HCV polyprotein, i.e. NS4A/NS4B/NS5A/NS5B [113–118].

Further to interacting with the NS3 serine protease of HCV, the NS4A protein may associate with host factors such as glyceraldehyde-2-phosphate dehydrogenase (GAPDH), and 1-phosphatidylinositol 3-phosphate 5-kinase (PI3P-5K) which is involved in the nuclear transport of cellular proteins [110].

1.2.2.5. NS4B

NS4B is a highly hydrophobic protein that consists of 261 amino acids with a molecular weight of 27kDa and is closely associated to the ER [56,119,120]. The protein encompasses several structural elements which serve a variety of functions during the proliferation of HCV. The N-terminus (aa 1 - 69) of NS4B features two amphipathic helices (AH1 and AH2), which may translocate post-translationally between the ER lumen and cytosol and have been implicated in the formation of ER derived lipid vesicles as well as the recruitment of LDs [119,121–124].

AH1 (aa 6 – 29) is a conserved structural motif that is flanked by positively charged amino acids. In terms of function, AH1 has diametric roles in the life cycle of HCV, i.e. HCV RNA replication and virus particle assembly [122]. Conversely, the 2nd N-terminal amphipathic helix (AH2) of NS4B (aa 42 – 66) consists of mainly hydrophobic residues and is essential to the conformational change of the NS4B N-terminal and, therefore, its localisation between the cytosol and ER lumen [119,122]. AH2 has been observed to preferentially associate with phosphatidyl inositol phosphates as well as various membrane structures depending on their lipid content [123]. Additionally, it has been reported that AH2 has an important function in homotypic oligomerisation of NS4B which contributes to the formation of the replication complexes (RCs) and the membranous web (MW) [125,126]. HCV replication occurs at the MW which is derived from ER membrane vesicles [121].

NS4B N-terminal AH2 may accumulate negatively charged lipids at the lipid bilayer and induce structural rearrangement whilst modulating biophysical properties, e.g. tensile strength, which may in turn affect the oligomeric state of NS4B [121]. It has also been reported that the N-terminus of NS4B is more effective in the targeting of LDs, owing to its hydrophobic residue content, than the C-terminus [119].

A central domain (aa 70 – 190) that has 4 - 5 TMDs therein, bridges the respective N- and C-termini of NS4B [127–129]. The function of this region has been attributed to a nucleotide binding motif (NBM) (aa 129 – 135) that is thought to be cytoplasmic and have GTPase activity, i.e. capable of nucleotide binding and hydrolysis [130].
The NBM of NS4B has been shown to be fundamental to HCV RNA replication and also, in terms of pathogenesis, the development of HCC progression due to its tumorigenic potential both *in vitro* and *in vivo* [130,131].

Amino acids 191 – 261 constitute the C-terminus of HCV NS4B which features an RNA binding domain that is rich in Arg residues, 2 alpha-helical regions (H1 and H2) which flank the nucleotide binding motif (NBM), and two palmitoylation sites which may not be of functional importance to the replication of HCV RNA [124,132–136].

Similar to the N-terminus, the C-terminus of NS4B also has a cytoplasmic orientation where it may localise and bind with cellular membranes, particularly those composed of phospholipids [133,137].

The association of host membranes with the NS4B C-terminus has been found to arise through electrostatic forces between the highly conserved and positively charged H1 domain and the negative charge carried by membranous components such as phospholipids and sphingomyelin [137].

Like AH2 at the N-terminus, H1 at the C-terminus (aa 201 – 213) of NS4B has been found to associate with phospholipid membranes depending on the their composition [124,137]. Similarly, H2 (aa 228 – 254) is a membrane associated domain with an affinity for phospholipids and a suspected role in membrane biogenesis and/or the assembly of viral progeny [138].Terminal Cys residues located at the end of the NS4B C-terminus serve as palmitoylation sites which, as seen in the AH2 domain of the N-terminus, are necessary for the oligomerisation of NS4B to occur [134]. Additionally, it has been found that NS4B, in conjunction with the viral NS3/4A protein, may regulate the phosphorylation status of NS5A (**section 1.2.2.6.**) [139].

Interestingly, it has been found that a variety of host proteins may interact with NS4B including stimulator of interferon genes (STING), a protein resident to the ER that is responsible for the induction of the interferon response via RIG-I, the 33kDa human vesicle-associated membrane protein associated protein (h-VAP-33) which is involved in RC formation on lipid rafts, and Reticulon 3 (RTN3) [140–143]. Of these proteins, RTN3 is of particular relevance as it is a host factor that is associated to the ER and required for the replication of many (+)-sense RNA enteroviruses [143].

A study by Wu *et al*., however, found the converse to be true for HCV where RTN3 served as a restriction factor with its 2nd TMD competitively binding to AH2 of the NS4B N-terminal that inhibited both self-oligomerisation and RNA replication [(143)]. Additionally, RTN3 is induced by CHOP and activating transcription factor 6 (ATF6) following ER stress which may induce the translocation of B-cell lymphoma 2 (Bcl-2) protein to the mitochondria to counteract the pro-apoptotic effects of ER stress [(144)].

1.2.2.6. NS5A

NS5A is a hydrophilic phosphoprotein that exists in two different phosphorylation states, i.e. basal- or hyper phosphorylated, that have a molecular weight of 56- and 58kDa, respectively [(145,146)]. Unlike NS4B, NS5A does not feature any TMDs, although it does localise at intracellular membranes due to the presence of an amphipathic alpha helix membrane anchor (aa 5 – 25) [(147)].

The N-terminus of NS5A contains a zinc-binding motif consisting of 4 cysteine residues that is required to maintain its structure and function and so NS5A is considered a zinc metalloprotein that is essential to virus replication [(148)].

Interestingly, NS5A has been found to co-localise with core protein on LDs at the ER, a finding which was found to occur pan-genotypically during virus particle assembly [(149)].

A study by Camus *et al*., explained this phenomenon whereby diacylglycerol acyl transferse-1 (DGAT1), an enzyme that uses triglycerides (TGs) as a substrate in the development of LDs at ER membranes, forms a complex with HCV proteins and facilitates their interaction with LDs [(150)]. Furthermore, Lin *et al*., found that Apolipoprotein J (ApoJ), a Golgi-associated chaperon that is induced by glucose and involved in regulating secretory protein folding, stabilises the interaction between core and NS5A during the production of infectious virus [(151)].

Although HCV NS5A expression is mainly cytoplasmic and membrane-bound, it has a hidden NLS in its N-terminal that is anchored to the ER [(53,55)]. Furthermore, the association between HCV NS5A and the ER has been found to affect intralumenal calcium stores via a mechanism that, unlike HCV core, is independent of SERCA pumps but involves the efflux of Ca^{2+} ions via inositol-1,4,5-triphosphate receptor (IP3R) channels [(152)].

The NLS of NS5A is exposed following caspase-mediated cleavage in apoptotic cells and, under regulation by protein kinase A (PKA), translocates to the nucleus to transcriptionally induce host genes such as lymphotoxin B (LTB) and NUAK family kinase 2 (NUAK2), both of which are involved in cell survival [(53)]. However, NUAK2, a member of the catalytic 5' AMP-activated protein kinase (AMPK) α-subunits, may alternatively be induced by metabolic stress such as that caused by glucose deprivation [(153)].

Additionally, NS5A may disturb glucose metabolism by another mechanism that concerns the gluconeogenic transcription factor, Forkhead-box 1 (FoxO1) [154]. HCV NS5A activates the serine-threonine kinase c-jun N-terminal kinase (JNK) via the generation of mitochondrial reactive oxygen species (ROS) [154]. Activated JNK leads to the reduced phosphorylation of FoxO1 and thereby causes its nuclear accumulation and the transcriptional induction of genes such as phosphoenolpyruvate carboxykinase (PCK2) and glucose-6-phosphatase (G6Pase) [154]. The activity of these genes, in turn, promotes endogenous glucose production (EGP) in hepatocytes which is thought to be a factor in the development of type 2 diabetes mellitus (T2DM) (**section 1.8.2.1.**) [154,155].

HCV NS5A may also interact with host factors that are related to cell growth. For instance, it has been reported that NS5A may disrupt the proliferation and differentiation of cells via a proline-rich motif in the NS5A C-terminus which binds to the Src homology 3 (SH3) domain of growth-factor-receptor-bound protein 2 (Grb2) adapter protein [156,157]. The direct interaction of NS5A and Grb2 results in the inhibition of extracellular signaling related kinase 1 and 2 (ERK1, ERK2) pathway, a subclass of mitogen-activated protein kinases (MAPK), that is otherwise activated by epidermal growth factor (EGF) [156]. Furthermore, the N-terminus of NS5A may complex with Grb2-associated binder 1 (Gab1) protein, albeit indirectly, through the p85 subunit of phosphatidylinositol 3-kinase (PI3K) which leads to its increased Tyr phosphorylation as well as that of downstream AKT serine/threonine protein kinase and thereby promotes cell survival and tumourigenesis [156].

MAPKs are also phosphorylated and activated downstream in response to interferon-α (IFN α) [158]. However, NS5A may disable this response through a region termed the interferon-α sensitivity determining region (ISDR) which correlates with viral resistance [159]. This occurs by NS5A interacting with the catalytic domain (aa 244 – 366) of protein kinase R (PKR) that is induced by interferon-stimulated genes (ISGs) to bind dsRNA and inhibit the translation of proteins via phosphorylation of the α subunit of eukaryotic translation initiation factor 2 (eIF2α) [159].

1.2.2.7. NS5B

NS5B is a 65kDa tail anchored protein that is central to virus replication as it functions as an RNA dependent RNA polymerase (RdRp), a property that has been attributed to a GDD motif which forms an RNA binding site with the C-terminal [160,161]. The structure of NS5B can be described as resembling a “right-hand” shape where the “thumb” and “finger” sub-domains enclose the GDD motif located in the “palm” domain [161]. The C-terminal tail folds across the “thumb” domain through the hydrophobic interaction of respective residues, and down into the active site of the NS5A “palm” domain forming an RNA binding groove with the GDD catalytic triad [161].

The NS5B RNA polymerase initiates transcription from the 98nt 3' X-tail of the (+)-sense genome to produce a (-)-sense intermediate that serves as a template for the synthesis of (+)-sense progeny genomes [162].

A study by Powdrill *et al.*, found the fidelity of HCV NS5B to be low with a relatively high error-rate of 10^{-3} mutations per copied nucleotide which contrasts with the RNA polymerase activity of another member of the *Flaviviridae*, Yellow Fever virus, which has a higher fidelity with an error rate of $1.9 – 2.3 \times 10^{-7}$ [163,164]. The HCV polymerase is error-prone due to its lack of proof-reading activity along with a mutational bias towards G:U/U:G mismatches [163].

However, the study by Powdrill *et al.*, involved the replication of HCV RNA in the presence of purified NS5B from a gt1b construct in a cell-free, biochemical assay, and so does not describe the fidelity of NS5B in other isolates of the virus [163]. Regardless, the error-rate of HCV NS5B may confer an evolutionary advantage to the virus by generating a population of viral quasispecies that are resistant to antiviral therapies over successive rounds of replication [163].

NS5B may interact with other viral non-structural proteins within replication complexes (RCs), e.g. NS3 and NS4A, NS4B, and NS5A, which are known to modulate polymerase activity of the protein [120,165,166]. Additionally, NS5B may regulate its own activity through the formation of homotypic oligomers [167].

Conversely, there is also evidence of NS5B interacting with host factors including eukaryotic translation initiation factor 4 A2 (eIF4A2) which functions as an RNA-dependent ATPase/helicase, PKC-related kinase which regulates NS5B polymerase activity by phosphorylation, and both h-VAP-33 and human p68 in the synthesis of (-)-sense genomic intermediates [168–171]. Another host protein that has been identified to interact with HCV NS5B is Nucleolin, a nucleolar phosphoprotein that functions as an RNA chaperone and escorts transcripts of host- and viral origin between nuclear and cellular compartments [172]. Nucleolin has been found to benefit HCV replication through the interaction of its C-terminus with NS5B which is thought to aid the binding of the RdRp to the viral genome and/or stabilise single HCV NS5B subunits for oligomerisation in RCs [172].

1.3. *In vitro* HCV infection systems

To date, the lack of animal models for HCV infection besides those of Chimpanzees and humanised mice with liver xenografts, and the partial recapitulation of the HCV life cycle by surrogate models, e.g. GB virus-B (GBV-B) in Tamarins, have hampered research into how the virus operates *in vivo*. However, there are a number of cell-based systems that have been developed which can be used to study the various molecular and cellular processes that are altered during HCV infection. These provide somewhat reliable models for both acute and chronic infection which can be used in basic research and drug development.

Tools that can used to study HCV include HCV pseudoparticles (HCVpp), HCV subgenomic replicons (HCV SGR), and cell culture-derived infectious HCV (HCVcc) e.g.bi-cistronic HCV chimeras such as JC1, and the gt2a JFH-1 isolate.

1.3.1. HCV pseudoparticles (HCVpp)

HCV pseudoparticles can be used to simulate host cell effects that are brought about during the early stages of HCV infection, i.e. virus entry [173]. HCVpp are essentially 'empty' virions comprised of the HCV envelope proteins, E1 and E2, exogenous retroviral Gag and Pol proteins from human immunodeficiency virus (HIV-1) to facilitate budding from the plasma membrane (PM), and a reporter gene such as green fluorescent protein (GFP) [174].

The construction of HCVpp involves the transfection of 3 vectors that encode the components HCV E1/E2, HIV-1 Gag-Pol, and GFP into 293T Human Embryo Kidney cells (HEK293T) [174]. HCV-like particles are then assembled and released by the transfected cells at low titre (~ 3×10^5 transducing units (TU) ml^{-1}) [174]. The resultant particles are then capable of receptor-mediated endocytosis that occurs during virus attachment and entry into Huh7 cells which is assessed by quantifying the expression of reporter genes [174]. However, HCVpp are not capable of producing high titre stocks via serial passage but require repeated rounds of transfection and so their use may be considered labour–intensive [175].

However, in spite of these considerations, HCVpp are a useful tool in the study of cellular receptors that mediate virus entry e.g. low density lipoprotein receptor (LDLR), CD81, and claudin-1 (CLDN-1) [174,176].

1.3.2. HCV subgenomic replicons (HCV SGR)

HCV subgenomic replicons (HCV SGR) feature the replicase genes (NS3 – NS5B) of the HCV genome and have the capacity to self-replicate in cells [177]. Instrumental to the development of all HCV-based replication systems was the cloning of a full length gt1b isolate known as consensus genome 1 (Con1) [177]. The Con1 replicon is a bi-cistronic construct that is comprised of 2 cassettes with different properties [177]. The structural genes of HCV are replaced with an exogenous internal ribosomal entry site (IRES) derived from encephalomyocarditis virus (EMCV) along with a selectable marker, i.e. neomycin phosphotransferase gene (*neo*) [177].

The presence of *neo* confers resistance to the antibiotic G418, which allows for selection of Huh7 cell transfectants that produce a high copy number (1,000 – 5,000) of replicated genomes per cell [177]. The genes that are downstream from the neomycin-IRES cassette represent the viral replicase of HCV, i.e. NS3-NS5B (**Figure 3**).

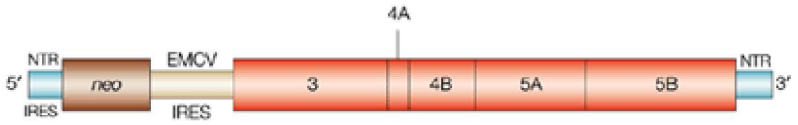


Figure 3 – The genomic organisation of HCV subgenomic replicons

5'- and 3'-nontranslated regions (NTRs) (blue) flank a gene conferring resistance to neomycin, *neo* (brown). An exogenous internal ribosomal entry site (IRES) from encephalomyocarditis virus (EMCV) drives the IRES-dependent translation of HCV proteins downstream from NS3 to NS5B [(83)].

While HCV SGR cells emulate the intracellular replication of HCV RNA when stably expressed, they are incapable of producing infectious virions due to the absence of HCV structural genes. Additionally, research has identified parallels between HCV SGR cells and the full-length virus model suggesting that both systems share commonalities, though differ in terms of magnitude, in virus replication e.g. impairment of mitochondrial fatty acid oxidation [(178)].

1.3.3. Infectious HCV models

A number of systems have been developed to investigate the molecular and cellular mechanisms of HCV that are considered to be representative of how virus infection occurs *in vivo*.

These *in vitro* models include the use of primary human hepatocytes (PHH) with HCV that is either derived from patient serum (HCVser) or cell culture (HCVcc) where the latter involves use of the JFH-1 (gt2a) molecular clone of the virus [(179–181)].

The JFH-1 isolate of HCV was developed by a group led by Takaji Wakita circa 2005 and involved cloning cDNA from an isolate derived from a Japanese patient with Fulminant Hepatitis [181]. This model recapitulates the entire hepatitis C virus life cycle including stages of attachment and host cell entry, replication and assembly, and virus egress to produce cell-culture derived virus particles (HCVcc) in a permissive cell line of human hepatoma cells termed Huh7 [181]. The JFH-1 model of HCV infection is a staple of HCV research in the development of therapeutic agents and understanding the viral mechanisms of pathology. Since its development, other variants of the JFH-1 Huh7 system have emerged such as the Huh7.5 mutant cell line that has a defective innate immune response, owing to a point mutation in retinoic acid-inducible gene-I (RIG-I), which is thought to contribute to its increased permissiveness to virus replication and production of higher virus titres compared to Huh7 cells [182,183]. In parallel, JFH-1 has been used to engineer other viral constructs of HCV such as the JC1 chimera [184].

JC1 is an intra-genotypic chimera that combines the JFH-1 replicase with the structural genes of J6 and has been said to yield infectious titres 100 – 1,000-fold greater than either of the parental isolates [184].

However, efficient replication and high titres of infectious JFH-1 may be achieved via serial passage of the virus and maintenance of persistently infected Huh7.5 cells [185].

This process gives rise to cell-culture adaptive mutations in viral proteins, e.g. core, E1, NS2, NS3, NS5A, and NS5B, of which those occurring in NS2, NS3, and NS5A were found to significantly increase virus assembly through the promotion of viral protein interactions [186,187].

The JFH-1 infection of Huh7 cells was the standard of research into HCV infection *in vitro* until August 2015, when Charles Rice's research group at The Rockefeller University identified a host-factor known as SEC14 Like Lipid Binding 2 (SEC14L2) that, when expressed, rendered a number of hepatoma cell lines permissive for pan-genotypic HCV replication [188]. Interestingly, SEC14L2 is a protein that is involved in the exchange of phosphorylated vitamin E (Tocopherol) with phosphatidylinositol, which is related to cholesterol biosynthesis and protection against lipid peroxidation [188,189].

In summary, there are several tools which can be used to study the mechanisms of HCV infection, though some are restricted to specific stages of the viral life cycle, e.g. HCVpp and HCV SGR cells, and therefore may not represent the scale of interactions that occur in full-length models where both structural and non-structural proteins are expressed in synergy. Thus, for comprehensive conclusions to be drawn, investigations should be carried out using both subgenomic and full-length systems of a consistent HCV genotype.

1.4. The HCV life cycle and Host Lipid Metabolism

The life cycle of HCV is largely dependent on the enhanced infectivity of virions that occurs through the complexing of virus particles with very-low density lipoproteins (VLDL) to produce lipoviroparticles (LVPs). Virus entry is facilitated by a combination of interactions that occur between the virus particle and cell receptors as well as co-receptors that bind to the VLDL component of the LVP (**Figure 4**) [190].

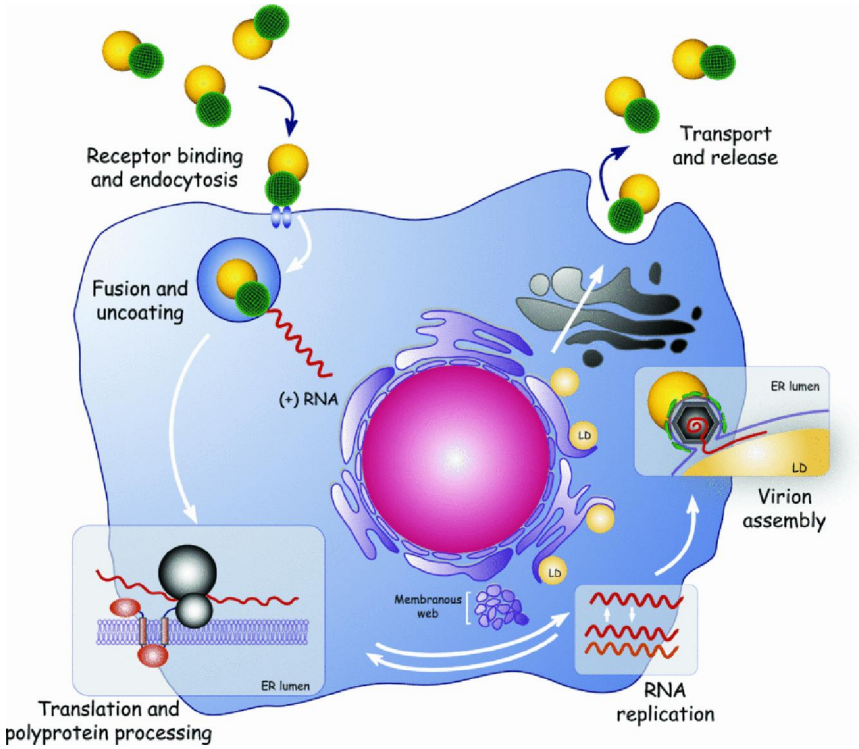


Figure 4 – The HCV life cycle

HCV virions (green spheres) complex with lipoproteins (yellow spheres) to form lipoviroparticles (LVPs) which enter naive liver cells via receptor-mediated endocytosis and membrane fusion. The nucleocapsid uncoats to release the viral genome which is translated to a single polyprotein that is processed by host- and viral proteases. HCV nonstructural proteins assemble replication complexes (RCs) within the membranous web which are adjacent to the ER and lipid droplets (LDs). Viral RNA is replicated and packaged in RCs which associate with very-low density lipoprotein (VLDL) precursor in the ER lumen to form immature lipoviroparticles (LVPs). Immature LVP are trafficked to the *trans* golgi network (TGN) where phosphatidylinositol-4-phosphate (PI4P) is localised and endosomal sorting complex required for transport complexes are recruited to facilitate virus egress [191–193].

The glycoprotein E1/E2 heterodimer that is expressed on the surface of the HCV particle docks with several receptors that are expressed on the surface of liver cells e.g. CD81, occludin (OCDN), claudin-1 (CLDN1) and scavenger receptor-β1 (SR-β1) [194,195]. Following receptor-binding, virion entry takes place via clathrin–dependent receptor mediated endocytosis, where cholesterol absorption and/or cholesterol homeostasis may be a factor due to the involvement of Niemann-Pick C1 Like 1 (NPC1L1) receptors [196,197]. After attachment, HCV fuses with an endosomal compartment to release the viral genome to the cytosol in a pH-dependent manner where it may be translated by ribosomes present on rough ER [198,199]. The synthesised viral polyprotein undergoes proteolytic processing via host and viral proteases and the viral genome replicates in replication complexes (RCs) that are shielded by the membranous web (MW) (**section 1.2.**). The 5'-UTR of nascent viral genomes are encapsidated by core protein in association with LDs at the ER membrane and, through interaction with E1 and E2 glycoproteins, the nucleocapsid buds into the lumen [200,201]. The ER lumenal space is the site where very low density lipoprotein (VLDL) begins to assemble via the microsomal triglyceride transfer protein (MTP) mediated lipidation of apolipoprotein B (ApoB) which complexes with E1/E2 glycoproteins on the enveloped nucleocapsid to form an immature lipoviroparticle (LVP) [202–204].

Through an as yet unknown mechanism, the immature LVP localises at the *trans* golgi network (TGN) that is enriched with phosphatidylinositol 4-phosphate (PI(4)P), a lipid species that recruits proteins involved in golgi trafficking to the TGN e.g. golgi phosphoprotein 3 (GOLPH3), oxysterol binding protein (OSBP), and the endosomal sorting complex required for transport (ESCRT) [192,205,206]. In addition to localising at the membranous web (MW), OSBP functions as a phosphatidylinositol 4-kinase (PI4K) effector and a regulator of cholesterol trafficking that is thought to play a role in the maturation of infectious virions [205,206]. Finally, the egress of LVPs from infected cells requires a system of cellular protein complexes termed ESCRT by which it can be said that HCV virion release exploits the anterograde transport of secretory proteins that is promoted by PI(4)P [193,207].

1.4.1. HCV and Lipid Species

The use of lipidome profiling in HCV infection has led to the identification of individual lipid species, as well as their mechanisms of biosynthesis, that are upregulated during virus infection [208–215].

A study by Diamond *et al*., found that changes in host metabolism, namely those pertaining to glycolysis and oxidative phosphorylation, are induced during HCV infection in Huh 7.5 cells that were found to promote lipid metabolism whilst maintaining the energy requirements of the cell during proliferation of the virus [208].

Phospholipids and sphingomyelins were among the lipid species found to be increased during HCV infection which indicates their involvement in virus assembly and secretion, a finding that concurs with the findings by Blackham *et al*., [208,214]. Phospholipids, however, primarily function in the structural repair of damaged intracellular membranes through recycling [216].

A study investigating the role of sphingomyelins, however, has shown that this lipid species is involved in the activation of the viral RNA-dependent RNA polymerase by enhancing the interaction of the Sphingomyelin Binding Domain (SBD) of NS5B and template RNA, though this region appears to be active only in gt1b isolates [209]. Furthermore, the SBD of the HCV NS5B RNA polymerase is also responsible for its localisation to lipid raft membranes [209]. Additionally, phosphatidylinositols such as phosphatidylinositol (4,5)-bisphophate ($PI[4,5]P_2$) and its precursor phosphatidylinositol 4-phosphate (PI(4)P) are lipids that have been identified as fulfilling many functions related to the plasma membrane and the mediation of cellular signaling pathways [210,217]. The amphipathic N-terminal of HCV NS5A is important to lipid membrane interactions [210]. Cho *et al*., attributed a conformational change in HCV NS5A to a specific binding motif within the viral protein that associates with $PI[4,5]P_2$ which was found to be essential for the replication of the HCV genome [210].

The relationship between phosphatidylinositol biosynthesis and HCV infection has led to studies of both upstream proteins such as the enzymes that are involved in their synthesis i.e. phosphatidylinositol kinases (PIKs) and phosphatidylinositol phosphatases such as PI4-kinase alpha (PI4Kα) and Sac1 phosphoinositide phosphatase (Sac1), respectively, as well as downstream effectors that include the Retromer complex and tail-interacting protein 47 (TIP47).

PI(4)P is derived from the phosphorylation of Inositol at position 4 of its group head by PI4Kα which has been found to be overexpressed in full length J6 and JFH-1 derived HCV SGR models [211]. PI(4)P primarily localises to the Golgi apparatus, although it has been observed to also localise to the endoplasmic reticulum (ER) in association with HCV NS5A prior to membrane rearrangement [211]. It has been proposed that HCV hijacks PI4Kα and increases PI(4)P synthesis as a means of mobilising viral replicase proteins via the nucleation of cellular vesicles to facilitate the formation of replication complexes (RCs) [211,213]. Similar mechanisms involving the dysregulation of host lipid metabolism have been observed in other species of *Flaviviridae* e.g. the NS3 protein of Dengue Virus overexpresses and recruits Fatty Acid Synthase (FASN) at sites of virus replication proximal to the ER to enhance lipogenesis [211].

Conversely, Li *et al.*, investigated Sac1, a key factor in the coatomer protein I (COPI) pathway, that dephosphosphorylates PI(4)P during retrograde transport from the golgi to the ER which has been found to inhibit HCV replication when overexpressed in infected cells [212,213]. A motif of Arg or Lys residues (aa 352 – 355) in HCV NS5A that is conserved among all HCV genotypes facilitates interaction with ADP-Ribosylation factor GTPase Activating Protein 1 (ARFGAP1), a cofactor for the Sac1 phosphatase-mediated regulation of PI(4)P abundance [212]. The importance of Sac1-activity, as well as its co-factors i.e. vesicular transport proteins ADP-ribosylation factor 1 (ARF1) and Golgi-specific Brefeldin A resistance factor 1 (GBF1), in HCV replication was demonstrated by the work of Zhang *et al.*, where the siRNA-mediated knockdown of ARF1 and GBF1 resulted in significant impairment of virus synthesis [213].

These studies, however, do not describe the functional importance or relevance of PI(4)P abundance to HCV replication which was clarified by Yin *et al.*, who investigated the role of the Retromer protein complex during HCV infection [218]. The Retromer complex is a part of the cellular transport machinery that has PI(4)P binding properties, and fulfils a role in the retrograde transport of cargo proteins from the *trans* golgi network (TGN) to subcellular locations enriched with PI(4)P that induces the unloading of protein cargoes [218]. Thus, Retromer has been found to localise with the RCs during HCV infection due to their abundance of PI(4)P.

The PI(4)P effector proteins that are conveyed by the Retromer complex include OSBP which associates with HCV NS5A, four phosphate adapter protein 2 (FAPP2) that functions in the transport of glycosphingolipids, and ceramide transfer protein (CERT) with golgi phosphoprotein 3 (GOLPH3) which are required for virion particle assembly [192,205,218]. In addition to these effector proteins, cation independent mannose-6-phosphate receptor (CIPMR) is another cargo protein of the Retromer complex which is involved in the transport of hydrolases and other proteins from the endosomal compartment to the TGN [218]. Additionally, tail-interacting protein 47 (TIP47) is also known to interact with CIPMR and may be important to the production of infectious HCV particles and the dysregulation of lipid metabolism as it is involved in the biogenesis of lipid droplets through the reorganisation of liposomes [218,219].

So far, it has been described how HCV exploits host metabolism through various interactions with host factors and cellular organelles to enhance its replication during infection. The following section outlines how the innate immune response may also contribute to the dysregulation of lipid metabolism during HCV infection.

1.5. HCV, Innate Immunity, and Lipid Metabolism

HCV utilises lipid droplets during the process of infectious virion assembly in the form of lipoviroparticles (LVPs) [220]. In addition to the mechanisms of lipogenesis that are to be investigated throughout this project, it has been demonstrated that host innate immunity is also associated with the formation of lipid droplets and, therefore, the propagation of HCV [221]. The HCV genome features a pathogen associated molecular pattern (PAMP) within the 3'-untranslated region (UTR), the presence of which is responsible for the induction of interferon (IFN) by the nuclear factor kappa B (NFκB) pathway [222]. The NFκB pathway involves the recruitment of the IκB kinases- alpha and beta (IKK-α, IKK-β) to the regulatory NFκB essential modifier (NEMO, IKKγ) protein to form the IKK complex which results in the phosphorylation and degradation of IκB following its dissociation from the RELA proto-oncogene NFκB subunit (RELA) and p50. Concomitantly, the liberated RELA protein and p50 complex translocate to the nucleus to transcriptionally induce NFκB-stimulated genes [221,222].

In addition to its involvement in the NFκB pathway, Li *et al.*, showed that IKK-α protein has a secondary role in the transcriptional induction of sterol regulatory element binding proteins (SREBPs) [222]. The key determinant underlying the dual antiviral and lipogenic properties of IKK-α depends on the interaction of the HCV genome 3'-UTR with the DExD box helicase, DEAD box polypeptide 3 X-linked (DDX3X) [221,222].

The association of DDX3X with HCV 3'-UTR leads to the phosphorylation of IKK-α and results in its translocation to the nucleus where it may complex with cyclic adenosine monophosphate response element binding protein (CBP) and the histone acetyltransferase, p300 [223]. Upon entry to the nucleus, the IKK-α/CBP/p300 complex transcriptionally induces sterol regulatory element binding protein-1 (SREBP-1) which, in turn, may induce the transcription of various lipogenic genes via association with the sterol regulatory elements (SREs) in their respective promoter regions which is speculated to be the initial step of HCV-induced lipogenesis (**Figure 5**) [221].

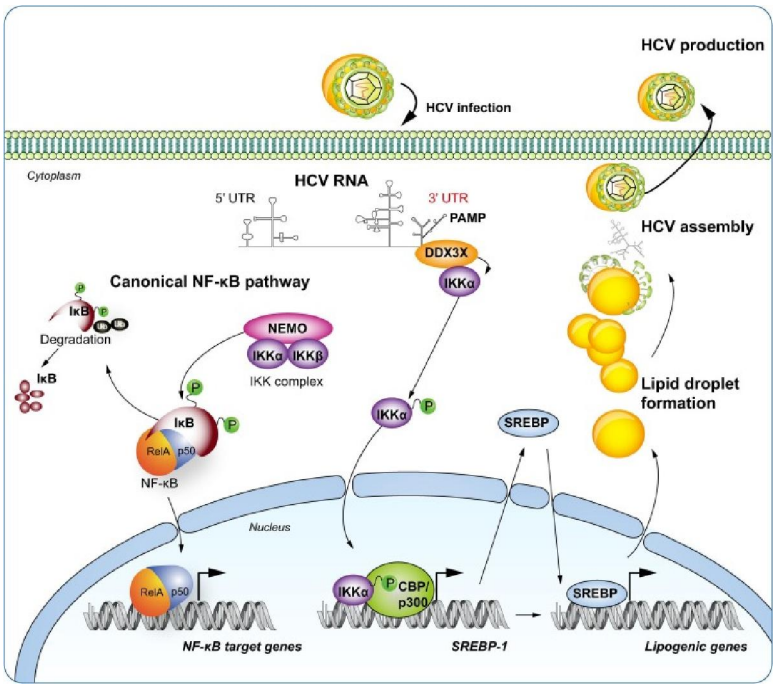


Figure 5 - HCV induced lipogenesis via IKKα

The 3'-UTR of the HCV genome recruits the DExD box helicase DDX3X and the IKKα subunit of the IKK complex that is involved in activation of the NFκB pathway. IKKα is phosphorylated and translocates to the nucleus where it complexes with cyclic adenosine monophosphate (cAMP) response element binding protein (CBP) and p300 to transcriptionally induce sterol regulatory element binding protein-1 (SREBP-1). SREBP proceeds to induce the transcription of various genes associated with the formation of lipid droplets [221].

1.5.1. HCV and Innate Immune Sensing

The innate immune response is activated following the detection of intrinsic features of viruses that are referred to as pathogen associated molecular patterns (PAMPs) e.g. dsRNA and 5'-triphosphates, by pathogen recognition receptors (PRRs) such as retinoic acid inducible gene-like receptors (RLRs) and Toll-like receptors (TLRs) [224,225].

1.5.1.1. HCV and Retinoic Acid Inducible Gene-like Receptors (RLRs)

The main retinoic acid induced gene-like receptor (RLR) that recognises HCV is retinoic acid inducible gene-I (RIG-I), a cytosolic RNA helicase that is comprised of 3 domains namely a carboxy terminus, a DExD/H box, and an amino terminus that features 2 CARD domains [226,227]. RIG-I detects HCV through the triphosphate group and a poly-U/UC region located at the respective 5'- and 3'-ends of the RNA genome [228,229]. Following HCV PAMP recognition by RIG-I, the oligomerisation of RIG-I is promoted along with its translocation from the cytosol to membranes of the mitochondria, peroxisomes, and mitochondrial associated membranes (MAMs) to associate with the mitochondrial antiviral signaling protein (MAVS) adapter protein [225–229]. This activation signal is then transduced via MAVS to activate the NFκB pathway, as well as proteins such as TANK binding kinase 1 (TBK1) and IKB Kinase ε (IKKε) which phosphorylate interferon regulatory factors 3 and 7 (IRF3, IRF7), to induce the transcription of interferon β (IFNβ) and interferon λ (IFNλ) [225].

However, it has been shown that expression of the HCV envelope protein heterodimer correlates with the downregulation of RIG-I [230]. Additionally, this pathway of interferon induction may be disabled by NS3/4A of HCV whereby the viral protease inhibits signal transduction by cleaving MAVS [231–233]. Additionally, the core protein may inhibit the dimerisation and phosphorylation of IRF3 which prevents the transcriptional induction of IFN-β [234].

1.5.1.2. HCV and Toll-like Receptors (TLRs)

Toll-like receptors (TLRs) are also a component of innate immune sensing that recognise intracellular pathogens [225]. TLR3 is the chief TLR that is expressed within hepatocytes and associated Kupffer cells that triggers innate immune responses upon the detection of viral nucleic acids [228,235,236]. The cytosolic C-terminus of TLR3 has Toll-IL1 receptor (TIR) homology that executes downstream signaling upon recognition of dsRNA [237]. Upon recognition of viral nucleic acid by TLR3, a signal is relayed by the TIR domain to the adapter protein Toll/IL-1 receptor domain-containing adaptor inducing IFN-β (TRIF) which activates the type I and III interferon response as well as inducing the expression of various pro-inflammatory cytokines and chemokines through IRF3 and NFκB pathways [237]. This method of innate immune sensing, however, may be circumvented by the envelope glycoproteins of HCV which have been found to coincide with the reduced expression of TLR3 *in vitro* [230].

Furthermore, in addition to MAVS, HCV NS3/4A is also capable of proteolytically cleaving TRIF and inhibiting the induction of the interferon by TLR3 [231–233]. As well as MAVS and TLR3, HCV also triggers another innate immune sensor, protein kinase R (PKR) [225]. PKR is a serine/threonine protein kinase that doubles as a PRR and serves roles in regulating protein synthesis, cell proliferation, programmed cell death, and cell signaling [225]. Upon binding to dsRNA, the kinase domain of PKR is activated and proceeds to phosphorylate the α subunit of eukaryotic translation initiation factor 2 (eIF2α) [238]. The phosphorylation of eIF2α by PKR is a mechanism by which cap-dependent host cell protein synthesis is inhibited, though translation of the HCV genome remains unaffected as synthesis of the viral polyprotein occurs via an internal ribosomal entry site (IRES) (**section 1.2.**) [238]. Moreover, HCV has also evolved to override the shutdown of host protein translation as a region of 8 amino acids in the E2 glycoprotein has been reported to inhibit the kinase activity of PKR [239]. As mentioned in **section 1.2.2.6.**, the interferon sensitivity determining region (ISDR) of HCV NS5A protein can also inhibit induction of the IFN response through interaction with the kinase catalytic domain of PKR [159].

To summarise, HCV may be detected by innate immune sensing mechanisms that involve the recognition of PAMPs i.e. dsRNA, 5'-triphosphates, 3'-poly U/UC tract by molecules such as PKR, RIG-I, and TLR3, respectively. Following PAMP recognition, a signal is transduced to downstream effector proteins, i.e. MAVS and TRIF, to elicit the antiviral effects of the interferon response (**Figure 6**).

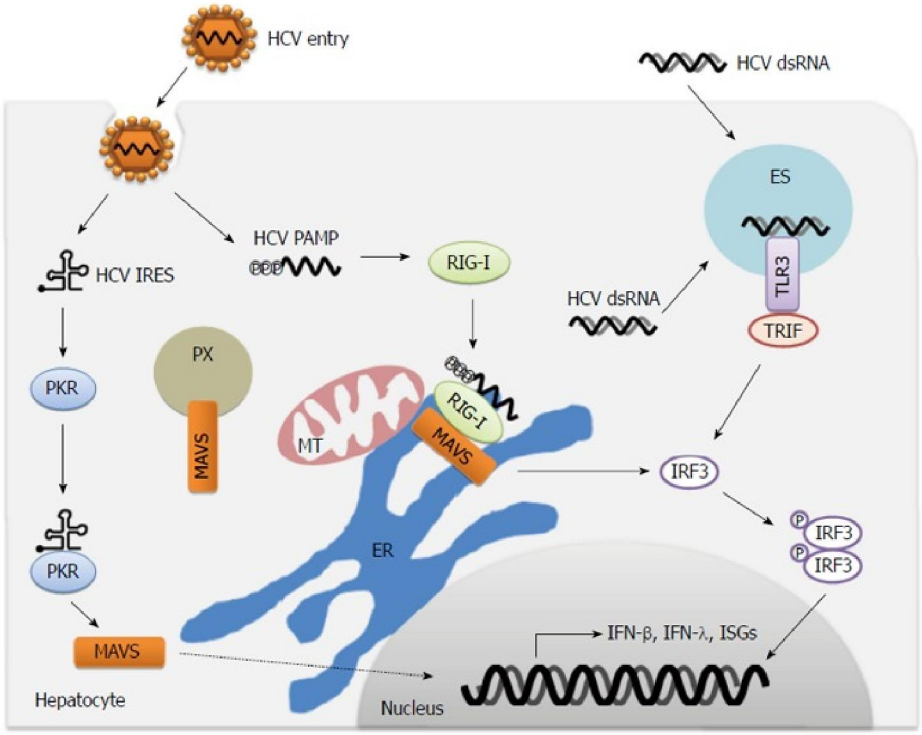


Figure 6 - Innate immune sensing of HCV to induce the interferon response

Intracellular HCV is detected by signaling molecules such as retinoic acid inducible gene I (RIG-I) and Toll/IL-1 receptor domain-containing adaptor inducing IFN-β (TRIF). The dsRNA within the IRES is detected by protein kinase R (PKR) which activates mitochondrial antiviral signaling protein (MAVS) and transduces the activation signal to TANK-binding kinase 1 (TBK1) and/or IKB kinase ε (IKK_ε) to phosphorylate Interferon Regulatory Factor 3 (IRF3) dimers. Phosphorylated IRF3 undergoes nuclear translocation to transcriptionally induce interferon genes (IFN-β, IFN-λ). Alternatively, MAVS may be activated by recognition of the 5'-triphosphate group of the viral genome by RIG-I. Additionally, HCV dsRNA may be detected by toll-like receptor 3 (TLR3) which together with the adapter protein Toll/IL-1 receptor domain-containing adaptor inducing IFN-β (TRIF) may also induce interferon production by IRF3 phosphorylation [(225)].

Given that HCV may induce the innate immune response by the recognition of PAMPs, the virus has evolved several defences to circumvent the antiviral effects of host innate immunity which may contribute to a persistent viral infection [(240)]. Such viral countermeasures involve the interaction of viral proteins with the adapter proteins of PRRs, i.e. MAVS and TRIF (**Figure 7**).

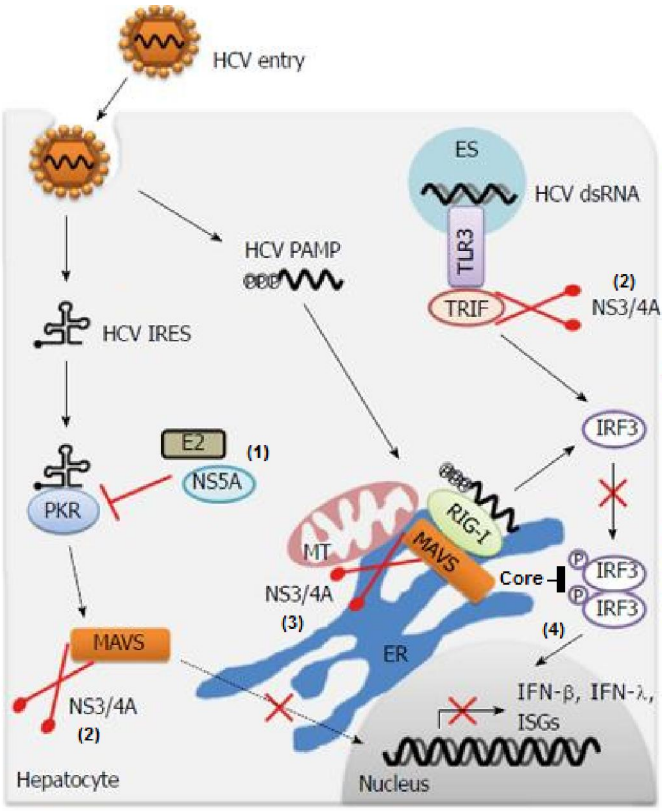


Figure 7 - Mechanisms of Innate Immune Evasion by HCV

(1) The secondary structure of the internal ribosomal entry site (IRES) binds to protein kinase R (PKR) to induce interferon (IFN) via mitochondrial antiviral signaling protein (MAVS) and is inhibited by HCV E2 and NS5A. **(2)** Viral dsRNA is detected by toll-like receptor 3 (TLR3) and the antiviral signal is transduced by the adapter protein TIR-domain-containing adaptor-inducing-interferon β (TRIF) which is also cleaved by HCV NS3/4A. **(3)** The 3'-triphosphate group of the HCV genome may be detected by RIG-I which associates with MAVS that is proteolytically cleaved by the serine/threonine protease activity of HCV NS3/4A. **(4)** The nuclear translocation of Interferon Regulatory Factor 3 via phosphorylation and dimerisation is inhibited by the expression of HCV core protein [(225)].

1.6. Diversity and Geographical distribution of HCV

Studies on the sequence diversity of HCV have shown that the virus has 6 main genotypes (gts) denoted by the number 1 – 6 which may be further categorised into around 67 epidemiological subtypes that are differentiated by lower case letters, e.g. gt2a [241,242]. The distinction between HCV gts is based on their distribution and prevalence around the world in addition to their whole genome sequences [241,243]. HCV gts 1 - 3 are most prevalent in regions such North America, Western Europe, Australasia, and East Asia [243]. Conversely, carriers of HCV in North Africa and the Middle-East are mostly infected with gts 1 and 4 [243]. Genotype 1 and 2 infections are localised to West Africa, and East Africa has a prevalence of gts 1 – 5 [243]. The majority of carriers in East Asia are infected with gt 6 [243]. Additionally, a 7th gt of HCV has been identified in central Africa, although gt 4 it is the most common isolate in the majority of HCV carriers in this region [243,244]. The worldwide distribution and prevalence of the most common HCV genotypes (1 – 6) is shown in **Figure 8**.

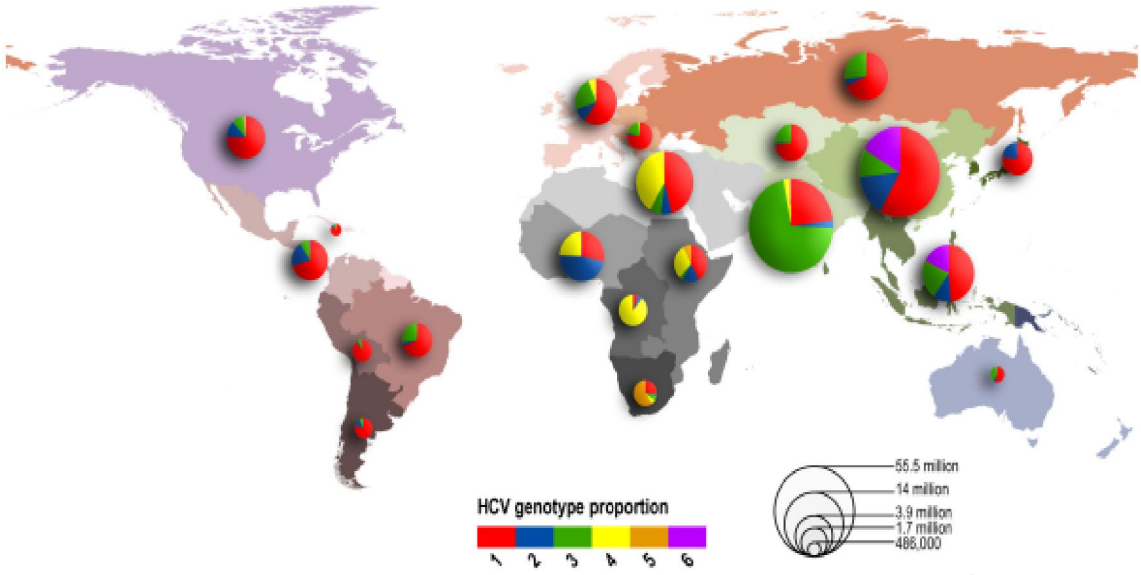


Figure 8 - The worldwide distribution and prevalence of HCV (gt 1- 6)

The worldwide prevalence of HCV is shown by pie-charts corresponding to colour-coded HCV genotypes for each country. Pie-chart size represents scale of infected individuals diagnosed [243].

A retrospective analysis of 1,217 studies concerning the national prevalence of HCV and incorporating estimates from the Global Burden of Disease project (GBD) between 1989 and 2013 reported that gt1 infections account for approximately half (46.2%) of global HCV incidence and gt3 was the second most common strain among the world's population of HCV carriers (30.1%) [243]. The authors of this study identified several trends with respect to global socio-economics. For example, infection with HCV gts 1 and 3 were mapped to countries of a higher national income in contrast to the higher prevalence of gt 4 and 5 infections found in lower income countries [243]. In addition there was an apparent association between HCV genotype and subtype with mode of transmission, e.g. higher incidence of HCV gt3 infection in intravenous drug abusers (IVDAs) [243].

1.6.1. Evolution of HCV Genotypes

With less than 72% sequence homology between genotypes, the variation in the genomic sequences of HCV strains exceed those found in human immunodeficiency virus type I (HIV-1) which is renowned for its high mutation rate (3×10^{-5} mutations per target base pair per replication cycle) [245,246]. The large population of HCV quasispecies within carriers is due to the error-prone activity of the NS5B RNA-dependent RNA polymerase and evolutionary pressure of the host microenvironment, e.g. drug therapy and immune responses [163,247]. Sarwar *et al.*, reported findings that were based on phylogenetic and amino acid sequence analysis of HCV NS4A using protein BLAST [247]. It was suggested that gt1b was likely to be the progenitor to all other HCV genotypes due to the conservation of amino acids in NS4B between geographically and epidemiologically distant strains e.g. Cys22 in gts 1a, 2, 3, and 6, Gln46 and Gln47 in gts 3 – 6, and Val29, Val30, and Val38 in gt 1a, 4, and 3 [247]. The authors of this study concluded that the amino acid sequences within the non-structural genes of HCV genotypes, though highly conserved, may have undergone substitution due to selective pressure by the immune response of the host [247].

However, this supposition assumes that only the immune response of the host is sufficient to promote viral evolution and does not acknowledge the effect of cell tropism, host metabolism and/or the integrity of cellular architecture on the evolution of HCV as HCV RNA isolated in tissue of the central nervous system (CNS) has been shown to have different sequences from hepatic isolates within the same host [13]. Furthermore, the diversity of HCV genotype correlates with distinct changes in host metabolism. Though metabolic complications may be a common feature among HCV genotypes, they may differ in their manifestations i.e. gts 1 and 4 are more associated with insulin resistance (IR) independent of steatosis whereas gt 3 may be directly steatogenic without incidence of IR [248–250]. These findings may represent how secondary complications may develop as a function of infecting HCV genotype.

Thus, in order to understand how metabolic disease pathologies may be brought about during HCV infection, the following section will describe glucose metabolism in homeostasis.

1.7. Homeostatic Glucose Metabolism

The key stages of glucose metabolism may be sub-divided into 3 main categories namely glucose uptake, glucose storage, and glucose metabolism i.e. glycolysis and the tricarboxylic (TCA) acid cycle. However, the metabolic pathologies of insulin resistance (IR), type 2 diabetes mellitus (T2DM), and hepatic steatosis that are associated with HCV infection may occur largely due to the improper metabolism of glucose and the production of substrates that are used for *de novo lipogenesis* (DNL).

1.7.1. Glucose Uptake

In the liver, glucose is primarily taken up cells from the serum by the membranous glucose transporter, GLUT2 [(251)]. GLUT2, along with the enzyme glucokinase (GCK) comprise the "glucose sensor" within cells, has a 2 - 3-fold lower affinity for glucose compared to GLUT1 but a higher capacity for glucose transport [(252,253)]. Furthermore, GLUT2 has been observed to be downregulated in HCV infection and may therefore be a contributing factor to the T2DM-like pathology that is associated with HCV [(254)].

1.7.2. Glucose Storage

In the event of intracellular glucose concentrations exceeding that sufficiently required to produce energy within hepatocytes, surplus glucose may be stored as a polymer in the form of glycogen, a process that is regulated by hormones including insulin, adrenaline, and glucagon [255]. This ensures that glucose may be available for ATP production during periods of fasting [253]. Following the phosphorylation of glucose to produce glucose-6-phosphate (G6P) and its conversion to glucose-1-phosphate (G1P) by the enzymes GCK and phosphoglucomutase (PGM), respectively, a short chain (3-4 residues) is formed through the covalent α-1,4-linkage between G1P monomers catalysed by glycogenin (GN) [255–257]. Subsequent polymerisation occurs by the enzyme glycogen synthase (GS) following its activation by glycogen synthase kinase 3 (GSK3), which is a downstream target of insulin-mediated Akt/PI3K signaling (**section 1.8.1**) [253,255,258]. Additionally, GS can be activated by G6P, thereby promoting Glycogenesis while protein kinase A (PKA) and 5' AMP-activated protein kinase (AMPK) are capable of inactivating GS through phosphorylation of Ser residues, though AMPK is reportedly inhibited in HCV infection [259–261]. Furthermore, GSK3 is also involved in lipid metabolism due to its targeting of SREBP-1 for phosphorylation during instances of cell senescence and mitochondrial dysfunction [262].

After short chains comprised of G1P subunits have been synthesised, a branching enzyme (BE) continues the process of glycogen polymerisation by catalysing the formation of α-1,6-linkages between chains of 11 – 14 glucose residues (**Figure 9**) [255,258].

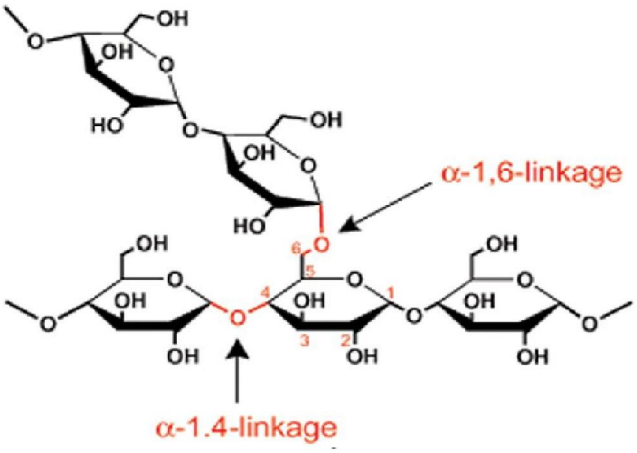


Figure 9 - The Chemical Structure of a Glycogen Short Chain

Glycogen short-chains are composed of a pentameric structure of 5 glucose monomer subunits involving a dimer covalently linked by α-1, 4-linkage, which branches to a trimer by an α-1,6-linkage. Carbon positions, and linkages therein are shown in orange [255].

During times of fasting, glycogen polymers are broken down by a process called glycogenolysis [253]. Glycogenolysis is catalysed by the enzyme glycogen phosphorylase (PYGL), which cleaves the α-1,4-glucosidic bonds of between glucose monomers and phosphorylates them to produce glucose-1-phosphate (G1P) [263]. A debranching enzyme (DBE), amylo-alpha-1,6-glucosidase, cleaves the α-1, 6-linkage between glycogen short chains [264].

The G1P residues yielded from the catabolism of glycogen are primed for metabolism following conversion to G6P by phosphoglucomutase (PGM) [257].

The metabolic pathways of glycogen i.e. glycogenesis and glycogenolysis, are shown in **Figure 10**.

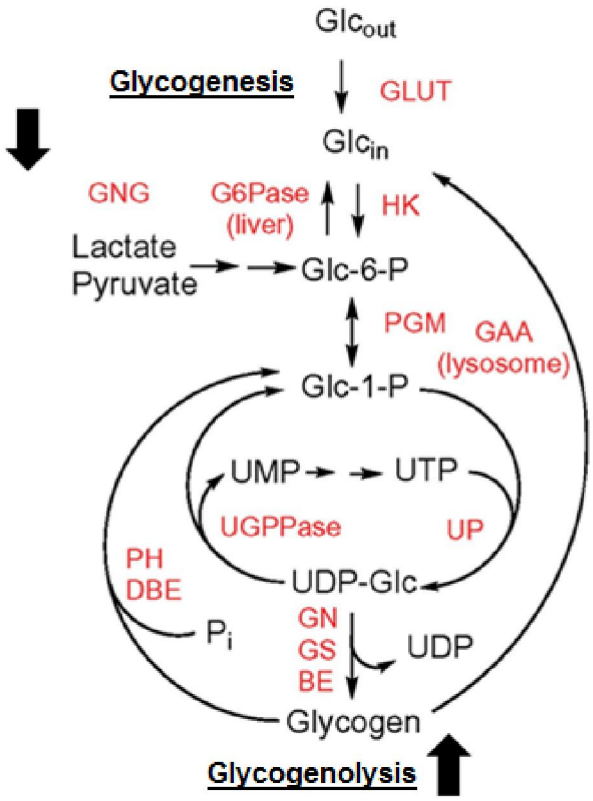


Figure 10 - Glycogen Metabolic Pathways

Extracellular glucose (Glc_{out}) is taken up by cells (Glc_{in}) via glucose transporters (GLUT) and is converted to its metabolically active form, glucose-6-phosphate (Glc-6-P) by hexokinase (HK). **Glycogenesis** Glycogen is synthesised from glucose-6-phosphate (Glc-6-P) that is produced from intracellular glucose (Glc_{in}) or obtained from lactate/pyruvate following gluconeogenesis (GNG) and the action of glucose-6-phosphatase (G6Pase). Glc-6-P is converted to Glc-1-P in a reversible reaction by phosphoglucomutase (PGM). Uridine triphosphate (UTP) is further catalysed into uridine diphosphate-glucose (UDP-Glc) by the enzyme uridine phosphorylase (UP). UDP-Glc may be recycled into uridine monophosphate (UMP) by UDP-glucose pyrophosphorylase (UGGPase) or polymerised into glycogen by the sequential action of glycogenin (GN), glycogen synthase (GS), and branching enzyme (BE). **Glycogenolysis** Glycogen may be broken down into glucose monomers by the action of lysosomal α-glucosidase (GAA) or into Glc-1-P through the enzymatic activities of debranching enzyme (DBE) and glycogen phosphorylase (PH) [(255)].

1.7.3. Glucose Metabolism

As summarised in the previous sections, glucose can be rendered intrahepatic either through the uptake from serum or via the catalysis of glycogen stores which is then metabolised to produce adenosine triphosphate (ATP) in order to satisfy the energetic requirements of various cellular functions. The metabolism of glucose may be described as a binary process involving 2 main processes, namely glycolysis and the tricarboxylic acid (TCA) cycle that are bridged by the process of oxidative phosphorylation. In mammalian cells, glucose is initially metabolised anaerobically in the cytosol by a cascade of biochemical reactions that are collectively referred to as glycolysis which involve the phosphorylation and oxidation of glucose-6-phosphate (G6P) to produce pyruvate via a series of intermediates [253].

1.7.3.1. Glycolysis

The first process of glucose metabolism, glycolysis, begins with the phosphorylation of monomeric glucose to its metabolically active form G6P by the rate-limiting enzyme glucokinase (GCK), a hexokinase that associates with the outer mitochondrial membrane (OMM) via its N-terminal domain [256,259]. Glucokinase is not inhibited by high G6P concentrations, and facilitates the storage of glucose as polymeric glycogen during fasting conditions [256]. Under these conditions, the enzyme exists in an inactive state and is bound to glucokinase regulatory protein (GKRP) within the nucleus [265,266].

However, it has been found that a combination of elevated glucose concentration resulting from cellular uptake, and not EGP, with insulin signaling may induce the dissociation of this complex and the cytosolic translocation of GCK [265–267]. The interplay between glucose- and lipid metabolism in the liver is further highlighted by GCK as it may be transcriptionally induced by pro-lipogenic transcription factors such as hepatocyte nuclear factor-4 (HNF-4) and sterol regulatory element binding protein-1c (SREBP-1c) via HNF-4 binding elements (HBEs) and sterol regulatory elements (SREs) in the GCK promoter [268–270].

However, the production of G6P by GCK results in the displacement of hexokinases from the outer mitochondrial membrane (OMM) which induces the transcription of enzymes related to glycolysis to promote further metabolism [271]. This has been suggested to occur via the spatial association between hexokinases and a transcription factor that is also resident to the OMM termed Max like protein (Mlx) in which displacement of the former causes the latter to complex with Max like interacting protein (MlxIP) [271]. The formation of this complex leads to the nuclear translocation of Mlx where it may transcriptionally induce genes encoding enzymes such as hexokinase II (HXK2), phosphofructokinase (PFK), glyceraldehyde-3-phosphate (GAPDH), and pyruvate kinase (PK) [271]. In addition, it has also been found that the transcription of thioredoxin interacting protein (TXNIP), a protein which strongly correlates with dysregulated lipid metabolism, is dependent on both glucose and Mlx activity [214,215,271].

The anaerobic process of glycolysis ultimately yields 2 molecules of adenosine triphosphate (ATP) and 2 molecules of the reduced form of nicotinamide adenine dinucleotide (NADH) per molecule of glucose (**Figure 11**) [253].

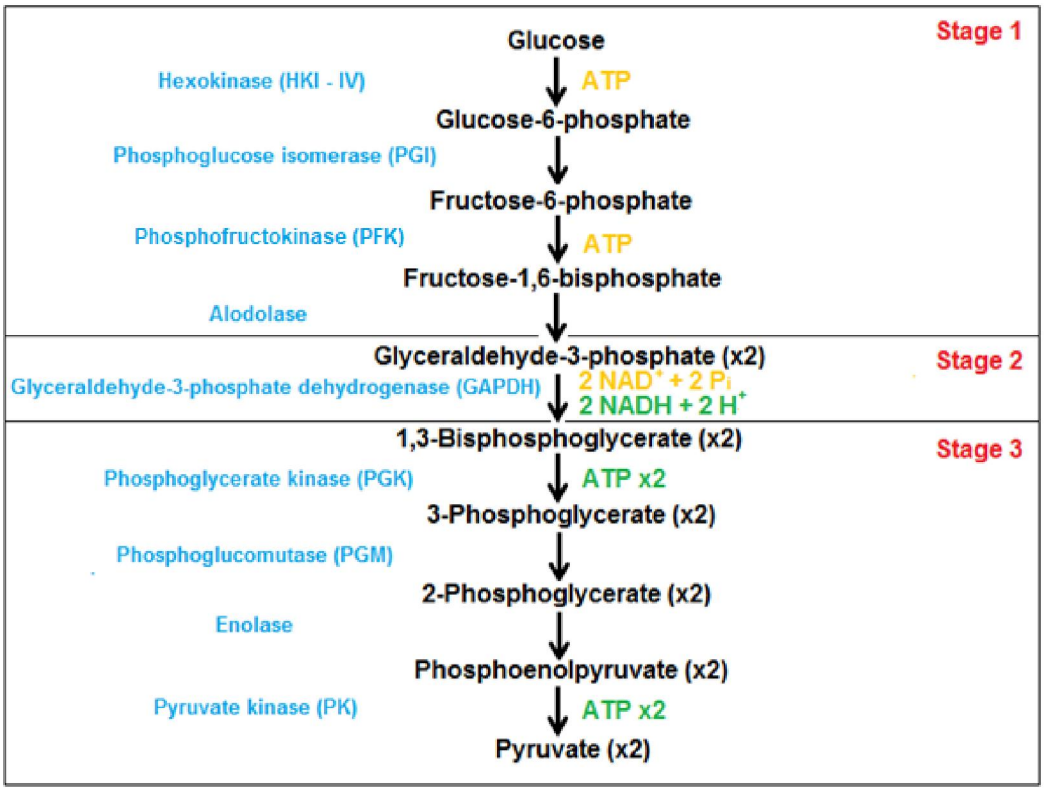


Figure 11 - The Glycolytic Pathway

Metabolites are shown in black, co-factors in yellow, enzymes in blue, and products in green. **Stage 1:** Intracellular glucose is phosphorylated to form its metabolically active form, Glucose-6-Phosphate (G6P) and irreversibly converted to fructose-1,6,-bisphosphate at the cost of 2 ATP molecules **Stage 2:** Fructose-1,6-bisphosphate is converted to glyceraldehyde-3-phosphate. **Stage 3:** The net gain of ATP, per molecule of glucose, is 2 molecules [272].

Alternatively, G6P may be metabolised by the pentose phosphate pathway (PPP) in which nicotinamide adenine dinucleotide phosphate (NADPH) and the phosphorylated pentose sugar, ribose-5-phosphate, are generated for the respective synthesis of fatty acids and ribonucleotides as seen during the metabolic shift in tumour cells and cancers e.g. hepatocellular carcinoma (HCC) [273–275]. However, HCV is known to upregulate glycolytic gene expression e.g. Hexokinase 1 (HXK1), via hypoxia-inducible factor 1α (HIF1α) which may explain why HCV replication is enhanced under hypoxic conditions and implies that the nonoxidative process of glycolysis is favoured by the host cell to metabolise glucose in response to virus infection [45,276,277].

The range of biochemical processes which are involved in the metabolism of glucose, and particularly the interplay between the TCA cycle (**section 1.7.3.2.**) and DNL are shown in **Figure 12** [253].

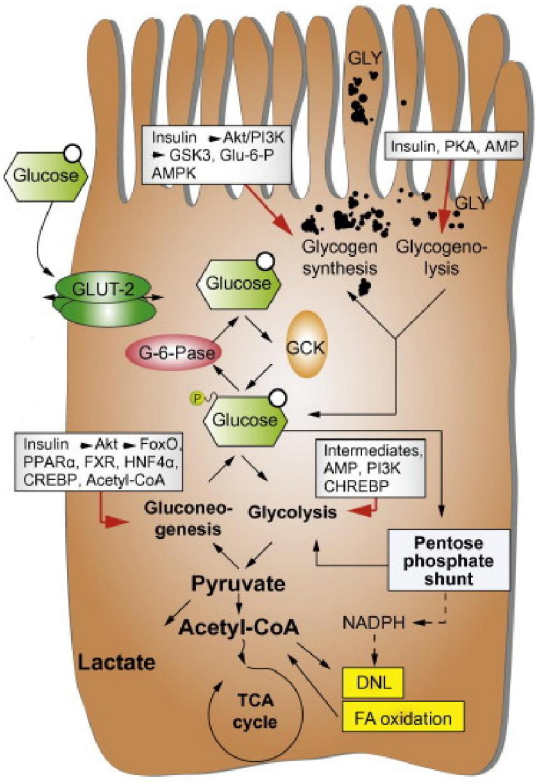


Figure 12 - The Network of Glucose Metabolic Pathways

Intracellular glucose occurs either through uptake from the extra milieu by the glucose transporter, GLUT-2, glycogenolysis that results from glycogen phosphorylase activity stimulated by insulin signaling, protein kinase A PKA, and/or adenosine monophosphate (AMP), or gluconeogenesis that results from insulin and downstream Akt signaling and induction by transcription factors; Forkhead box (FOXO) proteins, peroxisome proliferator activated receptor α (PPARα), carbohydrate response element bind protein (CREBP), nuclear receptors such as farnesoid X receptor (FXR) and hepatocyte nuclear factor 4α (HNF4α), or elevated [acetyl-CoA] using amino acids or pyruvate. Glucose may be used for glycogen (GLY) synthesis as initiated through insulin and signal transduction through Akt/PI3K signaling. Glucose is metabolised directly by glycolysis or indirectly via the pentose phosphate shunt. In glycolysis, glucose-6-phosphate is produced from the phosphorylation of glucose by the hexokinase, glucokinase (GCK) which is further metabolised to produce ATP. Pyruvate resulting from glycolysis is catalysed into either lactate, or acetyl-CoA which may also be produced from fatty acid (FA) oxidation. Acetyl-CoA is metabolised to generate energy or alternatively used in *de novo* lipogenesis (DNL) [253].

The pyruvate yielded from the glycolytic metabolism of glucose undergoes oxidative decarboxylation by pyruvate dehydrogenase (PDH) to form acetyl-CoA which may be further metabolised to produce ATP by the tricarboxylic acid (TCA) cycle in the mitochondrial matrix or, alternatively, stored as fat via *de novo* lipogenesis (DNL) [278].

1.7.3.2. The Tricarboxylic Acid (TCA) cycle

The overall purpose of the tricarboxylic acid (TCA) cycle is to support the energy produced in the metabolism of glucose by glycolysis through the conversion of pyruvate to carbon dioxide (CO_2) and water through a series of intermediates (**Figure 13**) [279].

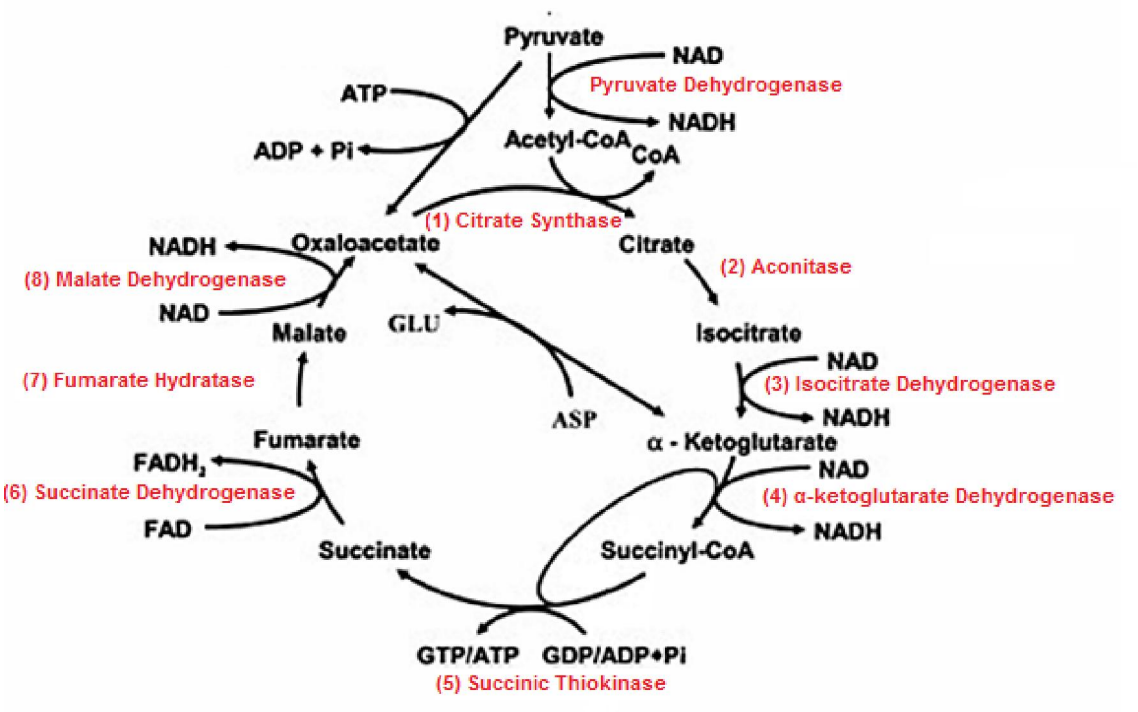


Figure 13 - The Tricarboxylic Acid (TCA) Cycle

Enzymes involved in the TCA cycle are shown in red. Pyruvate from glycolysis is oxidised by nicotinamide (NAD+) to acetyl-CoA which is converted to citrate and isocitrate. The catalysis of isocitrate to succinyl CoA via the production of intermediary α-ketoglutarate (AKG) is intensive on NAD+ supply. Alternatively, Asparagine (Asp) may be metabolised into Glutamate (Glu) which is broken down to produce pools of α-ketoglutarate (AKG) for oxaloacetate production. GTP or ATP is generated by the phosphorylation of nucleoside diphosphates during the catalysis of succinyl-CoA to succinate. The net ATP produced by this cycle is 30 molecules per molecule of glucose. Enzymes catalysing each stage are shown in red [279–281].

The TCA cycle constitutes the second series of reactions involved in the metabolism of glucose and occurs within the matrix of the mitochondria whereby the product from glycolysis, pyruvate, is further metabolised to yield ATP through the oxidation of Acetyl-CoA to CO_2 [279,281].

This pathway may be considered pivotal to cell metabolism and energy production as, together with the electron transport chain which includes the oxidative phosphorylation of the reduced forms of nicotinamide adenine dinucleotide (NADH) and flavin adenine dinucleotide ($FADH_2$), the majority of adenosine triphosphate (ATP) is produced (32 - 34 molecules of ATP per molecule of glucose) and approximately 2/3 of cellular oxygen is consumed to generate approximately 2/3 of systemic energy [279,282]. The TCA cycle is also capable of aerobically metabolising other substrates besides carbohydrates as a means to produce energy and maintain the pool size of carbon compounds when glucose concentrations are low [281,283]. Additional substrates that are also processed by the TCA cycle include fatty acids (FAs) which are oxidised to produce acetyl-CoA, NADH, FADH2, and ketone bodies resulting from the process of β-oxidation prior to TCA cycle entry, and amino acids including leucine (Leu), isoleucine (Ile), tyrosine (Tyr), phenylalanine (Phe), and tryptophan (Trp) [279,283,284]. Further to the catabolism of metabolites, the TCA cycle is also amphibolic in that it may synthesise glucose using amino acids via gluconeogenesis or the reverse TCA (rTCA) cycle, carry out the transamination and deamination of amino acids, and synthesise FAs [279,281].

To date, there are few disease states that have been linked to TCA cycle defects. Those that are known have been attributed to heritable genetic mutations e.g. Leigh's syndrome, a neurological disorder that has been mapped to mutations in the gene for the E1α subunit of the pyruvate dehydrogenase complex (PDHc) and to gene-deletions in the E3 binding protein (E3BP) [285]. Additionally, metabolic disorders can arise from deficient or inactive enzymes that are key to the TCA cycle e.g. α-ketoglutarate dehydrogenase complex (KGDHC) and succinate dehydrogenase (SDH), which contribute to Friedrich's ataxia and respiratory chain deficiency, respectively [286,287].

The TCA cycle is comprised of 8 stages that begins with the decarboxylation of pyruvate to produce the two-carbon molecule, acetyl-CoA which is condensed with oxaloacetate by citrate synthetase to produce the six-carbon intermediate, citrate [288,289]. Citrate is then dehydrated to form *cis*-aconitate and converted to isocitrate by an enzyme termed aconitase [290]. Isocitrate is decarboxylated to produce α-ketoglutarate (AKG) by the enzyme isocitrate dehydrogenase in a catalytic step that also involves the reduction of nicotinamide adenine dinucleotide (NAD^+) to NADH2 and the production of CO_2 [279]. α-ketoglutarate (AKG) is decarboxylated by the AKG dehydrogenation complex to produce succinyl-CoA which, through the action of succinate thiokinase (also referred to as succinyl CoA synthetase), is subsequently converted to succinate whilst generating ATP and GTP from their respective nucleoside diphosphates [291,292].

Succinate undergoes dehydration by the enzyme succinate dehydrogenase to form fumarate in a step that also results in the simultaneous reduction of FAD^+ to FADH2 [279]. The hydration of fumarate by fumarate hydratase (fumarase) leads to the formation of malate which is then oxidised by malate dehydrogenase to produce oxaloacetate in a reaction that also reduces NAD^+ to NADH2 [293,294]. Following entry to the electron transport chain (ETC), each NADH and FADH2 molecule produced per round of the TCA cycle is the equivalent of a further 3- and 2 molecules of ATP, respectively [279].

Repeated rounds of the TCA cycle are induced by the reaction between oxaloacetate and acetyl-CoA [279]. Overall, the net gain of ATP yielded by the combination of glycolysis, TCA cycle, and ETC in the metabolism of molecular glucose is 36 molecules [279].

1.7.3.3. Regulation of The TCA Cycle

Under physiological conditions, the TCA cycle may be affected by changes in intramitochondrial calcium ion concentration [Ca^{2+}] that may arise from endoplasmic reticulum (ER) stress and possibly lead to the induction of apoptosis via the mitochondria-associated pathway [295,296].

Following ER stress, Ca^{2+} ions are released from storage in the ER lumen through inositol-1,4,5-triphosphate receptor (IP3R) channels, which migrate across the cytosol to the mitochondria where they may be taken up by voltage dependent anion channels (VDACs) that are present on the outer mitochondrial membrane (OMM) [43,295,297]. VDACs, along with adenine nucleotide translocator (ANT) and cyclophilin D (CypD) that associates with a mitochondrial phosphate carrier (PiC), comprise the mitochondrial permeability transition pore (mPTP) [295,298]. Depending on the membrane potential generated by protons from the respiratory chain, VDACs can switch between "open" and "closed" conformations which give rise to states of either high- or low conductance that are selective for anions and cations, respectively [299,300]. Closure of VDACs renders them permissive for an increase in Ca^{2+} ion influx and impairs ATP efflux from the mitochondria which would otherwise occur in an "open" state [301,302].

Furthermore, excessive Ca^{2+} concentrations at the mitochondria may also induce dilation of mPTP and depolarisation of mitochondrial membranes which is characterised by a loss in mitochondrial membrane potential ($mt\Delta\Psi m$) [296]. Collectively, these hallmarks of mitochondrial dysfunction are indicative of the induction of apoptosis by the mitochondria-associated pathway [296,303].

Following the VDAC-mediated uptake of calcium by the mitochondria, Ca^{2+} ions in the intermembrane space (IMS) between the outer- and inner mitochondrial membranes (IMM) may enter the mitochondrial matrix as a function of osmosis by the action of the mitochondrial calcium uniporter (MCU), which is regulated by mitochondrial calcium uptake 1 (MICU1) protein, and may ultimately affect TCA cycle rate [299,304,305].

The energetic output of the TCA cycle, which relies on an abundance of acetyl co-A as a substrate, may also be affected by the concentration of intramitochondrial calcium through the stimulation of key enzyme activity i.e. pyruvate dehydrogenase phosphate phosphatase, NAD-isocitrate dehydrogenase, and α-ketoglutarate dehydrogenase (also referred to as oxoglutarate dehydrogenase (OGDH)) in the mitochondrial matrix [305–309].

Wan *et al*., investigated the effect of Ca^{2+} ions localised to the mitochondrial matrix on the concentrations of these enzymes and their substrates and found that AKG undergoes a 135% increase in ADP-stimulated oxidation under conditions of elevated [Ca^{2+}] [305].

The authors of this study also found that under conditions of depleted ADP and increased AKG, the cofactor NAD underwent increased reduction compared to controls, thereby contributing to ATP synthesis by the electron transport chain [305].

Interestingly, concentrations of pyruvate dehydrogenase (PDH), an enzyme that is responsible for producing acetyl-CoA as the key substrate for TCA cycling, was not affected by Ca^{2+} concentration. However, under conditions of pyruvate depletion and excess AKG, activity of PDH was reduced to 20% as an effect of substrate saturation though optimal activity was restored following an increase in mitochondrial [Ca^{2+}] [305]. The mechanism behind this finding was described by McCormack in an earlier study that found an increase in mitochondrial [Ca^{2+}] gave rise to a 7-fold increase in the activation of the pyruvate dehydrogenase complex (PDHc) by its dephosphorylation through the action of pyruvate dehydrogenase phosphatase [305,306].

These studies demonstrate the potential of intramitochondrial [Ca^{2+}] to stimulate the activity of TCA cycle enzymes. However, it has also been speculated that elevations in mitochondrial calcium may also result in an increased production of mitochondrial reactive oxygen species (ROS) as a consequence of mitochondrial dysfunction (**Figure 14**) [310,311].

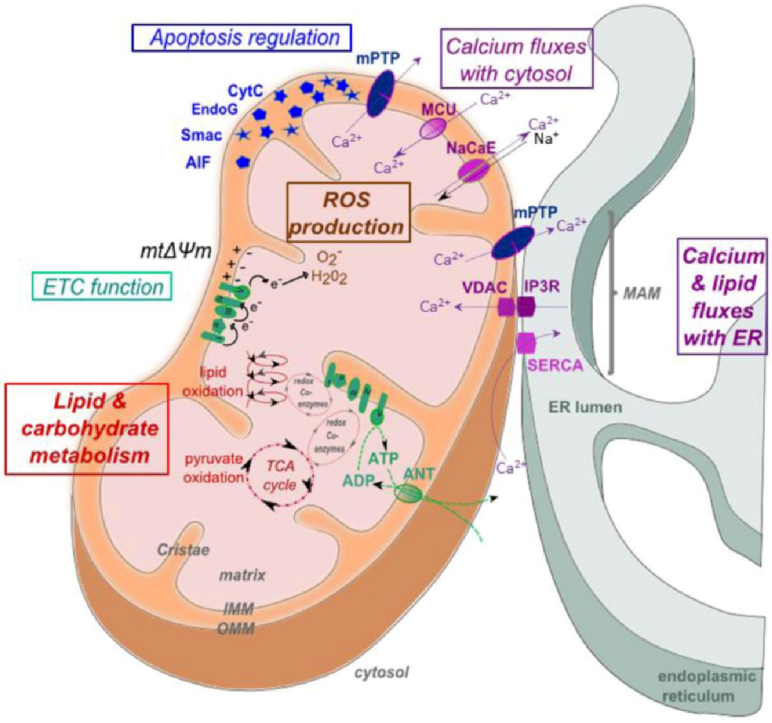


Figure 14 - Mitochondrial Ca^{2+} Import from the Endoplasmic Reticulum

Calcium ions (Ca^{2+}) enter the endoplasmic reticulum (ER) lumen through the sarco/endoplasmic reticulum Ca^{2+} ATPase (SERCA) pumps. Ca^{2+} ions migrate out of the ER through the Inositol-1,4,5-triphosphate receptor (IP3R) channels and are funnelled to the mitochondria across the cytosol by mitochondria associated membranes (MAMs). Depolarisation of the outer mitochondrial membrane (OMM) occurs and the mitochondrial membrane potential (mtΔΨm) is reduced. Mitochondrial pore transition protein (mPTP) increases, and OMM becomes permeable to Ca^{2+} ions. Ca^{2+} ions enter the mitochondrial intermembrane space between the outer- (OMM) and inner mitochondrial membranes (IMM) by the oscillation of voltage dependent anion channels (VDACs) or through the synergistic action of the sodium-calcium exchanger (NaCaE). Intramitochondrial Ca^{2+} may enter the site of the tricarboxylic acid (TCA) cycle, the mitochondrial matrix, through the action of the mitochondrial calcium uniporter (MCU) [127]. Mitochondrial dysfunction is induced by elevated intramitochondrial Ca^{2+} ions and disturbs the TCA cycle and thus the metabolism of carbohydrates and lipids. The incidence of mitochondrial dysfunction results in oxidative stress and the increased production of reactive oxygen species (ROS), e.g. Hydrogen Peroxide (H_2O_2) and singlet oxygen (O^{2-}), and also leads to the induction of the mitochondrial associated pathway of apoptosis which is characterised by secretion of cytochrome C (CytC), endonuclease G (EndoG), second mitochondria-derived activator of caspase (Smac), and apoptosis inducing factor (AIF) [311].

It is possible that calcium ion overload and ROS production may be induced through the intracellular activity of HCV proteins e.g. core, NS4B, NS5A, which in addition to direct physical interactions of viral proteins with the mitochondria, e.g. p7, NS4A, may result in mitochondrial dysfunction [40,74,152,312–314].

Mitochondrial dysfunction is a phenomenon that is characterised by increased mitochondrial [Ca^{2+}], decreased mitochondrial membrane potential ($mt\Delta\Psi_m$) and ATP production, as well as increased ROS production [315]. Furthermore, mitochondrial calcium ion flux may contribute to the imbalance of additional processes that regulate the rate of the TCA cycle, namely anaplerosis and cataplerosis, whereby mitochondrial anions are replenished and removed, respectively [281,316]. Both anaplerosis and cataplerosis regulate the production of intermediates that impair TCA cycle function and ATP production, i.e. four-carbon and five-carbon compounds derived from the metabolism of amino acids that cannot undergo full oxidation [281]. Anaplerosis involves the replacement of anions in the form of α-ketoglutarate (AKG), that is produced from the metabolism of amino acids such as glutamine (Gln), in order to sustain TCA cycle flux and balance the anions that are removed as citrate by cataplerosis [281,317]. Furthermore, the inter-relationship between glucose and lipid metabolism can also be demonstrated by the cataplerosis of citrate where it is translocated from the mitochondria to the cytosol, converted to acetyl-CoA by ATP-citrate lyase (ACLY), and serves as a precursor to fatty acid synthesis (**Figure 15**) [281,318,319].

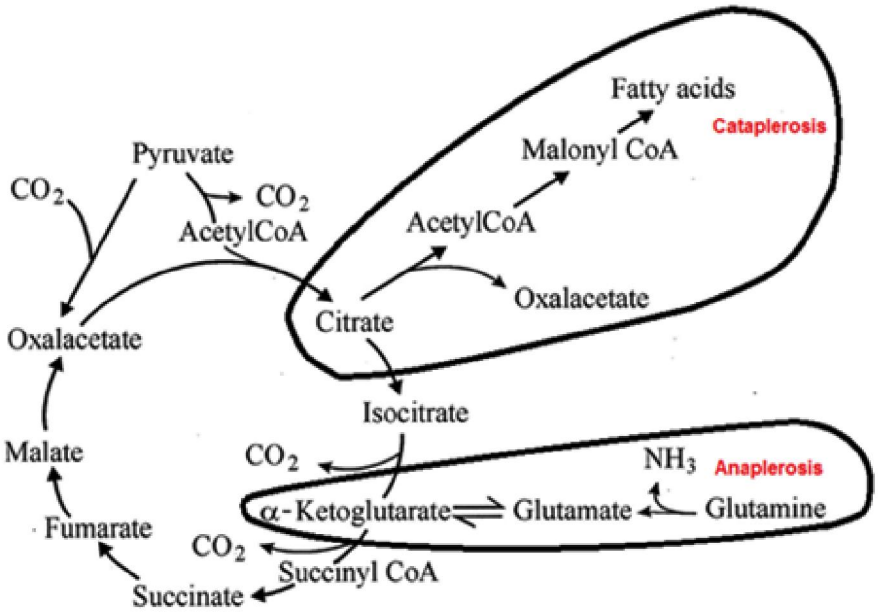


Figure 15 - Anaplerosis and Cataplerosis in the Tricarboxylic Acid (TCA) Cycle

Cataplerosis: The removal of the 6-carbon intermediate, Citrate, from the TCA cycle and the mitochondria for fatty acid synthesis and gluconeogenesis. **Anaplerosis:** The replenishment of the 4-carbon intermediate, α-ketoglutarate (AKG) from the deamination of glutamine that maintains TCA cycle function and ATP production [281].

In conclusion, the metabolism of glucose occurs in two stages namely glycolysis and the tricarboxylic acid (TCA) cycle to generate energy in the form of ATP. However, it appears that host lipid metabolism may occur as a consequence of an imbalance of anaplerosis and cataplerosis which serve to maintain TCA cycle flux. Glucose homeostasis may be compromised during HCV infection and give rise to the manifestation of secondary complications such as insulin resistance (IR), type II diabetes mellitus (T2DM), and hepatic steatosis. The pathogenesis of each condition during HCV infection is described as follows.

1.8. Metabolic Disorders associated with HCV infection

Chronic HCV infection may bring about pathologies that disturb host metabolism such as visceral obesity, low high-density lipoprotein (HDL) cholesterol, hyperglycaemia, hyperlipidaemia, and hypertension [320]. A clinical presentation of 3 of these disorders is termed metabolic syndrome (MS), a condition that is highly associated with HCV gt3 infection, disturbed lipid and glucose homeostasis, poor treatment outcome in chronic hepatitis C (CHC) patients, and associated with the development of insulin resistance (IR) [321,322]. Some reports suggest that HCV is an aetiological agent of IR, T2DM-like pathology, and MS e.g. there is a heightened incidence of T2DM occurring in infected recipients of liver transplants [323]. Conversely, a reduced incidence of T2DM also correlates with the attainment of a sustained virological response (SVR) following antiviral treatment [324]. The metabolic complications that are often associated with CHC infection, i.e. insulin resistance (IR), type 2 diabetes mellitus (T2DM), and hepatic steatosis are outlined in the following sub-sections.

1.8.1. Insulin Resistance (IR)

Insulin resistance (IR) is a manifestation that is characterised by the increased production of endogenous glucose from glycogen stores in the liver together with a decreased uptake of glucose by skeletal muscle cells, which is thought to arise from both defective insulin signalling and the compromised metabolism of glucose [325].

Under physiological conditions, upon binding of insulin by its cellular receptor, a signal is transduced by one of two functionally distinct insulin receptor substrate proteins, IRS-1 and IRS-2, that are concerned with the regulation of glucose synthesis and metabolism [325]. Insulin signaling is transduced by Tyr phosphorylation of insulin receptor substrates by protein kinases such as phosphatidylinositol-3-kinase (PI3K) and protein kinase B (Akt) that leads to glucose uptake, inhibition of gluconeogenesis, and glycogen synthesis [326,327]. Additionally, IRSs may be phosphorylated at Ser residues by other kinases e.g. protein kinase C (PKC), mTOR substrate p70 ribosomal S6 Kinase (S6K1), and c-jun N-terminal kinases (JNKs) which counteract Tyr phosphorylation and block PI3K/Akt-mediated signal transduction [327–330]. This may explain why concentrations of glucose are elevated in HCV-infected liver cells.

Additionally, PI3K may be indirectly affected by the action of protein tyrosine phosphatases (PTPs) and phosphatidylinositol phosphate phosphatases (PIPs) e.g. protein-tyrosine phosphatase 1b (PTP1b) and SH2-containing 5'-inositol phosphatase (SHIP2), respectively, which may be involved in T2DM and underlying insulin resistance on account of their ability to negatively regulate insulin signaling by dephosphorylating Tyr residues on IRSs and activated insulin receptors [331–333]. An example of this that has been found to underlie IR in HCV and involves the overexpression of protein phosphatase 2a (PP2A) as a response to ER stress and inhibition of the insulin signalling cascade through the dephosphorylation of Akt [334].

In addition, suppressors of cytokine signalling (SOCS) proteins such as SOCS1 and SOCS3 feature elongin BC-binding motifs that interact with the E3 ubiquitin ligase complex and are capable of disrupting insulin signaling by mediating the ubiquitin-dependent proteasomal degradation of IRS1 and IRS2 [(335)]. This particular mechanism of insulin-signaling blockade was found to be caused by the core protein of HCV *in vitro* whereby SOCS3 was upregulated and the expression of insulin receptor substrates 1 and 2 was reduced by proteasomal degradation [(336)]. The expression of HCV core may also lead to the production of ROS and an increased mitochondrial uptake of calcium which inhibits the initial step of mitochondrial respiration by electron transport chain complex I (NADH ubiquinone oxidoreductase) [(337–339)]. Furthermore, HCV core may be subject to ubiquitin-independent proteasomal degradation via the action of Proteasome Activator 28-γ (PA28γ) which has been linked to the development of IR and steatosis in transgenic mice [(340,341)].

1.8.2. Type 2 Diabetes Mellitus (T2DM)

The incidence of glucose intolerance may induce liver cells to undergo a diabetic state, referred to as type 2 diabetes mellitus (T2DM) which is characteristic of all liver diseases [(342)]. The mechanisms underlying this condition are described as follows.

1.8.2.1. Insulin Signaling in T2DM

T2DM in HCV patients has previously been attributed to defects in insulin signaling where the phosphorylation of IRS-1 Tyr residues by PI3K have been reported to be 2-fold lower in HCV carriers compared to controls [327]. An explanation for this has been proposed by Shinatni *et al*., based on data produced by examining insulin signaling in murine models [343]. The group suggest that HCV impairs the metabolism of glucose by mechanisms involving innate immunity as they observed that expression of HCV core protein in transgenic mice was capable of inducing a diabetic state, marked by high serum insulin and plasma glucose [343]. These characteristics of disordered glucose metabolism progressed to overt diabetes when a high-fat diet was fed to these animals [343]. The authors found that high expression of tumour necrosis factor α (TNFα) was responsible for the induction of glucose intolerance due to defective insulin signaling by suppressed Tyr phosphorylation of IRS-1 as the symptoms of T2DM in this model were alleviated through the administration of anti-TNFα antibodies [343].

In addition to the involvement of SOCS1 and SOCS3-mediated blockade of insulin signaling as mentioned in **section 1.8.1.**, HCV core from a gt3a isolate was found to bring about the degradation of IRS-1 by modulating SOCS7 expression via the nuclear receptor peroxisome proliferator activated receptor-γ (PPARγ) [344]. Additionally, the insulin signaling cascade was inhibited through mTOR by S6K1 in cells expressing the core protein from a gt1b isolate [345].

The activation of S6K1 results in the downregulation of the GLUT4 glucose transporter which leads to reduced glucose uptake, while the gluconeogenic enzyme phosphoenolpyruvate carboxykinase 2 (PCK2) is upregulated to facilitate EGP [345]. However, the underlying cause of T2DM in HCV may be due to the inappropriate anabolism of glucose via gluconeogenesis and glycogenolysis as opposed to defective insulin signaling. This is a reasonable assumption as *in vitro* models of HCV have reduced glucose uptake due to the decreased expression of glucose transporters GLUT1 and GLUT2, whilst chronic HCV patients often present elevated levels of endogenous glucose [254,325].

Collectively, these findings suggest that it may be possible for T2DM associated with HCV infection to share commonalities with non-viral T2DM but vary in terms of pathophysiology.

1.8.3. Hepatic steatosis

Despite a strong correlation between all genotypes of HCV infection and IR, there are differences when it comes to extent by which host lipid metabolism is dysregulated during infection. The association between HCV and hepatic steatosis is well established but whether this complication is caused by the virus directly as a cytopathic effect or by the host response to viral infection remains to be clarified.

Hepatic steatosis is often a hallmark of CHC infection where prevalence can be as high as 55% in patients, although this may vary depending on several other factors including lifestyle and infecting genotype [346,347]. However, irrespective of lifestyle factors, hepatic steatosis is commonly associated with gt3 infections of HCV compared to other genotypes which suggests that this particular genotype has a specific mechanism of inducing hepatocellular lipogenesis [347]. This has been investigated by studies that have attributed this phenomenon to the replication of the HCV genome as the quantity of intrahepatic (-)-sense RNA intermediates correlates with the incidence of steatosis which, in turn, accords with clearance of the virus by antiviral treatment [348,349]. In addition to the steatogenic (-)-sense RNA intermediate of HCV gt3, it has been reported that the core protein of gt3a may induce the accumulation of triglycerides and increase levels of cholesteryl esters, ceramides, and glycosylceramides thereby contributing to the synthesis of large lipid droplets (LDs) that are typical of infection with this genotype [48,350].

Furthermore, it has been found in a replicon model that a C-terminal region of NS5A may also be involved in the development of hepatic steatosis due to its inhibition of ApoB, a protein involved in VLDL synthesis and secretion (**section 1.4.**) [351]. However, there is evidence suggesting that a number of host factors such as nuclear receptors e.g. retinoid X receptor-α (RXRα) and peroxisome proliferator activated-receptor α (PPARα), and transcription factors such as sterol regulatory element binding proteins, e.g. SREBP-1c, are also involved in the dysregulation of lipid metabolism during HCV infection.

The nuclear receptors PPARα and RXRα form heterodimers in the presence of the high-affinity ligand, 9-*cis* retinoic acid, and bind to peroxisome proliferator activated receptor response elements (PPAR-REs) in target genes to induce their transcription [352,353]. The PPARα/RXRα heterodimer transcriptionally induces genes such as acyl CoA oxidase (AOX), L-peroxisomal bifunctional enzyme (L-PBE), 3-ketoacyl-CoA thiolase (PTL), and the cytochrome P450 4A isoforms CYP4A1 and CYP4A3 which concern the metabolism of very long chain fatty acids (VLCFAs) and long-chain fatty acids (LCFAs) via peroxisomal β-oxidation [354].

However, Cheng *et al*., found that the mRNA transcription and protein expression of PPARα, as well as carnitine palmitoyl acyl-CoA transferase 1a (CPT1a), a downstream target of PPARα that concerns the mitochondrial import of fatty acids for β-oxidation, to be downregulated during HCV infection [355]. Thus, with respect to this project, the role of nuclear receptors in the dysregulation of lipid metabolism during HCV infection can be ruled out.

1.9. Treatment for HCV infection

Until recently the standard treatment for hepatitis C virus infection was pegylated interferon-α in combination with Ribavirin, a nucleoside analogue. However, this treatment is associated with varied clinical outcomes as an effect of HCV genotype diversity.

However, a number of new therapeutics targeting either host factors or viral proteins have been developed that are reported to be both efficacious and well tolerated in HCV patients.

1.9.1. Ribavirin (RBA)

Ribavirin (RBA), the trade name for 1-beta-D-ribofuranosyl-1,2,4-triazole-3-carboxaminde, is a purine analogue that was first implemented in the treatment of children with respiratory syncitial virus (RSV) [356]. When RBA is used in conjunction with pegylated interferon-α (peg-IFN) in the treatment of HCV, efficacy of the latter has been shown to be greatly improved, although the mechanisms by which this occurs have not been well defined [356]. However, there have been a number of proposed mechanisms of action for RBA including the upregulation of interferon stimulated gene (ISG) expression, inhibition of host inosine monophosphate dehydrogenase (IMPDH), lethal mutagenesis when ribavirin triphosphate (RTP) is misincorporated into nascent viral genomes, and chain termination during viral RNA synthesis [357–359].

1.9.2. Interferon-based therapies

Interferons (IFN) are a class of signaling molecules that are a part of the innate immune response following pathogen recognition by dsRNA [360]. There are three classes of IFN that can be produced and released by virally infected cells i.e. type I such as IFN α- and β that can be expressed by most cells, type II which is also referred to as IFN γ which is limited to immune cells, and type III interferon, e.g. IFN λ, which is mainly expressed by epithelial cells and hepatocytes [361,362]. Interferons function as antiviral cytokines that inhibit HCV replication by inhibiting the IRES-mediated translation of viral genomes thereby limiting transcription and also through promoting the degradation of viral RNA by the RNAse L pathway through expression of 2'-5'-oligoadenylate synthase (OAS) [363,364].

1.9.2.1. Interferon (peg-IFN α, λ)

Treatment of HCV infection was limited to weekly injections of pegylated IFN α (peg-IFN α) which has a longer plasma half-life than IFN α due to the addition polyethylene glycol (PEG) [365,366]. The efficacy of the standard of care (SOC) treatment involving Ribavirin and peg-IFN α is varied, dose-dependent, and genotype specific, i.e. higher dosage of peg-IFN α is more effective at achieving SVR in gt3 (~80%) than gt1 infections (~42%) [367].

This variation in the efficacy of peg-IFN α has been found to negatively correlate with the frequency of amino acid mutations in a region called the interferon sensitivity determining region (ISDR) of HCV NS5A (**section 1.2.2.6.**) which presents a major limitation to the use of IFN-α based treatments against HCV [368]. However, Interferon λ (peg-IFN λ) may bind to receptors which are expressed by a smaller range of cells than Interferon α which allows them greater specificity in therapeutic applications. For example, IFN λ1 (IL-29) binds to IL-29 receptors that are mainly expressed by hepatocytes, as opposed to lymphocytes and monocytes, and thereby prevents immunological complications, e.g. leukopenia, that are often seen with peg-IFN α treatment [369,370]. Additionally, treatment of HCV with IFN λ demonstrates better safety and efficacy compared to peg-IFN α *in vivo*, and in suppressing viral RNA synthesis *in vitro* when it is used in combination with direct acting antivirals (DAAs) such as Daclatasvir (DCV) (**section 1.9.4.2**) [371].

1.9.3. 1st generation direct acting antivirals (DAAs)

The 1st generation of direct acting antivirals (DAAs) that were developed to treat HCV include the protease inhibitors (PI), Boceprevir and Telaprevir. These drugs inhibit the serine protease activity of HCV NS3 by occupying its active site through the reversible, covalent interaction between a featured ketoamide moiety and a catalytic residue (Ser139) that inhibits post-translational processing of the viral polyprotein [372,373].

However, the ketoamide binding site of both Boceprevir and Telaprevir is sensitive to amino acid sequence and, hence, conformation of the NS3 active site. Therefore, the 1st generation DAAs may not be effective at inhibiting pre-existing quasispecies that have variations in these residues, as seen in gt1 infections, as well as escape mutants that result from the selective pressure of such antiviral treatment [100,101,374].

1.9.4. 2nd generation direct acting antivirals (DAAs)

The drawbacks associated with Boceprevir and Telaprevir, such as resistance arising from amino acid variants in HCV quasispecies, led to the development of 2nd generation direct acting antivirals (DAAs) that target the replicase proteins of HCV, i.e. NS3 – NS5B, as a means to treat virus infection.

1.9.4.1. Simeprevir

Simeprevir is a 2nd generation HCV NS3/4A protease inhibitor that is both highly specific and potent [375]. Similar to the mechanism of action (MoA) of Boceprevir and Telaprevir, Simeprevir targets the active site of HCV NS3. However, unlike the 1st generation DAAs, Simeprevir is a non-covalent inhibitor that is associated with a better safety profile, relatively higher SVR rates, and more tolerable adverse drug reactions compared to peg-Interferon based therapies [376,377].

Additionally, the drug has been shown to be effective at low nanomolar concentrations against HCV gt1, although like Boceprevir and Telaprevir, Simeprevir is susceptible to resistance mutations [375,376]. Finally, Simeprevir has been found to decrease treatment duration and improve the efficacy of SOC treatment when included as part of triple therapy [377,378].

1.9.4.2. Daclatasvir (DCV)

Daclatasvir (DCV) is a potent, small molecule inhibitor of HCV NS5A where it is effective at picomolar concentrations against various HCV genotypes, including the JFH-1 isolate, *in vitro* [379]. Furthermore, the treatment of cirrhotic- and non-cirrhotic HCV gt3 patients with DCV and Sofosbuvir combination therapy is reported to have SVR rates of 59 - 69% and 94 - 97%, respectively [380].

The mechanism of action of DCV involves its binding to a poly-proline region between residues 31 - 93 within Domain I of HCV NS5A which affects both the localisation and function of the viral protein during HCV replication [381]. The association of DCV with HCV NS5A results in the redistribution NS5A from the endoplasmic reticulum (ER) to intracellular lipid droplets (LDs) as well as the inhibition of protein-protein interactions that are involved in the formation and function of RCs which, in turn, effects virus replication, virion assembly, and egress [381,382].

DCV is promising in the treatment of pan-genotypic HCV infection, although mathematical models along with experiments involving saturation mutagenesis and next-generation sequencing have revealed that DCV-resistant mutants, termed resistance-associated variants (RAVs) with substitutions in terminal residues i.e. aa positions 31 and 93 of HCV NS5A Domain I, may evolve if the drug is used as a standalone monotherapy [383,384]. However, the resistance of HCV to Daclatasvir has been reported to coincide with resistance to SOC treatment whilst appearing to enhance the sensitivity of RAVs to protease inhibitors [384].

1.9.4.3. Sofosbuvir

Sofosbuvir is a uridine phosphoramidate precursor that is metabolised in the liver to β-D-20-deoxy-20-R-fluoro-20-β-C-methyluridine nucleoside, an active uridine-triphosphate (UTP) analogue which functions as potent inhibitor of the HCV NS5B RNA-dependent RNA polymerase (RdRp) [385,386]. Sofosbuvir has demonstrated high rates of SVR in cirrhotic and non-cirrhotic HCV patients infected with genotypes 1, 2, 4, 5, and 6 infections when used with Velpatasvir, a pan-genotypic inhibitor of HCV NS5A, and also in gt2 and 3 infections when used in dual therapy with Ribavirin [387–389]. Additionally, Sofosbuvir as a dual-therapy with Ribavirin is well tolerated by recipients compared to Interferon-based treatments [390]. However, NS5B variants with a C136N/H polymorphism have been identified in treatment of naive patients with chronic HCV gt1b infection [391].

1.9.5. Host-Factor Therapeutics

In contrast to the advent of direct acting antiviral agents targeting viral proteins as a means to inhibit virus replication and the development of secondary complications, research into the development of antiviral therapeutics is currently examining the role of host factors that are recruited during the HCV life cycle.

1.9.5.1. Cyclophilin Inhibitors

Cyclophilins are a subgroup of enzymes with peptidyl-prolyl *cis-trans* isomerase (PPIase) activity that function in the isomerisation and post-translational folding of newly synthesised proteins [392,393]. These enzymes are resident to organelles such as the endoplasmic reticulum (ER), e.g. heat shock protein 47 (HSP47) and cyclophilin B (CypB), and the mitochondria, e.g. cyclophilin D (CypD) which may affect host metabolism by its involvement in opening the mitochondrial permeability transition pore (mPTP) (**section 1.7.3.3.**) [394–396]. Additionally, cyclophilins such as cyclophilin A (CypA) are targeted by cyclophilin inhibitors, e.g. cyclosporin A (CsA), which are often administered to recipients of organ transplants as immunosuppressants to reduce the likelihood of graft rejection.

For example, CsA dampens the innate immune response concerning natural killer (NK) cell activation by binding to CypA with high affinity and blocking the calcineurin-mediated nuclear translocation of nuclear factor of activated T-cells (NF-AT) to inhibit the transcriptional induction of cytokines, e.g. IL-2 [397–399]. Though treatment of Huh7 cells with CsA has been reported to induce the unfolded protein response (UPR), the mechanism of action for CsA in the inhibition of HCV replication and has been found to involve its interaction with the HCV NS5B polymerase [393,400]. Conversely, the mechanism of action for Alisporivir (ALV) is reported to involve the inhibition of HCV NS5A Domain II isomerisation by CypA [401].

Furthermore, CypD may play a role in regulating mitochondrial calcium ion concentrations which has consequences on the opening of mPTP and hence mitochondrial function (**section 1.7.3.3**), that may further explain why HCV replication is suppressed by CsA and ALV [395,396,400–403]. The application of ALV in triple therapy regimens with peg-IFN and Ribavirin is well tolerated with minimal adverse drug reactions (ADRs) in recipients and appears to be effective against HCV gt 1 - 4 infections [404].

1.9.5.2. Miravirsen

MicroRNAs (miRs) are short sequences (18 - 23nt) of non-coding RNA that play a role in the regulation of protein expression at either a transcriptional- or translational level by annealing to complementary sequences at the 3'-untranslated region (UTR) of target mRNAs and mediating their degradation [405].

Initially genes encoding miRs are transcribed in the nucleus by RNA Polymerase II (pol II) to produce long primary miR transcripts (pri-miRNAs) which are then processed into stem-loop structures of around 65 - 70nts (pre-miRNAs) by the nuclear microprocessor complex which is comprised of DGCR8, a dsRNA-binding protein called Pasha, and Drosha, an RNAse III enzyme [406–410]. Pre-miRNAs are subsequently exported from the nucleus to the cytoplasm by Exportin-5 (XPO5) in the presence of Ran-GTP where they are further processed into shorter (~22nts) mature miRNAs by the RNAse III enzyme, Dicer [408].

Upon maturation, miRNAs associate with Slicer (Ago2), an Argonaute protein that features Piwi-Argonaute-Zwille (PAZ) and MID domains which bind to the 3'-end and anchors the 5'-end of miRNA, respectively, and a P element-induced wimpy testes (PIWI) domain that has endonuclease activity to form the microRNA-containing-RNA-induced silencing complex (miRISC) [411,412]. However, this mechanism is contingent on 100% complementarity between the "seed region", i.e. nucleotide positions 2 - 8 of a given miR and the 3'-UTR of a target mRNA [405,413].

Alternatively, Ago proteins 1, 3, and 4 do not have endonuclease activity and may directly bind to miR-mRNA duplexes which thereby leads to repressed protein translation [412]. Protein expression may also be reduced by either mRNA destabilisation or, to a greater extent, translational inhibition even in the event of single mismatched base-pairs in either the "seed regions" or more commonly in the "centred sites" of bound miRs through disrupting translation initiation [414,415]. In this respect, the mechanism of action of miRNA is analogous to that of small interfering RNAs (siRNAs) which are commonly used in research as mRNA destabilisers and/or translational repressors of target genes. An exception to the microRNA dogma, however, is microRNA-122 (miR-122) in HCV infection. miR-122 is highly expressed in hepatocytes, accounting for approximately 70% of total miRNA in the liver and is involved in the regulation of genes that are associated with the synthesis of hepatic triglycerides e.g. fatty acid synthase (FASN), and mitochondria-associated acetyl-CoA carboxylase 2 (ACC2) [416–419].

miR-122 also demonstrates anti-tumour properties by regulating mRNA transcript abundance for cutlike homeobox1 (CUTL1), a gene that is implicated in hepatocellular carcinoma (HCC) due to its involvement in the proliferation and differentiation of liver cells [417,420].

In addition to regulating host genes, miR-122 may bind to S1 and S2 sites within the 5'-UTR together with an S3 site in the 3'-UTR of the HCV genome to enhance replication by recruiting Argonaute 2 protein which shields template RNA from degradation in the cytoplasm by 5'-3' exoribonuclease 1 (Xrn1) [421–423].

The occupation of S1, S2, and S3 sites by miR-122 and the resultant protection of the HCV genome from Xrn1 also increases translation due to the increased stability of viral RNA, and thus, miR-122 is an appealing target for the treatment of HCV [421,423].

Miravirsen is a specific inhibitor of both the biogenesis and function of miR-122 with pan-genotypic antiviral activity against HCV, including strains that have acquired resistance to direct acting antivirals (DAAs) [423]. Miravirsen is a synthetic, antisense oligonucleotide (ASO) therapy which consists of a phosphorothioate backbone with interspersed locked nucleic acid (LNAs) ribonucleotides [424]. The phosphorothioate modification to oligonucleotides confers resistance of the construct to nucleases and promotes its cellular uptake as well as its distribution to organelles such as the nucleus and mitochondria [425,426]. The LNAs in Miravirsen offer increased affinity of the oligonucleotide for miR-122, and further impairs the recruitment of exonucleases e.g. RNAse H, thereby extending its half-life due to improved stability [424,427].

The MoA of Miravirsen involves its high affinity binding to the stem-loops of both pri- and pre-miR-122 in the nucleus and inhibits processing by Drosha and Dicer, respectively, to ultimately inhibit the biogenesis of mature miR-122 [424].

Triple therapy of Miravirsen with peg-IFN α and Ribavirin is well tolerated and shown great efficacy in the treatment of chronic HCV gt1 infection where SVR has been achieved in recipients with no reported ADRs, off-target effects, or development of secondary complications, e.g. hepatocellular carcinoma (HCC) [428,429].

Additionally, Miravirsen monotherapy is effective in achieving HCV clearance albeit in a dose-dependent manner [430]. Besides inhibiting the replication of HCV, treatment with Miravirsen also results in reduced cholesterol which supports the notion that HCV is reliant upon elements of host lipid metabolism that are recruited by miR-122 during the life cycle of the virus [423]. Given that the 5'-UTR of HCV is highly conserved between genotypes and Miravirsen targets a host-factor, miR-122, this therapy is thought to present a high genetic barrier to the evolution of resistant strains, although point mutations in the HCV 5'-UTR following prolonged treatment with Miravirsen and serial passage of the virus *in vitro* have been reported [423,431].

Thus, the study of pathogen virulence factors is important to the understanding the mechanisms of disease pathogenesis and treatment thereof. However, a key concept in dissecting the underlying molecular biology of infection is identifying and characterising the influence of host factors.

1.10. Study of Host Factors in HCV Infection

The study of host factors and the modulation thereof by HCV may further the understanding of how certain biological processes are exploited or circumvented during infection and lead to the development of novel therapeutics. The implementation of methods such as microarray analysis and functional genomics in the study of HCV infection has demonstrated the interplay between virally encoded proteins and host molecular biology that occur throughout disease progression whilst revealing potential therapeutic targets in the process.

1.10.1. RNA Microarray

RNA microarray is a chip-based platform from that can yield vast amounts of data relating to cellular gene transcription under certain conditions, e.g. HCV infection over 48 hours, from which hypotheses can be formulated and tested using functional genomics e.g. RNAi [432]. The advantages of microarray are that thousands of genes can be assayed in a single experiment and the sensitivity of transcript detection is up to over four orders of magnitude [432]. Microarray data can also be analysed using gene ontology tools, e.g. GeneGO™ MetaCore™, to identify cellular pathways that involve genes which are differentially transcribed.

However, RNA microarray also has associated drawbacks. For example, because gene expression is measured in terms of transcript abundance, it is assumed that all RNA transcripts are expressed as protein without accounting for miRNA activity, regulation of protein translation, or mRNA stability. Another caveat in interpreting microarray data is that the intensity of the signal produced from the hybridisation of a labelled probe to target RNA cannot be distinguished as to whether it is generated due to a single cell expressing multiple transcripts or multiple cells expressing single transcripts [(432)]. Thus, microarray data is often validated using polymerase chain reaction (PCR) experiments and supported through proteomic techniques such as flow cytometry and Western Blotting.

1.10.2. Microarray in HCV

In a study by Wu *et* al., whole-genome microarray analysis was performed on cirrhotic liver tissue samples from a cohort of patients with HCV and HCV-related hepatocellular carcinoma (HCV-HCC) in which it was found that the development of complications such as hepatic steatosis and HCC in HCV infection could be attributed to abnormalities in host lipid metabolism that occur during virus infection [(433)].

The authors reported the transcription of genes involved in fatty acid biosynthesis and lipid metabolism was dysregulated in both HCV and in HCV-related HCC, e.g. fatty acid synthase (FASN, no fold-change in HCV; +2.70-fold in HCV-HCC), acyl-CoA synthetase long-chain family member 4 (ACSL4, +9.19-fold in HCV; +15.40-fold in HCV-HCC), and ELOVL fatty acid elongase 1 (ELOVL1, +1.81-fold in HCV; + 2.29-fold in HCV-HCC) [433]. Concomitantly, there was also a downregulation in the expression of genes involved in the catabolism of fatty acids, e.g. peroxisome proliferator-activated receptor α (PPARα, -2.04-fold in HCV; -3.60-fold in HCV-HCC), and peroxisome proliferator-activated receptor γ coactivator 1A (PPARGC1A, -1.93-fold in HCV; -6.53-fold in HCV-HCC) [433].

Similarly, it was also found that the transcription of genes associated with the synthesis, uptake, and transport of cholesterol were also dysregulated during HCV infection i.e. Very Low-Density Lipoprotein Receptor (VLDLR, + 4.25-fold in HCV; +3.56-fold in HCV-HCC), Niemann-Pick C1-like 1 (NPC1, -1.98-fold in HCV; -2.26-fold in HCV-HCC), and Apolipoprotein A-I (ApoA1, -1.50-fold in HCV; -1.77-fold in HCV-HCC) [433]. These findings were supported by biochemical assays in which serum-cholesterol and serum-triglycerides were lower and higher, respectively, in subjects with HCV-alone than in those with HCV-HCC [433]. The authors concluded that the *de novo* synthesis and uptake of fatty acids were enhanced which, together with reduced FA catabolism in HCV infection, contribute to the increased synthesis and retention of triglycerides in the liver [433].

RNA microarray was performed in a separate study which examined the regulation of host genes using an *in vitro* model for acute HCV infection, namely the JFH-1 isolate and Huh7 cells over the course of 48 hours, and also reported the virus to induce the differential transcription of genes involved in lipid metabolism, as well as those concerning oxidative stress, vesicle trafficking, and intracellular transport [(214)]. This investigation found over 2,000 genes to be differentially transcribed during replication of the full-length HCV genome compared to mock infected cells over 48 hours [(214)]. This finding contrasts with the effect seen in HCV SGR cells where the expression of the viral replicase affected the transcription of under 200 host genes [(214)]. Specifically, this study found that genes involved in the synthesis and transport of phospholipids and sphingolipids, e.g. sphingosine-1-phosphate phosphatase (SGPP1), serine-palmitoyl-CoA transferase 1 (SPTLC1), choline kinase α (CHKA), as well as that of fatty acids, e.g. ELOVL fatty acid elongase 4 (ELOVL4), fatty acid binding protein 3 (FABP3), and acyl-CoA synthetase long-chain family member 3 (ACSL3), were overexpressed during HCV infection [(214)]. Additionally, the increased anabolism of fatty acids occurred in synergy with a downregulation of genes concerning their degradation and oxidation e.g. acetyl-CoA acetyltransferase 2 (ACAT2) and short/branched chain specific acyl-CoA dehydrogenase (ACADSB) [(214)].

A 2-fold threshold of significance was used in selecting genes of interest for supporting RNAi experiments, where the siRNA-mediated knockdown of genes concerning lipid metabolism e.g. Thioredoxin-interacting protein (TXNIP, +20.51-fold at 24 hours p.i., +21.96-fold at 48 hours p.i.) and cytochrome P450 1A1 (CYP1A1, +5.19-fold at 24 hours p.i., +2.58-fold at 48 hours p.i.) resulted in an 85% and 60% reduction in viral RNA synthesis, respectively [214]. Furthermore, the siRNA-mediated knockdown of TXNIP and CYP1A1 in JFH-1 infected Huh7 cells lowered virus secretion by 90% and 75%, respectively [214]. This study indicated that TXNIP regulates the expression of downstream targets, e.g. TXNIP functions as a negative regulator of the mitochondrial β-oxidation of fatty acids (FAs) via PPARα, and that the modulation of genes such as TXNIP may affect cellular pathways e.g. lipid metabolism, upon which the HCV life cycle is dependent [214,434].

1.10.3. Functional genomics

The functions of differentially expressed host factors during virus infection identified from RNA microarray analyses can be validated and further investigated by incorporating techniques such as RNA interference (RNAi) and quantitative-reverse transcription polymerase chain reaction (qRT-PCR), along with supporting proteomics and biochemical assays, to determine the effect such proteins have on the replication of a pathogen.

For example, a study by Blackham involving JFH-1 infected Huh7 cells (MOI - 3) and qRT-PCR showed that TXNIP mRNA was upregulated by approximately 35-fold and 50-fold at 24 hours and 48 hours post-infection (p.i.), respectively, which contrasts with the ~20-fold increase seen at both timepoints in the microarray study [215].

In addition to this, the transcriptional fold-changes of a panel of genes involved in fatty acid (FA) metabolism including ELOVL4, ELOVL7, ACSL3, SREBP1, and PPARγ, as well as PPARGC1A (PGC1A) were also upregulated to levels higher than those observed in the microarray study [215]. Blackham also developed an HCV gt2a subgenomic replicon (SGR) cell line using Huh7 cells in which it was found that the expression of HCV NS proteins did not affect the transcription of genes concerned with the metabolism of FAs. In contrast, PPARGC1A is involved in the production of intracellular lipid droplets (LDs) and was found to undergo a significant (~6-fold) level of transcription in HCV SGR cells [215].

In addition to validating data from the microarray study, Blackham also performed small interfering RNA (siRNA) experiments which targeted TXNIP in JFH-1 infected Huh7 cells (MOI - 3), where an 90% suppression of this host protein resulted in a reductions of HCV RNA, extracellular virus titre, and HCV NS3 expression by 82%, 90%, and 80%, respectively [215].

Interestingly, the siRNA-mediated knockdown of TXNIP in JFH-1 infected Huh7 cells led to the increased expression of genes that are targeted by PPARα and related to host metabolism such as long chain-specific acyl-CoA dehydrogenase (LCAD), tribbles pseudokinase 3 (TRIB3), carnitine palmitoyl transferase 1a (CPT1a), pyruvate dehydrogenase kinase 4 (PDK4), enoyl-CoA hydratase 1 (ECH1), and acyl CoA oxidase 1 (ACOX1) [215]. In tandem, knockdown of TXNIP brought about the reduced expression of pro-lipogenic genes such as acyl-CoA synthetase long-chain family member 3 (ACSL3) and fatty acid transport protein 2 (SLC27A2) with no observable effects on cell viability [215]. Blackham also performed biochemical assays to determine the effect of viral protein expression on the intracellular concentration of lipid metabolites in JFH-1 and HCV SGR models in which an increased abundance of both triglycerides (TGs) and lipid droplets (LDs) was attributed to the overexpression of TXNIP.

1.10.4. Thioredoxin-interacting protein (TXNIP)

Thioredoxin-interacting protein (TXNIP) is a 50 kDa protein, consisting of 397 amino acids, that has structural homology to the arrestin family of proteins, i.e. arrestin-domain containing (ARRDC) proteins 1 – 5, which function as intracellular scaffolding molecules involved in receptor mediated endocytosis, ubiquitination, and signal transduction [435,436]. As described in the previous section, TXNIP is a factor in the dysregulation of host lipid metabolism during HCV infection in which it also appears to enhance proliferation of the virus.

Therefore, in order to understand how HCV may induce the overexpression of TXNIP, the mechanisms underlying the transcriptional induction and regulation as well as the functions of this protein will be described.

1.10.4.1. TXNIP Transcriptional induction

In the context of HCV infection, there are two mains sources of TXNIP expression, namely elevated glucose concentrations, via the transcriptional activity of Mlx-MlxIP heterodimers following their nuclear translocation, and oxidative stress brought by ROS and/or misfolded and oxidised proteins (**section 1.10.5.**).

As described in **section 1.7.3.1.**, the phosphorylation of glucose to glucose-6-phosphate by hexokinase (HXK2), causes displacement of the enzyme from the outer mitochondrial membrane which, in turn, induces the nuclear translocation of Max like protein (Mlx) by its complex with Max like protein-interacting protein (MlxIP) [271]. Following nuclear entry, Mlx may induce the transcription of either lipogenic genes such as TXNIP or other glycolytic targets e.g. HXK2, by binding to CACGTG E-box motifs that comprise carbohydrate response elements (ChoREs) within in their respective promoters [271,437,438]. Interestingly, the induction of TXNIP by Mlx-MlxIP heterodimers is reported to be promoted by the combination of hypoxic conditions, high glucose concentration, and an abundance of intracellular Ca^{2+} ions [271,438,439].

This phenomenon has been tested in neuronal cells both *in vivo* and *in vitro*, where the expression of TXNIP was pharmacologically inhibited with the use of calcium channel blockers, e.g. diltiazem, verapamil, and 2-aminoethoxydiphenyl borate (2-APB) [439]. The authors report that the treatment of cortical neurons with 2-APB, which prevents calcium store depletion through the inhibition of inositol-1,4,5-triphosphate receptors (IP3R), fully inhibited TXNIP expression, and contrasts with the blockade of calcium ion efflux from L-type calcium channels, analogous to voltage dependent anion channels, which significantly reduced TXNIP expression, although in a dose-dependent manner [439].

Similarly, Chen *et al*., investigated the mitochondrial localisation of TXNIP in diabetic cardiomyopathy and its involvement in the mitochondrial associated pathway of apoptosis, a process that is characterised by cytochrome C (CYCS) release, and caspase-3 cleavage [440,441]. Similar to the study by Kim *et al*., this study also found TXNIP expression as well as caspase-3 cleavage, and the apoptosis of cardiomyocytes to be reduced when verapamil was applied to a mouse model for obesity-induced diabetes [441]. The group remarked that calcium may contribute to the overexpression of TXNIP through the control of key transcriptional mediators such as MlxIP [441]. Furthermore, similar results were also found in pancreatic β-cells where loss of β-cell mass is symptomatic of diabetes [442].

Additionally, Xu *et al*., treated both INS-1 and primary human islet cells with Verapamil and found TXNIP expression to be inhibited *in vitro* [442]. The group also applied this treatment to streptozotocin- and obesity induced murine models for diabetes, where an improvement in endogenous insulin levels and glucose metabolism, as well as a prevention of T2DM was observed [442]. However, Xu *et al*, suggested an alternative mechanism for the promotion of β-cell survival which, in addition to a reduction of intracellular calcium, involved the transcriptional repression of TXNIP due to diminished occupation of the ChoRE in its promoter by Max like interacting protein like protein (MlxIPL), a paralog of MlxIP [271,442].

Collectively, these studies demonstrate that the concentration of intracellular calcium ions may be an important factor in the transcriptional induction, and therefore, overexpression of TXNIP that is mediated by Mlx [215,271,442,443]. Thus, the abundance and localisation of intracellular Ca^{2+} ions may be contributing factors in the dysregulation of host lipid metabolism during HCV replication.

1.10.4.2. TXNIP mRNA Regulation

TXNIP protein expression may be regulated at a post-transcriptional level through mechanisms that modulate the abundance of mRNA transcripts which occur due to the induction of the unfolded protein response (UPR), and the expression of both histone deacetylases (HDACs) and histone acetyltranferases (HATs).

1.10.4.2.1. TXNIP mRNA Regulation by the Unfolded Protein Response (UPR)

The abundance of TXNIP mRNA may be regulated post-transcriptionally via the action of microRNA 17 (miR-17) in a mechanism that is outlined in **section 1.9.5.2.**, which may be disabled following the induction of ER stress and the unfolded protein response (UPR).

Lerner *et al*., reported that TXNIP mRNA may be regulated by the endoribonuclease activity of inositol requiring enzyme-1α (IRE-1α) that follows the induction of the UPR in pancreatic β-cells [(444)]. In non-stressed cells, the 3 effector proteins of the UPR, i.e. IRE1-α, PKR-like ER Kinase (PERK), and activating transcription factor 6 (ATF6), are tethered to the ER by GRP78. However, perturbation of the ER membrane, as in the rearrangement induced by HCV NS4B, causes the release of activated IRE1-α, PERK, and ATF6 from GRP78, as a means to reduce protein synthesis at various levels [(445)]. miR-17 may regulate the translation of TXNIP through the destabilisation of mRNA transcripts. However, miR-17 is subject to degradation by the endoribonuclease properties of active IRE-1α following induction of the UPR, which leads to unregulated levels of TXNIP mRNA and, therefore, an overexpression of protein (**Figure 16**) [(444)].

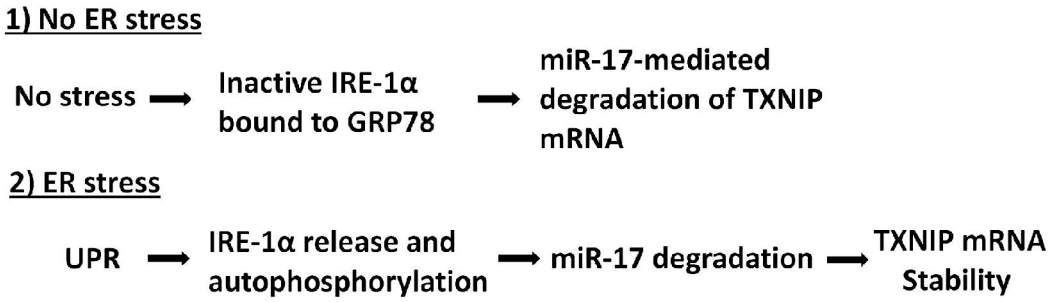


Figure 16 - TXNIP mRNA regulation by activated IRE-1α following ER stress

(1) No ER stress: Under physiological conditions, IRE-1α is inactive and bound to GRP78 and TXNIP mRNA is destabilised by the regulatory microRNA, miR-17. **(2) ER stress:** Following induction of the UPR, IRE-1α dissociates from GRP78, undergoes autophosphorylation, and miR-17 is degraded by the endoribonuclease activity of active IRE-1α. TXNIP mRNA is preserved as a result of diminished miR-17 levels due to active IRE-1α [(444)].

1.10.4.2.2. TXNIP mRNA Regulation by Histone Deactylases (HDACs) and Histone Acetyltransferases (HATs)

Nuclear DNA is packaged with proteins known as histones to form chromatin of which histone acetylation is a pre-requisite for chromatin structure and, therefore, gene expression [(446)]. Such histones feature conserved Lys residues that may be acetylated by histone acetylases (HATs) to promote gene transcription or, in the instance of TXNIP, deactylated by histone deacetylases (HDACs) to repress the transcription of its mRNA [(446)]. The transcription of TXNIP mRNA may be regulated by the action of the cytoplasmic class II histone deactylase, HDAC10 [(446)]. Lee *et al.*, targeted the expression of HDAC10 for siRNA-mediated knockdown which was found to increase both TXNIP mRNA and protein, intracellular ROS, and pro-apoptotic markers such as CYCS that are characteristic of the mitochondria-associated pathway of apoptosis being induced [(440,447)].

Thus, the authors of this study concluded that TXNIP expression may also be affected by the abundance of class II HDACs which affects both redox signaling and apoptosis in gastric cancer [447]. Conversely, elevated glucose in INS-1 and primary islet cells leads to the co-localisation of Mlx-MlxIPL heterodimers and p300 HAT protein at the ChoRE in the TXNIP promoter which enhances the transcription of TXNIP mRNA by acetylating histone H4 and facilitating the recruitment of RNA polymerase II [448].

1.10.5. TXNIP Function

Thioredoxin interacting protein (TXNIP) is primarily a regulator of cellular redox state that binds to and inhibits the activities of both isoforms of Thioredoxin (Trx1, Trx2), a thiol oxidoreductase [440,449]. In cells where the microenvironment is reduced, intermolecular disulfide bridges are formed between cysteine (Cys) residues between the Trx1 active site (Cys32, Cys35) and TXNIP (Cys63, Cys247). However, in the presence of ROS, both Cys32 and Cys35 of the Trx1 active site are oxidised and the Trx1-TXNIP complex dissociates to enable the reducing properties of Trx1 [435,440].

Conversely, Thioredoxin-2 (Trx2) is localised to the mitochondrial compartment where it is bound to and inhibits the mitogen activated protein kinase kinase kinase (MAPKKK), apoptosis signal-regulating kinase 1 (ASK1) [440].

However, TXNIP may also bind to Trx2 during oxidative stress which leads to the release of ASK1 in its active form to initiate the stress related, mitochondria-associated pathway of apoptosis (**section 1.10.4.1.**) [440,441].

1.10.5.1. TXNIP and Glucose Metabolism

The functions of TXNIP, in addition to binding Thioredoxin and inhibiting its thiol-oxidoreductase properties, include regulating the cellular metabolism of both glucose and lipids. The expression of TXNIP, as well as its paralog arrestin domain-containing 4 (ARRDC4) protein, has been found to correlate with the decreased uptake of glucose by cells but compensates for this by promoting endogenous glucose production (EGP) (**section 1.8.1**) [450,451]. This has been shown by Chutkow *et al.*, who engineered a strain of mice to have a liver-specific TXNIP-gene deletion and were characterised as having a hypoglycaemic and hyperinsulinaemic phenotype as well as impaired EGP [451]. It was found that hepatocellular glucose-release was 2-fold lower than controls, whereas the secretion of β-hydroxybutyrate, a ketone body resulting from the oxidation of fatty-acids, was 2.4-fold higher in this model [451]. EGP was not present in these animal models, where the absence of TXNIP expression did not affect the transcription of gluconeogenic genes such as phosphoenolpyruvate carboxykinase 1 (PCK1), G6Pase, and pyruvate carboxylase [451].

Furthermore, genes concerning lipid anabolism such as fatty acid synthase (FASN), acetyl co-A carboxylase 2 (ACC2) and carnitine palmitoyl transferase 1 (CPT1) were downregulated in this animal model, although transcription of lipoprotein lipase (LPL) was significantly increased (+3-fold) [451]. The authors of this work found that overexpression of wild-type TXNIP, but not a mutant variant featuring a mutation in Cys247 that is crucial to its interaction with Trx, rescued glucose production in TXNIP-null mice and concluded that TXNIP is important to the regulation of host metabolism [451].

1.10.5.2. TXNIP and Lipid Metabolism

The expression of TXNIP also correlates with the dysregulation of host lipid metabolism which occurs in parallel to processes that are involved in the production and utilisation of intracellular glucose. Many of the effects of TXNIP on host lipid metabolism are brought about via its activation of the NLRP3 inflammasome, a tri-partite protein complex that consists of NACHT, LRR, and PYD domains-containing 3 (NLRP3) protein in association with apoptosis-associated speck-like protein containing a caspase-recruitment domain (ASC) that recruits the active form of caspase-1 (CASP1) [452,453]. As mentioned in **section 1.10.4.**, TXNIP features arrestin domains in its respective amino- and carboxy terminals [453]. Current evidence suggests that during oxidative stress and the dissociation of TXNIP from Trx, the arrestin domains of TXNIP interact with the NACHT and LRR domains of NLRP3.

This activating signal is then transduced by the sequential recruitment of ASC and CASP1 to complete formation of the NLRP3 inflammasome complex in the perinuclear space between the endoplasmic reticulum (ER) and mitochondria [453–455]. Following assembly of the active NLRP3 inflammasome complex, CASP1 mediates the processing of immature interleukin-1β (IL-1β) and IL-18 that are induced by NF-κB signaling to produce bioactive and secretory pro-inflammatory cytokines, and activates sterol regulatory element binding proteins (SREBPs) that stimulate lipogenesis via the induction of genes, e.g. fatty acid synthetase (FASN) [85,456,457]. It has also been reported that the hepatocellular expression of HCV proteins can induce the upregulation of inflammasome components, i.e. NLRP3 and ASC, which together with the overexpression of TXNIP may account for the increased production of IL-1β and IL-18, as well as the dysregulation of lipid metabolism via SREBP-processing, e.g. SREBP-1c, that occurs during HCV infection [85,214,215,454,456–458]. Furthermore, the presence of intracellular ROS and NLRP3 inflammasome activation is reportedly suppressed following inhibition of mitochondrial VDACs which suggests that the source of TXNIP-Trx dissociation, and hence the dysregulation of lipid metabolism in HCV infection may be related to the perinuclear ER-mitochondrial interface [455]. Therefore, TXNIP overexpression may contribute to the dysregulation of host lipid metabolism and the proliferation of HCV by way of activating the NLRP3 inflammasome which processes SREBP-1c to transcriptionally induce lipogenic genes such as acetyl CoA-carboxylase (ACC), fatty acid synthase (FASN), pyruvate kinase (PK), and Glucokinase (GCK) [459].

Hypothesis & Aims

Hypothesis

The dysregulation of lipid metabolism caused by TXNIP overexpression during HCV infection can be suppressed through: the inhibition of pathways concerning Endoplasmic Reticulum (ER) stress and induction of the unfolded protein response (UPR), and mitochondrial dysfunction caused by calcium ion overload.

Aims

Microarray data concerning the JFH-1 infection of Huh7 cells over 48 hours will be re-evaluated using GeneGo™ Metacore™ software and examined for changes in gene transcription related to ER stress and the unfolded protein response (UPR) and to identify whether glucose may contribute to the dysregulation of lipid metabolism during HCV replication. To see if the induction of ER stress gives rise to disturbances in calcium homeostasis and host gene transcription, cytosolic calcium concentrations will be measured in HCV SGR- and JFH-1 infected Huh7 cells. To show whether host lipid metabolism is dysregulated in HCV replication models relative to uninfected controls, baseline measurements for TXNIP and downstream lipogenic gene transcription will be determined over 48 hours.

To observe the extent by which induction of the UPR contributes to the dysregulation of lipogenic gene transcription and the replication of replicon and virus, the IRE-1α arm of the UPR will be inhibited in both HCV SGR- and JFH-1 infected Huh7 cells and the effects determined over 48 hours.

The effects of alterations in Ca^{2+} homeostasis on genes involved in lipid and glucose metabolism will be examined in HCV gt2a infection models by measurement of mitochondrial calcium ion concentration and by inhibition of calcium ion overload. To determine whether mitochondrial dysfunction brought about by calcium ion overload contributes to the dysregulation of lipid metabolism and the replication of virus and replicon in HCV gt2a infection models, mRNA transcript abundance for genes concerning glucose and lipid metabolism, intracellular glucose and triglyceride concentration, together with glycogen and lipid droplet (LD) content, and virus replication will be measured.

Chapter 2: Materials & Methods

2.1. Materials

The items that were required during this project and the supplier from which they were obtained are listed as follows.

2.1.1. Reagents

Item	Supplier
DMEM high Glucose, GlutaMAX™, pyruvate.	Invitrogen, UK
DMEM, no Glucose	Invitrogen, UK
PBS, pH 7.4 (×10)	Invitrogen, UK
PBS 1× without calcium magnesium and phenol red	Fisher Scientific, UK
DMSO	Fisher Scientific, UK
Fetal Bovine Serum, qualified, E.U. approved, South America origin	Invitrogen, UK
Penicillin-Streptomycin	Invitrogen, UK
Geneticin (G418) [50 mg/ml]	Invitrogen, UK
TRIzol®	Invitrogen, UK
Chloroform	Sigma-Aldrich, UK
Nuclease Free Water	Invitrogen, UK
Isopropanol	VWR, UK
25:24:1 Phenol:Chloroform:Isoamyl Alcohol	Sigma-Aldrich, UK
Sodium Citrate [0.1M] Sodium citrate dehydrate Absolute Ethanol	 Sigma-Aldrich, UK VWR, UK
Sodium Acetate [3M] Sodium Acetate	 Sigma-Aldrich, UK
PCR Primers	Invitrogen, UK
Oligo(dT)18 Primer	Thermo Scientific, UK
Oligo d(T) primers	Invitrogen, UK
dNTP Mix	Promega, UK
Absolute Ethanol	VWR, UK

2.1.2. Consumables

Item	Supplier
6-Well Cell Culture Plates, Corning	VWR, UK
12-well plates, Corning® CellBIND® surface	VWR, UK
96-well F-bottom plate with lid	VWR, UK
60-well plates	VWR, UK
T75cm^2 cell culture flask, TC treated	VWR, UK
T25cm^2 cell culture flask, TC treated	VWR, UK
Cryogenic vial CryoTube internal thread 1ml	Fisher Scientific, UK
50ml freestanding centrifuge tubes	VWR, UK
15ml BD Falcon tubes	VWR, UK
Serological pipettes (5ml)	VWR, UK
Serological pipettes (10ml)	VWR, UK
Serological pipettes (25ml)	VWR, UK
1.7ml Axygen microtubes	Fisher Scientific, UK
0.45 µm Stericup® 150ml filter units	Fisher Scientific, UK
Amicon Ultra-15 Centrifugal Filter Unit with Ultracel-100 membrane	Millipore, UK
Rinzl Plastic Coverslips, Size 18x18mm	Emsdiasum, USA
Nitrocellulose Pre-Cut Blotting Membranes, 0.45 µm pore size	Invitrogen, UK
2 - 200µl yellow pipette tips	VWR, UK
50 - 1000µl blue pipette tips	VWR, UK
1-10µl Maximum recovery filter tip	Thistle Scientific, UK
20µl Maximum recovery filter tip	Thistle Scientific, UK
200µl Maximum recovery filter tip	Thistle Scientific, UK
1000µl Maximum recovery filter tip	Thistle Scientific, UK
Lightcycler Capillaries	Roche, UK
Shandon Microscope Slides	VWR, UK
Coverglass 20×20mm	VWR, UK

2.1.3. Enzymes

Item	Supplier
*Xba*I [20,000 units ml^{-1}]	New England Biolabs, USA
Mung Bean Nuclease	New England Biolabs, USA
10× Mung Bean Nuclease Buffer	New England Biolabs, USA
100× BSA	New England Biolabs, USA
Proteinase K (20mg/ml)	ThermoFisher Scientific, UK
M-MLV Reverse Transcriptase	Promega, UK
Recombinant RNAsin ribonuclease inhibitor (40 units μl^{-1})	Promega, UK
TURBO DNA-*free*™ (DNAse)	Invitrogen, UK

2.1.4. Kits

Item	Supplier
Mitochondrial ToxGlo® Assay	Promega, UK
Triglyceride Quantification kit	Abcam, UK
QuantiTect SYBR Green RT-PCR Kit	Qiagen, UK
Hs_miR-17_2 miScript Primer Assay	Qiagen, UK
Hs_RNU6-2_11 miScript Primer Assay	Qiagen, UK
miScript II RT Kit	Qiagen, UK
miScript SYBR Green PCR Kit	Qiagen, UK
QuantiTect SYBR Green PCR Kit	Qiagen, UK
2× PCRBIO UltraMix	PCR Biosystems, UK
QIAprep Spin Mini-prep kit	Qiagen, UK
T7 Megascript Kit	Invitrogen, UK

2.1.5. Markers

Item	Supplier
10kb DNA ladder	Promega, UK
Benchmark™ Pre-Stained Protein Ladder	Invitrogen, UK

2.1.6. Buffers

Item	Supplier
M-MLV Reverse Transcriptase Buffer Pack	Promega, UK
Resolving gel buffer	National Diagnostics, USA
Stacking gel buffer	National Diagnostics, USA
10× Tris/Glycine/SDS Running buffer	National Diagnostics, USA
6× DNA Loading Buffer	Promega, UK
NEBuffer 2	New England Biolabs, USA
4× Laemmli sample loading buffer	
Tris-HCl [50mM] (pH 6.8)	Sigma-Aldrich, UK
Glycerol (4% v/v)	VWR, UK
Ethylenediaminetetraacetic acid (EDTA) [12.5mM]	Sigma-Aldrich, UK
Bromophenol Blue (0.02% w/v)	BDH Laboratory Supplies, UK
Triton X-100 Lysis Buffer	
Tris-HCl [20mM]	Sigma-Aldrich, UK
Sodium chloride [150mM]	Sigma-Aldrich, UK
Ethylenediaminetetraacetic acid (EDTA) [1mM]	Sigma-Aldrich, UK
Triton X-100 (0.5% v/v)	Sigma-Aldrich, UK
HALT Protease Inhibitors [1×]	Thermo Scientific, UK
TBE buffer	
Tris Base [89mM]	Sigma-Aldrich, UK
Ethylenediaminetetraacetic acid (EDTA) [2mM]	Sigma-Aldrich, UK
Boric Acid [89mM]	Amresco, UK
TE Buffer (pH 8.3)	
Tris-HCL [10mM]	Sigma-Aldrich, UK
Ethylenediaminetetraacetic acid (EDTA) [1mM]	Sigma-Aldrich, UK
Transfer Buffer	
Tris/Glycine/SDS running buffer [1×]	National Diagnostics, USA
Methanol (20% v/v)	VWR, UK

Item	Supplier
TBS-T	
Tris [0.25 mM]	Sigma-Aldrich, UK
Sodium chloride [137mM]	Sigma-Aldrich, UK
Potassium chloride [2.7mM]	Sigma-Aldrich, UK
Tween-20 (0.05% v/v)	Sigma-Aldrich, UK
Mitochondrial Isolation Buffer	
Calcium chloride [0.75mM]	Sigma-Aldrich, UK
HEPES [20mM]	Sigma-Aldrich, UK
Sodium chloride [130mM]	Sigma-Aldrich, UK
Potassium chloride [4.5mM]	Sigma-Aldrich, UK
Magnesium chloride [1.2mM]	Sigma-Aldrich, UK
Disodium phosphate [1mM]	Sigma-Aldrich, UK
D-Glucose [21mM]	Sigma-Aldrich, UK
Sodium pyruvate [5mM]	Sigma-Aldrich, UK

2.1.7. Antibodies

Item	Supplier
Anti-HCV NS3 antibody (Mouse monoclonal)	Virogen, UK
Anti-Hepatitis C Virus Core Antigen antibody (C7-50)	Abcam, UK
Alexa Fluor® 594 Donkey Anti-Mouse IgG (H+L)	Invitrogen, UK
Alexa Fluor® 488 Donkey Anti-Mouse IgG (H+L)	Invitrogen, UK
Anti-HCV NS3 antibody (Mouse monoclonal)	Virogen, UK
Mouse Anti-TXNIP/VDUP1 JY1 clone antibody	MBL International, USA
Rabbit anti-Actin	Sigma-Aldrich, UK
Polyclonal Goat Anti-mouse Immunoglobulins HRP	Dako, UK

2.1.8. siRNA sequences (simplex) – Sigma-Aldrich

siRNA	Sequence
siTXNIP (TXNIP-1)	5'-CAUCCUUCAAAGGAAAAUA[dT][dT]-3'
siN/T	5'-GAUCAUACGUGCGAUCAGA[dT][dT]-3'
siMlx (Mlx-1)	5'-GAGUAUGCCUACAGCGACA[dT][dT]-3'

2.1.9. Primer Sequences – Invitrogen

2.1.9.1. Reference

Gene	Forward	Reverse
GAPDH	5'-CCCAATACGACCAAATCCG-3'	5'-CTCTGCTCCTCCTGTTCGAC-3'
HCV	5'-TCTGCGGAACCGGTGAGTA-3'	5'-TCAGGCAGTACCACAAGGC-3'

2.1.9.2. ER stress markers

Gene	Forward	Reverse
STC2	5'-TACCTCAAGCACGACCTGTG-3'	5'-AGCAAGTTCACGAGGTCCAC-3'
HSPA5	5'-CACAGTGGTGCCTACCAAGA-3'	5'-TGTCTTTTGTCAGGGGTCTTT-3'

2.1.9.3. Mitochondrial DNA (mtDNA)

Gene	Forward	Reverse
mtDNA	5'-TCTAAGCCTCCTTATTCGAGC-CGA-3'	5'-TTTCATCATGCGGAGATGTTGGA-TGG-3'

2.1.9.4. Glucose metabolism

Gene	Forward	Reverse
CYCS	5'-GGCGTGTCCTTGGACTTAGA-3'	5'-GTGTGGCACTGGGAACACTT-3'
ATP5L	5'-ATGGCCCAATTTGTCCGTAA-3'	5'-CAGCTCAACCTTGGCGTAGT-3'
NDUFAF4	5'-AGCAAGATGAAGCCCTCTGT-3'	5'-TCCTTCGGCTCTTGACATGT-3'
NDUFAF5	5'-TGCATCGAGACACAATGCTG-3'	5'-CCGGTGGCATAAGGTTGTTT-3'
OGDH	5'-GGCCAGATCCAGCTTTGATG-3'	5'-AGGAGGTCAAAGGGGAATGG-3'
ACLY	5'-CCACACTGCAAACTTCCTCC-3'	5'-GTGGTGCTCTTTCCTTGTGG-3'
PPARGC1A	5'-TCAAGCCACTACAGACACCG-3'	5'-GCCTCTCGTGCTGATATTCC-3'
MLX	5'-GTGTGTCTTCAGCTGGATCG-3'	5'-CCTCTTGTTGGCTGTTCTCC-3'

2.1.9.5. Lipid metabolism

Gene	Forward	Reverse
TXNIP	5'-ATAAAAGCCCTTTGAACCCC-3'	5'-GCTCAGTGCTCTGACACAGG-3'
ELOVL4	5'-CTGGTCCATCGCAGATAAGC-3'	5'-AGGTTCTCGGTCCTTCATCC-3'
ELOVL7	5'-CTATGGACTTTCTGCATTGGG-3'	5'-AACTGGCTTATGTGGATGGC-3'
FABP3	5'-AGTTCAGTCAGTGATGGGGC-3'	5'-GAACCTGAATTCTGGAAAGGG-3'
IRS2	5'-ACCTACGCCAGCATTGACTT-3'	5'-CATCCTGGTGATAAAGCCAGA-3'
ACSL3	5'-ACACAAGGGCGCATATCTTC-3'	5'-AGGGTGGCAAATGTTACAGC-3'
ARRDC4	5'-TTGGTTTTGTGAGCTGAGAGC-3'	5'-CAGTATTCTGCAGGGGAAGC-3'

2.1.10. Cells

Item	Supplier
Huh7	Dr. Marcus Dorner (Imperial College)
Huh7.5	Dr. Marcus Dorner (Imperial College)
HCV SGR (gt2a)	Samantha Blackham (Imperial College)

2.1.11. Plasmids

Item	Supplier
pJFH-1	Takaji Wakita (National Institute of Infectious Diseases)

2.2. Methods

2.2.1. Re-evaluation of Microarray Data

The datasets from a microarray study involving the infection of Huh7 cells with the JFH-1 isolate of HCV were downloaded as .CEL files from the Gene Expression Omnibus (accession: GDS4160) [214]. A database of genes was produced from the raw data using Partek software and analysed using Principle Components Analysis (PCA) with 2-way ANOVA. The Gene IDs and corresponding fold changes were cross-referenced with the GeneGO™ Metacore™ database for gene ontology and pathway analysis.

2.2.2. Cell culture

a) Propagation of cell lines:

Frozen stocks of cells were thawed and resuspended in 9 ml of complete DMEM in a T75cm^2 tissue culture flask. Growth medium was replaced 24 hours later and cells were grown to full confluence at 5% CO_2 and 37^{o}C. HCV SGR cells received a 1% (v/v) supplement of G418 (Geneticin) in complete DMEM.

b) Trypsinisation of cell lines:

T75cm^2 culture flasks were removed from incubation and cells were washed with phosphate buffered saline (PBS). Cells were treated with 1× Trypsin, incubated at 37^{o}C for 3 minutes, and displaced by agitation.

1× Trypsin was inactivated by the addition of complete DMEM. Trypsinised cells were centrifuged at 400×g for 5 minutes at room temperature, and resuspended in 5 ml of complete DMEM.

c) Quantification of cells:

This method was based on instructions provided by Abcam (http://www.abcam.com/protocols/counting-cells-using-a-haemocytometer). A 10µl aliquot of resuspended cells was diluted 1:2 to with Trypan Blue. Total cell number was determined by duplicate cell counts in 4 fields of a Neubauer haemocytometer using a ×10 objective lens under light microscopy.

d) Cell seeding densities for functional experiments:

Gene expression: 5×10^5 Huh7 cells for JFH-1 experiments and 4.5×10^5 cells for HCV SGR experiments were seeded into T25cm^2 tissue culture flasks.

Fluorometric/colourimetric analyses: 5×10^3 cells were seeded in triplicate wells of a 96-well plate.

ORO staining/siRNA transfection: 1.48×10^5 cells were seeded in triplicate wells of a 6-well plate.

Immunofluorescence: 6×10^4 cells were seeded onto Rinzl plastic coverslips.

JFH-1 virus titration: 9×10^4 Huh7.5 cells were seeded onto plastic square 18×18mm coverslips for titration of JFH-1 virus.

e) HCV gt2a infection models:

The JFH-1 infection of Huh7 cells was prepared by replacing the culture medium of Huh7 cells cultured in T25cm^2 flasks at 24 hours post-seeding with 5mls of complete DMEM.

Cells were infected with HCV at MOI – 7.5 or mock infected with an equal volume of conditioned medium. Cells were incubated at 37^{o}C and 5% CO_2, and analyses were carried out at 24 hours and 48 hours post-infection. HCV SGR experiments were performed by seeding Huh7 and HCV SGR cells into T25cm^2 tissue culture flasks and incubated at 37^{o}C and 5% CO_2. Analyses were carried out 24 hours and 48 hours post-seeding.

f) Treatment of cell lines:

HCV gt2a infection models were treated with 50 µM of STF-083010 or an equivalent volume of DMSO for ER stress and UPR experiments. For mitochondrial dysfunction and calcium homeostasis experiments, HCV gt2a infection models were treated with a volume of L-glutamate dissolved in complete DMEM [5 mM] at a final concentration of 0.5 mM.

g) Preparation of frozen stocks of cells:

Huh7 and HCV SGR cell lines were grown to confluence, washed, trypsinised, and resuspended in 1ml of foetal bovine serum with 10% (v/v) of DMSO in a 1ml cryogenic vial. Stocks were stored at -80^{o}C.

2.2.3. Isolation and Purification of Nucleic Acids

a) Cell Lysis using TRIzol® Reagent

This method was adapted from Blackham [(215)]. Growth media was removed from cells cultured in T25cm^2 flasks prior to treatment with 750 µl of TRIzol® reagent and incubation at room temperature for 5 minutes. TRIzol® lysates were homogenised and transferred to sterile 1.7 ml Eppendorf tubes.

b) Isolation of Total Cellular RNA

RNA was isolated by adding 200 µl of chloroform to TRIzol® lysate, shaken vigorously for 15 seconds, and incubated at room temperature for 3 minutes. Samples were spun at 12,201×g and 4˚C for 15 minutes in a Hawk 15/05 microcentrifuge (MSE, UK). The aqueous phase was transferred to a 1.7 ml Eppendorf tube and 500 µl of Isopropanol was added. Samples were mixed by inversion and incubated at room temperature for 10 minutes. Samples were centrifuged at 12,201×g for 10 minutes at 4˚C and supernatant was discarded. RNA pellets were washed with 1 ml of 75% (v/v) ethanol and centrifuged at 7,532×g for 5 minutes at 4^{o}C, the supernatant discarded, and the RNA pellet was air-dried for 15 minutes. Total cellular RNA was dissolved in 20 µl of nuclease-free water and genomic DNA was removed using the DNA-free Turbo DNAse kit according to manufacturer's instructions. The concentration and purity (A260/280) of RNA was determined using a NanoDrop Lite Spectrophotometer (Thermo Fisher Scientific, UK) prior to storage at -80^{o}C.

c) Isolation of Extracellular viral RNA

A 500 µl aliquot of growth medium was removed from JFH-1 infected Huh7 cell culture and cleared by centrifugation at 2,000×g for 5 minutes at room temperature before transfer to a new 1.7ml Eppendorf tube. TRIzol®/Chloroform extraction of RNA was performed as described (**section 2.2.3b.**).

d) Isolation of Total Cellular DNA

This method was based on manufacturer's instructions (Invitrogen, UK). 150 µl of ice cold absolute ethanol was added to the lower organic phases of TRIzol® lysates used to extract total RNA. Samples were mixed and incubated at room temperature for 5 minutes. Samples were centrifuged at 5,183×g for 5 minutes at 4^{o}C in a Hawk 15/05 microcentrifuge (MSE, UK) and the supernatant discarded. Nucleic acids were washed with 750 µl of 0.1M sodium citrate in 10% ethanol for 30 minutes at room temperature and pelleted via centrifugation at 5,183×g for 5 minutes at 4^{o}C in a Hawk 15/05 microcentrifuge (MSE, UK). The supernatant was discarded and the wash step repeated. The pellet was washed with 1 ml of 75% ethanol and incubated at room temperature for 1 hour. Samples were then centrifuged at 5,183×g for 5 minutes at 4^{o}C and the supernatant discarded. The DNA pellet was air-dried for 15 minutes, dissolved in 20 µl of nuclease-free water, and made to 350 µl with TE buffer. 350 µl of 25:24:1 phenol:chloroform:isoamyl alcohol was added and the mixture was shaken for 15 seconds prior to centrifugation at 15,682×g for 15 minutes at room temperature in a 5415 D microcentrifuge (Eppendorf, UK). The aqueous phases were transferred to 1.7 ml Eppendorf tubes and 0.1 volumes of 3M Sodium Acetate (pH 5.2) and 2.5 volumes of ice cold 100% ethanol were added. Mixtures were stored overnight at -80^{o}C, and centrifuged in a 5415 D microcentrifuge (Eppendorf, UK) at 15,682×g for 45 minutes at room temperature. The pellets were washed in 1 ml of 75% ethanol and centrifuged at 15,682×g for 5 minutes at room temperature before air-drying for 15 minutes.

DNA pellets were dissolved in 20 µl of nuclease-free water and the concentration and purity (A260/280) was determined using a NanoDrop Lite spectrophotometer (Thermo Fisher Scientific, UK).

2.2.4. PCR Primer Design

Primer sequences were obtained from previous work or via submission of the Human Genome Organisation (HUGO) name for genes of interest to the qPrimerDepot database (http://primerdepot.nci.nih.gov/) [214,215]. Sequences were cross-referenced for target specificity using PrimerBLAST. Primer annealing temperatures were optimised by preparing single qRT-PCR reactions using 200ng of template RNA and tested empirically at 50 – 60^{o}C.

2.2.5. Quantitative Reverse-Transcription Polymerase Chain Reaction (qRT-PCR)

This protocol was adapted from the method used by Blackham and used for measuring gene transcription in Huh7 and HCV SGR cells [215]. A PCR mastermix containing 2× QuantiTect SYBR Green (5 µl per reaction) and reverse transcriptase (RT, 0.1 µl per reaction) was prepared in a 1.7 ml Eppendorf tube and dispensed into separate Eppendorf tubes. To the reaction mix, 1 µl of forward and reverse primers [5mM] were added and the volume adjusted to 10 µl using nuclease-free water (minus the volume containing 400 ng of total cellular RNA (**section 2.2.3b.**)). PCR mixes were mixed and dispensed into PCR lightcycler capillaries in triplicate.

400 ng of total cellular RNA was added to each reaction and a no-template control (NTC) was included for each primer tested. The following program was used to perform qRT-PCR; 1 cycle at 50°C for 15 minutes (Reverse Transcription) and 40 cycles for qPCR; 95°C for 15 minutes (Activation), 50 - 60°C for 30 seconds (Annealing), 72°C for 30 seconds (Extension), and 94°C for 15 seconds (Denaturation). Relative gene expression was calculated using the $\Delta\Delta C_T$ equation (**Equation 1**) [460].

Equation 1. –The ΔΔCT Equation

1. $$\Delta\Delta CT = \mathbf{Test\ (Gene\ of\ Interest\ CT - Reference\ Gene\ CT)} - \mathbf{Control\ (Gene\ of\ Interest\ CT - Reference\ Gene\ CT)}$$

$$\boldsymbol{Relative\ Fold\ change\ in\ Gene\ transcription} = 2^{-\Delta\Delta CT}$$

2. $$\boldsymbol{Negative\ inverse} = \frac{-1}{\Delta\Delta CT}$$

2.2.6. Isolation of JFH-1 Plasmid DNA (pJFH-1) from bacterial stocks

Frozen stocks of *E. coli* cells containing the pJFH-1 plasmid construct (pJFH-1) were picked and spread on LB Agar plates before overnight incubation at 37°C. Colonies were picked and used to inoculate 5 ml of Luria Broth [50 µg ml^{-1} Ampicillin] prior to overnight incubation at 220rpm and 37°C in a shaking incubator.

Bacterial sub-cultures were centrifuged at 1,261×g for 10 minutes at room temperature and pJFH-1 plasmid DNA was extracted using a QIAprep Spin Mini-prep kit according to manufacturer's instructions.

2.2.7. Preparation of pJFH-1 Plasmid DNA

13 µg of pJFH-1 plasmid DNA was linearised by adding 0.5 µl of 100× BSA, 1 µl of *Xba*I [20,000 units ml^{-1}], 5 µl of 10× NEBuffer 2, 2 µg of pJFH-1, and the volume made to 50 µl with nuclease-free water. The mixture was incubated at 37^{o}C for 6 hours and heat-inactivated at 65^{o}C for 20 minutes. 2 µl Mung Bean Nuclease (10,000u ml^{-1}), 2.5 µl 10× Mung Bean Nuclease Buffer, and 10.5 µl nuclease-free water was added to 10 µl of linearised JFH-1 DNA, and the reaction mix was incubated in a water bath at 37^{o}C for 1 hour. The reaction was inactivated by proteinase K digestion and JFH-1 DNA was extracted using sodium acetate/ethanol precipitation (**section 2.2.3d.**)

2.2.8. *In vitro* transcription of JFH-1 RNA

JFH-1 RNA was synthesised using the T7 Megascript kit according to manufacturer's instructions. In summary, a 20 µl T7 Megascript reaction mix was prepared in a 1.7 ml Eppendorf tube containing 2 µl of each ribonucleotide (rATP, rUTP, rGTP, and rCTP), ~1 µg of linearised JFH-1 DNA, 2 µl of 10× Reaction Buffer, 2 µl of Enzyme Mix, and the volume made to 20 µl using nuclease-free water. The transcription reaction was incubated overnight in a water bath at 37^{o}C, and JFH-1 RNA was isolated using TRIzol® extraction (**section 2.2.3b.**).

2.2.9. Production of infectious Hepatitis C virus (JFH-1)

This method was adapted from Baillie [461]. 6×10^{5} Huh7.5 cells were seeded into a well of a 6-well plate in 2 ml of DMEM supplemented with 10% FBS without antibiotics and incubated overnight at 37^{o}C and 5% CO_2. Cells were removed from incubation and culture medium was replaced with 1 ml OptiMEM transfection medium and returned to incubation for 1 hour. 2 µg of T7 JFH-1 RNA in 500 µl of OptiMEM was incubated at room temperature for 20 minutes to prepare a JFH-1 RNA mastermix. 4 µl of Lipofectamine 3000™ in 500 µl of OptiMEM was incubated at room temperature for 5 minutes to prepare a Lipofectamine mastermix. JFH-1 RNA and Lipofectamine 3000™ mastermixes were combined, mixed, and incubated at room temperature for 20 minutes. Cells were removed from incubation and OptiMEM was replaced with 1 ml of Lipofectamine 3000™/JFH-1 RNA mix.

Cells were incubated overnight and transfection media was replaced with 2 ml of antibiotic-free DMEM the following day.

2.2.10. Production of JFH-1 virus stocks via serial passage

This method was based on a protocol published by Yi [462]. Huh7.5 cells were prepared 1:4 in T75cm^2 cell culture flasks (**section 2.2.2.**). The following day, growth media was removed and the cells treated with 1.5 ml of JFH-1 infectious media and incubated at 37^{o}C and 5% CO_2 for four hours before a further 13.5 ml of complete DMEM was added. Infected

2.2.11. Preparation of JFH-1 virus stocks

Infectious media was collected every 4 days and cleared by centrifugation at 2,000×g for 5 minutes. The supernatant was filtered through a 0.45µm 150 ml filter unit and concentrated using an Amicon® Ultra-15 Centrifugal Filter Device by centrifugation at 4,000×g and 4^{o}C for 20 minutes. Growth media from naive Huh7.5 cells was collected, cleared, filtered, and concentrated as above to prepare conditioned medium for mock infected controls.

2.2.12. Immunostaining of HCV Antigens

At 24 hour and 48 hour time points, cells were removed from incubation, growth media was discarded and the cells washed with PBS. Cells were fixed with 4% paraformaldehyde for 30 minutes at room temperature. Fixed cells were permeabilised using 0.1% Triton X-100 in PBS for 20 minutes at room temperature and blocked with 1% BSA in PBS for 30 minutes. 1% BSA in PBS was removed and the cells were incubated with 1/100 mouse anti-HCV NS3 antibody (HCV SGR, Huh7 cells), or 1/200 mouse anti-HCV core C7-50 (mock, JFH-1 infected Huh7 cells) for one hour at room temperature. The cells were washed three times with PBS for 5 minutes at room temperature and incubated with either 1/200 Alexa Fluor 488 donkey-anti mouse (HCV SGR, Huh7 cells) or 1/600 Alexa Fluor 594 donkey-anti mouse (mock, JFH-1 infected Huh7 cells) antibodies for one hour at room temperature. The cells were washed three times with PBS for 5 minutes at room temperature and coverslips were mounted onto Shandon microscope slides using 1/1000 4',6-diamidino-2-phenylindole (DAPI) in Mowiol mounting medium. Slides were observed under a Nikon TE2000-S fluorescent microscope and images were captured with Lucia G software.

2.2.13. Titration of JFH-1 infectivity

9×10^4 Huh7.5 cells were seeded onto 0.1% gelatin-coated plastic coverslips in a 12-well plate and incubated at 37°C and 5% CO_2 overnight. At time of infection, growth media was replaced with 650 µl of DMEM. Duplicate wells were inoculated with a 100 µl volume of concentrated JFH-1 virus stock in DMEM that corresponded to 1×10^{-2}, 1×10^{-3}, or 1×10^{-4} dilutions. Infected cells were incubated at 37°C and 5% CO_2 for 48 hours, after which the infectious media was discarded, cells were fixed and stained for HCV core (**section 2.2.12.**). Focus Forming Units (FFUs) of HCV core protein were counted and the titre of the virus stock calculated.

2.2.14. cDNA synthesis (Two-step PCR)

This method was taken from Blackham and used for measuring gene transcription in Mock- and JFH-1 infected Huh7 cells [215]. 1µg of d(T) primers were added to 2 µg of total RNA from mock and JFH-1 infected Huh7 cells and the volume made to 12.5 µl with nuclease-free water. Samples were incubated at 70°C for 5 minutes in a Progene DNA Thermocycler (Techne, UK), and placed on ice for 2 minutes. 1 µl of M-MLV Reverse Transcriptase (200 units μl^{-1}), 5 µl of 5× M-MLV Reverse Transcriptase Buffer, 0.625 µl of Recombinant RNAsin ribonuclease inhibitor (40 units μl^{-1}), 5 µl of dNTP mix (10 mM), and 0.875 µl of nuclease-free water were added to each reaction.

Reactions were incubated at 42°C for 60 minutes in a Progene DNA Thermocycler (Techne, UK) and cDNA concentration was determined using a NanoDrop Lite spectrophotometer (Thermo Fisher Scientific, UK) prior to storage at -20°C. qPCR reactions to measure gene transcription in JFH-1 infected Huh7 cells were prepared by combining 2× QuantiTect SYBR Green PCR Mastermix (5 µl per reaction), 1 µl of forward and reverse primer mix [5 mM], and the volume adjusted to 10 µl using nuclease-free water (minus the volume containing 900 ng of cDNA). PCR mixes were mixed and dispensed into PCR lightcycler capillaries in triplicate. 900 ng of cDNA was added to each reaction and a no-template control (NTC) was included for each primer tested. The PCR program was run under the same conditions as described **section 2.2.5.**, and fold changes were calculated using the $\Delta\Delta C_T$ method (**Equation 1**).

2.2.15. Absolute Quantitation of Intracellular/Extracellular HCV

qRT-PCR reactions were prepared as described in **section 2.2.5.** using 1 µg of total RNA from HCV SGR- or JFH-1 infected Huh7 cells (**section 2.2.3b**) for intracellular virus quantitation, or 0.1 volumes of RNA isolated from infectious media (**section 2.2.3c**) for extracellular virus quantitation along with a series of JFH-1 RNA standards [6 ng – 60 fg]. A standard curve was generated using Roche Lightcycler software and the second derivative maximum method. Absolute values (computed concentration) were converted to genome copy number by **Equation 2** [215].

Equation 2. – Calculation of Absolute Genome Copy Number

$$Genome\ copy\ no. = \frac{Computed\ concentration \times PCR\ Amplicon\ RMM}{Avogadro's\ constant}$$

Therefore:

$$Genome\ copy\ no. = \frac{Computed\ concentration \times 50826}{6 \times 10^{23}}$$

2.2.16. Preparation of Total Cellular Protein

a) Cell Lysis

HCV gt2a infection models were removed from incubation at 37°C and 5% CO_2 at 24 hour and 48 hour time points and growth medium was discarded. The cells were washed with room temperature PBS, treated with 1 ml of Triton X-100 lysis buffer and incubated at room temperature for 5 minutes. The cell lysates were transferred to 1.7 ml Eppendorf tubes and stored at 4°C for 30 minutes, followed by centrifugation in a Hawk 15/05 microcentrifuge (MSE, UK) at 11,984×g and 4˚C for 20 minutes. Protein supernatants were transferred to 1.7 ml Eppendorf tubes before quantification using the Bradford assay.

b) Bradford Assay

2 µl of protein lysate was dispensed into triplicate wells of a 96-well plate along with bovine serum albumin (BSA) standards [0.25 – 2.5 mg ml^{-1}] in Triton X-100 lysis buffer.

Samples were treated with 98 µl of Bradford reagent and incubated at room temperature for 5 minutes before absorbance was read at 595nm in a Multiskan™ GO Microplate reader (Thermo Fisher Scientific, UK).

c) Concentration of Total Cellular Protein Lysates

Total cellular protein lysates were mixed with 1 ml of ice cold acetone and stored at -80^{o}C for 1.5 hours. The mixtures were centrifuged in a Hawk 15/05 microcentrifuge (MSE, UK) at 12,201×g and 4˚C for 20 minutes, the supernatant discarded, and the pellet air dried for 15 minutes prior to resuspension in 100 µl of Triton-X 100 lysis buffer. Protein concentrate was quantified using the Bradford assay (**section 2.2.16b.**).

2.2.17. miR-17 Expression (miScript PCR)

300 ng of Total cellular RNA (**section 2.2.3b.**) was used to synthesise miR-17 cDNA using the miScript II RT kit as suggested by the manufacturer. 3 ng of miR-17 cDNA was used to perform qRT-PCR with miR-17 and U6 (internal control) primers in triplicate using the miScript primer assay kit according to manufacturer's instructions.

2.2.18. 2% TBE Agarose Gel Electrophoresis

50 ml of 1× Tris-Borate EDTA buffer (TBE) was filtered into a conical flask. 1 g of molecular grade agarose was dissolved by heating and allowed to cool before 3 µl of Sybr Safe was added. Agarose gel was poured into an electrophoresis tank and allowed to set prior to immersion in 1× TBE buffer. 12 µl of PCR product in 6× DNA loading buffer and nuclease-free water, and a 10kb DNA Ladder was loaded before the gel was run at 60v for 50 minutes. Visualisation was performed using a Molecular Imager® Gel Doc XR+ (Bio Rad, UK) and images were taken using Image 4.1 software.

2.2.19. Measurement of Intracellular Calcium

a) Cytosolic calcium

This protocol was modified from a method published by Griffiths *et al* [463]. At 24 hour and 48 hour time points, growth media was removed from HCV gt2a infection models. The cells were washed twice with Ca^{2+}/Mg^{2+}-free PBS, treated with Indo-1 [10µM] in Ca^{2+}/Mg^{2+}-free PBS, and incubated at 37°C and 5% CO_2 for 30 minutes. The Indo-1 stain was removed and the cells were washed twice with Ca^{2+}/Mg^{2+}-free PBS. The cells were rested in Ca^{2+}/Mg^{2+}-free PBS for 15 minutes before cytosolic calcium was measured by reading absorbance at 405nm using a Multiskan™ GO Microplate reader (Thermo Fisher Scientific, UK).

b) Mitochondrial calcium

Following measurement of cytosolic calcium ion concentration, Ca^{2+}/Mg^{2+}-free PBS was removed and the cells were treated with 150 µl of Mitochondrial Isolation Buffer. The cells were incubated at room temperature for 2.5 hours and 37°C and 5% CO_2 for an additional 1.5 hours. Mitochondrial Isolation Buffer was removed following incubation and the cells were washed twice with Ca^{2+}/Mg^{2+}-free PBS. The cells were rested in Ca^{2+}/Mg^{2+}-free PBS at room temperature for 15 minutes before Mitochondrial calcium was measured by reading absorbance at 405nm in a Multiskan™ GO Microplate reader (Thermo Fisher Scientific, UK).

2.2.20. Measurement of Reactive Oxygen Species (ROS)

At 24 hour and 48 hour time points, growth medium was removed from HCV gt2a infection models, the cells washed twice with PBS, and stained with 2',7'-dichlorofluoroscein diacetate (H2DCFDA) [50 µM] in PBS. The cells were incubated at 37°C and 5% CO_2 for 30 minutes. The stain was removed, the cells washed twice with PBS, and rested in PBS for 15 minutes. Absorbance was read at 490nm in a Multiskan™ GO Microplate reader (Thermo Fisher Scientific, UK).

2.2.21. Determination of Mitochondria-Associated Apoptotsis Activity (Mitochondrial ToxGlo™)

At 24 hour and 48 hour time points, Huh7 and HCV SGR cells were removed from incubation, the growth medium removed, and the cells washed with PBS. The cells were treated with 30 µl of bis-AAF-R110 in Assay Buffer and incubated at 37^{o}C and 5% CO_2 for 30 minutes before fluorescence was measured at 485nm in a Multiskan™ GO Microplate reader (Thermo Fisher Scientific, UK) in accordance with manufacturer's instructions. A standard curve was prepared by treating Huh7 cells with H_2O_2 [10 µM – 10 nM] and incubating at 10% CO_2 and 37^{o}C for 30 minutes prior to assay.

2.2.22. Assessment of Mitochondrial Membrane Potential

At 24 hour and 48 hour time points, growth medium was removed and cells were treated with 50 µl of tetramethyl rhodamine ethyl ester (TMRE) [500 nM] in DMEM and incubated at 37^{o}C and 5% CO_2 for 20 minutes. Cells were washed once in 0.2% bovine serum albumin in PBS and rested in 50 µl of 0.2% BSA for a further 15 minutes. A subset of cells was treated with carbonyl cyanide-4-(trifluoromethoxy)phenyl hydrazone (FCCP) as a control. Fluorescence was measured at 549nm by reading in a Multiskan™ GO Microplate reader (Thermo Fisher Scientific, UK).

2.2.23. Long PCR of Mitochondrial DNA (mtDNA)

This protocol was modified from that published by Santos *et al* [464]. Reactions were prepared using 75 ng of total cellular DNA (**section 2.2.3d.**), 12.5 µl of 2× PCRBIO Ultra Mix™, 1 µl of forward and reverse primer mix [5µM] and the volume adjusted to 25 µl using nuclease-free water. PCR reactions were run in a Progene thermocycler (Techne, UK) under the following cycling conditions; 75°C for 2 minutes (activation), 94°C for 1 minute (denaturation), 19 cycles of 94°C for 15 seconds followed by 64°C for 12 minutes, 72°C for 10 minutes (extension), and 25°C (final hold). PCR products were run on a 2% TBE agarose gel (**section 2.2.18.**).

2.2.24. Staining of Intracellular Lipid Droplets (LDs)

a) Oil-Red-O staining:

Fixed HCV gt2a infection models were stained with 500 µl of Oil-Red-O and placed on an orbital shaker at 100rpm for 30 minutes. The ORO stain was removed and the cells differentiated using 1 ml of 60% isopropanol at room temperature for 5 minutes. Cells were washed with 1 ml of dH_2O and the nuclei were counterstained with 500 µl of Harris' Haematoxylin. Cells were placed on an orbital shaker at 100rpm for 1 minute. The cells were rinsed with 1 ml of dH_2O following removal of Harris' Haematoxylin and placed on an orbital shaker at 100rpm for 10 minutes. Cells were examined under light microscopy using a ×40 objective lens on a Nikon TE2000-S microscope. Images were acquired with ACT-1 software.

b) Quantitation of intracellular lipid droplets using ImageJ:

This method was taken from that published by Deutsch *et al* [465]. Lipid quantitation, expressed as % area of image was achieved by converting original microscope images into an RGB stacked Montage, setting the threshold to include specific ORO stains, and percentage area measured using ImageJ software.

2.2.25. Determination of Intracellular [glucose]

This method was taken from The University of Maryland and prepared by Nam Sun Wang. 3.75 µg of total cellular protein in Triton X-100 lysis buffer (**section 2.2.16c.**) was made to 150 µl using dH_2O in sterile 0.6 ml microfuge tubes and 150 µl of 3',5'-Dinitrosalicylic acid (DNS) reagent solution was added. Samples were incubated at 90^{o}C for 15 minutes. 40% (v/v) potassium sodium tartrate solution was added to each sample before cooling to room temperature for 30 minutes. The absorbance for each sample was measured at 575nm in a Multiskan™ GO Microplate reader (Thermo Fisher Scientific, UK).

2.2.26. Determination of Intracellular glycogen content

This method was taken from that published by Kumari e*t al* [466]. 3.75 µg of whole cell protein lysate in Triton X-100 lysis buffer was dispensed in triplicate wells of a 96-well plate and adjusted to 25 µl using Triton X-100 protein lysis buffer. 25 µl of Iodine-Potassium Iodide (IKI) working solution was added to each well and the plate was incubated on ice for 20 minutes. Absorbance was measured at 560nm using a Multiskan Go™ plate reader (Thermo Fisher Scientific, UK).

2.2.27. Quantification of Intracellular [triglyceride]

The Triglyceride Quantification kit (Abcam) was used according to manufacturer's instructions. 5 µg of total cellular protein in Triton X-100 lysis buffer was dispensed into triplicate wells of a 96-well plate. 1 µl of Lipase was added to each sample and the volume adjusted to 25 µl using triglyceride assay buffer. Reactions were incubated at room temperature for 20 minutes. 23 µl of triglyceride assay buffer, 1 µl of triglyceride probe, and 1 µl of triglyceride enzyme mix were added to each reaction. Reactions were incubated at room temperature for 1 hour and absorbance was read at 570nm in a Multiskan™ GO Microplate reader (Thermo Fisher Scientific, UK).

2.2.28. Western Blotting of Host and Viral Protein expression

This method was adapted from a method published by Bio-Rad. Samples were prepared by combining 50 µg of protein lysate with an equal volume of 4× Laemmli sample loading buffer and the volume adjusted to 50 µl using dH_2O. Samples were incubated at 95^oC for 5 minutes and placed on ice. Protein samples were loaded onto a 12% acrylamide gel along with 5 µl of Benchmark™ pre-stained protein standard and run at 200v for 45 minutes. Gel transfer was performed in 1× Transfer buffer at 100v for 1.5 hours and washed twice with 0.05% TBST for 5 minutes at room temperature, and blocked using 4% dry milk in TBST for one hour at room temperature. Proteins of interest were stained using primary antibodies (1/1000 dilution of mouse anti-VDUP1 (TXNIP) Clone JY1 Clone, 1: 2,000 rabbit anti-actin, 1/100 mouse anti-HCV NS3, mouse anti-HCV core) in 4% dry milk overnight at 4^oC. The membrane was washed three times with TBST for 5 minutes at room temperature and incubated with HRP-conjugated secondary antibodies (1/10,000 anti-mouse IgG, 1/10,000 anti-rabbit IgG) for one hour at room temperature. The membrane was washed three times with TBST for 5 minutes and treated with Clarity™ Luminol Enhancer reagent. Visualisation was performed in a Fusion FX7/SL Advance gel dock (Peqlab) and images were taken using Fusion-Capt Advance software.

2.2.29. siRNA-Mediated Knockdown of Host Genes

This method was obtained from Blackham [215]. HCV gt2a infection models were removed from incubation and growth medium was discarded. The cells were washed with 1 ml of OptiMEM before treatment with 500 µl of fresh OptiMEM and incubated at 37°C and 5% CO_2 for 1 hour. siRNA mixes were prepared using [25 nM] (siTXNIP) or [50 nM] (siMlx, siGAPDH) in 500 µl of OptiMEM and incubated at room temperature for 5 minutes. Lipofectamine 3000™ mixes were prepared by adding 1 µl of Lipofectamine 3000™ in 500 µl of OptiMEM and incubated at room temperature for 5 minutes. siRNA and Lipofectamine 3000™ mixes were combined and incubated at room temperature for 20 minutes. The cells were treated with siRNA and Lipofectamine 3000™ transfection mixes for and incubated at 37°C and 5% CO_2 for 8 hours. Transfection mixes were removed and replaced with 1 ml of antibiotic-free DMEM. Total cellular RNA from cell transfectants (**section 2.2.3b.**) and extracellular viral RNA (**section 2.2.3c.**) from infectious media was isolated at 24 hour and 48 hour time points.

2.2.30. Statistical Analysis

Statistical analysis was performed using single-factor ANOVA (MS Excel 2007) on triplicate $2^{-\Delta\Delta CT}$ values, calculated genome copy numbers, and fluorometric/colourimetric measurements ($\alpha = 0.05$).

Chapter 3: ER stress and Dysregulated Lipid Metabolism in HCV Infection

3.1. Overview:

The datasets from the microarray study of JFH-1 infected Huh7 cells by Blackham *et al*., were downloaded from the Gene Expression Omnibus (accession: GDS4160) and re-evaluated using Partek software with gene ontology analysis (GeneGO™ Metacore™) to identify cellular pathways that were disrupted during HCV infection. Two pathways that were induced during HCV infection included the glucose-dependent synthesis of polyunsaturated fatty acids (PUFAs) and the induction of the unfolded protein response (UPR) that follows Endoplasmic Reticulum (ER) stress. Initial transcriptomic profiling and measurement of intracellular [glucose] in HCV SGR cells cultured under glucose rich (control) and glucose-free conditions confirmed the results from the re-evaluated microarray data. Lerner *et al*., reported that TXNIP mRNA is regulated by mIR-17 abundance that is subject to degradation by the endoribonuclease activity of the UPR effector, inositol-requiring enzyme 1α (IRE-1α), which in turn can be inhibited by STF-083010. STF-83010 was applied to HCV gt2a models of infection and the effects on lipogenic gene transcription and HCV replication were measured using qRT-PCR. Inhibition of IRE-1α led to a downregulation of lipogenic gene transcription and a significant ($p= 5.4\times10^{-4}$) 3-fold reduction in intracellular virus replication in HCV SGR cells at 48 hours post-treatment whereas little difference was observed in the JFH-1 model. Data from this investigation suggest that UPR induction is more involved in the TXNIP-mediated dysregulation of lipid metabolism and replication of viral RNA in the HCV SGR model than in JFH-1 infected Huh7 cells.

3.2. Results & Discussion

As an initiative for this project, where the mechanisms by which TXNIP is overexpressed during HCV infection was investigated, the datasets from the microarray study of JFH-1 infected Huh7 cells by Andrew Baillie and Samantha Blackham (Imperial College) was obtained from the Gene Expression Omnibus and re-evaluated in collaboration with Dr. Stathis Giotis (Imperial College) [214].

3.2.1. Gene Ontology pathway analysis of re-evaluated Microarray data (PUFA Biosynthesis)

GeneGO™ Metacore™ pathway analysis was carried out using the re-evaluated datasets from the microarray study of JFH-1 infected Huh7 cells over 48 hours to identify candidate pathways that related to the upregulation of ELOVL4, ELOVL7, and ACSL3 that occurs during HCV infection as reported by Blackham (**Figure 17**) [214,215].

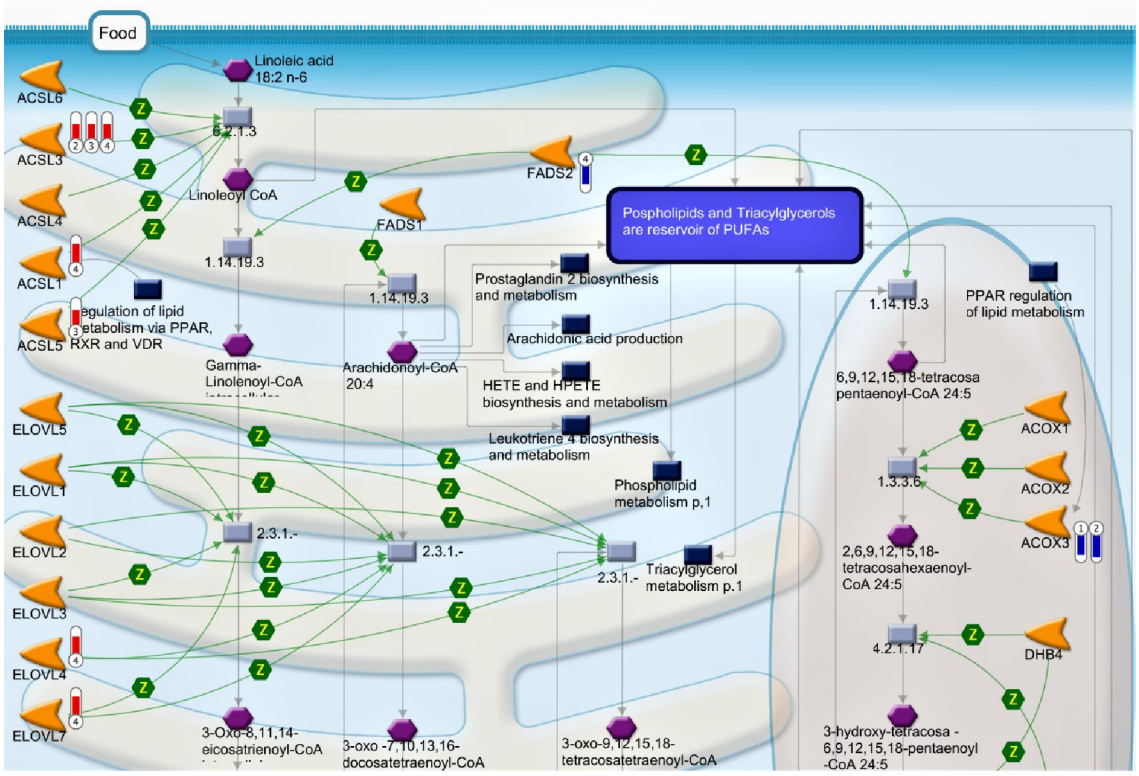


Figure 17 - GeneGO™ Metacore™ pathway analysis from re-evaluated microarray data (PUFA Biosynthesis)

PUFA biosynthesis is dysregulated during HCV infection. Red thermometers indicate gene upregulation and blue thermometers flag genes that are downregulated. Numbers 3 and 4 on each thermometer correspond to 24 hours and 48 hours post-infection, respectively. Genes of interest related to PUFA biosynthesis can be seen on the far-left of the diagram: **ACSL3** (+2.18-fold at 24 hours, p= 4.23×10^{-11}; +2.05-fold at 48 hours, p= 1.65×10^{-10}), **ELOVL4** (+2.38-fold at 48 hours, p= 1.62×10^{-8}), **ELOVL7** (+2.61-fold at 48 hours, p= 2.13×10^{-15}) [214,215].

Figure 17 supports the observations made by Blackham and shows that the upregulation of genes involved in fatty acid elongation (ELOVL4, ELOVL7) and fatty acid condensation (ACSL3) occurs during HCV infection. These are related to the biosynthesis of polyunsaturated fatty acids (PUFAs) which are reported to inhibit HCV replication [214,467].

These genes may be induced as a response to the intake of dietary glucose (food) during HCV replication and so preliminary studies involving the cell culture of Huh7- and HCV SGR cells under glucose-rich [25mM] (control) and glucose-free conditions were conducted to examine the influence of glucose concentration in the extracellular milieu on the transcription of TXNIP and lipogenic genes of interest over the course of 48 hours. The rationale for this experiment was to simulate the effect of glucose intolerance that is commonly seen in HCV and to identify other cellular pathways that may be peripheral to the dysregulation of host lipid metabolism which occurs during HCV RNA replication.

qRT-PCR was used to measure the transcription of genes examined in previous work that were considered to be representative of dysregulated lipid metabolism in JFH-1 infected Huh7 cells, i.e. lipogenesis (TXNIP), lipid droplet formation (ACSL3), fatty acid synthesis (ELOVL4, ELOVL7), and fatty acid transport (FABP3), along with glyceralde-3'-phosphate dehydrogenase (GAPDH) as an internal control at 24 hours and 48 hours post-seeding (**Figure 18 (A, B)**) [(215)].

3.2.2. Lipogenic Gene Transcription in HCV SGR cells +/- glucose (24, 48 Hours)

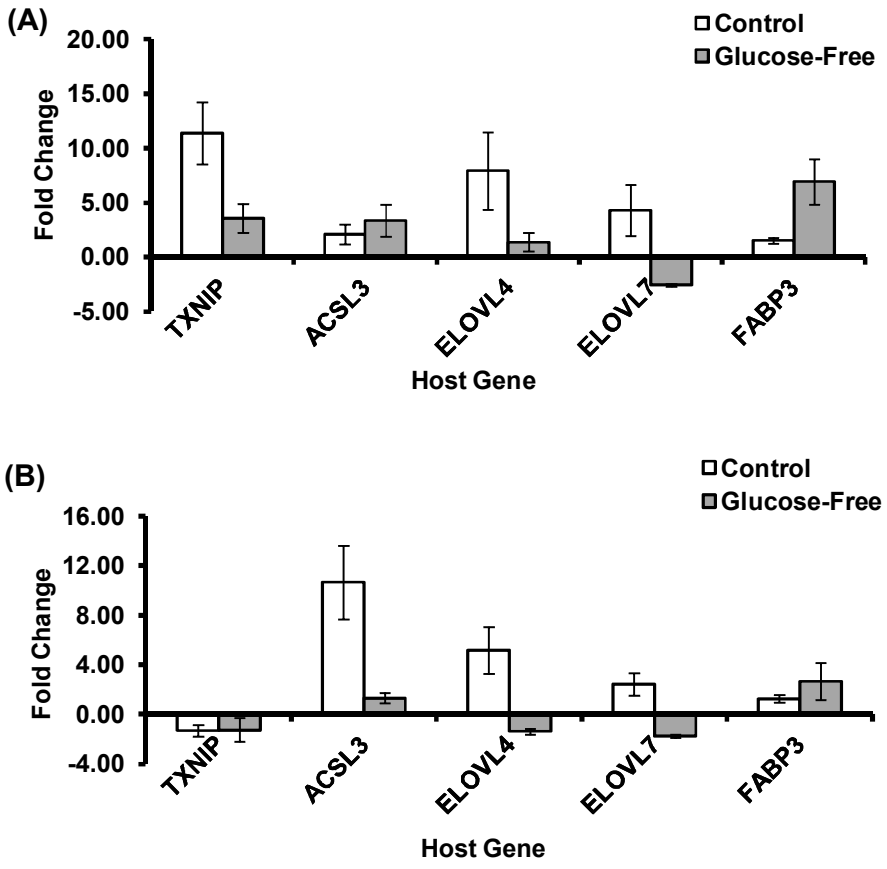


Figure 18 (A, B) – Lipogenic gene transcription in HCV SGR cells +/- glucose [25 mM] (24, 48 Hours)

Relative fold changes of lipogenic gene transcription measured in HCV SGR cells, compared to Huh7, seeded in control (white columns) and glucose-free (grey columns) culture medium at 24 hours and 48 hours post-seeding. Huh7- and HCV SGR cells were seeded under these conditions from a stock grown under glucose rich conditions. **(A)** Mean fold changes in HCV SGR gene transcription at 24 hours. **(B)** Mean fold changes in HCV SGR gene transcription at 48 hours. Genes assayed; Thioredoxin-interacting Protein (**TXNIP**), Acyl CoA synthetase long chain family member 3 (**ACSL3**), ELOVL Fatty Acid Elongase 4 (**ELOVL4**), ELOVL Fatty Acid Elongase 7 (**ELOVL7**), Fatty Acid Binding Protein 3 (**FABP3**). Data shown are averages of triplicate measurements from a single experiment with error bars representing standard deviation (SD). Graphs representing differences in cycle thresholds (ΔC_T) between cell lines under these conditions are shown in **Appendix A1.1 (A, B)**.

As shown in **Figure 18 (A)**, genes such as TXNIP (+11.40-fold, SD +/- 2.86), ELOVL4 (+7.92-fold, SD +/- 3.56), and ELOVL7 (+4.31-fold, SD +/- 2.35) are upregulated in HCV SGR cells under control conditions at 24 hours post-seeding. However, there is a significant (p= 0.05) reduction in the transcription of TXNIP (+3.58-fold, SD +/- 1.33), and a noticeable decrease in the mRNA abundance of downstream effectors of fatty acid synthesis, i.e. ELOVL4 (+1.39-fold, SD +/- 0.83) and ELOVL7 (-2.57-fold, SD +/- 0.13) when HCV SGR cells are cultured under glucose-free conditions at this time point. This finding indicates that glucose is a contributing factor to the transcription of TXNIP. However, FABP3, a protein that binds to and transports the phospholipid intermediate, lysophosphatidic acid (LPA), from the cytoplasm to the nucleus is upregulated (+6.93-fold, SD +/- 2.07) at 24 hours post-seeding when HCV SGR cells are deprived of glucose, which contrasts with that measured under the control condition (+1.53-fold, SD +/- 0.27) [468,469]. Additionally, the transcription of ACSL3, which is associated with the degradation of fatty acids as well as their condensation to form LDs at the ER is upregulated (+3.37-fold, SD +/- 1.46) under conditions of glucose deprivation and is comparable to transcription of this gene measured in HCV SGR cells under control conditions (+2.10-fold, SD +/- 0.93) at 24 hours post-seeding. This result could either mean that there is an increase in the mitochondrial or peroxisomal β-oxidation of fatty acids or, alternatively, that LD formation is upregulated in HCV SGR cells under conditions of glucose deprivation at 24 hours post-seeding [470,471].

The upregulation of lipogenic gene transcription in HCV SGR cells, in the absence of glucose, may result from ER stress and induction of the UPR that has been found to occur in the absence of glucose [472].

Figure 18 (B) shows that TXNIP transcription is downregulated in HCV SGR cells cultured under both control (-1.33-fold, SD +/- 0.47) and glucose-free conditions (-1.25-fold, SD +/- 0.95) at 48 hours post-seeding that suggests there is a refractory period in which the stimulus of TXNIP induction subsides. Moreover, the transcription of lipogenic genes downstream of TXNIP induction are downregulated less than 2-fold in HCV SGR cells grown under glucose-free conditions. This finding contrasts with the transcript abundance of ACSL3 (+10.65-fold, SD +/- 2.98), ELOVL4 (+5.17-fold, SD +/- 1.89), and ELOVL7 (+2.44-fold, SD +/- 0.91), that remain upregulated in HCV SGR cells cultured under control conditions which implies that intracellular glucose is a factor in PUFA biosynthesis and LD biogenesis in cells expressing HCV NS proteins over 48 hours post-seeding.

To see whether the presence of glucose in the extracellular milieu of Huh7- and HCV SGR cells corresponded to alterations in the transcription of genes concerned with glucose metabolism and calcium homeostasis, qRT-PCR was also performed to measure the transcript abundance of Max like protein (Mlx) and stanniocalcin 2 (STC2) in HCV SGR cells under control and glucose-free conditions at 24 hours and 48 hours post-seeding (**Figure 19 (A, B)**).

3.2.3. Gene Transcription of STC2 and Mlx in HCV SGR cells +/- glucose (24, 48 Hours)

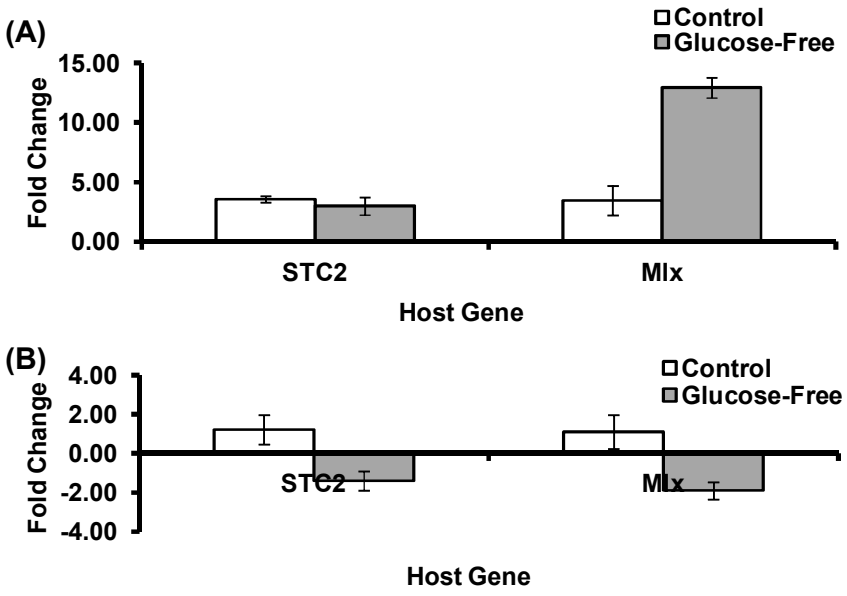


Figure 19 (A, B) - Gene transcription of STC2 and Mlx in HCV SGR cells +/- glucose [25 mM] (24, 48 Hours)

Relative fold changes in transcription of genes related to calcium regulation (STC2) and glucose metabolism (Mlx) measured in HCV SGR cells, compared to Huh7, seeded in control (white columns) and glucose-free (grey columns) culture medium at 24 hours and 48 hours post-seeding. Huh7- and HCV SGR cells were seeded under these conditions from a stock grown under glucose rich conditions. **(A)** Mean fold changes of gene transcription in HCV SGR cells at 24 hours. **(B)** Mean fold changes of gene transcription in HCV SGR cells at 48 hours. Data shown are averages of triplicate measurements from a single experiment with error bars representing standard deviation (SD). Genes assayed; Stanniocalcin 2 (**STC2**), Max like protein (**Mlx**). Graphs representing differences in cycle thresholds (ΔC_T) between cell lines under these conditions are shown in **Appendix A1.2 (A, B)**.

Figure 19 (A) shows that glucose concentration in the extracellular milieu does not affect the disturbance of calcium homeostasis, characterised by STC2 transcription, in HCV SGR cells as mRNA abundance is comparable under both control (+3.58-fold, SD +/- 0.25) and glucose-free (+3.02-fold, SD +/- 0.75) conditions.

This result also indicates that ER stress may be induced by the expression of HCV NS proteins as STC2 functions in the negative regulation of store operated calcium entry (SOCE) and the promotion of cell survival following induction of the unfolded protein response (UPR) [(473)].

Conversely, the transcript abundance of Max like protein (Mlx) is upregulated in HCV SGR cells under both control (+3.49-fold, SD +/- 1.25) and glucose-free (+12.96-fold, SD +/- 0.86) conditions. This is curious under glucose-free conditions as Mlx is a glucose-responsive protein that is displaced from the outer mitochondrial membrane (OMM), in tandem with hexokinase II, by glucose-6-phophate (G6P) in the initial stage of glycolysis. However, the upregulation of this gene may arise due to endogenous glucose production (EGP) via glycogenolysis or gluconeogenesis as a response to glucose deprivation which could explain the increase seen in TXNIP transcription at 24 hours post-seeding [(271)].

Figure 19 (B) shows that the transcription of both STC2 and Mlx in HCV SGR cells normalise to basal levels (< 2-fold) under both control and glucose-free conditions at 48 hours post-seeding which implies that the transcriptional induction of STC2, Mlx and TXNIP is an acute response to HCV NS protein expression in HCV SGR cells.

Thus, the DNS assay was performed on whole cell protein lysates isolated from Huh7 and HCV SGR cells cultured under control and glucose-free conditions to determine whether the upregulation in Mlx and TXNIP mRNA in HCV SGR cells were reflective of changes in intracellular glucose concentration via EGP (**Figure 20 (A, B)**).

3.2.4. Intracellular glucose concentration in Huh7 and HCV SGR cells +/- glucose (24, 48 Hours)

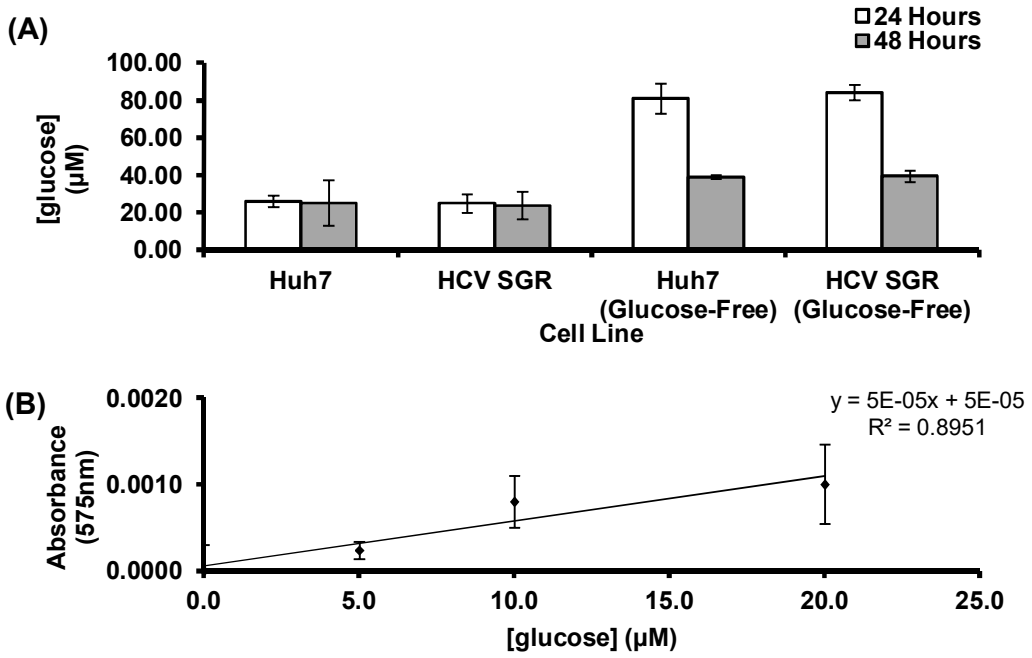


Figure 20 (A, B) - Average intracellular [glucose] (µM) in Huh7 and HCV SGR cells +/- glucose [25 mM] (24, 48 hours)

Intracellular [glucose] measured in Huh7 and HCV SGR cells cultured under control (glucose [25 mM]) and glucose-free conditions at 24 hours (white columns) and 48 hours (grey columns) post-seeding. Huh7- and HCV SGR cells were seeded under these conditions from a stock grown under glucose rich conditions. **(A)** Intracellular glucose concentrations (µM) measured in Huh7 and HCV SGR cells grown in control and glucose-free DMEM. **(B)** The standard curve produced at the time of assay using D-glucose standards [0 – 20 µM]. Data shown are averages of triplicate measurements from a single experiment with error bars representing standard deviation (SD).

Figure 20 (A) shows that intracellular glucose concentration does not alter in either Huh7 or HCV SGR cells cultured in medium containing high glucose [25mM] over 48 hours (mean= 25.05 μM, SD +/- 0.91). However, intracellular glucose concentration is higher at 24 hours and 48 hours post-seeding in both cell lines under glucose-free conditions, in comparison to controls, which suggests EGP is active under conditions of glucose deprivation. Given that TXNIP mRNA is elevated in HCV SGR, compared to Huh7 cells, at 24 hours post-seeding and intracellular glucose concentration is comparable between both cell lines over 48 hours, it can be said that the upregulation of TXNIP mRNA is not involved in the production of endogenous glucose in HCV SGR cells [(451)].

Thus, to examine whether the reduced overexpression of TXNIP had an effect on the replication of viral RNA under glucose-free conditions, absolute quantitation of HCV genome copy number was performed using one-step qRT-PCR, JFH-1 RNA standards [6 ng – 60 fg], and total cellular RNA isolated from HCV SGR cells cultured under control and glucose-free conditions at 24 hours and 48 hours post-seeding (**Figure 21**).

3.2.5. Intracellular HCV SGR genome copy number in HCV SGR cells +/- glucose (24, 48 Hours)

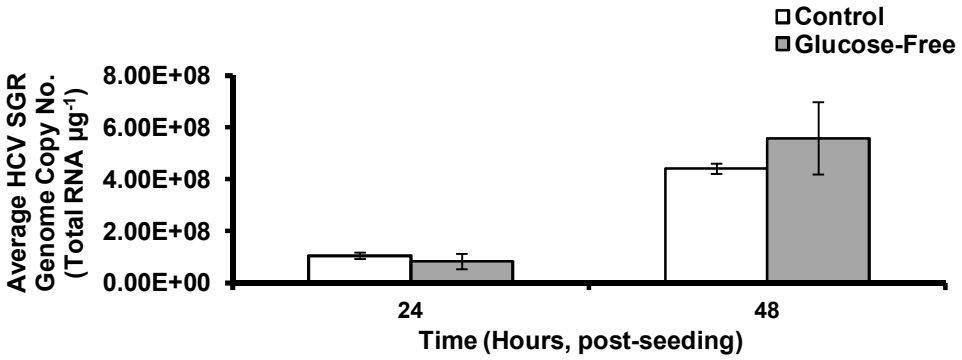


Figure 21 - Intracellular HCV SGR replication in HCV SGR cells +/- glucose [25 mM] (24, 48 hours)

Intracellular HCV SGR genome copy number measured in HCV SGR cells seeded in control (white columns) and glucose-free culture medium (grey columns) at 24 hours and 48 hours post-seeding. HCV SGR cells were seeded under these conditions from a stock grown under glucose rich conditions. Data shown are averages of triplicate measurements from a single experiment with error bars representing standard deviation (SD).

Figure 21 shows that 24 hours post-seeding, intracellular HCV SGR genome copy number is comparable between HCV SGR cells under both conditions (mean= 9.50×10^7 genome copies, SD +/- 1.49×10^7). However, at 48 hours post-seeding, intracellular virus is slightly higher in HCV SGR cells grown under glucose-free conditions (5.58×10^8 genome copies, SD +/- 1.48×10^8) than those cultured in medium containing high-glucose (4.41×10^8 genome copies, SD +/- 1.97×10^7). This result illustrates that the replication of intracellular viral RNA is not significantly affected by glucose concentration in the extracellular milieu.

The data from these experiments performed on gt2a HCV SGR cells collectively suggest that TXNIP overexpression occurs, in part, due to the concentration of glucose in the extracellular milieu but may be exacerbated by other cellular pathways such as ER stress, inferred by the comparable levels of STC2 upregulation seen at 24 hours post-seeding under both control and glucose-free conditions [(473)]. The re-evaluated data from the microarray study of JFH-1 infected Huh7 cells found STC2 transcription to be upregulated at 24 hours (+22.27-fold, $p= 1.29\times10^{-16}$) and 48 hours (+14.37-fold, $p= 1.88\times10^{-15}$) post-infection in accordance with levels previously reported by Blackham [(214)]. Thus, gene ontology pathway analysis was performed on the re-evaluated microarray data using GeneGO™ Metacore™ to identify genes involved in the unfolded protein response (UPR) that also undergo differential transcription during HCV infection (**Figure 22**).

3.2.6. Gene Ontology pathway analysis of re-evaluated microarray data (UPR induction)

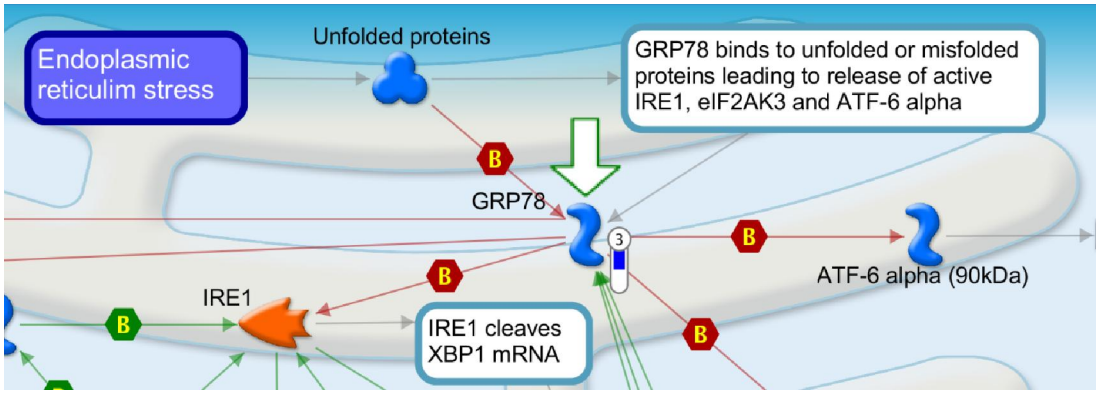


Figure 22 – GeneGO™ Metacore™ pathway analysis from re-evaluated microarray data (UPR induction)

Re-evaluated data from the Microarray study of Human hepatoma cells infected with the JFH-1 isolate of HCV was analysed by GeneGO™ Metacore™ software to reveal that endoplasmic reticulum stress and the unfolded protein response (UPR) are induced during HCV infection which is characterised by the release of IRE-1α (IRE1) and ATF-6 from the anchor protein, GRP78. Gene downregulation at 24 hours post-infection is indicated by number 3 on the blue thermometer. Genes of interest; **GRP78** (-2.04 at 24 hours, $p = 2.98 \times 10^{-10}$), **IRE1** (No change), **ATF-6** (No change).

Figure 22 shows that glucose regulated protein 78 (GRP78) is significantly ($p = 2.98 \times 10^{-10}$) downregulated (-2.04-fold) at 24 hours post-infection in the microarray study of JFH-1 infected Huh7 cells. GRP78 is the protein encoded by the heat shock protein family A member 5 (HSPA5) gene that functions as a calcium dependent ER-chaperone and an inhibitory anchor protein of the UPR effectors, i.e. inositol-requiring enzyme 1α (IRE-1α) and activating transcription factor 6 (ATF6) [474,475]. These proteins are concerned with reducing accumulated proteins at various levels of synthesis following the induction of ER stress.

IRE-1α is associated with the degradation of mRNAs localised to the ER and ATF6 induces the transcription of ER chaperones via ER stress response elements (ESREs) in the promoters of target genes [444,475]. Following the induction of ER stress and the release of intralumenal Ca^{2+} ions, GRP78 dissociates from the UPR effector proteins which leads to their activation, as GRP78 facilitates the removal of unfolded proteins from the ER by autophagy and translocates to the mitochondria to inhibit mitochondrial dysfunction caused by calcium ion overload [445,474–476].

Thus, to indicate whether or not the UPR was induced in both HCV gt2a infection models, control data for STC2 transcription in HCV SGR cells (**Figure 19**) was compared to that measured in JFH-1 infected Huh7 cells along with the quantification of HSPA5 mRNA abundance (**Figure 23 (A, B)**).

3.2.7. Gene Transcription of STC2 and HSPA5 in HCV gt2a Infection Models (24, 48 Hours)

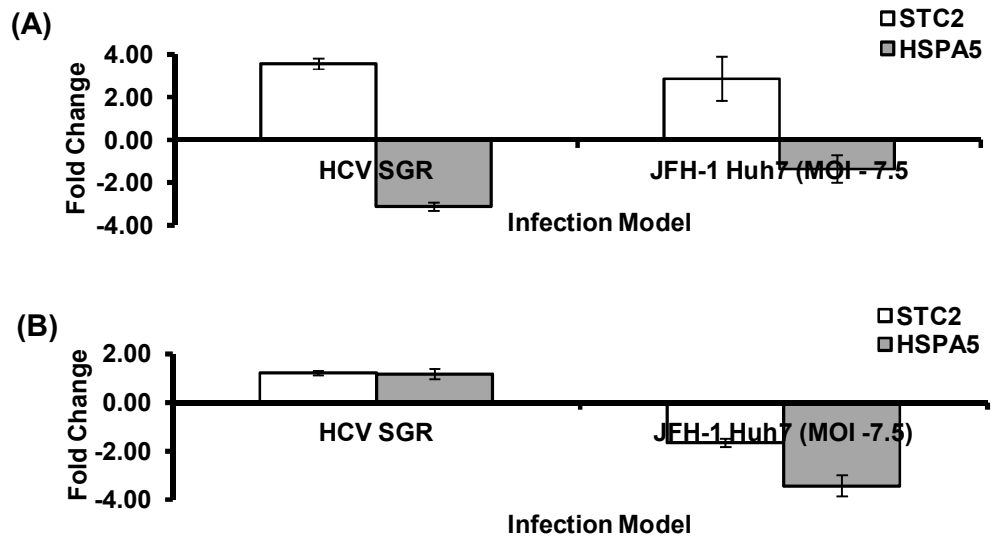


Figure 23 (A, B) – Gene Transcription of STC2 and HSPA5 in HCV gt2a infection models (24, 48 hours)

Relative fold change in transcription of STC2 (white columns) and HSPA5 (grey columns) measured in HCV SGR and JFH-1 infected Huh7 cells, compared to controls, at 24 hours and 48 hours post-seeding and post-infection, respectively. **(A)** Mean fold changes in HCV SGR and JFH-1 infected Huh7 cells at 24 hours. **(B)** Mean fold changes in HCV SGR and JFH-1 infected Huh7 cells at 48 hours. Genes assayed; Stanniocalcin 2 (**STC2**), Heat shock 70kDa protein A5 (**HSPA5**). Data shown are averages of triplicate measurements from a single experiment with error bars representing standard deviation (SD). Graphs representing differences in cycle thresholds (ΔC_T) between cell lines under these conditions are shown in **Appendix A1.3 (A, B)**

Figure 23 (A) shows that stanniocalcin 2 (STC2) is elevated in both HCV SGR (+3.58-fold, SD +/- 0.25) and JFH-1 infected Huh7 cells (+2.87-fold, SD +/- 1.03), compared to controls at 24 hours post-seeding and post-infection, respectively. Conversely, HSPA5 transcription is downregulated in both HCV SGR (-3.12-fold, SD +/- 0.20) and JFH-1 infected Huh7 cells (-1.35-fold, SD +/- 0.64) at this time point.

At 48 hours, levels of STC2 transcription recover to below a 2-fold threshold of significance in both HCV gt2a infection models. However, while there is no change, i.e. < 2-fold, in HSPA5 transcription in HCV SGR cells, transcription of HSPA5 mRNA is further downregulated (-3.42, SD +/- 0.22) in JFH-1 infected Huh7 cells. The downregulation of HSPA5 transcription has been found to be characteristic of ER stress induction and elevated intracellular calcium. Additionally suppression of this gene may enhance apoptosis by upregulating the expression of C/EBP-homologous protein (CHOP) [(477)]. Thus, these data so far indicate that ER stress and the UPR are induced in both the acute and chronic models of HCV replication.

Given that the lumenal space of the ER is a store for calcium ions and that calcium store depletion may occur through the incidence of ER stress, HCV gt2a infection models were stained with Indo-1 and fluorescence (405nm) was measured at 24 hour and 48 hour time points to determine whether the induction of ER stress and the UPR gave rise to alterations in cytosolic concentrations of calcium (**Figure 24**) [(473)].

3.2.8. Cytosolic Ca^{2+} in HCV gt2a Infection Models (24, 48 Hours)

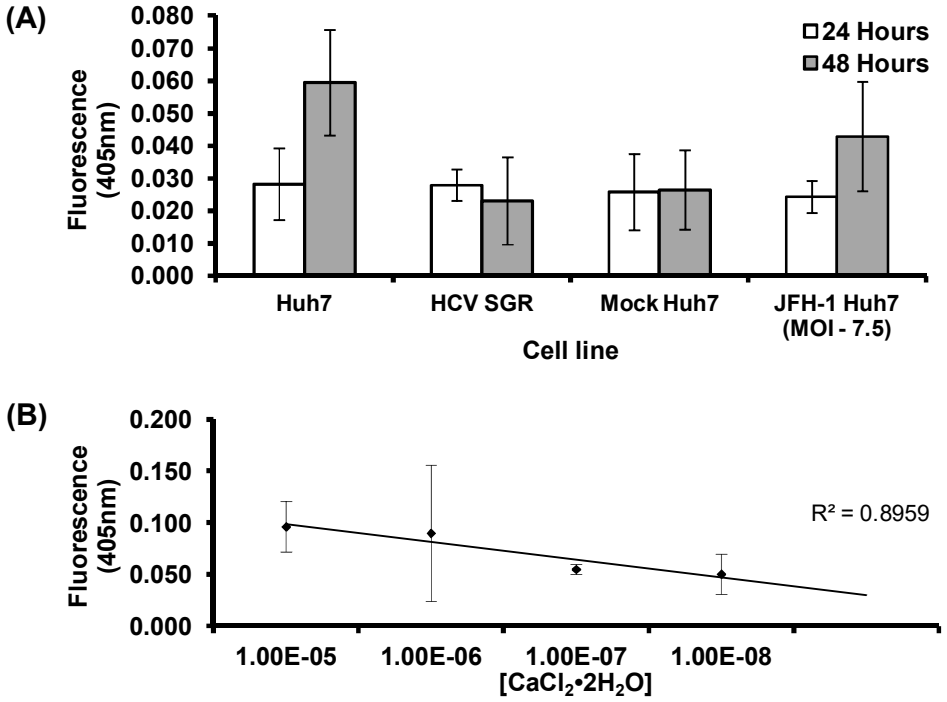


Figure 24 - Cytosolic Ca^{2+} in HCV gt2a Infection Models (24, 48 hours)

Cytosolic calcium measured in HCV SGR and JFH-1 infected Huh7 cells, compared to controls, at 24 hours and 48 hours post-seeding and post-infection, respectively. **(A)** Cytosolic calcium measured in Huh7 and HCV SGR, mock- and JFH-1 infected Huh7 cells at 24 hour (white columns) and 48 hour (grey columns) time points. **(B)** A standard curve produced at the time of the assay using calcium chloride dihydrate dissolved in H_2O [10 µM – 10 nM]. Data shown are averages of triplicate measurements from a single experiment with error bars representing standard deviation (SD).

Figure 24 (A) shows a comparable level of fluorescence detected at 405nm following Indo-1 staining in both HCV SGR- and JFH-1-infected cells, as well as controls, at 24 hours post-seeding and post-infection, respectively (mean= 0.0266, SD +/- 0.002). The concentration of cytosolic calcium in Huh7 and HCV SGR cells increase and decrease, respectively, at 48 hours post-seeding.

Conversely, cytosolic [calcium] in mock infected Huh7 cells remains stable at both time points, whereas that measured in JFH-1 infected Huh7 cells (MOI – 7.5) increases at 48 hours post-infection. The elevation in cytosolic calcium in both Huh7 and JFH-1 infected Huh7 cells at 48 hours may be explained by increased influx of Ca^{2+} ions from the culture medium as it is formulated with calcium chloride. However, the reduced cytosolic [Ca^{2+}] seen in HCV SGR cells at 48 hours may occur as a consequence of the increased transcription of STC2 seen at 24 hours as it inhibits the import of extracellular calcium in response to calcium store depletion following ER stress [(473)].

These results suggest that disturbances in cytosolic calcium ion concentration may arise from HCV protein expression in HCV SGR- and JFH-1 infected Huh7 cells which may also have consequences in ATP production as the mitochondria buffers intracellular Ca^{2+} concentration (**section 1.7.3.3.**) [(478)]. Considering the GeneGo™ Metacore™ pathway analysis, the differential transcription of STC2 and HSPA5 implicating the UPR to be active in HCV SGR- and JFH-1 infected Huh7 cells, and the findings by Lerner *et al*., it was hypothesised that the endoribonuclease activity of IRE-1α may be involved in the regulation of TXNIP mRNA transcript abundance in HCV gt2a infection models [(444)].

To test whether TXNIP mRNA is regulated by miR-17, which in turn is modulated by the endoribonuclease activity of IRE-1α following UPR induction, HCV SGR cells were treated with a cell permeable inhibitor, STF-083010, and miR-17 expression levels were measured in total RNA isolated at 24 hours and 48 hours post-seeding by using qRT-PCR and U6 as an internal control (**Figure 25 (A, B)**).

3.2.9. miR-17 expression in HCV gt2a Infection Models (24, 48 Hours)

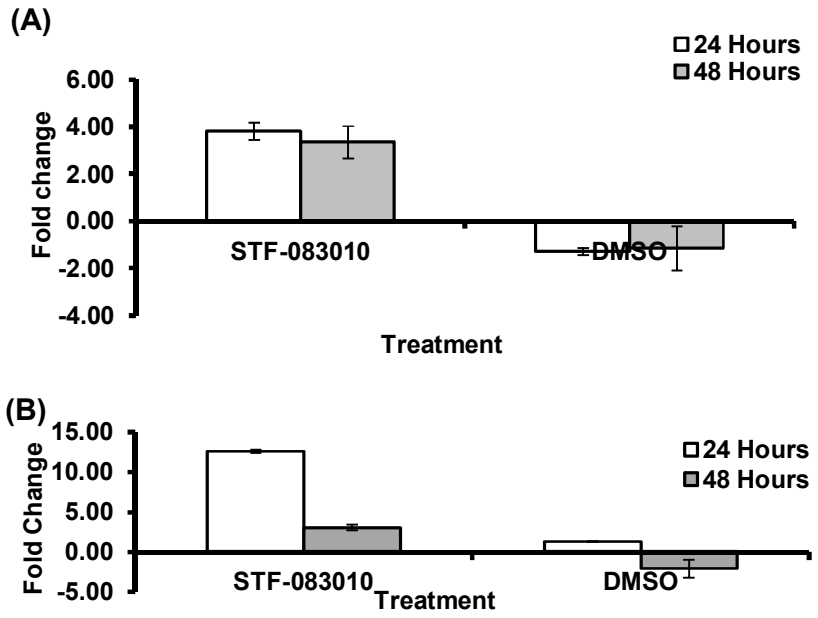


Figure 25 (A, B) - miR-17 expression levels in HCV gt2a infection models treated with STF-083010 (24, 48 hours)

miR-17 expression levels measured in HCV gt2a infection models treated with STF-083010, compared to DMSO controls, at 24 hour and 48 hour time points. **(A)** miR-17 expression in HCV SGR cells, compared to Huh7 cells, treated with STF-083010 or DMSO measured at 24 hours (white columns) and 48 hours (grey columns) post-seeding. **(B)** miR-17 expression in JFH-1 infected Huh7 cells, compared to mock infected Huh7 cells, treated with STF-083010 or DMSO measured at 24 hours (white columns) and 48 hours (grey columns) post-infection. Data shown are averages of triplicate measurements from a single experiment with error bars representing standard deviation (SD). Graphs representing differences in cycle thresholds (ΔC_T) between cell lines under these conditions are shown in **Appendix A1.4 (A - D)**.

As shown in **Figure 25 (A)**, miR-17 is significantly ($p= 8.1\times10^{-3}$) upregulated (+3.81-fold, SD +/- 0.36) in HCV SGR cells treated with STF-083010 which contrasts with the DMSO-treated control where miR-17 is downregulated (-1.29-fold, SD +/- 0.15) at 24 hours post-seeding. The upregulation of miR-17 expression in STF-083010-treated HCV SGR cells is also significant ($p= 3.1\times10^{-3}$) at 48 hours (+3.35-fold, SD +/- 0.69) post-seeding, whereas miR-17 expression is at basal levels in the DMSO control (-1.15-fold, SD +/- 0.93). The difference in the abundance of miR-17 between STF-083010 treated HCV SGR cells and the DMSO control is representative of the UPR being induced during HCV RNA replication. Furthermore, the inhibitory effects of STF-083010 on the endoribonuclease domain of IRE-1α appear to be active in HCV SGR cells. The endoribonuclease domain of IRE-1α serves to suppress ER protein translation through the degradation of mRNAs and enhance protein folding through the activation of X-box binding protein 1 (XBP1), via the cleavage of a 26nt intron, during irremediable ER stress [(444)].

Figure 25 (B) shows that miR-17 abundance is increased (+12.64-fold, SD +/- 0.20) in STF-083010 treated JFH-1 infected Huh7 cells, compared to mock infected cells, at 24 hours post-infection. This contrasts with JFH-1 infected Huh7 cells that were treated with DMSO, where there is a low abundance of miR-17 (+1.31-fold, SD +/- 0.01). However, miR-17 expression is reduced (+3.09-fold, SD +/- 0.34) in STF-083010-treated JFH-1 infected Huh7 cells, whilst that in the DMSO-control is suppressed (-2.09-fold, SD +/-1.13) at 48 hours post-infection.

These data further demonstrate that ER stress and the UPR are induced in HCV gt2a infection models and that the stability of miR-17 may be increased by inhibiting the endoribonuclease activity of IRE-1α.

To correlate the involvement of miR-17 abundance in the regulation of TXNIP mRNA, as well as downstream lipogenic gene transcription, namely those involved PUFA biosynthesis (ELOVL4, ELOVL7), fatty acid transport (FABP3), and lipid droplet formation (ACSL3), qRT-PCR was performed using total RNA that was isolated from HCV SGR cells treated with STF-083010 and DMSO at 24 hours and 48 hours post-seeding (**Figure 26 (A, B)**).

3.2.10. Lipogenic Gene Transcription in HCV gt2a Infection Models Treated with STF-083010 (24, 48 Hours)

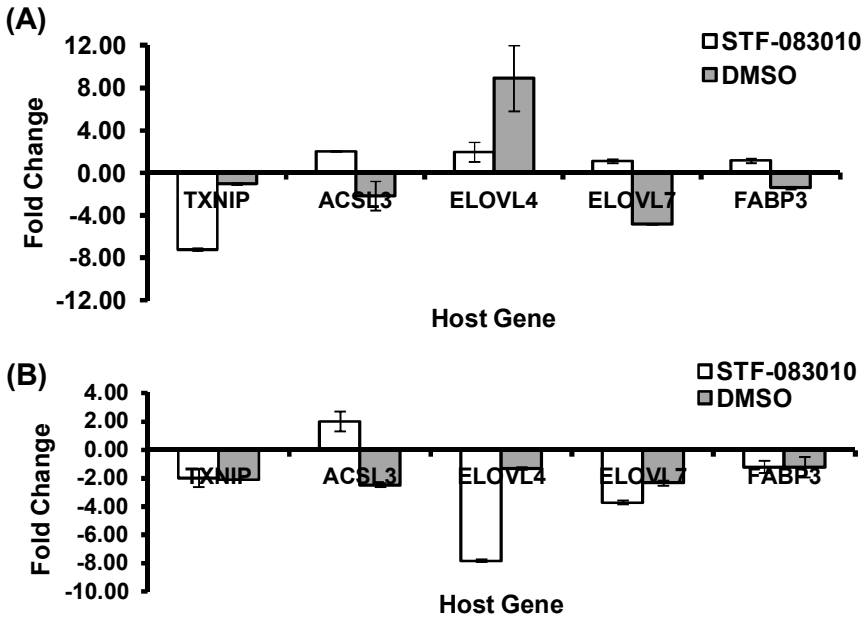


Figure 26 (A, B) - Lipogenic gene transcription in HCV SGR cells treated with STF-083010 (24, 48 Hours)

Relative fold change of lipogenic gene transcription measured in HCV SGR cells, compared to Huh7 cells, treated with STF-083010 (white-columns) or DMSO (grey columns) at 24 hours and 48 hours post-seeding. **(A)** Mean fold changes in HCV SGR cells at 24 hours post-seeding. **(B)** Mean fold changes in HCV SGR cells at 48 hours post-seeding. Genes assayed; Thioredoxin-interacting Protein (**TXNIP**), Acyl CoA synthetase long-chain family member 3 (**ACSL3**), ELOVL Fatty Acid Elongase 4 (**ELOVL4**), ELOVL Fatty Acid Elongase 7 (**ELOVL7**), Fatty Acid Binding Protein 3 (**FABP3**). Data shown are averages of triplicate measurements from a single experiment with error bars representing standard deviation (SD). Graphs representing differences in cycle thresholds (ΔC_T) between cell lines under these conditions are shown in **Appendix A1.5 (A, B)**.

As shown in **Figure 26 (A)**, the treatment of HCV SGR cells with STF-083010 results in a general suppression of lipogenic gene transcription that corresponds with the upregulation of miR-17 abundance seen at 24 hours post-seeding.

The downregulation of TXNIP mRNA transcription (-7.21-fold, SD +/- 0.13) is significant ($p= 1.1\times10^{-4}$) at 24 hours post-seeding which may also account for the basal transcription of downstream lipogenic genes, i.e. ACSL3, ELOVL4, ELOVL7, and FABP3, at this time point. The treatment of HCV SGR cells with DMSO, however, produces a similar effect by suppressing the transcription of TXNIP and downstream lipogenic genes to basal levels, i.e. <2-fold, at 24 hours post-seeding with the exception of ELOVL4 where mRNA is upregulated (+8.94-fold, SD +/- 3.08).

Figure 26 (B) shows the decrease in TXNIP and downstream lipogenic gene transcription in HCV SGR cells treated with STF-083010 is maintained at 48 hours post-seeding where the greatest effect is seen in ELOVL4 transcription (-7.85-fold, SD +/- 0.10). ACSL3 mRNA transcription, however, recovers to levels that are just below threshold of significance (+1.99-fold, SD +/- 0.71). In DMSO-treated HCV SGR cells, the transcription of all genes examined in the panel for dysregulated lipid metabolism during HCV replication are downregulated approximately 2-fold.

These results suggest that induction of the UPR, following ER stress, is integral to the transcription of TXNIP and downstream lipogenic genes during genome replication in HCV SGR cells which may be suppressed by targeting the endoribonuclease activity of IRE-1α.

The suppression of TXNIP using STF-083010 accords with the findings by Lerner *et al*., where it was reported that the inhibition of IRE-1α activity by STF-083010 increases the abundance of miR-17 which, in turn, destabilises TXNIP mRNA and prevents activation of the NLRP3 inflammasome in the induction of programmed cell death following irremediable ER stress [(444)].

Thus, the protocol of STF-083010 treatment and relative quantification of lipogenic gene transcription was also applied to JFH-1 infected Huh7 cells to examine whether the IRE-1α arm of the UPR also contributes to the dysregulation of lipogenic gene transcription in HCV infection. This was determined by using qPCR to measure lipogenic gene transcription in cDNA synthesised from total cellular RNA of mock- and JFH-1 infected Huh7 cells, co-treated with STF-083010 or DMSO, at 24 hours and 48 hours post-infection (**Figure 27 (A, B)**).

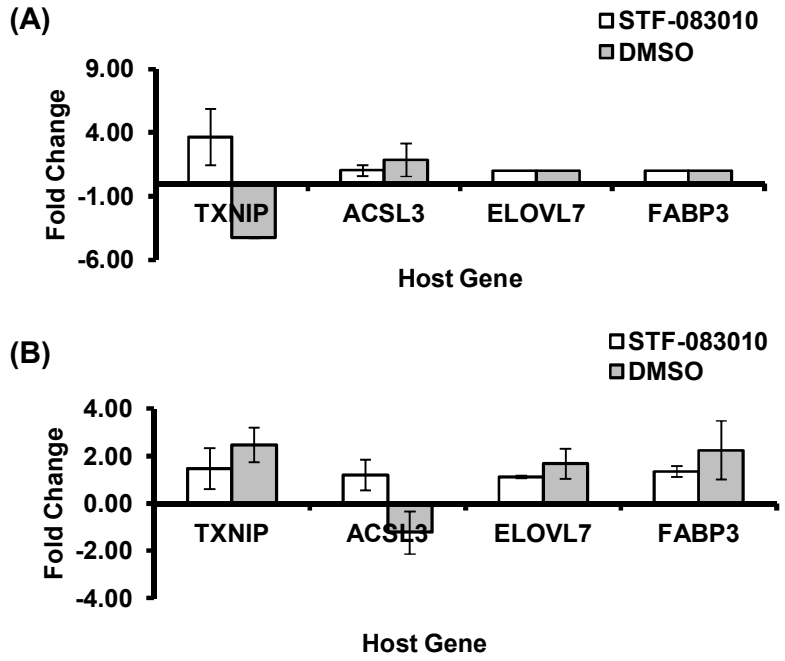


Figure 27 (A, B) - Lipogenic gene transcription in JFH-1 infected Huh7 cells treated with STF-083010 (24, 48 Hours)

Relative fold changes of lipogenic gene transcription measured in JFH-1 infected Huh7 cells, compared to mock infected Huh7 cells, treated with STF-083010 (white-columns) or DMSO (grey columns), at 24 hours and 48 hours post-infection. **(A)** Mean fold changes in JFH-1 infected Huh7 cells at 24 hours post-infection. **(B)** Mean fold changes in JFH-1 infected Huh7 cells at 48 hours post-infection. Genes assayed; Thioredoxin-interacting Protein (**TXNIP**), Acyl CoA synthetase long-chain family member 3 (**ACSL3**), ELOVL Fatty Acid Elongase 7 (**ELOVL7**), Fatty Acid Binding Protein 3 (**FABP3**). Data shown are averages of triplicate measurements from a single experiment with error bars representing standard deviation (SD). Graphs representing differences in cycle thresholds (ΔC_T) between cell lines under these conditions are shown in **Appendix A1.6 (A, B)**.

Figure 27 (A) shows that the transcript abundance of TXNIP mRNA remains upregulated (+3.69-fold, SD +/- 2.23) in JFH-1 infected Huh7 cells that were co-treated with STF-083010 at 24 hours post-infection. This contrasts with the downregulation of TXNIP seen in HCV SGR cells following co-treatment with STF-083010, as well as the downregulation of TXNIP transcription in DMSO treated JFH-1 infected Huh7 cells (-4.25-fold, SD +/- 0.02).

However, ACSL3 mRNA transcription is at a basal level (+1.05-fold, SD +/- 0.42), and the transcript abundance of ELOVL7 as well as FABP3 remain unaltered in STF-083010 treated JFH-1 infected Huh7 cells. Likewise, there is a < 2-fold change in lipogenic gene transcription following the treatment of JFH-1 infected Huh7 cells with DMSO at 24 hours post-infection.

Figure 27 (B) shows that the suppression of lipogenic gene transcription following the treatment of JFH-1 infected Huh7 cells with STF-083010 is maintained at 48 hours post-infection where no changes are observed in the transcription of TXNIP (+1.47, SD +/- 0.47), ACSL3 (+1.20-fold, SD +/- 0.65), ELOVL7 (+1.12-fold, SD +/- 0.05), or FABP3 (+1.35-fold, SD +/- 0.22). A similar effect is seen in DMSO-treated cells, where lipogenic gene transcription is stabilised at around a 2-fold level of transcription. ELOVL4 was excluded from the panel of genes used to characterise dysregulated lipid metabolism in JFH-1 infected Huh7 cells as transcription of this gene did not change in control experiments, i.e. no qPCR amplification was observed after 36.00 cycles.

The levels of lipogenic gene transcription in JFH-1 infected Huh7 cells treated with STF-083010 and DMSO are comparable which suggests that the latter is largely responsible for the downregulation of lipogenic gene transcription as it is the solvent in which the former is dissolved.

Furthermore, data from this experiment indicates that ER stress and UPR induction of are not as involved in the dysregulation of lipid metabolism in the JFH-1 model of HCV infection as they appear to be in HCV SGR cells.

To observe how the suppression of dysregulated host lipid metabolism affects the replication of HCV RNA, intracellular virus was quantitated by qRT-PCR using JFH-1 RNA standards [6 ng – 60 fg] and total RNA extracted from STF-083010-treated HCV SGR cells and controls at 24 hours and 48 hours post-seeding (**Figure 28**).

3.2.11. HCV genome copy number in HCV gt2a Infection Models Treated with STF-083010 (24, 48 Hours)

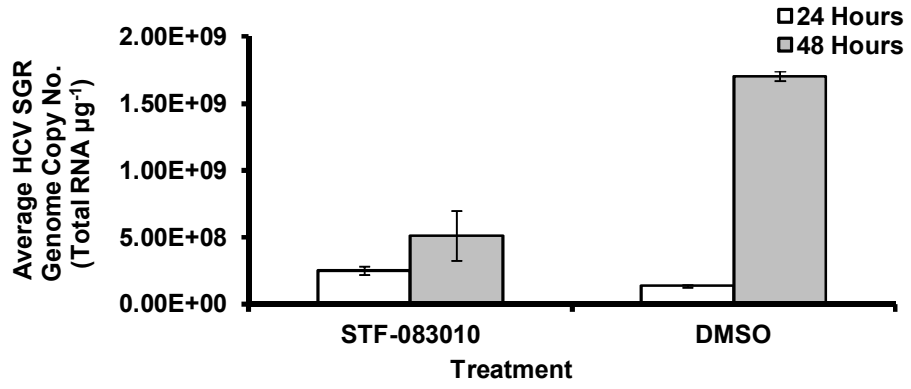


Figure 28 - Intracellular HCV SGR replication in HCV SGR cells +/- STF-083010 (24, 48 hours)

Intracellular virus genome copy number measured in HCV SGR cells treated with STF-083010 or DMSO at 24 hours (white columns) and 48 hours (grey columns) post-seeding. Data shown are averages of triplicate measurements from a single experiment with error bars representing standard deviation (SD).

Figure 28 shows that HCV SGR cells treated with STF-083010 have an increase in HCV SGR genome replication (2.51×10^{8} genome copies, SD +/- 3.25×10^{7}) compared to the DMSO control (1.35×10^{8} genome copies, SD +/- 1.18×10^{7}) at 24 hours post-seeding. Conversely, there is a significant ($p= 5.4\times10^{-4}$) 3.33-fold reduction in HCV genome copy number in STF-083010-treated HCV SGR cells (5.12×10^{8} genome copies, SD +/- 1.85×10^{8}) relative to those treated with DMSO (1.70×10^{9} genome copies, SD +/- 1.67×10^{8}) at 48 hours post-seeding.

Similarly, to examine the suppression of dysregulated lipid metabolism brought about by inhibition of IRE-1α on virus replication in JFH-1 infected Huh7 cells co-treated with STF-083010, intracellular virus was quantitated using qRT-PCR, JFH-1 RNA standards [6 ng – 60 fg], and total RNA harvested at 24 hours and 48 hours post-infection (**Figure 29**).

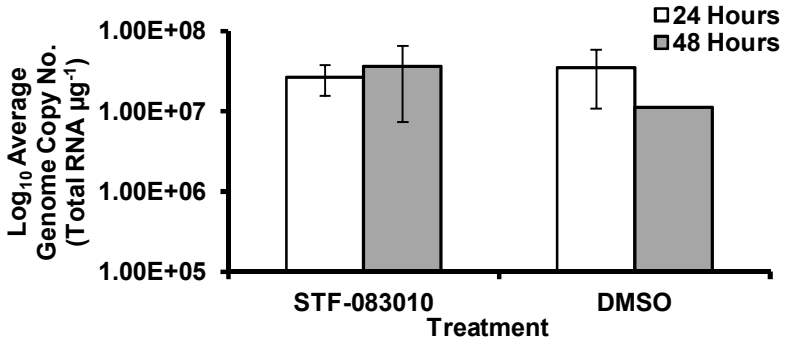


Figure 29 - Intracellular HCV replication in JFH-1 infected Huh7 cells (MOI – 7.5) +/- STF-083010 (24, 48 hours)

Intracellular virus genome copy number measured in JFH-1 infected cells treated with STF-083010 or DMSO at 24 hours (white columns) and 48 hours (grey columns) post-infection. Data shown are averages of triplicate measurements from a single experiment with error bars representing standard deviation (SD).

Figure 29 shows that there is little difference in genome copy number between JFH-1 infected Huh7 cells treated with STF-083010 (2.67×10^7 genome copies, SD +/- 1.10×0^7) and DMSO (3.50×10^7 genome copies, SD +/- 1.42×10^7) at 24 hours post-infection. However, intracellular HCV replication increases slightly in JFH-1 infected Huh7 cells treated with STF-083010 (3.67×10^7 genome copies, SD +/- 2.92×10^7) at 48 hours post-infection, whereas intracellular virus titre is reduced in the DMSO control (5.65×10^6 genome copies, SD +/- 1.96×0^6) at this time point.

The effects of STF-083010 treatment on extracellular virus secretion was also determined in the JFH-1 Huh7 model of HCV infection by using viral RNA harvested from infectious media at 24 hours and 48 hours post-infection, JFH-1 standards [6 ng – 60 fg] and qRT-PCR (**Figure 30**).

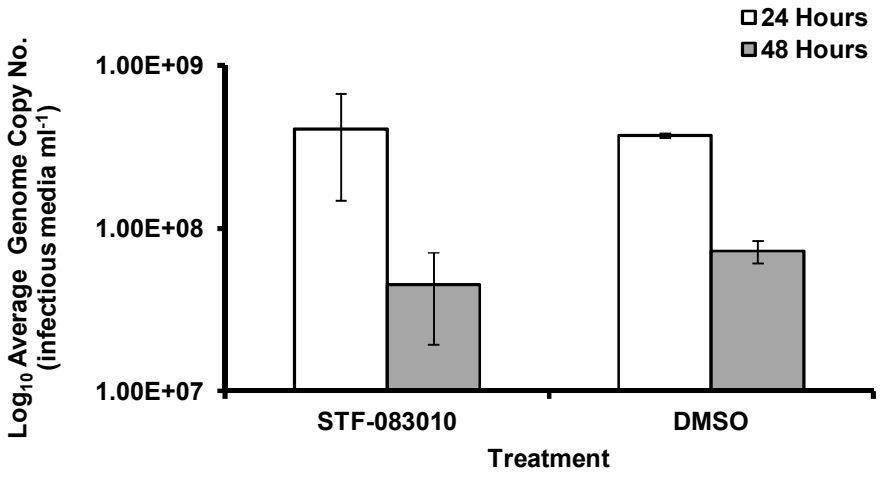


Figure 30 - Extracellular HCV secretion in JFH-1 infected Huh7 cells (MOI – 7.5) +/- STF-083010 (24, 48 hours)

Extracellular viral RNA measured in culture media from JFH-1 infected Huh7 cells treated with STF-083010 or DMSO at 24 hours (white columns) and 48 hours (grey columns) post-infection. Data shown are averages of triplicate measurements from a single experiment with error bars representing standard deviation (SD).

Figure 30 shows that no difference is seen in extracellular virus secretion between JFH-1 infected Huh7 cells co-treated with STF-083010 and DMSO at either 24 hours or 48 hours post-infection.

The findings from this series of experiments show that while the levels of UPR induction, as indicated by the differential transcriptional of STC2 and HSPA5, are similar between HCV gt2a infection models, the effects of inhibiting IRE-1α endoribonuclease activity on the regulation of TXNIP mRNA and the induction of downstream lipogenic targets involved in fatty acid synthesis (ELOVL4), condensation (ACSL3) and transport (FABP3), and intracellular virus replication, in HCV SGR- and JFH-1 infected Huh7 cells are different.

As the inhibition of IRE-1α activity was more effective in suppressing lipogenic gene transcription and replication of viral RNA in the HCV SGR model of HCV infection, Western Blotting using whole cell protein lysates prepared from HCV SGR cells treated with STF-083010 and controls at 24 hours and 48 hours post-seeding was performed to see if the effects observed on host gene transcription and intracellular virus replication corresponded to changes in host (TXNIP) and viral (HCV NS3) protein expression (**Figure 31**).

3.2.12. Host and Viral Protein Expression in HCV SGR cells Treated with STF-083010 (24, 48 Hours)

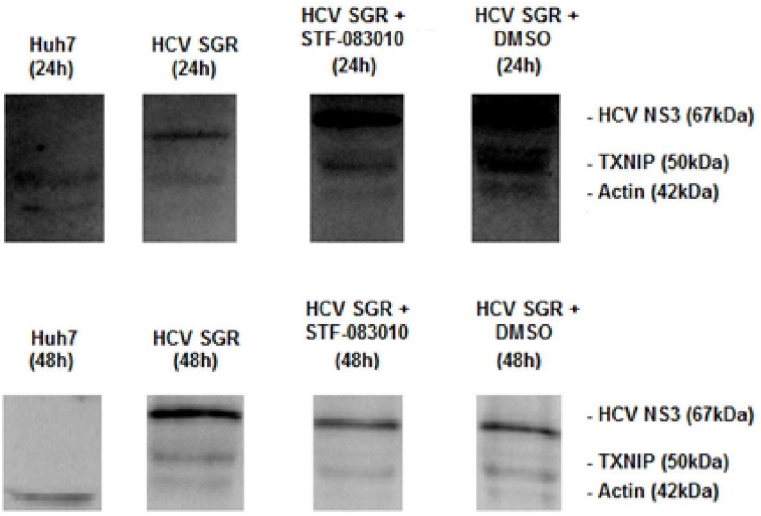


Figure 31 - Protein quantification in Huh7 and HCV SGR cells +/- STF-083010 (24, 48 hours)

Western Blot on 12% SDS-PAGE of intracellular protein (HCV NS3, TXNIP, β-actin) isolated from STF-083010 treated Huh7 and HCV SGR cells, and controls at 24 hours (24h) and 48 hours (48h) post-seeding.

As shown in **Figure 31**, there is high background staining in the Western Blot of host and viral proteins at 24 hours post-seeding which may be due to the method used, i.e. triple-staining of proteins using mouse and rabbit antibodies, being sub-optimal. However, due to time constraints, this experiment was not repeated and so the protein bands produced from this Western Blot were quantified by densitometry analysis using ImageJ software (**Figure 32**).

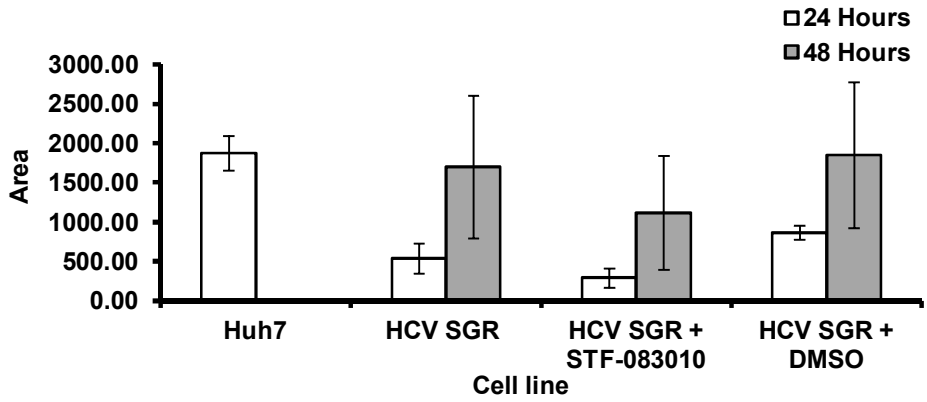


Figure 32 – Densitometry analysis of TXNIP protein expression in Huh7 and HCV SGR cells +/- STF-083010 (24, 48 hours)

Densitometry analysis of protein bands (TXNIP) following the Western Blot of intracellular protein isolated from HCV SGR cells treated with STF-083010 and controls at 24 hours (white columns) and 48 hours (grey columns) post-seeding. Data shown are averages of triplicate densitometry measurements from a single experiment with error bars representing standard deviation (SD).

Figure 32, shows that TXNIP expression is higher in Huh7 cells at 24 hours post-seeding than in HCV SGR cells, which is most likely to arise from the process of trypsinisation during the preparation of this experiment as the enzymatic cleavage of cell adhesion molecules in the sub-culture of confluent cells may induce changes in the expression of proteins that regulate cell metabolism and mitochondrial electron transport, e.g. glutamate dehydrogenase and ATP synthase subunit β [(479)]. However, TXNIP expression is lower in HCV SGR cells where IRE-1α endoribonuclease activity is inhibited using STF-083010 at 24 hour and 48 hour time points, compared to untreated cells and the DMSO control. These data further demonstrate that the UPR is active during HCV replication, and that TXNIP mRNA transcript abundance is regulated by miR-17 abundance which can be increased through the inhibition of IRE-1α in accordance with the findings by Lerner *et al* [(444)].

In addition, densitometry analysis was also used to quantify HCV NS3 to confirm the effects of miR-17-mediated destabilisation of TXNIP mRNA on viral protein expression in HCV SGR cells co-treated with STF-083010 (**Figure 33**).

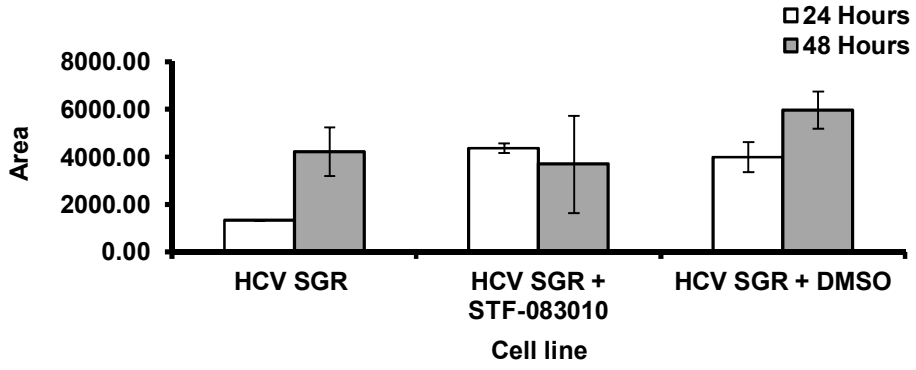


Figure 33 – Densitometry analysis of HCV NS3 protein expression in HCV SGR cells +/- STF-083010 (24, 48 hours)

Densitometry analysis of protein bands (HCV NS3) following the Western Blot of intracellular protein isolated from HCV SGR cells treated with STF-083010 and controls at 24 hours (white columns) and 48 hours (grey columns) post-seeding. Data shown are averages of triplicate measurements from a single experiment with error bars representing standard deviation (SD).

Figure 33 shows that there is minimal expression of HCV NS3 in untreated HCV SGR cells (536.17, SD +/- 189.45) at 24 hours post-seeding. The expression of HCV NS3 is significantly enhanced (p= 0.02) following treatment of HCV SGR cells with STF-083010 which supports data showing an increase in HCV RNA synthesis seen under this condition, compared to controls, at this time point (**Figure 28**). However, HCV NS3 expression is lower in HCV SGR cells treated with STF-083010 (3698.32, SD +/- 2056.04) than in untreated cells (4228.23, SD +/- 1032.20) and the DMSO control (5979.09, SD +/- 778.32) at 48 hours post-seeding which accords with the qRT-PCR data for HCV RNA replication.

This experiment supports the findings that induction of the UPR and ER stress are actively involved in the dysregulation of lipid metabolism in the HCV SGR model of HCV RNA replication. However, this experiment cannot be relied upon to draw conclusions as the control band (β-Actin) produced in the blot at 24 hours is not well defined.

3.3. Conclusion

In summary, initial studies involving the culture of HCV SGR cells under both glucose-free and control conditions showed similar levels of STC2 upregulation which suggests that intracellular calcium homeostasis is dysregulated and that this may be a factor in the upregulation of TXNIP and downstream lipogenic gene transcription. Moreover, intracellular [glucose] appears to be comparable between HCV SGR- and Huh7 cells over 48 hours post-seeding, though this does not appear to affect HCV SGR replication. However, additional studies showed that ER stress and the UPR are factors relevant to the regulation of TXNIP mRNA which may affect downstream lipogenic gene transcription and the replication of viral RNA in HCV SGR cells. TXNIP transcript abundance is regulated via miR-17 which, in turn, is regulated by the endoribonuclease domain of IRE-1α. The inhibition of IRE-1α endoribonuclease activity by STF-083010 is more effective in the HCV SGR model than in JFH-1 infected Huh7 cells, which indicates that ER stress is more involved in the dysregulation of lipid metabolism that is brought about during viral RNA replication in the absence of HCV structural proteins.

The key findings from this series of experiments and how they relate to the pathways involved in the upregulation of TXNIP in HCV SGR cells are shown in **Figure 34**.

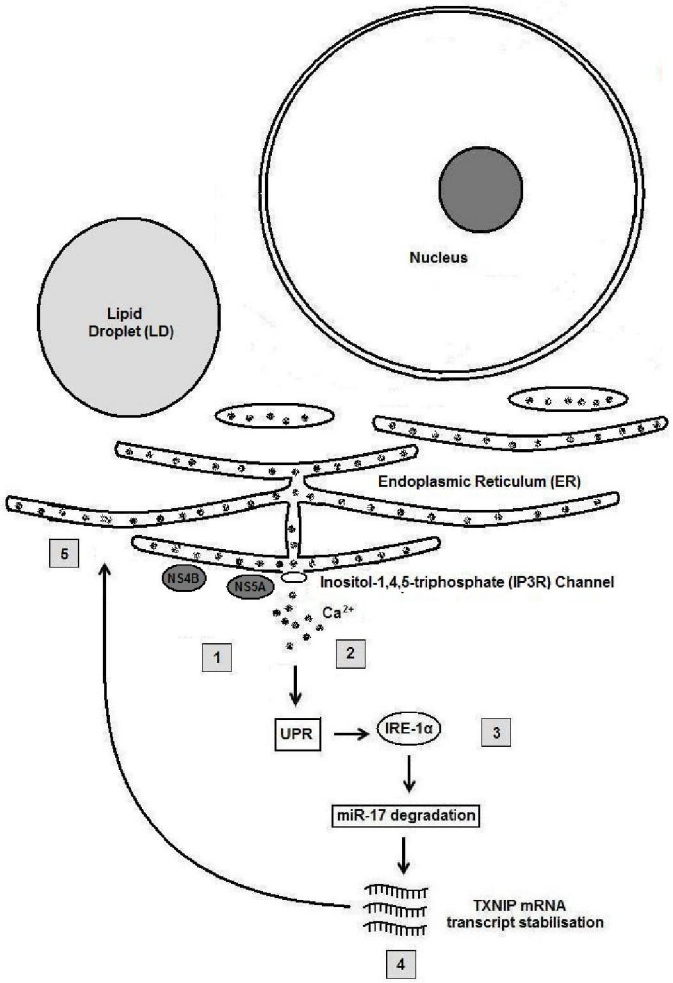


Figure 34 - ER Stress Induced Mechanism of TXNIP Overexpression

A diagram of how the induction of ER stress and the UPR contribute to the upregulation of TXNIP. **(1)** HCV NS4B induces stress at the endoplasmic reticulum (ER) membrane and causes perturbations in membrane arrangement. **(2)** HCV NS5A induces the efflux of intralumenal calcium ions from the ER by inositol-1,4,5-triphosphate (IP3R) channels. **(3)** Unfolded protein response (UPR) is activated leading to the autophosphorylation of the endoribonuclease, IRE-1α. IRE-1α has endoribonuclease activity degrades target RNAs including messenger RNAs (mRNAs), and micro RNAs (miRs). **(4)** miR-17, which regulates the abundance of TXNIP mRNA, is degraded by active IRE-1α. **(5)** Degradation of miR-17 leads to increased TXNIP mRNA stability and therefore feeds back into the translation machinery of the ER.

Chapter 4: Mitochondrial Dysfunction and dysregulated Lipid Metabolism in HCV infection

4.1. Overview

The phenomenon of ER stress was evident in both HCV SGR and JFH-1 Huh7 models of HCV infection which could have been behind the variations seen in cytosolic calcium concentration as shown in **Chapter 3**. Given that the mitochondria of eukaryotic cells are adjacent to the ER where they may buffer intracellular calcium ion concentration and this may consequently affect cellular metabolism, the possibility of mitochondrial dysfunction contributing to the dysregulation of lipid metabolism, mediated by Thioredoxin-interacting protein (TXNIP), was investigated in HCV gt2a infection models. The mitochondrial uptake of intracellular calcium by voltage dependent anion channels (VDACs), as described in **section 1.7.3.3.**, was inhibited through the treatment of HCV gt2a infection models with L-glutamate. This treatment gave rise to a reduction in TXNIP and downstream lipogenic gene transcription, triglyceride concentration, lipid droplet (LD) formation, apparent restoration of cellular glucose metabolism, and a considerable decrease in intracellular virus replication in JFH-1 infected Huh7 cells, compared to controls, at 24 hours and 48 hours post-infection.

4.2. Results & Discussion

As shown in **Chapter 3**, the concentration of intracellular calcium was altered following ER stress in HCV gt2a infection models which may, in turn, give rise to differences in concentrations localised to the mitochondria. Thus, mitochondrial calcium ion (Ca^{2+}) abundance was examined in HCV gt2a infection models. This was achieved by staining intracellular calcium with the Indo-1 fluorophore, removal of cytosolic calcium via the activation of cellular anion pumps by heat-treatment in a mitochondrial isolation buffer, and the fluorescence (405nm) was measured at 24 hour and 48 hour time points (**Figure 28 (A, B)**) [463].

4.2.1. Mitochondrial Ca^{2+} in HCV gt2a Infection Models (24, 48 Hours)

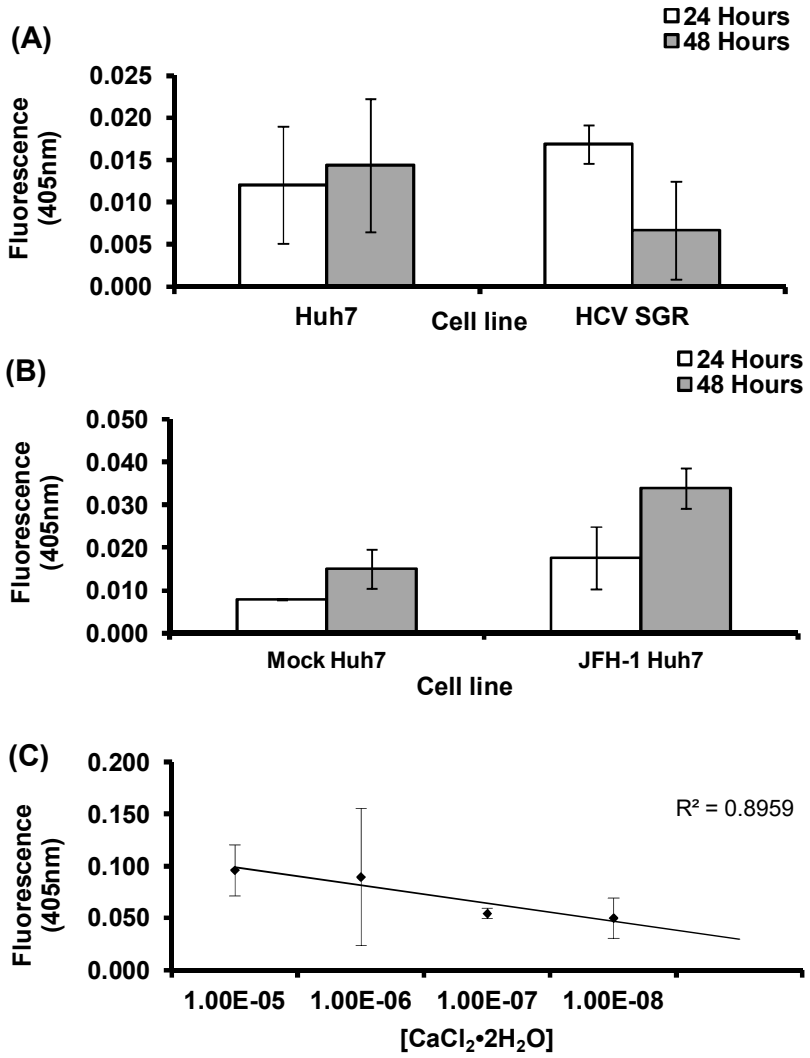


Figure 35 (A - C) - Mitochondrial Ca^{2+} in HCV gt2a Infection Models (24, 48 hours)

Mitochondrial calcium measured in HCV gt2a infection models at 24 hour (white columns) and 48 hour (grey columns) time points. **(A)** Mitochondrial calcium measured in Huh7 and HCV SGR cells at 24 hours and 48 hours post-seeding. **(B)** Mitochondrial calcium measured in mock- and JFH-1 infected Huh7 cells at 24 hours and 48 hours post-infection. **(C)** The standard curve, demonstrating linearity, produced at the time of the assay using calcium chloride dihydrate dissolved in H_2O [10 µM – 10 nM]. Data shown are averages of triplicate measurements from a single experiment with error bars representing standard deviation (SD).

Figure 35 (A) shows that mitochondrial Ca^{2+} is higher in HCV SGR cells (0.0169, SD +/- 0.002) compared to Huh7 cells (0.0121, SD +/- 0.007) at 24 hours post-seeding. However, at 48 hours post-seeding, the abundance of mitochondrial calcium ions is lower in HCV SGR cells (0.0067 SD +/- 0.006) than that measured in Huh7 cells (0.0144, SD +/- 0.008).

Figure 35 (B) illustrates that the abundance of Ca^{2+} ions at the mitochondria in JFH-1 infected Huh7 cells (0.0177, SD +/- 0.007) is higher than that measured in mock infected Huh7 cells (0.0079, SD +/- 0.001) at 24 hours post-infection. Similarly, mitochondrial calcium is greater in JFH-1 infected Huh7 cells (0.0339, SD +/- 0.004) than mock infected Huh7 cells (0.0151, SD +/- 0.004) at 48 hours post-infection. Furthermore, there is comparable +1.90-fold increase in mitochondrial calcium in both mock- and JFH-1 infected Huh7 cells at this time point.

The data from this experiment indicate that the abundance of calcium ions at the mitochondria is generally higher in the JFH-1 model of HCV infection than in the HCV SGR model of HCV replication. This phenomenon may occur as Ca^{2+} ions are released from the ER lumen via Inositol-1,4,5-triphosphate (IP3R) channels, following the induction of ER stress, and localise to the mitochondria via the action of the transmembrane GTPase, mitofusin II [43,295,480].

It has been reported that calcium ion overload at the mitochondria may induce dilation of the mitochondrial permeability transition pore (mPTP), swelling of the mitochondrial matrix, rupture of the outer mitochondrial membrane (OMM), increase the mitochondrial production of reactive oxygen species (ROS), and incur oxidative damage to mitochondrial DNA (mtDNA) [481–483].

To qualitatively assess the integrity of mtDNA in the JFH-1 model of HCV, 2% agarose gel electrophoresis was performed to detect a large fragment (~9kb) of mtDNA that was amplified using long PCR and total cellular DNA isolated from mock- and JFH-1 infected Huh7 cells at 24 hours and 48 hours post-infection (**Figure 36**).

4.2.2. Mitochondrial DNA (mtDNA) in JFH-1 infected Huh7 cells (24, 48 Hours)

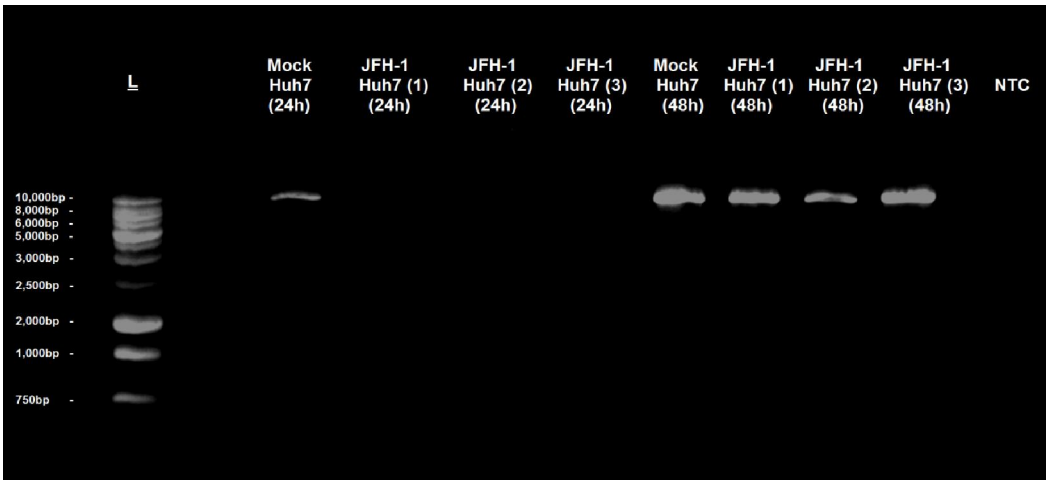


Figure 36 - PCR Amplification of Mitochondrial DNA (mtDNA) in Mock- and JFH-1 infected Huh7 cells (MOI – 7.5) (24, 48 Hours)

Large mitochondrial DNA amplified using total cellular DNA isolated from mock- and JFH-1 infected Huh7 cells at 24 hours and 48 hours post-infection. **L**: Reference marker (10,000bp DNA ladder). **NTC**: No template control.

As shown by **Figure 36**, a band of around 9kb can be seen in the lane which ran PCR product that was amplified using long PCR and total cellular DNA isolated from mock infected Huh7 cells at 24 hours (24h) post-infection, whereas there is an absence of detectable product amplified from the DNA of JFH-1 infected Huh7 cells. This indicates that mtDNA is intact in mock infected Huh7 cells whilst mtDNA may be damaged by ROS through the occurrence of DNA lesions and strand breaks in JFH-1 infected Huh7 cells. Furthermore, the impact of HCV infection on mitochondrial DNA was reported by a cohort study where mtDNA was found to be reduced in CHC patients by 19% [483,484].

Conversely, bands of around 9kb are detectable for both mock- and JFH-1 infected Huh7 cells at 48 hours (48h) post-infection, which suggests enzymes involved in the base excision repair (BER) of mtDNA, e.g. polymerase β (Polβ) and polymerase γ (Polγ) are induced [485]. However, the induction of DNA repair mechanisms was not assessed in this project due to time constraints. Furthermore, the integrity of mtDNA in HCV SGR cells was also investigated but proved inconclusive (data not shown).

The data shown in **Figure 35** and **Figure 36** suggest that mitochondrial calcium ion overload is present in human hepatoma cells that express HCV proteins and this appears to coincide with the compromised integrity of mtDNA in the JFH-1 model. Therefore, the phenomenon of calcium-dependent mitochondrial dysfunction was further characterised and tested as a potential source of dysregulated lipid metabolism in HCV gt2a infection models.

To determine whether uptake of calcium ions could be inhibited via mitochondrial voltage dependent anion channels (VDACs), the abundance of mitochondrial Ca^{2+} ions in L-glutamate treated HCV gt2a infection models and controls was determined by Indo-1 staining, removal of cytosolic calcium, and measuring fluorescence (405nm) at 24 hour and 48 hour time points. These data was compared to control conditions (**Figure 35 (A – C)**) and are shown in **Figure 37 (A – C)** [486].

4.2.3. Inhibition of Mitochondrial Ca^{2+} Uptake in HCV gt2a Infection Models (24, 48 Hours)

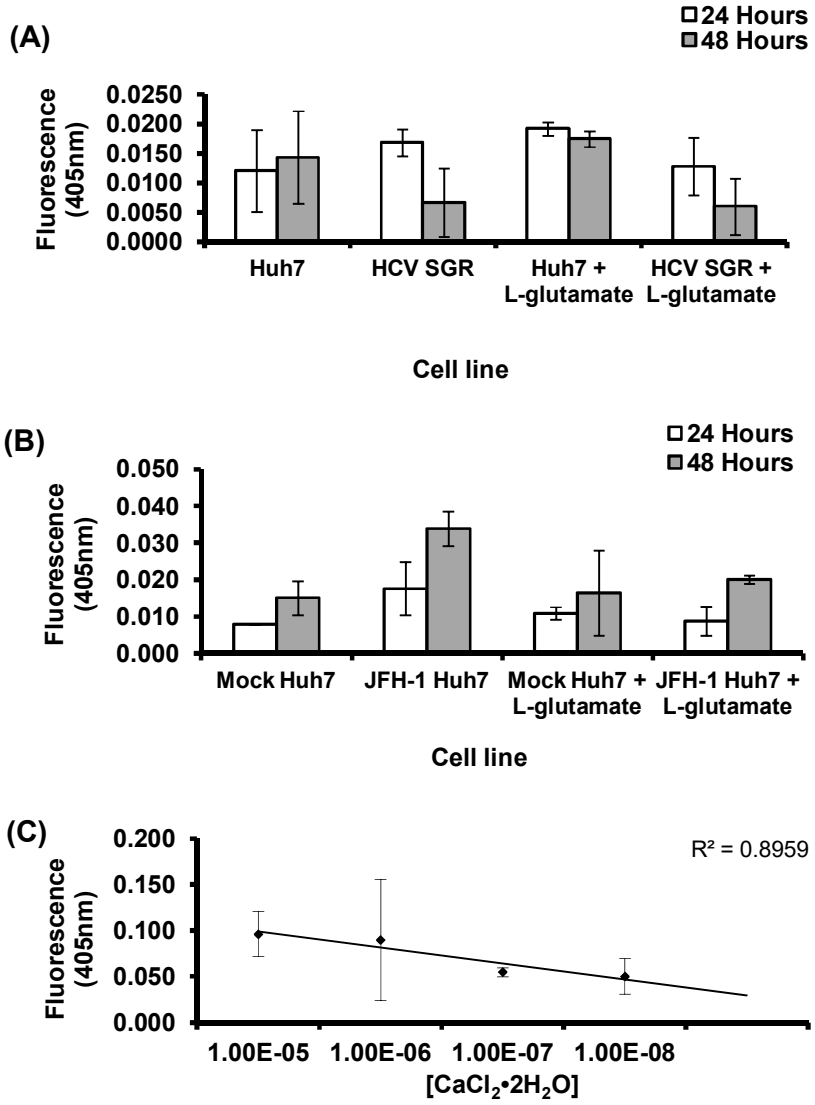


Figure 37 (A - C) - Mitochondrial Ca^{2+} ions in HCV gt2a infection models +/- L-glutamate (24, 48 hours)

Mitochondrial calcium measured in control and L-glutamate treated HCV gt2a infection models at 24 hour (white columns) and 48 hour (grey columns) time points. **(A)** Mitochondrial Calcium ions measured in control and L-glutamate treated Huh7 and HCV SGR cells at 24 hours and 48 hours post-seeding. **(B)** Mitochondrial Calcium ions measured in control and L-glutamate treated mock- and JFH-1 infected Huh7 cells at 24 hours and 48 hours post-infection. **(C)** The standard curve, demonstrating linearity, produced at the time of the assay using calcium chloride dihydrate dissolved in H_2O [10 µM – 10 nM]. Data shown are averages of triplicate measurements from a single experiment with error bars representing standard deviation (SD).

As shown in **Figure 37 (A)**, control HCV SGR cells have a higher abundance of mitochondrial calcium ions (0.0169, SD +/- 0.002) than that observed in control Huh7 cells (0.0121, SD +/- 0.0069) at 24 hours post-seeding. However, treatment with L-glutamate appears to increase mitochondrial calcium content in Huh7 cells (0.0192, SD +/- 0.0012) whilst comparatively reducing that measured in HCV SGR cells (0.0129, SD +/- 0.0049) at this time point. Conversely, L-glutamate appears to have little effect at 48 hours post-seeding as mitochondrial Ca^{2+} ions in L-glutamate treated Huh7 (0.0144, SD +/- 0.0079) and HCV SGR (0.0060, SD +/- 0.0048) cells are comparable to that measured in the respective controls.

Figure 37 (B) shows that mock infected Huh7 cells have a moderate presence of mitochondrial calcium ions (0.0079, SD +/- 0.0001) which is almost half (44.6%) of that seen in control JFH-1 infected Huh7 cells (0.0177, SD +/- 0.007) at 24 hours post-infection. The measurement of Ca^{2+} ions in L-glutamate treated mock- (0.0110, SD +/- 0.0016) and JFH-1 infected Huh7 cells (0.0088, SD +/- 0.0038) is comparable to the untreated mock control at this time point.

At 48 hours post-infection, the treatment of mock infected Huh7 cells with L-glutamate results in a slight increase in mitochondrial calcium (0.0165, SD +/- 0.011) that is comparable to the untreated control (0.0151, SD +/- 0.004) while mitochondrial Ca^{2+} ions are significantly (p= 0.04) reduced in L-glutamate treated JFH-1 infected Huh7 cells (0.0201, SD +/- 0.001) compared to the control (0.0339, SD +/- 0.004) at this time point.

These results demonstrate that the treatment of HCV gt2a infection models with L-glutamate is effective at reducing calcium localised to the mitochondria at 24 hours. This effect is retained at 48 hours in the JFH-1 model, though mitochondrial calcium levels are comparable between L-glutamate treated HCV SGR cells and the control at this time point.

With mitochondrial calcium ion abundance reduced at 24 hours in HCV gt2a infection models treated with L-glutamate, the effect on mitochondrial membrane potential ($mt\Delta\Psi m$) was examined as calcium ion overload is associated with a loss of mitochondrial membrane polarity [487]. This was achieved by staining control and L-glutamate [0.5 mM] treated HCV gt2a infection models with a cationic dye, Tetramethylrhodamineethyl ester (TMRE), that preferentially binds to depolarised outer mitochondrial membranes, and measuring fluorescence (549nm) at 24 hour and 48 hour time points (**Figure 38 (A, B)**).

4.2.4. Mitochondrial Membrane Potential (mtΔΨm) in HCV gt2a Infection Models (24, 48 Hours)

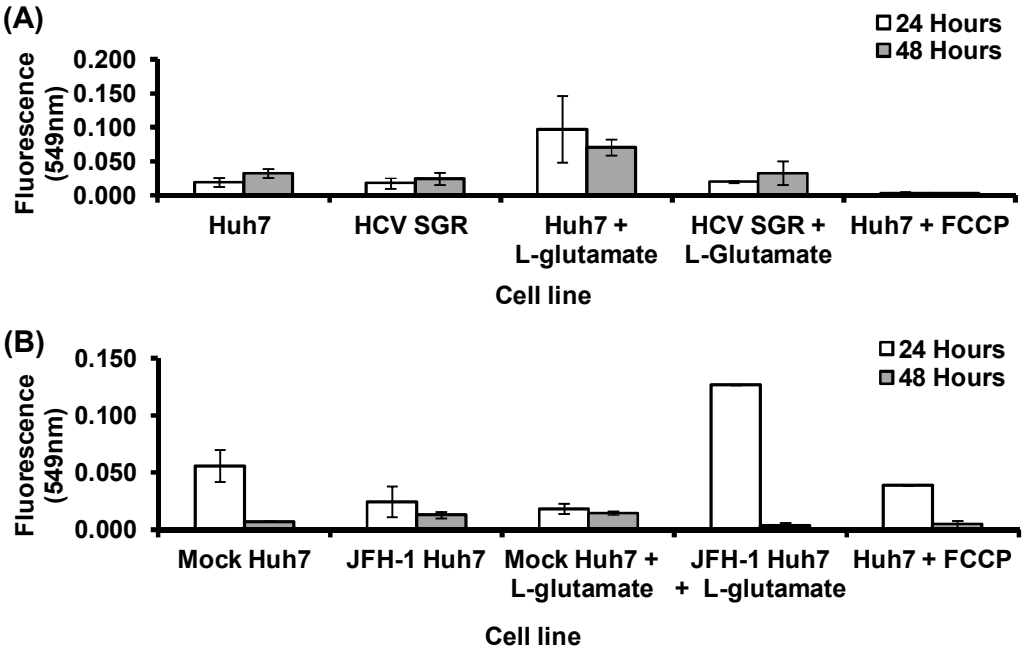


Figure 38 (A, B) – Mitochondrial Membrane Potential (mtΔΨm) in HCV gt2a Infection Models +/- L-glutamate (24, 48 hours)

Mitochondrial membrane potential (mtΔΨm) measured in control and L-glutamate treated HCV gt2a infection models at 24 hour (white columns) and 48 hour (grey columns) time points. Huh7 cells treated with carbonyl cyanide-4-(trifluoromethoxy)phenylhydrazone (FCCP) were included as a positive control. **(A)** Mitochondrial membrane potential in control and L-glutamate treated Huh7 and HCV SGR cells at 24 hours and 48 hours post-seeding. **(B)** Mitochondrial membrane potential measured in control- and L-glutamate treated mock- and JFH-1 infected Huh7 cells at 24 hours and 48 hours post-infection. Data shown are averages of triplicate measurements from a single experiment with error bars representing standard deviation (SD).

Figure 38 (A) shows there is little difference in mtΔΨm between Huh7 and HCV SGR controls as well as L-glutamate treated HCV SGR cells (mean= 0.019, SD +/- 0.001) at 24 hours post-seeding, although L-glutamate treated Huh7 cells have an elevated mitochondrial membrane potential (0.097, SD +/- 0.049) at this time point.

A similar pattern is seen at 48 hours post-seeding where there is little difference in the mtΔΨm of control Huh7 and HCV SGR cells as well as HCV SGR cells treated with L-glutamate (mean= 0.030, SD +/- 0.004), whereas Huh7 cells treated with L-glutamate have a high mtΔΨm (0.071, SD +/- 0.012).

Figure 38 (B) shows that mtΔΨm is markedly reduced in control JFH-1 infected Huh7 cells (0.0244, SD +/- 0.0135) compared to that seen in the mock infected control (0.0557, SD +/- 0.0139). Conversely, mitochondrial membrane potential is significantly ($p= 1\times10^{-3}$) enhanced following treatment of JFH-1 infected cells with L-glutamate (0.1266, SD +/- 0.0004), whereas that measured in L-glutamate treated mock infected cells is reduced (0.0183, SD +/- 0.0045) at 24 hours post-infection.

The mitochondrial membrane potential in all control and L-glutamate treated cells is generally decreased at 48 hours post-infection (mean= 0.0115, SD +/- 0.004), though L-glutamate treated JFH-1 infected cells have the greatest reduction in mtΔΨm (0.0036, SD +/- 0.002) at this time point. Furthermore, there is little difference seen in mitochondrial membrane potential of mock infected Huh7 cells treated with L-glutamate between 24 hours and 48 hours post-infection.

The efflux of calcium ions from the ER may accumulate at the mitochondria and induce depolarisation of the inner mitochondrial membrane (IMM) for which Tetramethylrhodamine ethyl ester (TMRE), a lipophilic, cationic ionophore, has a high binding affinity [488,489].

The reduced mt$\Delta\Psi$m observed in control JFH-1 infected Huh7 cells is validated by the treatment of Huh7 cells with carbonyl cyanide-4-(trifluoromethoxy)phenylhydrazone (FCCP) which activates proton conductance in the uncoupling of mitochondrial oxidative phosphorylation and induces depolarisation of the IMM [(490)]. Given that mitochondrial membrane potential is reduced in the JFH-1- and the HCV SGR models of HCV at 24 hours post-infection and 48 hours post-seeding, respectively, this may reflect differences in the induction of ER stress and mitochondrial dysfunction caused by the expression of HCV structural proteins in addition to the viral replicase.

The data from this experiment illustrate that the potential between the inner- and outer mitochondrial membranes is reduced in JFH-1 infected Huh7 cells and further indicate that mitochondrial dysfunction may be induced during virus replication as a consequence of calcium ion overload.

Further studies were conducted to see if the mitochondrial-associated pathway of apoptosis was induced in the HCV SGR model as pro-apoptotic caspases, e.g. caspase-3, are released from the mitochondria in the instance of calcium ion overload which may indicate a disruption in the the functional capacity of this organelle.

Thus, the Mitochondrial ToxGlo™ assay was used to measure the activity of "Dead Cell Protease", presumably caspase-3, in HCV SGR cells over the course of 48 hours post-seeding (**Figure 39 (A, B)**).

4.2.5. Mitochondrial-Associated Apoptosis in HCV SGR cells (24, 48 Hours)

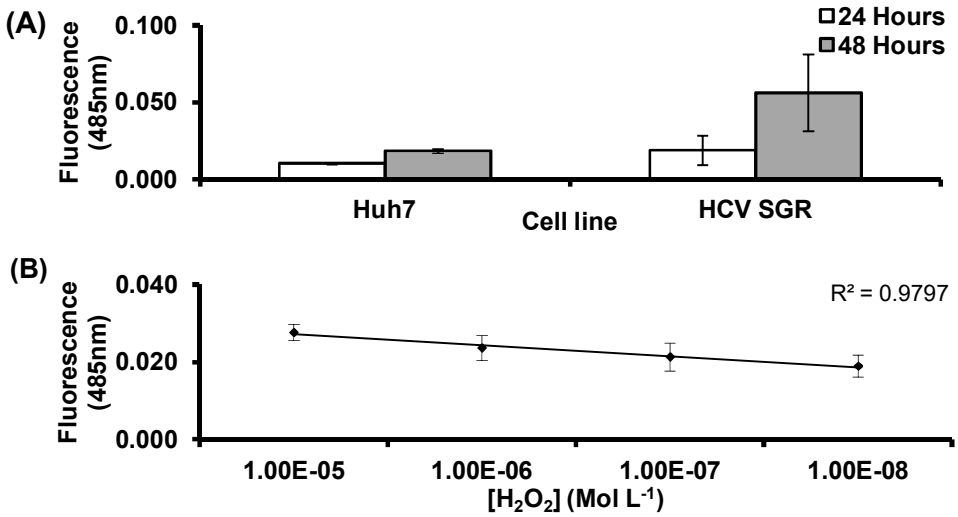


Figure 39 (A, B) – Induction of Mitochondria-Associated Apoptosis in HCV SGR cells (24, 48 Hours)

"Dead cell protease" activity measured in Huh7 and HCV SGR cells at 24 hours and 48 hours post-seeding. **(A)** Apoptotic protease activity measured in Huh7 and HCV SGR cells at 24 hours (white columns) and 48 hours (grey columns) post-seeding. **(B)** The standard curve produced at the time of assay for dead cell protease activity in Huh7 cells treated with H_2O_2 [10 µM – 10 nM]. Data shown are averages of triplicate measurements from a single experiment with error bars representing standard deviation (SD).

Figure 39 (A) shows that there is little mitochondrial apoptotic protease activity Huh7 cells (0.0101, SD +/- 0.0003) at 24 hours, though this increases (0.0183, SD +/- 0.0013) at 48 hours post-seeding. In contrast, HCV SGR cells have high "Dead Cell Protease" activity (0.0190, SD +/- 0.009) at 24 hours post-seeding, that increases 2.95-fold (0.0561, SD +/- 0.02) at 48 hours.

The increased activity of “Dead Cell Protease” in HCV SGR cells shown by the higher fluorescence (485nm), compared to Huh7 cells, at 24 hours and 48 hours post-seeding demonstrates that the mitochondria-associated pathway of apoptosis is induced in this model.

The induction of programmed cell death via the mitochondria may be related to the upregulation of TXNIP that follows the induction of ER stress by the viral replicase proteins in HCV SGR cells at 24 hours post-seeding (**Chapter 3**) [491]. It has been previously shown that the mitochondrial-associated pathway of apoptosis may occur through oxidative stress causing TXNIP to dissociate from Trx1 in the cytoplasm or, alternatively, induce the nuclear export and mitochondrial translocation of TXNIP where it may competitively bind to Trx2 and induce the release of apoptosis signaling kinase 1 (ASK1) to bring about caspase-mediated apoptosis [435,440,491]. The measurement of “Dead Cell Protease” activity could not performed in the JFH-1 model due to the requirement for live cells and containment level 3 (CL3) restrictions.

As an alternative means of assessing mitochondrial function in the JFH-1 model, the transcription of genes related to the oxidative phosphorylation of glucose in control and L-glutamate treated HCV gt2a infection models was measured using qRT-PCR and qPCR over 48 hours to assess whether the induction of apoptosis via the mitochondria had consequence on the transcription of genes concerned with the metabolism of glucose.

A panel of genes was selected from the re-evaluated microarray data (data not shown), and included Max like protein (Mlx) due to its involvement in the transcriptional induction of glycolytic genes and TXNIP (**Figure 40 (A, B)**) [215,443].

4.2.6. Oxidative Phosphorylation Gene Transcription in HCV gt2a Infection Models +/- L-glutamate (24, 48 Hours)

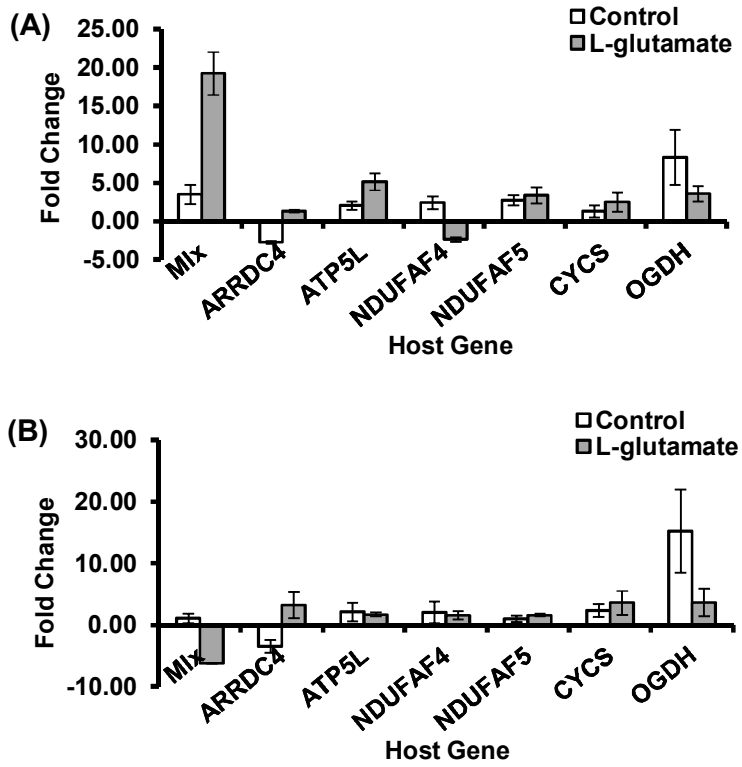


Figure 40 (A, B) – Oxidative Phosphorylation gene transcription in HCV SGR cells +/- L-glutamate (24, 48 hours)

Relative fold change in transcription of genes related to oxidative phosphorylation measured in control and L-glutamate treated (grey columns) HCV SGR cells, compared to Huh7 cells, at 24 hours and 48 hours post-seeding. **(A)** Mean fold changes in HCV SGR cells at 24 hours post-seeding. **(B)** Mean fold changes in HCV SGR cells at 48 hours post-seeding. Genes assayed; Max like protein (**Mlx**), Arrestin domain containing 4 (**ARRDC4**), ATP Synthase subunit G (**ATP5L**), NADH Dehydrogenase (Ubiquinone) Complex I, Assembly Factor 4 (**NDUFAF4**), NADH Dehydrogenase (Ubiquinone) Complex I, Assembly Factor 5 (**NDUFAF5**), Cytochrome C (**CYCS**), Oxoglutarate Dehydrogenase (**OGDH**). Data shown are averages of triplicate measurements from a single experiment with error bars representing standard deviation (SD). Graphs representing differences in cycle thresholds (ΔC_T) between cell lines under these conditions are shown in **Appendix A2.1 (A, B)**.

As shown in **Figure 40 (A)**, there is an upregulation of Mlx mRNA in HCV SGR cells treated with L-glutamate at 24 hours post-seeding (+19.24-fold, SD +/- 2.79) compared to the transcript abundance seen in the untreated control (+3.49-fold, SD +/- 1.25) which indicates that glucose uptake and the transcription of glucose-responsive genes are enhanced under this condition [492,493]. This finding is supported by the transcriptional data for ARRDC4, a paralog of TXNIP that is repressed by glucose deprivation, where transcript abundance is downregulated (-2.70-fold, SD +/- 0.16) in the untreated control and transcribed at basal levels in HCV SGR cells treated with L-glutamate (+1.34-fold, SD +/- 0.17) [493].

Gene transcription for the G subunit of the ATP Synthase (ATP5L) is upregulated in HCV SGR cells treated with L-glutamate (+5.16-fold, SD +/- 1.10) at 24 hours post-seeding which contrasts with that measured for the untreated control (+2.06-fold, SD +/- 0.52) at this time point. The gene product of ATP5L has a transmembrane segment that forms the F_0 domain of ATP synthase (complex V) which is embedded in the inner mitochondrial matrix (IMM) as part of a H^+ channel that facilitates the proton motive force generated by complex I of the mitochondrial respiratory chain to produce ATP in the initial stages of oxidative phosphorylation [494–496]. The transcription of complex I assembly factors, NDUFAF4 and NDUFAF5, are upregulated by +2.45-fold, SD +/- 0.83 and +2.76-fold, SD +/- 0.63, respectively, in control HCV SGR cells at 24 hours post-seeding.

However, treatment of this model with L-glutamate leads to a repression in NDUFAF4 transcription (-2.34-fold, SD +/- 0.29) whilst promoting the transcript abundance of NDUFAF5 (+3.38-fold, SD +/- 1.06) at this time point. In control HCV SGR cells, cytochrome C (CYCS) transcription undergoes fold-changes of +1.30-fold, SD +/- 0.79 and +2.38-fold, SD +/- 1.06 at 24 hours and 48 hours post-seeding, respectively. This upregulation may result from the ROS-mediated degradation of cardiolipin and release of CYCS from the mitochondria, or through the homooligomerisation of the pro-apoptotic proteins, Bax and Bak [481,497]. However, following the treatment of HCV SGR cells with L-glutamate, transcription of this gene is upregulated by +2.54-fold, SD +/- 1.26 and +3.60-fold, SD +/- 1.94 at 24 hours and 48 hours post-seeding, respectively, that suggests the enhancement of respiratory chain function through the inhibition of mitochondrial Ca^{2+} uptake due to the reduced oscillation of mitochondrial VDACs.

At 24 hours post-seeding, the transcript abundance of oxoglutarate dehydrogenase (OGDH), which catalyses the conversion of oxoglutarate (α-ketoglutarate) to succinyl-co A and CO_2 during the tricarboxylic acid (TCA) cycle, is upregulated in control HCV SGR cells (+8.33-fold, SD +/- 3.60), and to a lesser extent in those treated with L-glutamate (+3.60, SD +/- 1.94). This effect is maintained at 48 hours post-seeding (**Figure 40 (B)**), where OGDH transcription is maintained at a comparable level in HCV SGR cells treated with L-glutamate (+3.67, SD +/- 2.20), but is highly upregulated (+15.23-fold, SD +/- 6.71) in the untreated control.

Additionally, the treatment of HCV SGR cells with L-glutamate appears to generally stabilise the transcription of genes related to oxidative phosphorylation at 48 hours post-seeding, where the transcript abundance of ATP5L, NDUFAF4, and NDUFAF5 is < 2-fold. However, ATP5L and NDUFAF4 remain slightly upregulated in the untreated control with fold changes of +2.14-fold, SD +/- 1.49, and +2.08-fold, SD +/- 1.79, respectively. Moreover, at 48 hours post-seeding, Mlx mRNA is downregulated (-6.20-fold, SD +/- 0.08) and ARRDC4 transcript abundance is upregulated (+3.25-fold, SD +/- 2.13) in HCV SGR cells treated with L-glutamate whilst Mlx transcription is basal (+1.08-fold, SD +/- 0.77) and ARRDC4 remains downregulated (-3.46-fold, SD +/- 1.02) in the untreated control.

These results suggest that in the HCV SGR model of HCV replication, L-glutamate treatment may enhance oxidative phosphorylation as an effect of inhibiting mitochondrial dysfunction induced by calcium ion overload. Thus to observe the effects in the JFH-1 model of HCV infection, a similar panel of genes were assessed in JFH-1 infected Huh7 cells treated with L-glutamate and compared to controls using qPCR and cDNA synthesised from total RNA isolated at 24 hours and 48 hours post-infection (**Figure 41 (A, B)**).

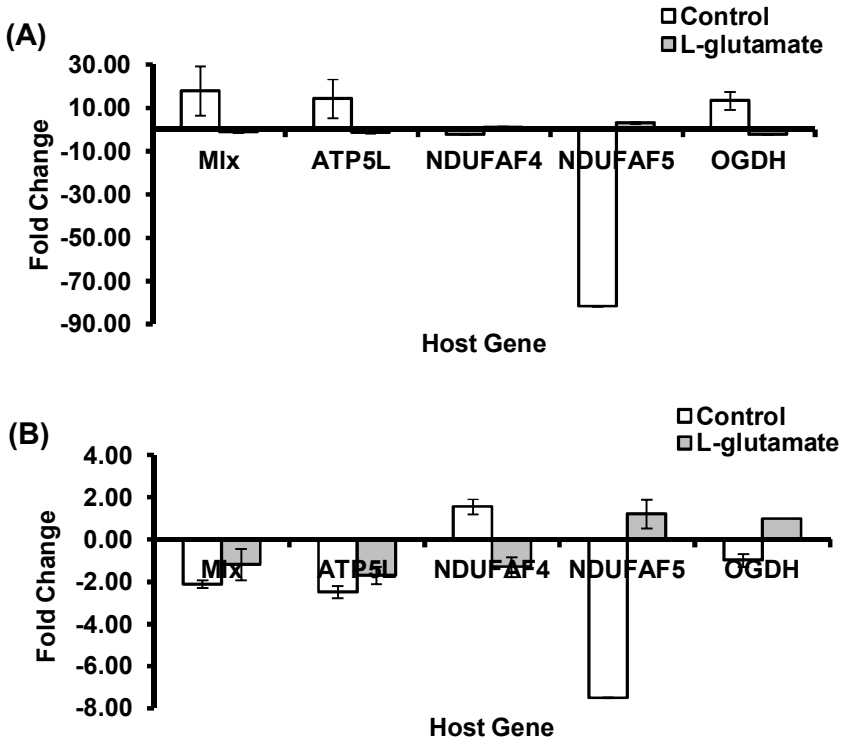


Figure 41 (A, B) – Oxidative phosphorylation gene transcription in JFH-1 infected Huh7 cells (MOI – 7.5) +/- L-glutamate (24, 48 hours)

Relative fold change in transcription of oxidative phosphorylation-related genes measured in control (white columns) and L-glutamate treated (grey columns) JFH-1 infected Huh7 cells, compared to mock infected Huh7 cells, at 24 hours and 48 hours post-infection. **(A)** Mean fold changes in JFH-1 infected Huh7 cells at 24 hours post-infection. **(B)** Mean fold changes in JFH-1 infected Huh7 cells at 48 hours post-infection. Genes assayed; Max like protein (**Mlx**), ATP Synthase (**ATP5L**), NADH Dehydrogenase (Ubiquinone) Complex I, Assembly Factor 4 (**NDUFAF4**), NADH Dehydrogenase (Ubiquinone) Complex I, Assembly Factor 5 (**NDUFAF5**), Oxoglutarate Dehydrogenase (**OGDH**). Data shown are averages of triplicate measurements from a single experiment with error bars representing standard deviation (SD). Graphs representing differences in cycle thresholds (ΔC_T) between cell lines under these conditions are shown in **Appendix A2.2 (A, B)**.

As shown in **Figure 41 (A)**, transcription of Max like protein (Mlx) is upregulated in control JFH-1 infected Huh7 cells (+17.98-fold, SD +/- 11.33) compared to the mock infected Huh7 cells, and is suppressed following treatment with L-glutamate (-1.04-fold, SD +/- 0.32) at 24 hours post-infection.

Similarly, ATP5L transcription is upregulated (+14.27-fold, SD +/- 9.00) in control JFH-1 infected Huh7 cells but is downregulated following treatment with L-glutamate (-1.23-fold, SD +/- 0.57) at 24 hours post-infection. NDUFAF4 transcription is downregulated (-2.13-fold, SD +/- 0.08) in control JFH-1 infected Huh7 cells but is maintained at basal levels following treatment with L-glutamate (+1.40-fold, SD +/- 0.02). NDUFAF5 mRNA, however, is significantly ($p= 4.47\times10^{-10}$) downregulated (-81.61-fold, SD +/- 0.01) in control JFH-1 infected Huh7 cells but significantly ($p= 6.32\times10^{-4}$) upregulated (+3.10-fold, SD +/- 0.55) following treatment with L-glutamate.

Figure 41 (B) shows that there is basal transcription, i.e. < 2-fold, of all genes related to oxidative phosphorylation under both control and L-glutamate treated conditions at 48 hours post-infection, with the exception of NDUFAF5 where mRNA abundance is significantly ($p= 1.46\times10^{-7}$) downregulated in control JFH-1 infected Huh7 cells (-7.50-fold, SD +/- 0.02). In contrast, the treatment of JFH-1 infected Huh7 cells with L-glutamate augments NDUFAF5 transcription to basal levels (+1.22-fold, SD +/- 0.68) at this time point. ARRDC4 was not included in this experiment as this gene was not transcriptionally altered in control JFH-1 Huh7 infection experiments.

These data indicate that the regulation of glucose metabolism by oxidative phosphorylation is disordered in HCV infection but may be alleviated by inhibiting the mitochondrial uptake of calcium through treatment with L-glutamate.

It can be said from this experiment that mitochondrial dysfunction, induced by calcium ion overload, is evident to different degrees in both HCV gt2a infection models and that treatment with L-glutamate can produce significant effects on the transcription of genes relating to oxidative phosphorylation, an intermediary stage in the metabolism of intracellular glucose that bridges the metabolic processes of glycolysis and the TCA cycle.

To observe whether the differential transcription of genes concerning oxidative phosphorylation translated to differences in intracellular [glucose] in HCV SGR- and JFH-1 infected Huh7 cells, the 3',5'-dinitrosalicylic acid (DNS) assay was performed using whole cell protein lysate isolated from control and L-glutamate treated HCV gt2a infection models and absorbance (575nm) was measured at 24 hours and 48 hour time points (**Figure 42 (A - C)**).

4.2.7. Intracellular [Glucose] in HCV gt2a Infection Models +/- L-glutamate (24, 48 Hours)

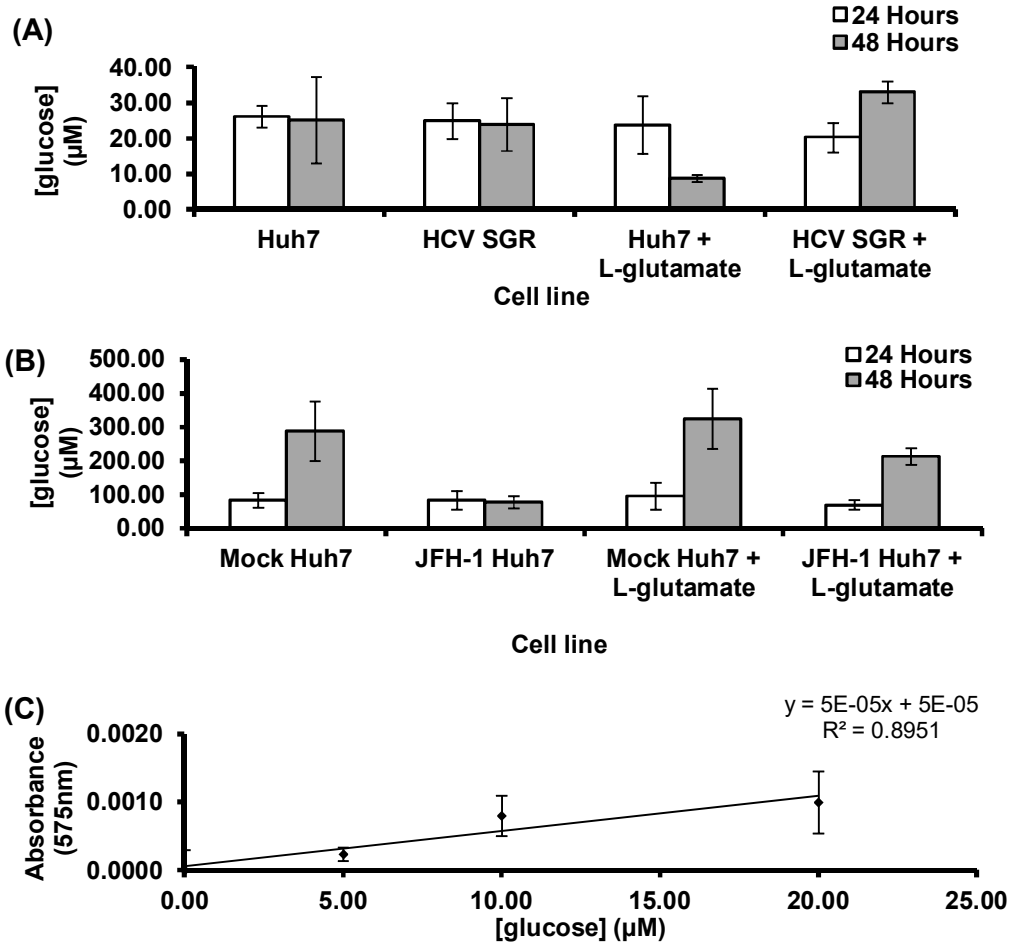


Figure 42 (A – C) - Average intracellular [glucose] (μM) in HCV gt2a Infection Models +/- L-glutamate (24, 48 hours)

Intracellular [glucose] measured in control and L-glutamate [0.5 mM] treated HCV gt2a infection models at 24 hour (white columns) and 48 hour (grey columns) time points. **(A)** Intracellular glucose concentrations (μM) measured in control and L-glutamate treated Huh7 and HCV SGR cells at 24 hours (white columns) and 48 hours (grey columns) post-seeding. **(B)** Intracellular glucose concentrations (μM) measured in control and L-glutamate treated mock- and JFH-1 infected Huh7 cells at 24 hours and 48 hours post-infection. **(C)** The standard curve using D-glucose standards [0 – 20 μM] produced at the time of assay from which intracellular glucose concentrations were deduced. Data shown are averages of triplicate measurements from a single experiment with error bars representing standard deviation (SD).

Figure 42 (A) shows that comparable glucose concentrations (mean= 23.79 μM, SD +/- 2.52) are seen in control and L-glutamate treated Huh7 and HCV SGR cells at 24 hours post-seeding. Likewise, a similar concentration of intracellular glucose (mean= 24.56 μM, SD +/- 0.89) is seen in both the Huh7 and HCV SGR control at 48 hours post-seeding. However, a lower concentration of intracellular glucose is present in Huh7 cells treated with L-glutamate (8.76μM, SD +/- 1.01) at 48 hours post-seeding, whereas the concentration of glucose in L-glutamate treated HCV SGR cells increases (33.05μM +/- 3.03).

As shown in **Figure 42 (B)**, intracellular glucose concentrations in mock- and JFH-1 infected Huh7 cells are comparable (mean= 68.93 μM, SD +/- 10.50) under both control and L-glutamate treated conditions at 24 hours post-infection. At 48 hours post-infection, however, there is a 3.4-fold increase in intracellular [glucose] in mock infected Huh7 cells (mean= 305.67 μM, SD +/- 25.59) under both control and L-glutamate treated conditions. Conversely, intracellular glucose concentration does not significantly change between 24 hours (83.05 μM, SD +/- 27.76) and 48 hours (76.98 μM, SD +/- 18.12) post-infection in control JFH-1 infected hepatocytes. However, there is an approximate 3.06-fold increase in intracellular [glucose] in L-glutamate treated JFH-1 infected Huh7 cells between 24 hours (69.48 μM, SD +/- 13.75) and 48 hours (212.81 μM, SD +/- 24.20) post-infection.

The data presented here indicate that control Huh7 and HCV SGR cells have similar concentrations of intracellular [glucose] where little difference is observed over 48 hours post-seeding. However, treatment with L-glutamate results in decreased and increased intracellular [glucose] in Huh7 and HCV SGR cells, respectively, at 48 hours post-seeding. JFH-1 infected Huh7 cells have a similar pattern of intracellular [glucose], though higher in comparison by almost 4-fold, to that seen in control Huh7 and HCV SGR cells where glucose concentration does not appear to alter over 48 hours and reflects data for the JFH-1 model previously shown by Blackham [(215)]. However, L-glutamate treatment noticeably increases glucose concentration in JFH-1 infected Huh7 cells, compared to the untreated control, at 48 hours post-infection.

Thus, to determine whether the differences in intracellular [glucose] in control and L-glutamate treated HCV gt2a infection models corresponded to changes in intracellular glycogen over the course of 48 hours, the Iodine-Potassium Iodide (IKI) method was performed on whole cell protein lysates isolated from control and L-glutamate treated HCV gt2a infection models and absorbance (560nm) was measured at 24 hour and 48 hour time points (**Figure 43 (A, B)**).

4.2.8. Intracellular Glycogen Content in HCV gt2a Infection Models +/- L-glutamate (24, 48 Hours)

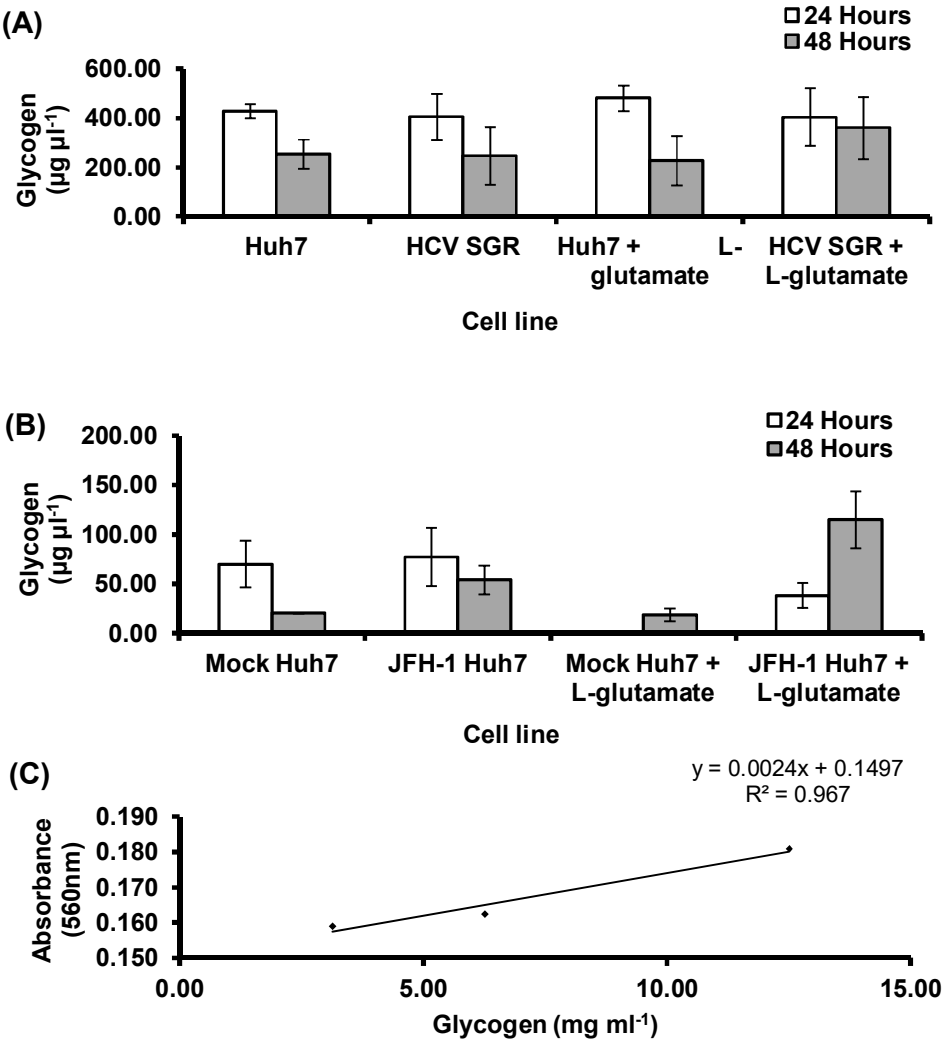


Figure 43 (A - C) - Intracellular Glycogen Content (µg µl^{-1}) in HCV gt2a Infection Models +/- L-glutamate (24, 48 Hours)

Intracellular glycogen content measured in control and L-glutamate [0.5 mM] treated HCV gt2a infection models at 24 hour (white columns) and 48 hour (grey columns) time points. **(A)** Intracellular glycogen (µg µl^{-1}) measured in control and L-glutamate treated Huh7 and HCV SGR cells at 24 hours (white columns) and 48 hours (grey columns) post-seeding. **(B)** Intracellular glycogen (µg µl^{-1}) measured in control and L-glutamate treated mock- and JFH-1 infected Huh7 cells at 24 hours (white columns) and 48 hours (grey columns) post-infection. **(C)** The standard curve produced at the time of assay using glycogen standards [3.125 – 12.5 mg ml^{-1}] from which intracellular glycogen content was deduced. Data shown are averages of triplicate measurements from a single experiment with error bars representing standard deviation (SD).

Figure 43 (A) shows that intracellular glycogen content in Huh7 and HCV SGR cells under both control and L-glutamate treated conditions are comparable at 24 hours post-seeding (mean= 429.13 µg µl^{-1}, SD +/- 35.76). Intracellular glycogen content in

control Huh7 and HCV SGR cells, as well as L-glutamate treated Huh7 cells, comparably decrease to similar levels (mean= 243.14 µg $µl^{-1}$, SD +/- 14.06) at 48 hours post-seeding. However, intracellular glycogen content in HCV SGR cells treated with L-glutamate increases by 39.7% (360.23 µg $µl^{-1}$, SD +/- 126.61) compared to the control at this time point (257.71. µg $µl^{-1}$, SD +/- 116.81). This indicates that there is a surplus of intracellular glucose that is stored as glycogen polymers.

As shown in **Figure 43 (B)**, the glycogen content in control mock- and JFH-infected cells is comparable at 24 hours post-infection (mean= 73.74 µg $µl^{-1}$, SD +/- 5.12) that is substantially lower than the results for the HCV SGR model at this time point. No data was obtained when intracellular glycogen was measured in mock infected Huh7 cells treated with L-glutamate at 24 hours post-infection. However, glycogen content in L-glutamate treated JFH-1 infected Huh7 cells is lower (38.35 µg $µl^{-1}$, SD +/- 12.69) than that seen in the untreated control at 24 hours post-infection which supports the observations indicating that glucose metabolism in HCV gt2a infection models is stimulated by this treatment.

At 48 hours post-infection, intracellular glycogen in control mock infected Huh7 cells (20.52, µg $µl^{-1}$, SD +/- 5.22) is comparable to that in L-glutamate treated mock infected Huh7 cells (18.71 µg $µl^{-1}$, SD +/- 6.43). Conversely, control JFH-1 infected

Huh7 cells contain a higher level of glycogen (54.06 μg μl^{-1}, SD +/- 14.28,) and there is a significant ($p= 1.64\times10^{-3}$) increase in intracellular glycogen in L-glutamate treated JFH-1 infected Huh7 cells (114.93 μg μl^{-1}, SD +/- 29.84) at 48 hours post-infection [(498)].

These data suggest that mitochondrial dysfunction caused by calcium ion overload is evident in both HCV gt2a infection models which may account for disturbances in glucose metabolism at the point of oxidative phosphorylation, and, which may also affect glycogen synthesis. However, this experiment shows that these effects of mitochondrial dysfunction may be alleviated by L-glutamate treatment, possibly as a result of reducing mitochondrial calcium uptake.

To examine the effects of inhibiting mitochondrial dysfunction on the dysregulation of lipid metabolism at a transcriptional level, qRT-PCR was used to measure the mRNA transcript abundance of genes characterising dysregulated lipid metabolism in HCV infection using total RNA isolated from control and L-glutamate treated Huh7 and HCV SGR cells at 24 hours and 48 hours post-seeding. The results obtained were compared to the control data from **Chapter 3** (**Figure 44 (A, B)**).

4.2.9. Lipogenic Gene Transcription in HCV gt2a Infection Models +/- L-glutamate (24, 48 Hours)

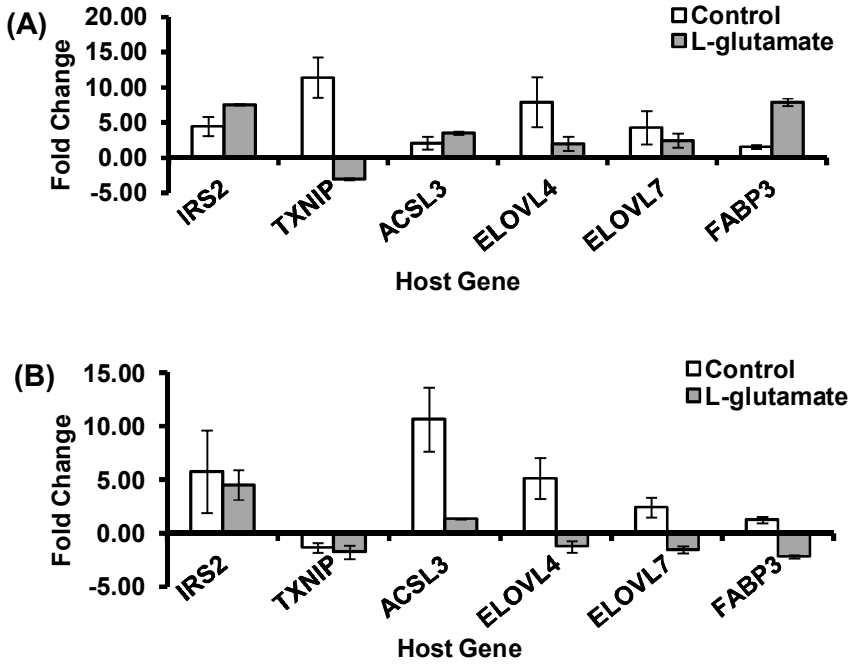


Figure 44 (A, B) – Lipogenic gene transcription in HCV SGR cells +/- L-glutamate (24, 48 hours)

Relative fold change of transcription of lipogenic genes measured in control (white columns) and L-glutamate treated (grey columns) HCV SGR cells, compared to Huh7 cells, at 24 hours and 48 hours post-seeding. **(A)** Mean fold changes in HCV SGR cells at 24 hours post-seeding. **(B)** Mean fold changes in HCV SGR cells at 48 hours post-seeding. Genes assayed; Insulin receptor substrate 2 (**IRS2**), Thioredoxin-interacting Protein (**TXNIP**), Acyl CoA synthetase long-chain family member 3 (**ACSL3**), ELOVL Fatty Acid Elongase 4 (**ELOVL4**), ELOVL Fatty Acid Elongase 7 (**ELOVL7**), Fatty Acid Binding Protein 3 (**FABP3**). Data shown are averages of triplicate measurements from a single experiment with error bars representing standard deviation (SD). Graphs representing differences in cycle thresholds (ΔC_T) between cell lines under these conditions are shown in **Appendix A2.3 (A, B)**.

As shown in **Figure 44 (A)**, treatment of HCV SGR cells with L-glutamate enhances IRS2 transcription (+7.54-fold, SD +/- 0.10) compared to the control (+4.49-fold, SD +/- 1.34) at 24 hours post-seeding.

Conversely, the treatment of HCV SGR cells with L-glutamate gives rise to a significant (p= 0.04) reduction in TXNIP transcription (-3.03-fold, SD +/- 0.16) compared to the control (+11.40-fold, SD +/- 2.86) at 24 hours post-seeding.

However, ACSL3 transcription increases in L-glutamate treated HCV SGR cells (+3.53-fold, SD +/- 1.01) compared to the control (+2.10-fold, SD +/- 0.93) at this time point which may give rise to an increase in either the degradation of fatty acids via β-oxidation or the formation of lipid droplets (LDs) [470,471]. Additionally, there is a significant (p= 0.05) reduction in ELOVL4 transcription in L-glutamate treated HCV SGR cells (+2.01, SD +/- 0.99) compared to the control (+7.92-fold, SD +/- 3.96) which occurs in tandem with a reduction in ELOVL7 mRNA (+2.44-fold, SD +/- 0.53) compared to the control (+4.31-fold, SD +/- 2.35) at 24 hours post-seeding. FABP3 transcription is significantly (p= 0.01) increased (+7.89-fold, SD +/- 2.16) in L-glutamate treated HCV SGR cells at 24 hours post-seeding relative to that measured in the untreated control (+1.53-fold, SD +/- 0.27) which suggests an increase in fatty acid transport from the cytoplasm to the nucleus [468].

Figure 44 (B) shows that the suppression of lipogenic gene transcription in HCV SGR cells by L-glutamate treatment is sustained at 48 hours post-seeding. However, insulin receptor substrate 2 (IRS2) mRNA remains upregulated (+4.54-fold, SD +/- 1.38) in L-glutamate treated HCV SGR cells though this measurement is lower than that found in the control (+5.80-fold, SD +/- 3.85) at this time point.

IRS2 was assayed in this experiment due to its upregulation (+5.26-fold, p= 5.35×10^{-19}) at 48 hours post-infection in the current microarray data analysis and is of relevance to this study as this gene is reported to stimulate pro-lipogenic effects which may contribute to the development of hepatic steatosis [499].

The qRT-PCR data from this experiment, however, suggests that the transcriptional induction of this gene is not related to the incidence of mitochondrial dysfunction in HCV SGR cells [(499)].

The effects of L-glutamate treatment on lipogenic gene transcription was also measured in the JFH-1 model using qPCR and cDNA synthesised from total RNA that was isolated at 24 hours and 48 hours post-infection. The results were compared to the control data described in **Figure 18 (A, B)** (**Figure 45 (A, B)**).

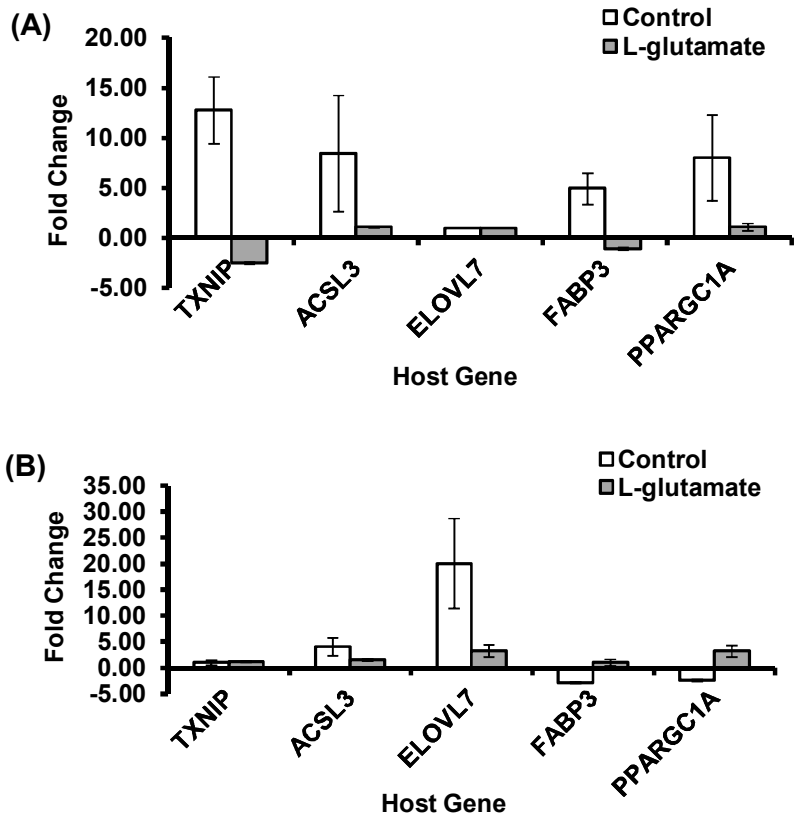


Figure 45 (A, B) – Lipogenic gene transcription in JFH-1 infected Huh7 cells (MOI – 7.5) +/- L-glutamate (24, 48 hours)

Relative fold change of transcription in lipogenic genes measured in control (white columns) and L-glutamate treated (grey columns) JFH-1 infected Huh7 cells, compared to mock infected Huh7 cells, at 24 hours and 48 hours post-infection. **(A)** Mean fold changes in JFH-1 infected cells at 24 hours post-infection. **(B)** Mean fold changes in JFH-1 infected cells at 48 hours post-infection. Genes assayed; Thioredoxin-interacting Protein (**TXNIP**), Acyl CoA synthetase long-chain family member 3 (**ACSL3**), ELOVL Fatty Acid Elongase 7 (**ELOVL7**), Fatty Acid Binding Protein 3 (**FABP3**), Peroxisome proliferator activated receptor-γc1a (**PPARGC1A**). Data shown are averages of triplicate measurements from a single experiment with error bars representing standard deviation (SD). Graphs representing differences in cycle thresholds (ΔC_T) between cell lines under these conditions are shown in **Appendix A2.4 (A, B)**.

As shown in **Figure 45 (A)**, the treatment of JFH-1 infected Huh7 cells with L-glutamate leads to a significant ($p= 1.37\times10^{-4}$) reduction in TXNIP transcription (-2.50-fold, SD +/- 0.09) at 24 hours post-infection, compared to that observed in the control (+12.77-fold, SD +/- 3.34).

ACSL3 mRNA transcripts are also lower in L-glutamate treated JFH-1 infected Huh7 cells (+1.07-fold, SD +/- 0.04) compared to the control (+8.45-fold, SD +/- 5.81) at 24 hours post-infection. Additionally, transcription of FABP3 in L-glutamate treated JFH-1 infected Huh7 cells is significantly (p= 0.03) downregulated (-1.11-fold, SD +/- 0.13) compared to the control (+4.93-fold, SD +/- 1.57), and PPARGC1A mRNA is transcribed at basal levels (+1.08 fold, SD +/- 0.37) which contrasts with the levels of upregulation seen in the control (+7.99-fold, SD +/- 4.29) at this timepoint.

Figure 45 (B) shows that the transcription of lipogenic genes in JFH-1 infected Huh7 cells treated with L-glutamate is comparable to the levels seen in the untreated control at 48 hours post-infection. However, ELOVL7 transcript abundance is significantly ($p= 9\times10^{-3}$) reduced (+3.31-fold, SD +/- 1.16) in comparison to the control (+20.16-fold, SD +/- 8.66). Similarly, PPARGC1A is upregulated (+3.21-fold, SD +/- 1.08) in L-glutamate treated JFH-1 infected Huh7 cells relative to the untreated control (-2.38-fold, SD +/- 0.19) which may be relevant to the alleviation of disturbances in glucose and lipid metabolism that are brought about by HCV infection as PPARGC1A transcriptionally co-activates genes that are associated with gluconeogenesis, oxidative metabolism, mitochondrial biogenesis, and lipid transport [(500)].

Generally, the transcription of TXNIP and downstream lipogenic genes are suppressed in both HCV SGR- and JFH-1 infected Huh7 cells following treatment with L-glutamate.

However, the panel of genes used to characterise dysregulated lipid metabolism in control and L-glutamate treated HCV gt2a infection models differed slightly as the transcript abundance of IRS2 and ELOVL4 was not altered in control JFH-1 experiments, i.e. no data produced after 36.00 cycles.

To observe whether the differences in TXNIP and downstream lipogenic gene transcription manifested phenotypically in the HCV gt2a infection models, intracellular triglyceride concentrations were quantified using the Triglyceride Quantification Kit, whole cell protein lysate isolated from control and L-glutamate treated HCV SGR and JFH-1 infected Huh7 cells, and the absorbance (570nm) was measured at 24 hour and 48 hour time points (**Figure 46 (A - C)**).

4.2.10. Intracellular [triglyceride] in HCV gt2a Infection Models +/- L-glutamate (24, 48 Hours)

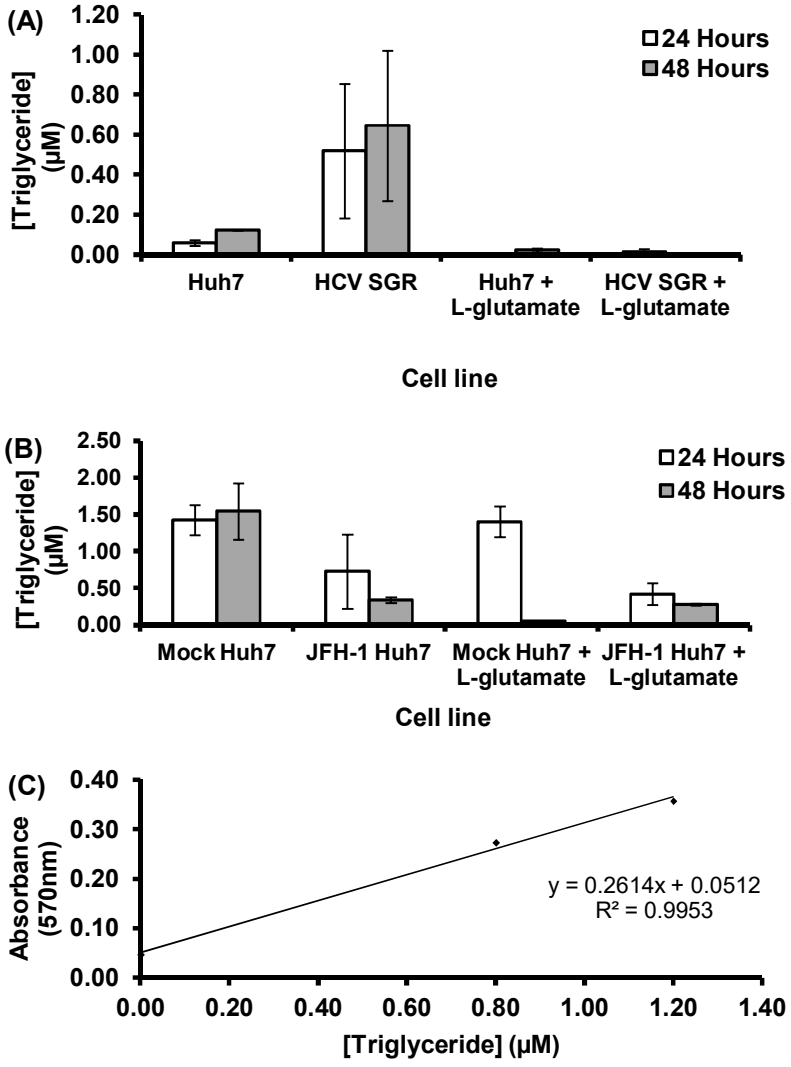


Figure 46 (A - C) - Intracellular [triglyceride] (µM) in HCV gt2a Infection Models +/- L-glutamate (24, 48 Hours)

Intracellular triglyceride concentration (µM) measured in control and L-glutamate treated HCV gt2a infection models at 24 hour and 48 hour time points. **(A)** Intracellular triglyceride concentration in control and L-glutamate treated Huh7 and HCV SGR cells at 24 hours (white columns) and 48 hours (grey columns) post-seeding. **(B)** Intracellular triglyceride concentration in control and L-glutamate treated mock- and JFH-1 infected Huh7 cells at 24 hours (white columns) and 48 hours (grey columns) post-infection. **(C)** The standard curve produced using triglyceride standards [0 – 1.2 µM] at the time of assay from which intracellular [triglyceride] was deduced. Data shown are averages of triplicate measurements from a single experiment with error bars representing standard deviation (SD).

As shown in **Figure 46 (A)**, control Huh7 cells have a low concentration (0.06 μM, SD +/- 0.01) of triglycerides at 24 hours post-seeding that increases approximately 20-fold (0.12 μM, SD +/- 0.0014) at 48 hours post-seeding. In comparison, there is a greater concentration of intracellular triglycerides in control HCV SGR cells at 24 hours (0.52 μM, SD +/- 0.33) and 48 hours (0.64 μM, SD +/- 0.30) post-seeding. The concentration of triglycerides in L-glutamate treated HCV SGR cells is reduced compared to the control at 24 hours (0.02 μM, SD +/- 0.01) and is undetectable at 48 hours post-seeding. These data reflect the differences in lipogenic gene transcription shown by the qRT-PCR analyses.

Figure 46 (B) shows mock infected Huh7 cells have a high intracellular [triglyceride] at 24 hours (1.42 μM, SD +/- 0.20) and 48 hours (1.54 μM, SD +/- 0.38) post-infection. In comparison, intracellular triglyceride concentration is reduced by 53.3% (0.72 μM, SD +/- 0.50) and 78% (0.34 μM, SD +/- 0.04) in untreated JFH-1 infected Huh7 cells at 24 hours and 48 hours post-infection, respectively. This may occur as a consequence of virus assembly, egress, and the overexpression of genes involved in intracellular transport of secretory vesicles, e.g. RAB27A, RAB27B, being active in the JFH-1 model of HCV infection [214].

Meanwhile, the treatment of mock infected Huh7 cells with L-glutamate results in an intracellular triglyceride concentration that is comparable to the untreated control (1.39 μM, SD +/- 0.20), whereas that measured in JFH-1 infected Huh7 cells treated with L-glutamate (0.41 μM, SD +/- 0.15) is lower than the control (0.73 μM, SD +/- 0.50) at 24 hours post-infection.

However, at 48 hours post-infection, a significant ($p= 0.03$) decrease in intracellular triglyceride is seen in L-glutamate treated mock infected Huh7 cells (0.05 μM, SD +/- 0.01) relative to the mock infected control, and little difference in intracellular [triglyceride] (mean= 0.31 μM, SD +/- 0.04) can be seen between control and L-glutamate treated JFH-1 infected Huh7 cells.

This experiment shows that JFH-1 infected Huh7 cells have a higher concentration of intracellular triglycerides than the HCV SGR model which is most likely due to the presence of structural proteins compounding the dysregulation of lipid metabolism caused by the viral replicase proteins. Furthermore, the intracellular [triglyceride] in HCV gt2a infection models reflect the fold-changes seen in the transcription of TXNIP and downstream lipogenic genes as well as the suppression thereof by treatment with L-glutamate.

To observe the effect of inhibited mitochondrial calcium ion uptake, and so reduced intracellular triglyceride concentration, on the formation of lipid droplets (LDs) in HCV gt2a infection models, L-glutamate treated HCV SGR- and JFH-1 infected Huh7 cells and controls were stained with Oil-Red-O, a specific stain for LDs and neutral triglycerides at 24 hour and 48 hour time points, and examined using light microscopy (**Figures 47 - 50**) [(501)].

4.2.11. Intracellular Lipid Droplets (LDs) in HCV gt2a Infection Models +/- L-glutamate (24, 48 Hours)

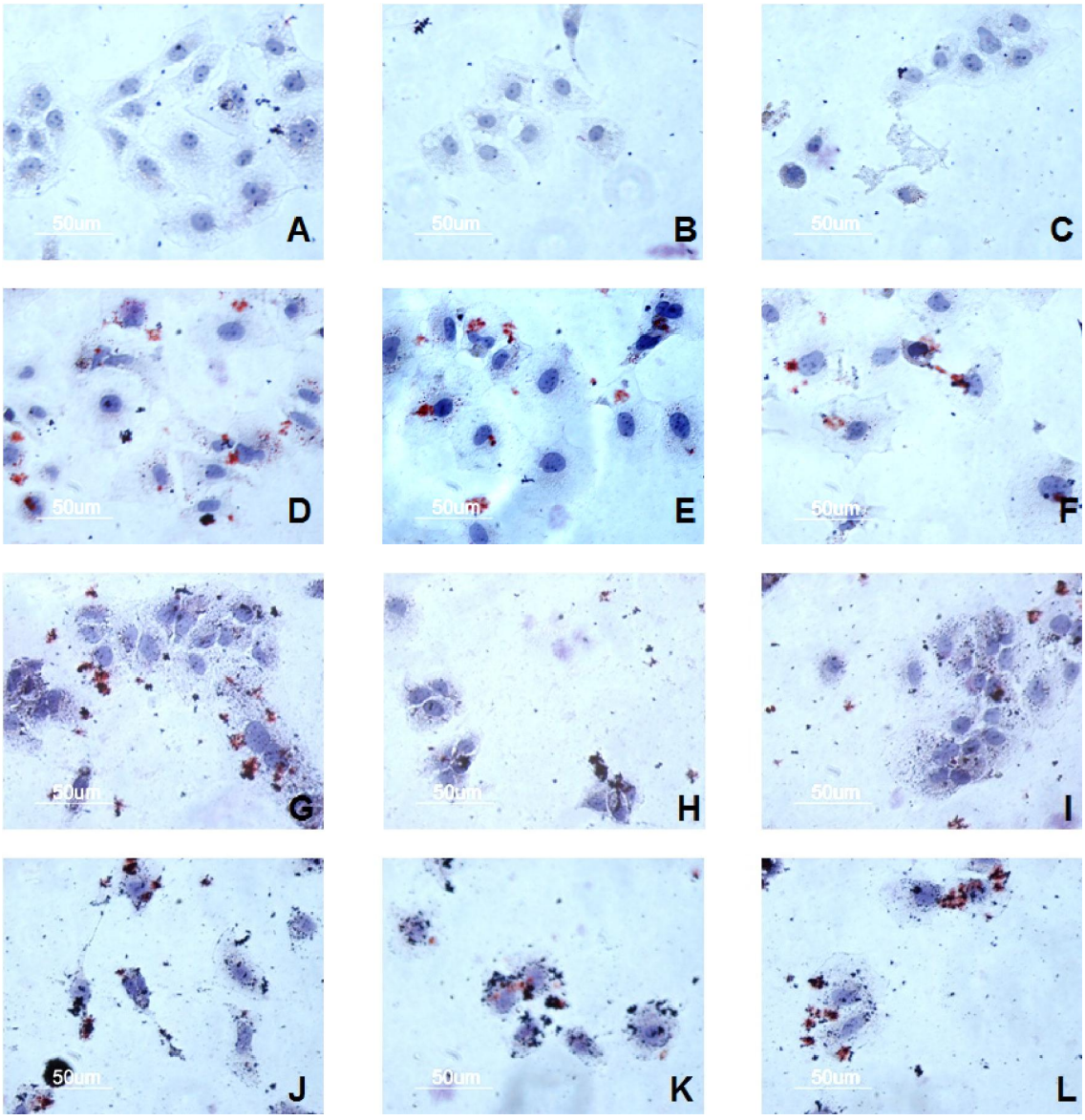


Figure 47 (A – L) - Oil-Red-O stained Huh7 and HCV SGR cells (24, 48 hours)

Huh7 and HCV SGR cells were stained for lipid droplets using Oil-Red-O under control conditions at 24 hours and 48 hours post-seeding. Nuclei are stained blue. Lipids are stained red. **A – C;** Huh7 cells are negative for the presence of lipid at 24 hours post-seeding. **D – F;** HCV SGR cells are positive for the presence of lipid at 24 hours post-seeding. **G – I;** Huh7 cells show limited staining for the presence of lipid at 48 hours post-seeding. **J – L;** ORO staining of lipid in HCV SGR cells is of greater intensity at 48 hours post-seeding. Images shown represent 3 fields of view of for each condition.

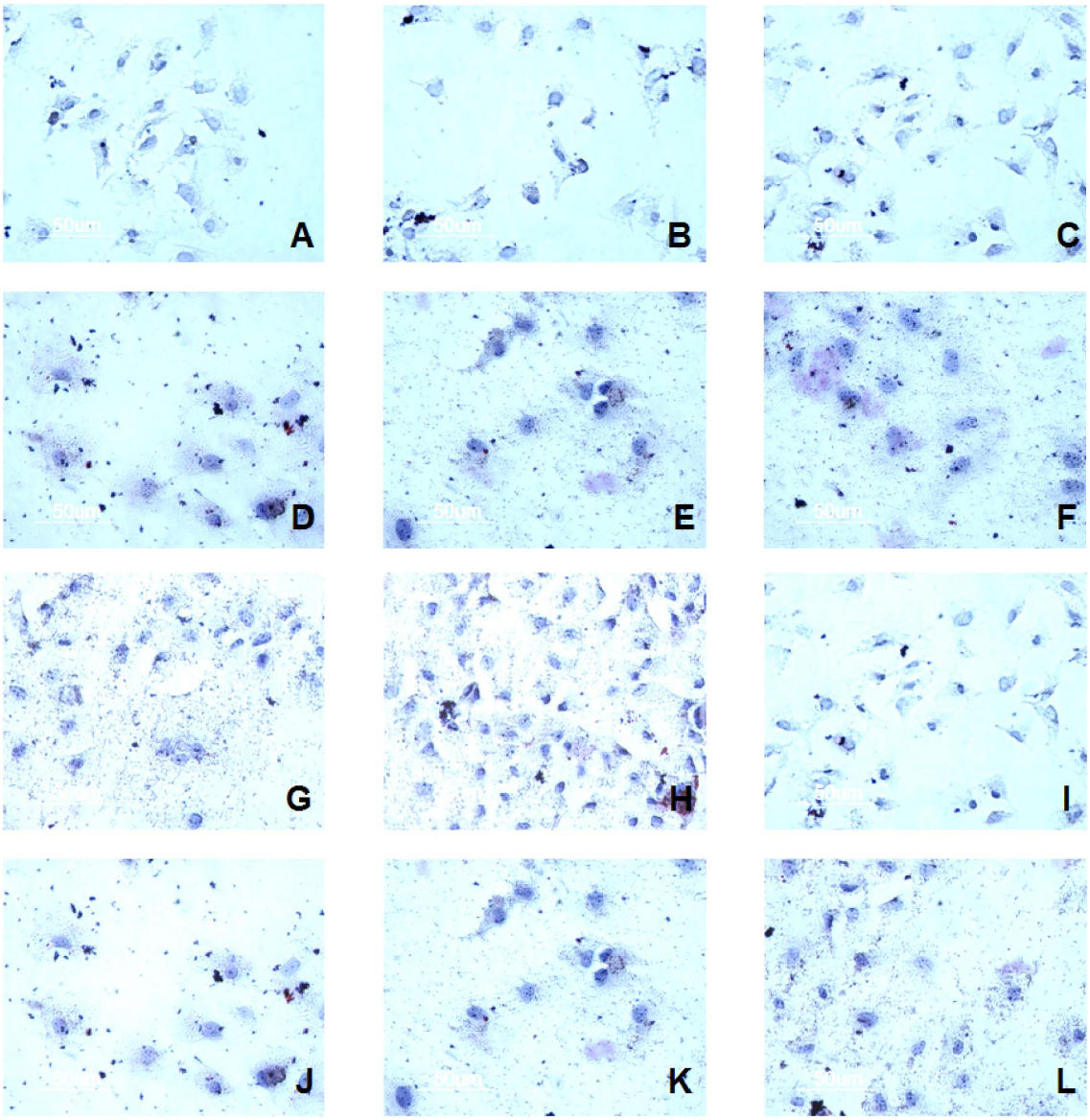


Figure 48 (A – L) - Oil- Red-O stained Huh7 and HCV SGR cells + L-glutamate (24, 48 hours)

Huh7 and HCV SGR cells were stained for lipid droplets using Oil-Red-O following treatment with L-glutamate at 24 hours and 48 hours post-seeding. Nuclei are stained blue. Lipids are stained red. **(A – C)** Huh7 cells are negative for the presence of lipid at 24 hours post-seeding. (**D – F)** HCV SGR cells are negative for the presence of lipid at 24 hours post-seeding. (**G – I)** Huh7 cells show limited staining for the presence of lipid (red stains) at 48 hours post-seeding. **(J – L)** ORO staining of intracellular lipid is undetectable in HCV SGR cells at 48 hours post-seeding. Images shown represent 3 fields of view of for each condition.

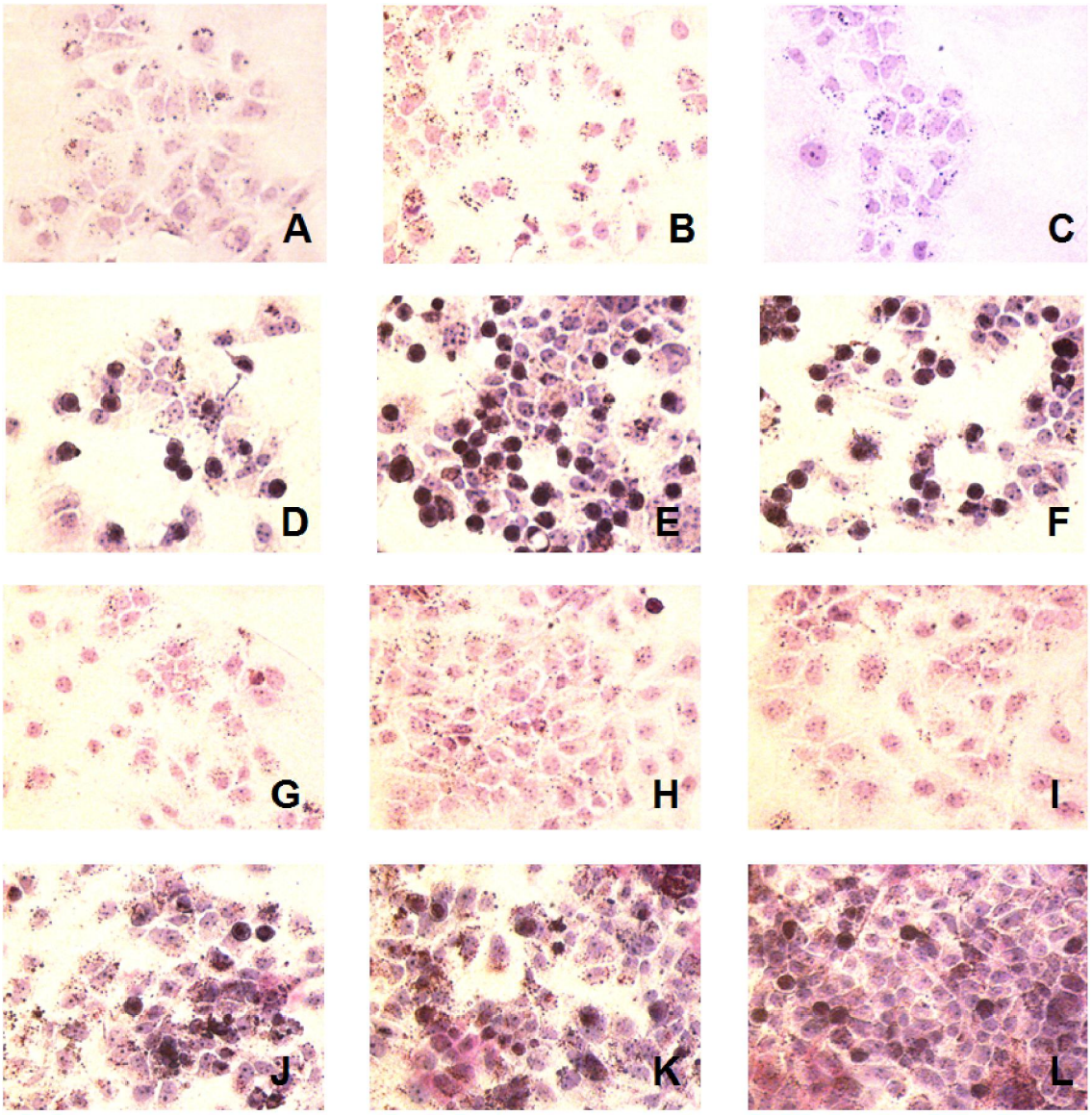


Figure 49 (A – L) - Oil-Red-O (ORO) staining of intracellular lipid droplets in Mock- and JFH-1 infected Huh7 cells (MOI – 7.5) (24, 48 Hours)

Mock- and JFH-1 infected Huh7 cells were stained for lipid droplets using Oil-Red-O under control conditions at 24 hours and 48 hours post-infection. Nuclei are stained blue. Lipids are stained red. **(A – C)** Mock infected Huh7 cells are negative for the presence of lipid at 24 hours post-infection. **(D – F)** JFH-1 infected Huh7 cells are positive for a nuclear localisation of lipid (purple nuclei) at 24 hours post-infection. **(G – I)** Mock infected Huh7 cells show limited staining for the presence of lipid at 48 hours post-infection. **(J – L)** ORO staining of lipid in JFH-1 infected Huh7 cells is of greater intensity at 48 hours post-infection. Images shown represent 3 fields of view of for each condition.

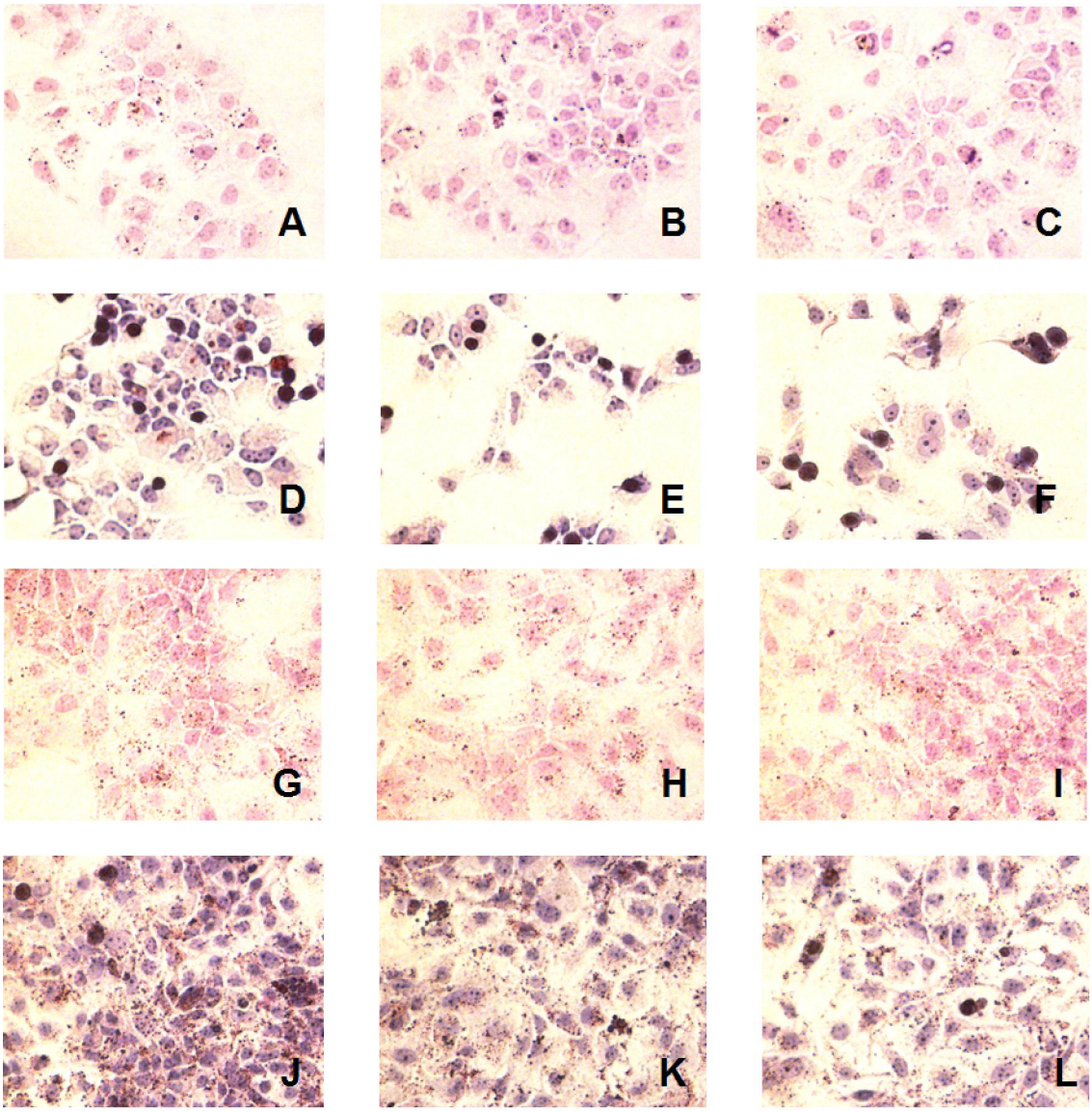


Figure 50 (A – L) - Oil-Red-O (ORO) staining of intracellular lipid droplets in Mock- and JFH-1 infected Huh7 cells (MOI – 7.5) + L-glutamate (24, 48 Hours)

Mock- and JFH-1 infected Huh7 cells were stained for lipid droplets using Oil-Red-O following treatment with L-glutamate at 24 hours and 48 hours post-infection. Nuclei are stained blue. Lipids are stained red. **(A – C)** Mock infected Huh7 cells + L-glutamate are negative for the presence of lipid at 24 hours post-infection. **(D – F)** JFH-1 infected Huh7 cells + L-glutamate have limited staining of nuclear lipid (purple nuclei) at 24 hours post-infection. **(G – I)** Mock infected Huh7 cells are negative for the presence of lipid at 48 hours post-infection. **(J – L)** JFH-1 infected Huh7 cells + L-glutamate have a limited amount of lipid at 48 hours post-infection. Images shown represent 3 fields of view of for each condition.

The treatment of HCV gt2a infection models with L-glutamate results in a substantial reduction of intracellular LDs at 24 hour and 48 hour time points. To confirm this, the images produced from this experiment were quantitated using a ImageJ software (**Figure 51 (A, B)**) [465].

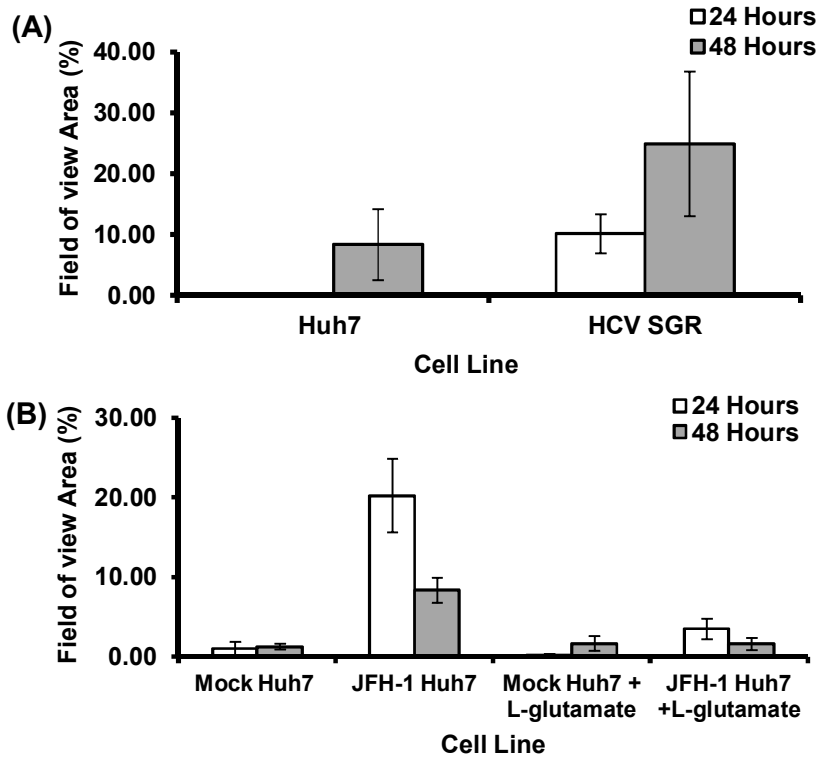


Figure 51 (A, B) - Quantification of ORO stained intracellular LDs in HCV gt2a infection models +/- L-glutamate (24, 48 Hours)

Images of ORO stained lipid droplets (LDs) in HCV gt2a infection models were converted to 8-bit RGB stacks using ImageJ. Thresholds for LD were set and percentage area per field of view area was determined. **(A)** Quantification of LD abundance in control Huh7 and HCV SGR cells at 24 hours (white columns) and 48 hours (grey columns) post-seeding**.** No data was obtained for Huh7 or HCV SGR cells treated with L-glutamate. **(B)** Quantification of LD abundance in mock- and JFH-1 infected Huh7 cells +/- L-glutamate at 24 hours (white columns) and 48 hours (grey columns) post-infection**.** Data shown are averages of triplicate measurements from a single experiment with error bars representing standard deviation (SD).

As shown in **Figure 51 (A)**, control Huh7 cells do not stain for lipid droplets (LDs) using ORO at 24 hours post-seeding, although a low abundance (8.35%, SD +/- 5.83) is present at 48 hours post-seeding.

However, LDs are detectable in control HCV SGR cells at 24 hours (10.14%, SD +/- 3.26) which increases by approximately 2.5-fold at 48 hours (24.95%, SD +/- 11.94) post-seeding. Huh7 and HCV SGR cells are negative for the presence of ORO-stained LDs at 24 hours and 48 hours post-seeding following treatment with L-glutamate. This indicates that the formation of LDs in the replicon model of HCV replication is largely dependent on mitochondrial dysfunction caused by calcium ion overload.

Figure 51 (B) represents the quantitation of ORO-stained LDs in mock- and JFH-1 infected Huh7 cells treated with L-glutamate and controls at 24 hours and 48 hours post-infection. In control mock infected Huh7 cells, there is a minimal presence of intracellular LDs at both 24 hours (1.02%, SD +/- 0.81) and 48 hours (1.26%, SD +/- 0.38) post-infection. However, LDs are significantly abundant in control JFH-1 infected Huh7 cells at 24 hours (20.23%, SD +/- 4.26) ($p= 0.02$) and 48 hour (8.32%, SD +/- 1.59) ($p= 1.6\times10^{-3}$) time points in relation to mock infected Huh7 cells. There are trace amounts of LDs in mock infected Huh7 cells, following treatment with L-glutamate, at both 24 hours (0.21%, SD +/- 0.10) and 48 hours (1.64%, SD +/- 0.93) post-infection.

Similarly, there is a significant (p= 0.03) reduction in intracellular LDs in L-glutamate treated JFH-1 infected Huh7 cells at 24 hours (3.47%, SD +/- 1.29) and 48 hours (1.58%, SD +/- 0.78) ($p= 2\times10^{-3}$) post-infection compared to the control which suggests that mitochondrial dysfunction induced by calcium ion overload is also a contributing factor to the development of intracellular LDs in HCV infection.

This experiment suggests that both HCV gt2a models of infection share a common pathway in the formation of LDs during virus replication, namely the incidence of mitochondrial dysfunction which may occur as a consequence of ER stress induction. However, as shown by the images taken of HCV gt2a infection models stained with ORO, control HCV SGR cells have a clear cytoplasmic localisation of LDs while those in the JFH-1 model appear to have a nuclear localisation. HCV core protein has been reported to localise to the nucleus in many different liver cell types, as well as with large lipid droplets in the case of stellate cells [(41)]. Furthermore, HCV core has been shown to be instrumental to the redistribution of LDs to the perinuclear compartment in infected cells [(502)]. These data also appear to correlate with the reduction of triglycerides that were measured in HCV gt2a infection models following treatment with L-glutamate (**Figure 46 (A, B)**).

Thus, intracellular virus was quantitated using qRT-PCR, total cellular RNA isolated from HCV SGR cells treated with L-glutamate and controls, and JFH-1 RNA standards [6 ng – 60 fg] to examine the effects of suppressed lipid metabolism, induced through glutamate treatment, on virus replication at 24 hours and 48 hours post-seeding (**Figure 52**).

4.2.12. HCV genome copy number in HCV gt2a Infection Models +/- L-glutamate (24, 48 Hours)

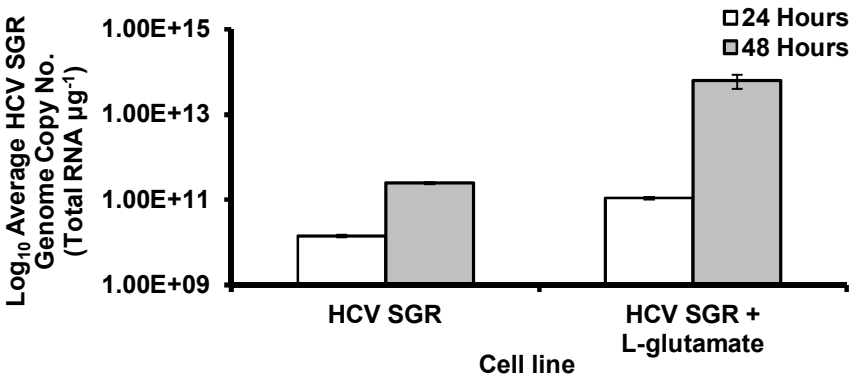


Figure 52 - Intracellular HCV SGR replication in HCV SGR cells +/- L-glutamate (24, 48 Hours)

Intracellular HCV SGR genome copy number measured in control and L-glutamate treated HCV SGR cells at 24 hours (white columns) and 48 hours (grey columns) post-seeding. Data shown are averages of triplicate measurements from a single experiment with error bars representing standard deviation (SD).

As shown in **Figure 52**, intracellular replicon transcript in HCV SGR cells treated with L-glutamate is significantly ($p= 0.03$) higher (1.08×10^{11}, SD +/- 6.30×10^{9}) than the control (1.41×10^{10}, SD +/- 6.35×10^{8}) at 24 hours post-seeding. HCV SGR RNA replication is also greater in HCV SGR cells treated with L-glutamate (6.30×10^{13}, SD +/- 2.29×10^{13}) relative to the untreated control (2.45×10^{11}, SD +/- 1.37×10^{10}) at 48 hours post-seeding.

Likewise, to determine the effects of suppressed lipid metabolism via inhibited mitochondrial dysfunction on intracellular virus replication in the JFH-1 model of HCV infection, absolute viral genome copy number was quantitated using qRT-PCR, JFH-1 RNA standards [6 ng – 60 fg], and total cellular RNA isolated from JFH-1 infected Huh7 cells treated with L-glutamate and controls at 24 hours and 48 hours post-infection (**Figure 53**).

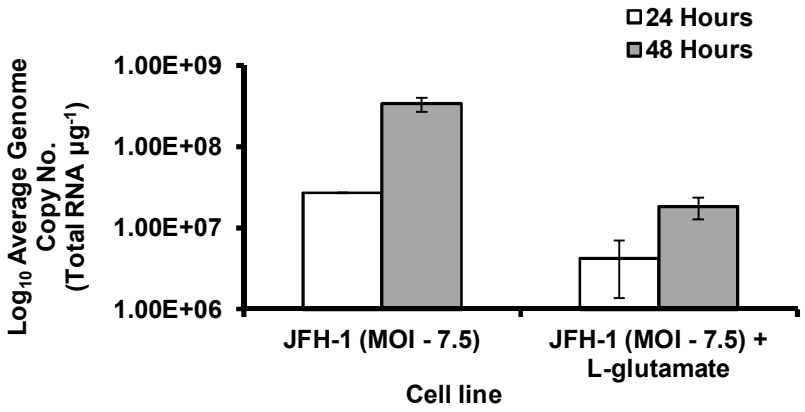


Figure 53 - Intracellular HCV replication in JFH-1 infected Huh7 cells (MOI – 7.5) +/- L-glutamate (24, 48 Hours)

Intracellular virus genome copy number measured in control and L-glutamate treated JFH-1 infected Huh7 cells at 24 hours (white columns) and 48 hours (grey columns) post-infection. Data shown are averages of triplicate measurements from a single experiment with error bars representing standard deviation (SD).

Figure 53 shows that treatment of JFH-1 infected Huh7 cells with L-glutamate significantly ($p= 7.57\times10^{-3}$) reduces intracellular virus genome copy number (4.24×10^{6}, SD +/- 2.85×10^{6}) compared to the untreated control (2.74×10^{7}, SD +/- 3.54×10^{5}) at 24 hours post-infection.

Similarly, there is a significant ($p= 2.9\times10^{-4}$) reduction in intracellular genome copy number in L-glutamate treated JFH-1 infected Huh7 cells (1.84×10^{7}, SD +/- 5.58×10^{6}), compared to the untreated control (3.41×10^{8}, SD +/-6.67×10^{7}), at 48 hours post-infection.

To determine the effects of inhibited mitochondrial dysfunction, and the suppressed dysregulation of lipid metabolism, on extracellular virus titre in the JFH-1 model, HCV genome copy number was quantitated using qRT-PCR, JFH-1 RNA standards [6 ng – 60 fg], and RNA isolated from media used to culture L-glutamate treated JFH-1 infected Huh7 cells and controls at 24 hours and 48 hours post-infection (**Figure 54**).

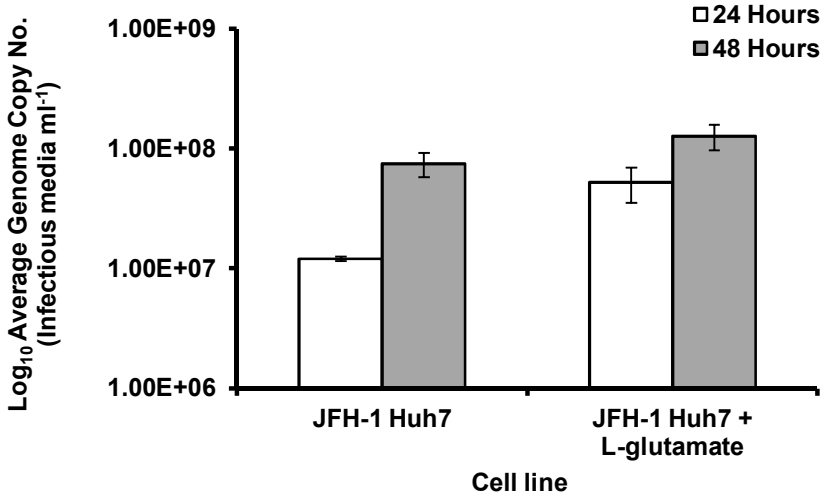


Figure 54 - Extracellular HCV secretion in JFH-1 infected Huh7 cells (MOI – 7.5) +/- L-glutamate (24, 48 Hours)

Extracellular virus genome copy number measured in RNA isolated from media used to culture control and L-glutamate treated JFH-1 infected Huh7 cells at 24 hours (white columns) and 48 hours (grey columns) post-infection. Data shown are averages of triplicate measurements from a single experiment with error bars representing standard deviation (SD).

As **Figure 54** shows, treatment of JFH-1 infected Huh7 cells with L-glutamate gives rise to a significant (p= 0.02) increase in extracellular virus secretion (5.24×10^7, SD +/- 2.26×10^6) compared to the control (1.20×10^7, SD +/- 5.17×10^6) at 24 hours post-infection.

This effect is also seen at 48 hours post-infection where there is a significant (p= 0.01) 1.7-fold increase in extracellular virus (1.28×10^8, SD +/- 3.06×10^7) in JFH-1 infected cells treated with L-glutamate relative to the untreated control (7.51×10^7, SD +/- 1.71×0^7). Taken together, data for intra- and extracellular virus in JFH-1 infected Huh7 cells treated with L-glutamate indicate that this treatment may promote HCV particle secretion.

With L-glutamate appearing to affect both lipogenic gene transcription and virus replication in treated HCV gt2a infection models, Western Blotting was performed on whole cell protein lysates isolated from L-glutamate treated HCV SGR cells and JFH-1 infected Huh7 cells, as well as controls, to quantify both host (TXNIP) and viral (HCV NS3, HCV core) protein expression at 48 hours post-seeding (**Figures 55 - 57**).

4.2.13. Host and Viral Protein Expression in HCV gt2a Infection Models +/- L-glutamate (48 Hours)

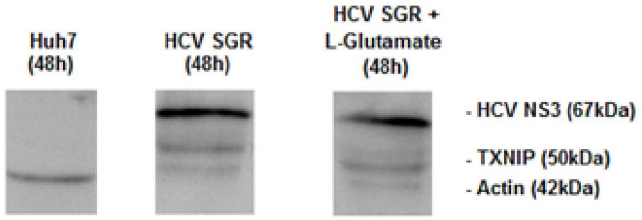


Figure 55 - Protein quantification (HCV NS3, TXNIP, Actin) in Huh7 and HCV SGR cells +/- L-glutamate (24, 48 hours)

Western Blot on 12% SDS-PAGE of intracellular protein (HCV NS3, TXNIP, β-Actin) isolated from control and L-glutamate treated Huh7 and HCV SGR cells at 48 hours (48h) post-seeding.

The protein expression of TXNIP relative to β-Actin in Huh7- and HCV SGR cells under control and L-glutamate treated conditions were quantified via densitometry using ImageJ software at 48 hours post-seeding (**Figure 56**).

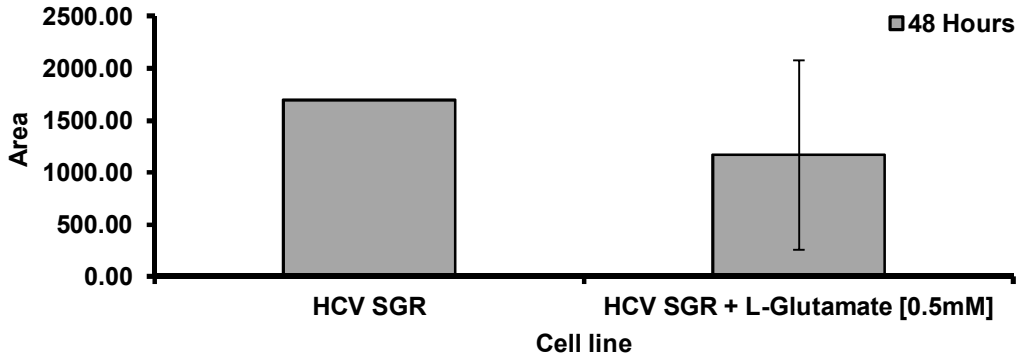


Figure 56 - Densitometry analysis of TXNIP protein expression in Huh7 and HCV SGR cells +/- L-glutamate (48 Hours)

Densitometry analysis of protein bands (TXNIP) following the Western Blot of intracellular protein isolated from control and L-glutamate treated Huh7 and HCV SGR cells at 48 hours (grey columns) post-seeding. Data shown are averages of triplicate densitometry measurements from a single experiment with error bars representing standard deviation (SD).

Figure 56 shows that there is an approximate 3-fold increase (1696.88, SD +/- 907.35) in TXNIP expression in control HCV SGR cells whilst that in L-glutamate treated HCV SGR cells is reduced by ~31.1% (1169.88, SD +/- 576.43) at 48 hours post-seeding.

This result supports the qRT-PCR data for TXNIP transcription in L-glutamate-treated HCV SGR cells where a downregulation of mRNA at 24 hours post-seeding corresponds to a suppression of protein expression at 48 hours.

To examine the effect of reduced TXNIP expression on that of viral protein in HCV SGR cells, HCV NS3 was also quantified in control and L-glutamate treated HCV SGR cells using densitometry analysis (**Figure 57**).

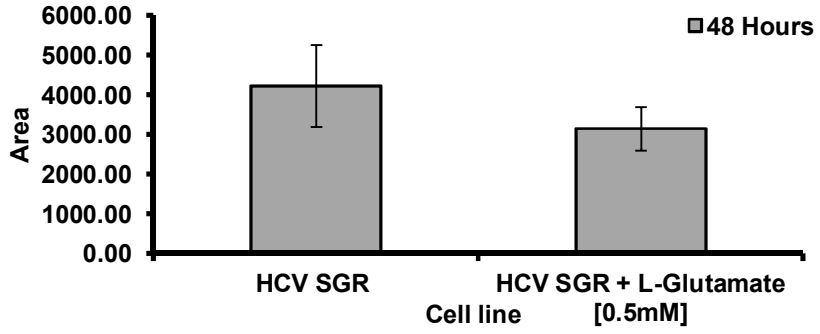


Figure 57 - Densitometry analysis of HCV NS3 protein expression in HCV SGR cells +/- L-glutamate (48 Hours)

Densitometry analysis of protein bands (HCV NS3) following the Western Blot of intracellular protein isolated from control and L-glutamate treated HCV SGR cells at 48 hours (grey columns) post-seeding. Data shown are averages of triplicate measurements from a single experiment with error bars representing standard deviation (SD).

Figure 57 shows that the untreated control shows a high level of HCV NS3 protein expression (4228.28, SD +/- 1032.20) which is comparatively reduced (3154.83, SD +/- 544.49) in HCV SGR cells treated with L-glutamate at 48 hours post-seeding

The effect of L-glutamate treatment on the expression of TXNIP and HCV core was also verified in the JFH-1 model by Western Blotting but produced unsatisfactory results.

Thus, to investigate whether the accumulation of mitochondrial calcium ions contribute to the presence of intracellular reactive oxygen species (ROS) and, hence, the transcriptional induction of TXNIP in HCV infection, mock- and JFH-1 infected Huh7 cells were stained with 2',7'-dihydrofluoroscein diacetate (H2DCFDA) under control and L-glutamate treated conditions and fluorescence (490nm) was measured at 24 hours and 48 hours post-infection (**Figure 58 (A, B)**).

4.2.14. Intracellular reactive oxygen species (ROS) in JFH-1 infected Huh7 cells +/- L-glutamate (24, 48 Hours)

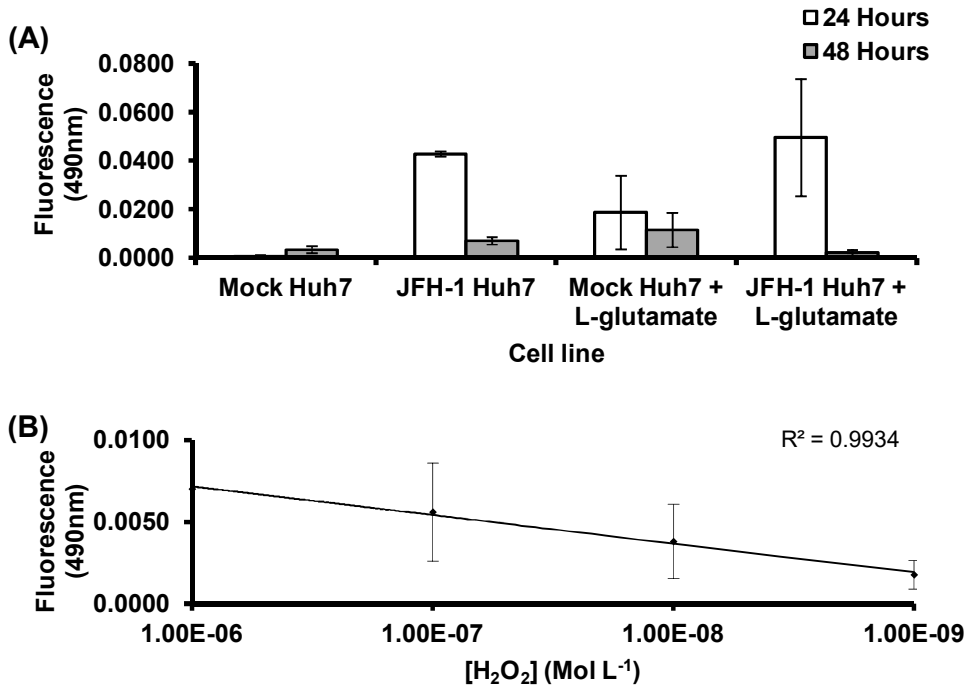


Figure 58 (A, B) - Fluorometric analysis of reactive oxygen species (ROS) in Mock- and JFH-1 infected Huh7 cells +/- L-glutamate [0.5 mM] (24, 48 Hours)

Intracellular ROS in mock- and JFH-1 infected Huh7 cells under both control and L-glutamate treated conditions at 24 hours and 48 hours post-infection. **(A)** Intracellular ROS in control and L-glutamate treated mock- and JFH-1 infected Huh7 cells at 24 hours (white columns) and 48 hours (grey columns) post-infection. **(B)** The standard curve produced at the time of assay using Huh7 cells treated with H_2O_2 [1 µM – 1 nM] to demonstrate linearity. Data shown are averages of triplicate measurements from a single experiment with error bars representing standard deviation (SD).

As shown in **Figure 58 (A)**, the presence of intracellular reactive oxygen species (ROS) in the mock control is baseline (0.0005, SD +/- 0.0002) at 24 hours post-infection, which contrasts with the abundance measured in control JFH-1 infected Huh7 cells (0.0427, SD +/- 0.001). However, L-glutamate treatment leads to an increase in intracellular ROS in both mock (0.019, SD +/- 0.015) and JFH-1 infected Huh7 cells (0.050, SD +/- 0.024).

Additionally, there is an incremental increase in ROS abundance in control mock infected Huh7 cells (0.0033, SD +/- 0.0013) whilst that measured in Huh7 cells infected with the JFH-1 isolate of HCV decreases (0.0071, SD +/- 0.0015) at 48 hours post-infection. Treatment with L-glutamate, however, reduces the abundance of ROS in both mock (0.0115, SD +/- 0.007) and JFH-1 infected Huh7 cells (0.002, SD +/- 0.001) at this time point.

Furthermore, this experiment was performed using HCV SGR cells that were treated with L-glutamate and the effects on intracellular ROS abundance were measured at 24 hours and 48 hours post-seeding. However, no difference was seen between treatments (data not shown).

Additionally, this experiment suggests that the source of intracellular ROS, and possibly the source of TXNIP overexpression, is not related to the mitochondrial generation of physiological ROS, i.e. the diffusion of superoxide anions ($O_2^{-\cdot}$) from the mitochondrial matrix to the cytosol via VDACs where they are catalysed into H_2O_2 by superoxide dismutase 1 (SOD1) [503,504].

4.3. Conclusion

This investigation aimed to study the occurrence of mitochondrial dysfunction and its involvement in the dysregulation of lipid metabolism during HCV infection. Experiments assessing the concentration of calcium ions localised to the mitochondria, thought to originate from ER stress, indicated that mitochondrial dysfunction was evident in both HCV SGR- and JFH-1 infected Huh7 cells.

This phenomenon was further characterised by examining changes in mitochondrial membrane potential, the initial stages of mitochondrial respiration (oxidative phosphorylation), and lipogenic gene transcription over the course of 48 hours in HCV gt2a infection models.

Mitochondrial dysfunction was found to correlate with abnormalities in intracellular glucose and glycogen concentrations, as well as the upregulated transcription of TXNIP and downstream lipogenic genes which may account for an increase in intracellular triglycerides (TGs), lipid droplets (LDs), and intracellular virus titres in HCV gt2a infection models. Disturbances in host metabolism were tested by inhibiting the mitochondrial uptake of calcium ions by mitochondrial voltage dependent anion channels (VDACs) using a high concentration of L-glutamate [0.5 mM]. This treatment was previously reported to reduce the concentration of calcium ions in isolated mitochondria but is shown here, for the first time, to be effective in decreasing mitochondrial Ca^{2+} when applied to whole cells.

In conclusion, the treatment of HCV gt2a infection models with L-glutamate generally led to a stimulation of glucose metabolism that is thought to arise from anaplerosis, a suppression of TXNIP and downstream lipogenic gene transcription, a reduction in intracellular triglycerides and lipid droplets, and a decrease intracellular virus replication in JFH-1 infected Huh7 cells.

The findings from this study of mitochondrial dysfunction in the context of dysregulated lipid metabolism during HCV infection and the pathways to which they relate require further investigation but are putatively illustrated in **Figure 59**.

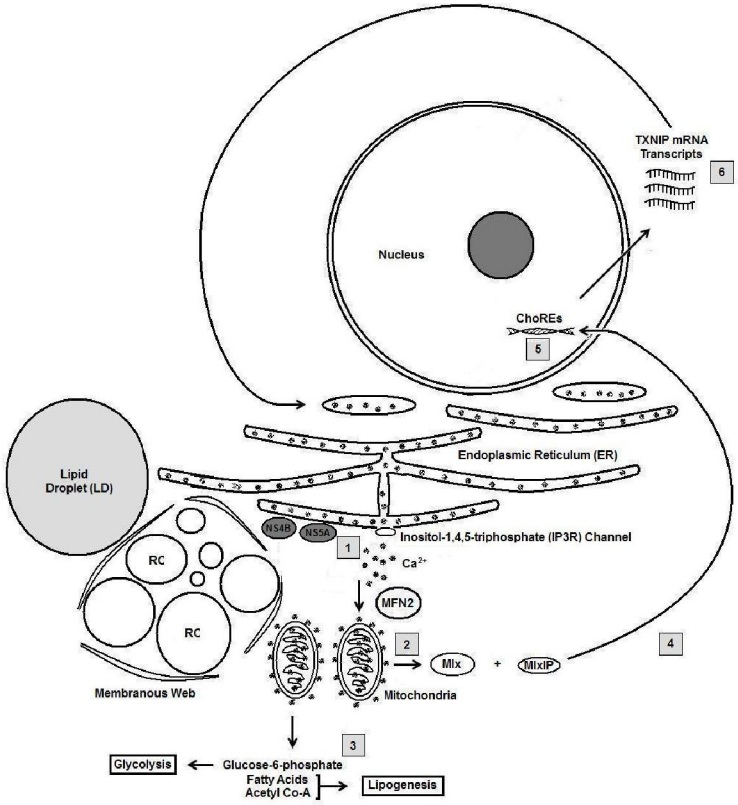


Figure 59 – TXNIP upregulation through mitochondrial dysfunction induced by calcium ion overload following ER stress

(1) HCV NS5A induces the efflux of intralumenal calcium ions from the ER by inositol-1,4,5-triphosphate (IP3R) channels to the cytosol following ER stress induced by HCV NS4B. **(2)** Cytosolic calcium localises at the mitochondria via the action of Mitofusin 2 (MFN2), causing dilation of voltage dependent anion channels (VDACs) an increase in mitochondrial permeability pore transition, and possibly displacement of Max like protein (Mlx). **(3)** Mitochondrial respiratory function is compromised and further metabolism of energetic substrates, e.g. glucose-6-phosphate (G6P), Fatty acids (FAs), and Acetyl Co-A is impaired. **(4)** Mlx complexes with Max like protein-interacting protein (MlxIP) to facilitate nuclear entry. **(5)** Mlx transcriptionally activates genes involved in glycolysis, as well as TXNIP, via interaction with the carbohydrate response elements featured within their promoters. **(6)** Abundant TXNIP mRNA transcripts lead to an increase in TXNIP protein turnover.

Chapter 5: The Role of Host Genes in HCV Replication

5.1. Overview

To investigate the interplay of host gene expression and HCV replication, a series of siRNA experiments were conducted to validate the effect of suppressing TXNIP mRNA on replicon replication in HCV SGR cells in comparison to previous work that used the JFH-1 model [215]. Additionally, the transcriptional induction of Thioredoxin-interacting protein (TXNIP) by Max-like protein (Mlx) was studied using siRNA where it was found that the knockdown of Mlx gave rise to a 3.5-fold reduction in intracellular replicon RNA. However, TXNIP transcript abundance remained upregulated by 2-fold which indicates that factors besides Mlx may be active in the overexpression of TXNIP in HCV SGR cells.

5.2. Results and Discussion

To further the study the impact of host-gene transcription on the replication of HCV, a series of siRNA experiments were conducted to knock down host genes that were related to the transcription of TXNIP while assessing the effects on the replication of viral RNA in HCV SGR cells. The siRNA sequences used in this series of experiments were identical to those used in previous work where they were used to investigate the role of host genes, e.g. TXNIP and Mlx, in JFH-1 infected Huh7 cells [214,215].

As a control to validate the results of TXNIP suppression reported in **Chapter 3** and **Chapter 4**, and for consistency with the work performed by Blackham, siRNA targeting TXNIP (TXNIP 1), referred to henceforth as siTXNIP, was transfected into HCV SGR cells to examine the effects of TXNIP knockdown on mRNA transcript abundance using qRT-PCR and total RNA isolated at 24 hours and 48 hours post-transfection (**Figure 60**) [214,215].

5.2.2. Effects of TXNIP Silencing in HCV SGR Cells (24, 48 Hours)

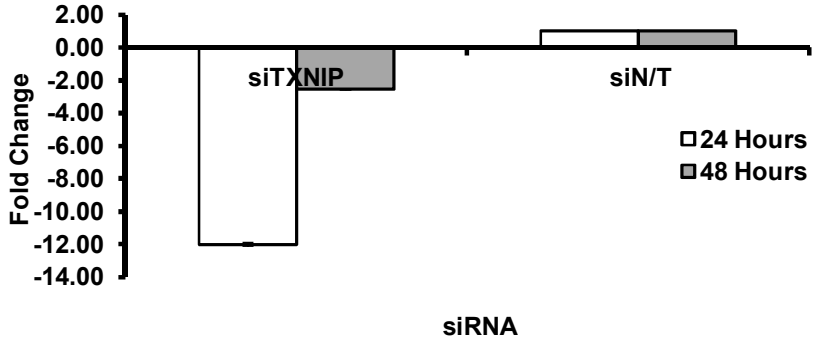


Figure 60 - TXNIP transcription in HCV SGR cells transfected with siRNA targeting TXNIP (siTXNIP) (24, 48 Hours)

Relative fold change of TXNIP transcription in HCV SGR cells transfected with either targeting (siTXNIP) or non-targeting (siN/T) siRNA at 24 hours (white columns) and 48 hours (grey columns), post-transfection. Data shown are averages of triplicate measurements from a single experiment with error bars representing standard deviation (SD). A graph representing differences in cycle thresholds (ΔC_T) between cell lines are shown in **Appendix A3.1**.

As shown in **Figure 60**, TXNIP mRNA transcription is downregulated (-11.99, SD +/- 0.09) in HCV SGR cells transfected with siTXNIP relative to the non-targeting control (siN/T) at 24 hours post-transfection and remains downregulated, albeit to a lesser extent, at 48 hours post-transfection (-2.53, SD +/- 0.03).

To examine the effect of TXNIP knockdown on the replication of replicon RNA in HCV SGR cell transfectants, in comparison to the effects reported by Blackham in the JFH-1 model, intracellular virus was quantitated using qRT-PCR, JFH-1 RNA standards [6 ng – 60 fg], and total RNA isolated at 24 hours and 48 hours post-transfection (**Figure 61**) [214,215].

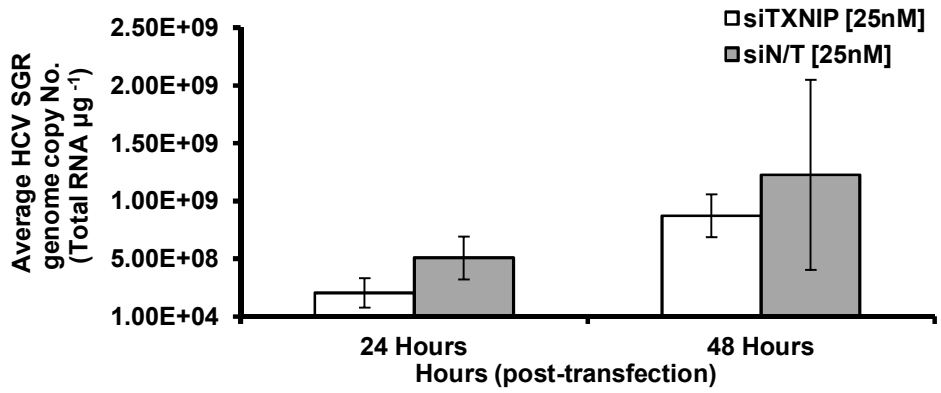


Figure 61 - Intracellular HCV SGR replication in HCV SGR cells transfected with siRNA targeting TXNIP (siTXNIP) (24, 48 Hours)

Intracellular HCV SGR genome copy number measured in HCV SGR cells transfected with either targeting (siTXNIP, white columns) or non-targeting (siN/T, grey columns) siRNA at 24 hours and 48 hours post-transfection. Data shown are averages of triplicate measurements from a single experiment with error bars representing standard deviation (SD).

Figure 61 shows that HCV replication in HCV SGR cells is reduced by 59.6% following transfection with siTXNIP (2.05×10^8 genome copies, SD +/- 1.26×10^8), relative to the genome copy number measured in the non-targeting control (5.07×10^8 genome copies, SD +/- 1.84×10^8) at 24 hours post-transfection. This level of suppression is comparable to the reduced viral RNA synthesis in JFH-1 infected Huh7 cells found by Blackham and translates to a 2.48-fold reduction in intracellular replicon replication [(215)].

The siRNA-mediated downregulation of TXNIP continues to impair virus replication at 48 hours post-transfection where there is a 29.11% reduction in replicon replication in HCV SGR cells transfected with siTXNIP (8.72×10^8 genome copies, SD +/- 5.19×10^8) compared to the non-targeting control (1.23×10^9 genome copies, SD +/- 8.23×10^8).

This finding confirms the importance of TXNIP to HCV RNA replication and so efforts were made to investigate whether upstream induction was brought about by mechanisms additional to that of IRE-1α degradation of miR-17, specifically focussing on the Mlx pathway.

5.2.3. Effects of Mlx Silencing in HCV SGR Cells (24, 48 Hours)

siRNAs targeting Max like protein (siMlx, referred to as Mlx 1 by Blackham), as well as non-targeting siRNAs (siN/T), were transfected into HCV SGR cells and the effects on Mlx transcription determined using qRT-PCR and total RNA isolated from HCV SGR cell transfectants at 24 hours and 48 hours post-transfection (**Figure 62**) [215].

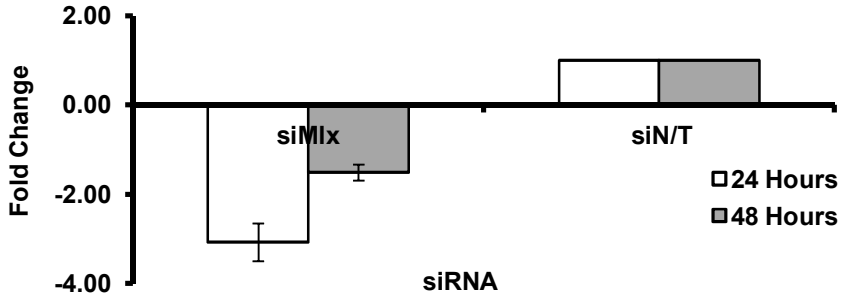


Figure 62 - Mlx transcription in HCV SGR cells transfected with siRNA targeting Mlx (siMlx) (24, 48 Hours)

Relative fold change of Mlx transcription in HCV SGR cells transfected with either targeting (siMlx) or non-targeting (siN/T) siRNA at 24 hours (white columns) and 48 hours (grey columns), post-transfection. Data shown are averages of triplicate measurements from a single experiment with error bars representing standard deviation (SD). A graph representing differences in cycle thresholds (ΔC_T) between cell lines are shown in **Appendix A3.2**.

Figure 62 shows that transcription of Mlx in HCV SGR cells transfected with targeting siRNA (siMlx) is downregulated (-3.07-fold, SD +/- 0.43), compared to the non-targeting control, at 24 hours post-transfection. However, Mlx transcription recovers to basal levels (-1.51-fold, SD +/- 0.18) in Mlx-targeted transfectants compared to the non-targeting control at 48 hours post-transfection. This experiment was elaborated upon by measuring the effects of Mlx knockdown on the transcription of TXNIP mRNA in HCV SGR cells at 24 hours and 48 hours post-transfection (**Figure 63**).

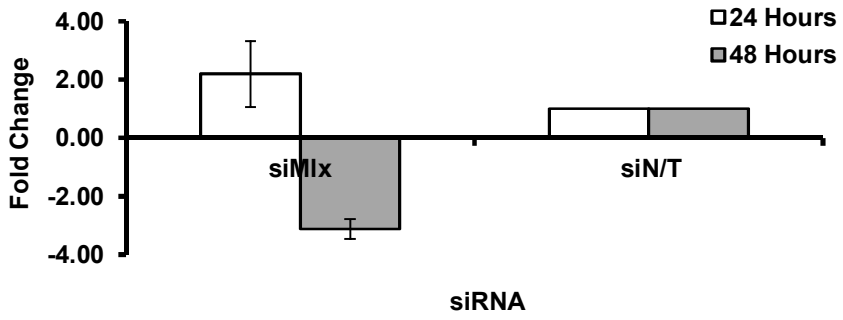


Figure 63 - TXNIP transcription in HCV SGR cells transfected with siRNA targeting Mlx (siMlx) (24, 48 Hours)

Relative fold change of TXNIP transcription in HCV SGR cells treated with either targeting (siMlx) or non-targeting (siN/T) siRNA at 24 hours (white columns) and 48 hours (grey columns), post-transfection. Data shown are averages of triplicate measurements from a single experiment with error bars representing standard deviation (SD). A graph representing differences in cycle thresholds (ΔC_T) between cell lines are shown in **Appendix A3.3**.

As shown by **Figure 63**, the siRNA-mediated knockdown of Mlx has a downstream effect on TXNIP transcription where mRNA abundance is slightly upregulated (+2.21-fold, SD +/- 1.77) at 24 hours, and is downregulated (-3.12-fold, SD +/- 0.34) at 48 hours post-transfection.

This experiment suggests that the upregulation of TXNIP in HCV SGR cells may be dependent on factors other than the glucose-responsive, Mlx-mediated transcriptional induction as discussed in **Chapter 4**.

To determine the effects of suppressed TXNIP transcription on virus replication in HCV SGR cells transfected with siMlx, intracellular replicon RNA was measured using qRT-PCR, JFH-1 RNA standards [6 ng – 60 fg], and total RNA isolated from HCV SGR cells transfectants at 24 hours and 48 hours post transfection (**Figure 64**).

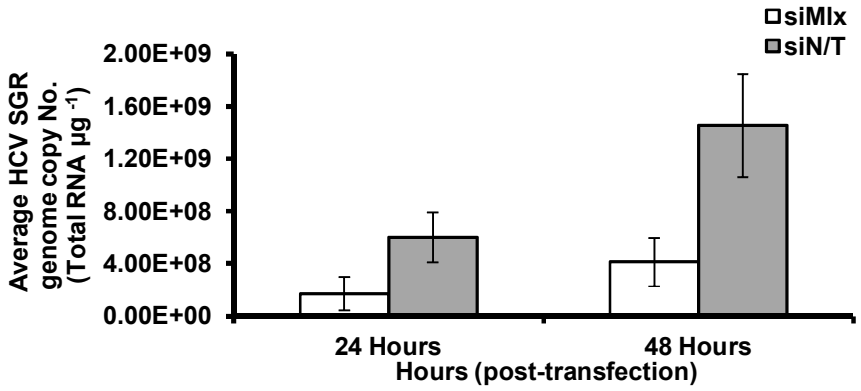


Figure 64 - Intracellular HCV SGR replication in HCV SGR cells transfected with siRNA targeting Mlx (siMlx) (24, 48 Hours)

Intracellular HCV SGR genome copy number measured in HCV SGR cells transfected with either targeting (siMlx, white columns) or non-targeting (siN/T, grey columns) siRNA at 24 hours and 48 hours post-transfection. Data shown are averages of triplicate measurements from a single experiment with error bars representing standard deviation (SD).

Figure 64 shows that the siRNA-mediated silencing of Mlx transcription in HCV SGR cells results in a significant (p= 0.006) 4.02-fold reduction (1.72×10^{8} HCV SGR genome copies, SD +/- 4.12×10^{7}) in intracellular replicon replication, compared to the non-targeting control (6.02×10^{8} HCV SGR genome copies, SD +/- 9.08×10^{7}) at 24 hours post-transfection.

Additionally, a significant (p= 0.01) decrease in intracellular virus replication is seen in HCV SGR cells transfected with siMlx (4.13×10^8 HCV SGR genome copies, SD +/- 1.91×10^8) compared to the non-targeting control (1.46×10^9 HCV SGR genome copies, SD +/- 3.93×10^8) at 48 hours post-transfection which suggests that Mlx transcription of glucose responsive genes is important to HCV replication. Thus, it could be said that that genes involved in the metabolism of glucose, particularly glycolysis, may contribute to HCV replication and the dysregulation of lipid metabolism.

Additionally, data presented here may be reflective of HCV replication being dependent on substrates produced by glycolysis as genes associated with this form of anaerobic glucose metabolism are transcriptionally induced by Mlx [437,505]. Therefore, the re-evaluated data from the Microarray experiment of JFH-1 infected Huh7 cells was inspected for fold-changes in the transcription of glycolytic genes e.g. lactate dehydrogenase A, phosphofructokinase (PFK), and Aldolase, as well as Hexokinase II (HXK2) to support the hypothesis that Mlx is responsible for the transcriptional induction of TXNIP [437].

Following analysis of the re-evaluated microarray data (data not shown) it was found that lactate dehydrogenase A was not transcriptionally altered in the JFH-1 infected Huh7 cells and PFK (-2.04-fold, p= 4.58×10^{-8}) and Aldolase A (-2.08-fold, p= 2.45×10^{-9}) were downregulated at 24 hour and 48 hour time points (data not shown). Conversely, HXK2 was identified as being significantly upregulated at both 24 hours and 48 hours post-infection (**Figure 65**).

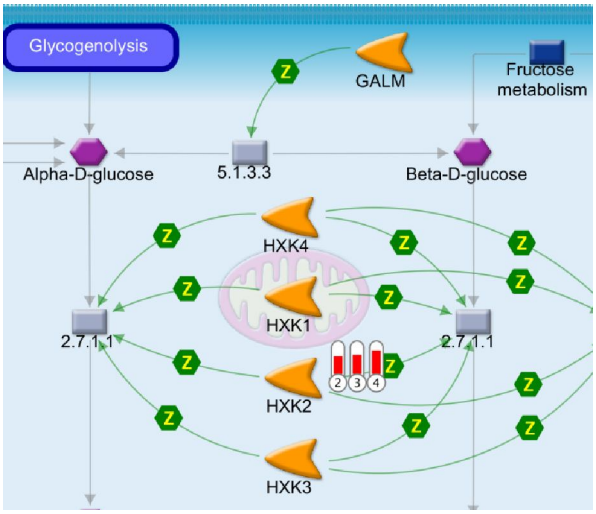


Figure 65 - GeneGO™ Metacore™ pathway analysis from re-evaluated microarray data (Hexokinase 2 (HXK2) Transcription)

The re-evaluated data from the Microarray study of Human hepatoma cells infected with the JFH-1 isolate of HCV was analysed by GeneGO™ Metacore™ software to further validate the findings of Blackham and identify genes and pathways of interest for this study. Hexokinase 2 (HXK2) transcription is dysregulated during HCV infection. Red thermometers indicate gene upregulation. Numbers 3 and 4 on each thermometer correspond to 24 hours and 48 hours post-infection, respectively. **HXK2** is upregulated at 24 hours (+2.49-fold, p= 5.79×10^{-12}) and 48 hours (+3.08-fold, p= 1.68×10^{-13}) post-infection.

The analysis shown in **Figure 65** suggests that HXK2 transcription is upregulated in JFH-1 infected Huh7 cells at 24- and 48 hours post-infection. This finding indicates that the process of glycolysis and thus the transcriptional activity of Mlx are favoured during HCV infection, which support the findings shown in **Chapter 4** as the promoter of HXK2 is transcriptionally induced by Mlx [271].

5.3 Conclusion

This series of experiments sought to validate the dependence of HCV replication on the transcriptional activity of TXNIP by Mlx in HCV SGR cells. The findings presented here may go some way to support the hypothesis that virus replication is dependent on glucose metabolism, and that the dysregulation of lipid metabolism occurs as a consequence of impairment of this pathway (**Chapter 4**). This is also supported by knockdown experiments in which Max like protein (Mlx), an upstream transcription factor of TXNIP that is glucose-responsive, was targeted for knockdown. However, the knockdown of Mlx in HCV SGR cells showed that TXNIP remains upregulated ~2-fold which suggests that other factors, besides Mlx, may be responsible its induction (**Chapter 3**).

Finally, studies investigating the siRNA-mediated knockdown of TXNIP confirmed that RNA replication in HCV SGR cells could be impaired by targeting this host-factor, thus validating the results seen in **Chapter 3** and **Chapter 4**.

Chapter 6: General Discussion & Conclusion

6. General Discussion

The objective of this Ph.D. project was to investigate the cause(s) of Thioredoxin-interacting protein (TXNIP) overexpression during HCV infection which was observed in previous work that involved the microarray analysis of host gene expression in JFH-1 infected Huh7 cells over 48 hours [214,215,461].

The datasets from the microarray study were re-evaluated and gene ontology analysis was performed using Partek software and GeneGO MetaCore™, respectively, in collaboration with Dr. Stathis Giotis of the Skinner Lab at Imperial College in order to identify gene networks that were peripheral to the dysregulation of lipid metabolism during HCV infection and previously unreported [214]. Following the re-evaluation, no significant differences were observed in lipogenic gene expression between the re-evaluated microarray data and those reported by Blackham *et al*., [214]. However, several genes relating to the induction of ER stress (HSPA5, STC2) and the metabolism of glucose (ARRDC5, ATP5L, CYCS, NDUFAF4, and NDUFAF5) were identified to be differentially transcribed in JFH-1 infected Huh7 cells during the microarray data re-evaluation. Thus, inhibition of the unfolded protein response and mitochondrial dysfunction was studied to examine their contribution to the dysregulation of lipid metabolism in HCV gt2a infection models, i.e. HCV SGR- and JFH-1 infected Huh7 cells.

From the outset, 24 hours and 48 hours post-infection were chosen as the time points of interest as these were the intervals in which the transcription of TXNIP and the majority of other host genes were found to be differentially transcribed in the microarray study of JFH-1 infected Huh7 cells [214]. However, 24 hours and 48 hours post-seeding were used for studies involving the model for chronic HCV replication, i.e. HCV SGR cells. Following the optimisation of each protocol used during this project, single experiments for the transcriptomic, biochemical, and proteomic analyses were performed on HCV gt2a infection models as a biological triplicate from which technical triplicates were acquired for statistical purposes. The datasets produced from this study remained consistent and several significant observations were made despite the regular passage and maintenance of cell lines.

In this study, TXNIP transcription was found to be increased in both HCV SGR- and JFH-1 infected Huh7 cells (MOI – 7.5) at 24 hours post-seeding and post-infection, respectively, with a recovery to basal levels of transcription observed at 48 hours. This finding contrasts with previous work where TXNIP mRNA was upregulated approximately +5-fold and +50-fold in HCV SGR and JFH-1 infected Huh7 cells (MOI – 3) at 24 hours post-seeding and post-infection, respectively [214,215,461].

The JFH-1 model was optimised by infecting Huh7 cells with newly synthesised JFH-1 virus stock at a range (0.001 – 7.5) of multiplicity of infection (MOI) (data not shown). TXNIP mRNA abundance was quantified using qPCR where transcription was found to be upregulated at 24 hours post-infection using an MOI of 7.5.

Thus, MOI – 7.5 was used for all experiments involving the JFH-1 isolate of HCV as TXNIP transcript abundance was similar to that observed in HCV SGR cells at 24 hours post-seeding when comparable cell-seeding densities, i.e. ~5×10^5 cells, were used. Several reasons may underlie the differences in TXNIP transcription seen in this study and previous work including differences in virus preparation, experimental set-up, cell passage, and seeding density.

Finally, though not demonstrated in this project, TXNIP expression has been reported to activate the NLRP3 inflammasome during HCV infection where it is responsible for the processing of SREBP-1 and, therefore, the downstream expression of genes related to fatty acid synthesis, which may explain its role in the dysregulation of lipid metabolism during HCV infection [85,444,453,454,457,506].

6.1. ER stress and Dysregulated Lipid Metabolism during HCV infection

The re-evaluated microarray data and gene ontology pathway analysis indicated that pathways related to the onset of ER stress and the induction of the unfolded protein response (UPR) may be related to the biosynthesis of polyunsaturated fatty acids (PUFAs) and that this may, therefore, contribute to the dysregulation of lipid metabolism caused during HCV infection [214,215]. Furthermore, the uptake of dietary glucose (food) was suggested to be a contributing factor to the transcriptional induction of genes related to PUFA biosynthesis, e.g. ELOVL4, ELOVL7, and ACSL3.

Thus, to investigate the source of TXNIP overexpression and dysregulated lipid metabolism during HCV infection in the context of glucose supplementation, experiments were initially conducted using Huh7 and HCV SGR cells cultured under control (glucose [25mM]) and glucose-free conditions. In HCV SGR cells it was found that TXNIP transcription is upregulated at 24 hours post-seeding compared to Huh7 cells grown under both conditions. However, the fold-change in TXNIP mRNA in HCV SGR cells cultured under glucose-free conditions was significantly ($p= 0.03$) lower than that found in HCV SGR cells grown in glucose-rich [25 mM] growth medium. This indicates that the uptake of glucose, as opposed to endogenous glucose production (EGP), significantly contributes to the upregulation of TXNIP transcription during HCV replication. However, it has been reported that glucose-deprivation may also induce ER stress, as well as the unfolded protein response (UPR), and so interpretation of the results from these preliminary experiments should acknowledge that the absence of glucose in the extracellular milieu may exacerbate lipogenic responses in HCV SGR cells [472,507].

Additionally, it was suggested that ER stress may be induced due to the transcriptional upregulation of stanniocalcin 2 (STC2) which is involved in the negative regulation of store operated calcium entry (SOCE) at 24 hours (+22.3-fold, $p= 1.29\times10^{-16}$) and 48 hours (+20.9-fold, $p= 2.58\times10^{-21}$) post-infection as reported previously and confirmed by the re-evaluated microarray data [214,473].

The differential transcription of this gene was comparable in both HCV SGR- and JFH-1 infected Huh7 cells over 48 hours, and so calcium homeostasis was further investigated by measuring cytosolic calcium ion (Ca^{2+}) levels.

A decrease in cytosolic Ca^{2+} was observed in HCV SGR cells, compared to Huh7 cells, at 48 hours post-seeding which accords with the inhibition of calcium uptake from the extracellular milieu as per the induction of STC2. However, cytosolic [Ca^{2+}] was increased in JFH-1 infected Huh7 cells at 48 hours post-infection. This difference may be due to the induction of chronic ER stress by the constitutive expression of HCV NS proteins in the HCV SGR model of HCV replication as opposed to the acute insult brought by newly translated HCV proteins in the JFH-1 model. Furthermore, the HSPA5 gene, which encodes the GRP78 protein that functions as an anchor protein of the UPR effectors (IRE-1α, ATF6, and PERK), was found to be downregulated in both HCV gt2a infection models, and indicated that apoptosis may be enhanced through the upregulation of CCAAT-enhancer binding protein (C/EBP) homologous protein (CHOP) following ER stress [(477)]. These findings led to the induction of the unfolded protein response (UPR) being further investigated in HCV SGR- and JFH-1 infected Huh7 cells to identify whether this process was involved in the transcriptional induction of TXNIP and the dysregulation of lipid metabolism in HCV gt2a infection models (**Chapter 3**).

Following the induction of stress and the accumulation of unfolded proteins in the endoplasmic reticulum, GRP78 releases IRE-1α where it dimerises and, following autophosphorylation of its allosteric kinase domain, exerts endoribonuclease activity through the degradation of untranslated mRNA [508,509].

Additionally, the endoribonuclease activity of IRE-1α may process X-box binding protein 1 (XBP1) mRNA, whereby a 26nt intronic sequence is removed and the exons are ligated by RNA ligase, to produce an active truncated isoform that induces the transcription of ER chaperone proteins [510].

However, Lerner *et al*., reported that TXNIP mRNA abundance is also affected by the activity of IRE-1α in pancreatic β cells and tested this using an inhibitor, STF-083010 [444,511]. Thus, the association between ER stress, TXNIP transcript abundance and dysregulated lipid metabolism during HCV infection was tested by treating HCV gt2a infection models with STF-083010 at a 50 μM concentration [444]. This concentration was based on a method published by Lerner *et al*., and was supported by studies that involved the optimisation of [STF-083010] in HCV SGR cells which found 50 μM to be optimal for functional experiments (data not shown) [512]. The treatment of HCV SGR cells with STF-083010 gave rise to a 4-fold increase in miR-17, a 7-fold decrease in TXNIP mRNA, and a 3.33-fold reduction in the replication of HCV replicon RNA over 48 hours post-seeding.

Conversely, a 50 μM concentration of STF-083010 had no effect on the upregulation of TXNIP mRNA or virus replication in JFH-1 infected Huh7 cells despite an approximate 12-fold increase in miR-17 abundance at 24 hours post-infection.

Thus, the difference in suppressing TXNIP and downstream lipogenic gene transcription and, by proxy, virus replication through the inhibition of IRE-1α endoribonuclease activity in HCV gt2a infection models indicates that UPR induction is not as involved in the dysregulation of lipid metabolism and virus replication during HCV infection as it appears to be in the HCV SGR model of replication.

6.2. Mitochondrial Dysfunction and Dysregulated Lipid Metabolism during HCV infection

The differences in cytosolic calcium ion concentration observed in HCV gt2a infection models indicated that the incidence of ER stress and calcium store depletion via inhibition of SERCA activity and Ca^{2+} ion efflux via IP3R channels may also affect the function of the mitochondria to generate ATP from the metabolism of glucose and fatty acids [43–45]. Thus, to examine if changes in intracellular calcium may correlate with the overexpression of TXNIP and the dysregulation of lipid metabolism in HCV gt2a infection models, the incidence of mitochondrial dysfunction due to mitochondrial calcium ion overload was investigated.

Initially, total cellular calcium was measured following the staining of HCV gt2a infection models with Indo-1. However, through the use of a modified protocol involving a mitochondrial isolation buffer and heat-treatment to remove cytosolic calcium through the activation of cellular anion pumps, the abundance of calcium ions at the mitochondria could be determined [96].

Indeed, mitochondrial calcium ion overload was present in both HCV SGR- and JFH-1 infected Huh7 cells where fluorescence (405nm) was higher than that observed in controls at 24 hours post-seeding and post-infection, respectively [463].

Collectively, the consequences of calcium ion overload, i.e. mitochondrial permeability transition (MPT), reduced mitochondrial membrane potential (mt$\Delta\Psi$m), and the ROS-mediated degradation of mitochondrial contents, e.g. mtDNA, were found to be particularly evident in the JFH-1 infection model of HCV infection [296,482,484]. Furthermore, there was an increase in apoptotic enzyme activity in HCV SGR cells which indicated that expression of HCV non-structural proteins may lead to changes that are characteristic of the mitochondria-associated pathway of apoptosis being induced [441,513].

Therefore, to investigate the effects of mitochondrial dysfunction on the metabolism of glucose in HCV gt2a infection models, the re-evaluated microarray data was examined to identify whether genes concerning the oxidative phosphorylation of glucose were affected at a transcriptional level during HCV infection.

It was found that the transcription of ARRDC4, a TXNIP paralog that is induced in response to elevated cellular glucose, was significantly upregulated at 24 hours (+11.3-fold, $p= 3.42 \times 10^{-15}$) and 48 hours (+10.7-fold, $p= 4.96 \times 10^{-15}$) post-infection (data not shown).

However, when ARRDC4 transcript abundance was quantified using qRT-PCR, this gene was found to be downregulated in HCV SGR cells at 24 hours and 48 hours post-seeding, whilst no change was observed in JFH-1 infected Huh7 cells at either time point.

The re-evaluated microarray data showed that Hexokinase 2 (HXK2), an enzyme that couples glycolysis to mitochondrial oxidative phosphorylation, was also significantly upregulated at 24 hours (+2.49-fold, $p= 5.79\times10^{-12}$) and 48 hours (+3.08-fold, $p= 1.68\times10^{-13}$) post-infection [514]. Additionally, other genes involved in the oxidative phosphorylation (OXPHOS) of glucose such as ATP5L, NDUFAF4 and NDUFAF5 were found to be upregulated approximately +2-fold at 48 hours post-infection in the re-evaluated microarray data (data not shown), and so transcription of these genes was measured in HCV SGR- and JFH-1 infected Huh7 cells at 24 hours and 48 hours post-seeding and post-infection, respectively.

The transcriptional fold changes of ATP5L, NUDFAF4 and NDUFAF5 in HCV SGR cells were upregulated approximately +2-fold at 24 hours and 48 hours post-seeding whereas the transcript abundance of ATP5L and NDUFAF5 was greatly downregulated at 24 hours and 48 hours post-infection in JFH-1 infected Huh7 cells. These results demonstrate that the mitochondrial respiration of glucose is highly impaired during oxidative phosphorylation when the entire life cycle of HCV is recapitulated.

The differential transcription of genes involved in oxidative phosphorylation also reflected a common phenotypic difference in glucose metabolism between HCV gt2a infection models, i.e. glucose intolerance, as intracellular glucose concentrations did not alter over the course of 48 hours in accordance with data previously shown by Blackham [215].

The accumulation of calcium ions at the mitochondria, in addition to the effects observed on the transcription of OXPHOS genes and intracellular glucose concentration, appeared to coincide with the upregulation of TXNIP transcription and downstream lipogenic genes. It has been reported that the treatment of isolated mitochondria with L-glutamate reduces the uptake of intracellular calcium through binding specifically to Asp-rich sites within mitochondrial voltage dependent anion channels (VDACs) where oscillation between closed and open conformations are induced, and channel conductance is inhibited along with the opening of mPTP (**section 1.7.3.3**) [486].

However, a working concentration of L-glutamate [0.5mM] was used to treat whole cells in this experiment based on a method published by Gincel *et al*., where the dilation of VDACs were inhibited in isolated mitochondria. Thus, this concentration may be excessive and so further study may be required to optimise the effective dose *in cellulo* [(486)].

Thus, studies involving the inhibition of calcium ion uptake by mitochondrial VDACs in HCV gt2a infection models were carried out using L-glutamate with the effects on glucose and lipid metabolism, as well as virus replication, measured over 48 hours [(486)]. Treatment of both HCV SGR- and JFH-1 infected Huh7 cells with L-glutamate resulted in reduced amounts of mitochondrial calcium, increases in mitochondrial membrane potential, and a general regulation of OXPHOS gene transcription in comparison to untreated controls. In addition, intracellular glucose concentrations remained stable in untreated HCV gt2a infection models but an increase was seen in both HCV SGR- and JFH-1 infected Huh7 cells at 48 hours following treatment with L-glutamate.

Additionally, similar findings were made when intracellular glycogen content was measured in HCV gt2a infection models treated with L-glutamate.

These results suggest that the mitochondrial respiration of glucose, i.e. the TCA cycle, is enhanced in HCV gt2a infection models following treatment with L-glutamate and may be due to the anaplerosis of key metabolites, e.g. α-ketoglutarate, or due to the preservation of mitochondrial membrane potential when the mitochondrial uptake of calcium ions by VDACs is limited.

Furthermore, the transcription of TXNIP and downstream lipogenic genes associated with fatty acid elongation (ELOVL4, ELOVL7) and condensation (ACSL3) in both HCV SGR- and JFH-1 infected Huh7 cells also correlated with that of OXPHOS genes where the transcription profiles of both pathways were normalised, i.e. < 2-fold, following treatment with L-glutamate.

The normalisation of lipogenic gene transcription, following treatment of HCV gt2a infection models with L-glutamate was verified biochemically by measuring intracellular triglyceride (TG) concentration and using Oil-Red-O (ORO) to stain intracellular lipid droplets (LDs). Both the measurement of intracellular TG and LD in HCV SGR- and JFH-1 infected Huh7 cells showed an abundance in untreated controls that was reduced to trace amounts following treatment with L-glutamate which contrasts with reports that suggest that ER stress, calcium release, and mitochondrial dysfunction may occur as an effect of lipotoxicity rather than a cause dysregulated lipid metabolism [(309)].

The abundance of LD in HCV SGR cells may have arisen due to co-treatment with Geneticin (G418) which was used on the basis of neomycin resistance being a selectable marker for the expression of HCV NS proteins in this model. However, this is unlikely as ORO staining was also applied to JFH-1 infected Huh7 cells which do not require G418 and so confirm that the expression of HCV proteins correlate with an increase in intracellular LDs.

However, intracellular LDs are present in different cellular compartments between HCV gt2a infection models, i.e. HCV SGR cells have a cytoplasmic distribution of LDs presumably due to initial budding from the ER, whilst JFH-1 infected Huh7 cells appear to have a nuclear localisation which may serve as a reservoir of fatty acids for the nuclear membrane [515]. The images acquired from the ORO stain of JFH-1 infected Huh7 cells have poor differentiation compared to those obtained from the ORO stain of HCV SGR cells and so this experiment needs to be repeated before any conclusions can be made. However, the implied nuclear LDs correlate with the increased transcription of FABP3 in JFH-1 infected Huh7 cells under control conditions observed at 24 hours post-infection as this gene is involved in the delivery of fatty acids and other lipid-based molecules to the nucleus [468]. Furthermore, a study identified the presence of nuclear LDs, separate to cytoplasmic LDs invaginated by the nuclear envelope, in serial liver sections isolated from a patient infected with the gt1b isolate of HCV through the use of electron microscopy [515].

The reduced FA and LD content observed in HCV gt2a infection models treated with L-glutamate corroborate the effects of this amino acid derivative on cell metabolism that were previously reported to occur in HA1ER cells, a human embryonic kidney cell line in which HRas Proto-Oncogene (HRAS) is transgenically expressed [516]. Kaadige *et al* describe how the anti-lipogenic effects of glutamine occur through the inhibition of glucose-derived citrate export, which otherwise provides substrates for FA biosynthesis, that follows mitochondrial anaplerosis and the replenishment of TCA cycle intermediates via glutaminolysis. However, the authors also comment that the repression of TXNIP following glutamine supplementation may only be relevant to highly glycolytic tumour cells [516].

Furthermore, Kaadige *et al.*, show that the addition of glutamine, a precursor to glutamate, may lead to the repression of TXNIP, and therefore stimulate the uptake of glucose, by blockade of transcriptional induction by Mlx through the recruitment of a histone-deactylase dependent corepressor to the NH_3 terminus of MlxIP via mitochondrial anaplerosis [516]. Thus, whether this activity is responsible for the downregulation of TXNIP, in addition to a decrease in mitochondrial calcium, in L-glutamate treated HCV gt2a infection models remains to be determined [516].

This phenomenon seems likely as initial transcriptomic studies involving the treatment of HCV SGR cells with 4,4′-diisothiocyanatostilbene-2,2′-disulfonic acid (DIDS), which exclusively inhibit the uptake of Ca^{2+} ions by mitochondrial VDACs, showed that TXNIP mRNA downregulation was not as great at either 24 hours (+1.29-fold, SD +/- 0.43) or 48 hours (+1.79-fold, SD +/- 0.66) post-seeding in comparison to those treated with L-glutamate (data not shown)[517].

Taken together with data from **Chapter 3**, these results suggest that LD formation may be a general response to cellular stress in which mitochondrial dysfunction and metabolic reprogramming to favour glycolysis manifest under hypoxic conditions during HCV infection [276,518]. Additionally, these results indicate that the transcriptional induction of TXNIP by Mlx may be conditional on an increase in mitochondrial calcium [215,271,439,441–443].

The effects of suppressed TXNIP and downstream lipogenic gene transcription, as well as LD biosynthesis, on HCV replication and secretion was also examined in HCV gt2a infection models co-treated with L-glutamate over 48 hours.

In HCV SGR cells, increased HCV genome replication was observed at both 24 hours and 48 hours post-seeding, whereas intracellular HCV genome copy number in L-glutamate treated JFH-1 infected Huh7 cells was comparable to that seen in the untreated control at 24 hours post-infection.

Additionally, there was a significant ($p= 0.004$) decrease in intracellular virus in JFH-1 infected Huh7 cells following treatment with L-glutamate at 48 hours post-infection.

Treatment of JFH-1 infected Huh7 cells with L-glutamate also produced increased secretion of extracellular virus at 24 hours, though this decreased to a comparable titre measured in the untreated control at 48 hours post-infection.

However, the infectivity of extracellular virus secreted by JFH-1 infected Huh7 cells following L-glutamate treatment remains to be determined and is worth investigating in future studies given that abundance of intracellular LDs are diminished following the inhibition of mitochondrial calcium ion uptake.

The transcriptional data for TXNIP and HCV genome copy number in control and L-glutamate treated HCV gt2a infection models was verified using Western Blotting and densitometry analysis.

In HCV SGR cells treated with L-glutamate, TXNIP expression was lower than levels seen the untreated control at 48 hours post-seeding. This finding accords with that from the qRT-PCR analysis, where TXNIP mRNA was downregulated in HCV SGR cells following treatment with L-glutamate at both 24 hours and 48 hours post-seeding.

However, expression of HCV NS3 protein was also found to be lower in L-glutamate treated HCV SGR cells which conflicts with the higher measurement of replicon transcripts, compared to the control, at 48 hours post-seeding. The discrepancy between the Western Blot and qRT-PCR data in HCV SGR cells at 48 hours post-seeding may be due to the methodology, i.e. triple staining with antibodies, being sup-optimal and so this experiment will need to be repeated in future work.

The data from this series of experiments highlight a fundamental difference between JFH-1 and HCV SGR models where the cellular pathways on which virus replication are associated appear to diverge, i.e. full-length HCV infection relates to mitochondrial dysfunction whereas HCV SGR genome replication correlates with the induction of ER stress.

The overexpression of TXNIP in HCV may also signify that the products from glycolysis are used as substrates for *de novo lipogenesis* (DNL), instead of being further metabolised by the mitochondria via oxidative phosphorylation and the tricarboxylic acid (TCA) cycle, as a result of mitochondrial dysfunction being induced in HCV gt2a infection models [253,278]. Thus, TXNIP may have an indirect role in sensing mitochondrial integrity whereby its expression may reflect the capacity of the mitochondria to further metabolise glucose [443].

Finally, the concentration of intracellular ROS was determined in HCV gt2a infection models treated with L-glutamate to assess whether physiological ROS, e.g. H_2O_2, $O_2^{-\cdot}$, emanating from the mitochondria contributes to the induction of TXNIP during HCV replication [519].

This experiment found that the inhibited dilation of mitochondrial VDACs in HCV gt2a infection models lead to an increase in intracellular ROS which contrasts with the findings by Tikunov *et al*., where it was reported that closure of mitochondrial VDACs using G3139, an 18mer phosphorothioate oligonucleotide, exacerbates calcium induced mPTP and oxidative stress by preventing the efflux of $O_2^{-\cdot}$ [520]. This finding suggests that the abundance of intracellular ROS during HCV replication is not generated by the mitochondria.

Collectively, data from these experiments show a correlation between the TXNIP-mediated dysregulation of lipid metabolism and intracellular virus replication in the replicon model of HCV whereby the former may be suppressed through targeting calcium ion overload at the site of mitochondrial VDACs.

6.3. The Role of Host Genes in HCV Replication

The role of host genes in the replication of HCV was further investigated by carrying out a series of experiments involving the siRNA-mediated knockdown of genes relating to the transcriptional induction of TXNIP in HCV SGR cells. The siRNA sequence used for TXNIP knockdown (TXNIP-1, siTXNIP) in JFH-1 infected Huh7 cells was transfected into HCV SGR cells to validate the targeting of this host gene as a strategy to impair HCV replicon replication [(215)].

Following the transfection of HCV SGR cells with TXNIP-1 siRNA, referred to as siTXNIP in this work, a 92% knockdown in TXNIP transcript abundance was seen compared to the non-targeting control at 24 hours post-transfection which led to a 59.6% reduction in HCV replicon replication at this time point and accords with the findings reported by Blackham in the JFH-1 model of HCV infection [(215)].

However, at 48 hours post-transfection, HCV genome replication is impaired by 29.11% which is likely due to the decreased stability of targeting siRNA or dilution thereof as an effect of cell proliferation [(521)].

Thus, with the impairment of virus replication by suppression of TXNIP validated through siRNA-mediated knockdown, the same method was applied to Mlx, an upstream transcription factor of TXNIP, as a means to confirm its role in response to intracellular glucose as described in **Chapter 3** and **Chapter 4** [(271)].

Transfection of HCV SGR cells with siRNA targeting Mlx resulted in an 8.52-fold downregulation of Mlx transcription whilst that of TXNIP was at the threshold of significance (2-fold) at 24 hours post-transfection. The knockdown of Mlx also brought about a significant ($p= 0.001$) reduction in HCV replication in HCV SGR cells at 48 hours post-transfection which confirms that TXNIP, by way of glucose-induced Mlx transcriptional induction, plays a significant role in the replication of HCV.

6.4. Conclusion

In summary, it can be said from this study that both ER stress and mitochondrial dysfunction may play a crucial and synergistic role in the TXNIP-mediated dysregulation of lipid metabolism during HCV infection. However, virus quantitation carried out during the suppression of TXNIP via these pathways showed varying effects between HCV gt2a infection models suggesting that there are inherent differences in the pathways that are induced and exploited during virus replication. Furthermore, downregulation of TXNIP in the JFH-1 model by the aforementioned pathways gave rise to equivalent or heightened levels of extracellular virus in comparison to the untreated controls at 24 hours. This indicates that TXNIP expression, along with defects in lipid metabolism, may arise as a host response to organelle stress induced by the virus that serves a role in the post-replicative steps of the virus life cycle.

Thus, the assembly of intact lipoviroparticles (LVPs) and the infectivity of the virus produced in cells where the upregulation of TXNIP has been inhibited by the mechanisms described in this project are worth investigating in future research.

Another issue that may be addressed by future research is whether the targeting of TXNIP by these pathways ameliorates the metabolic complications that are associated with chronic HCV infection e.g. T2DM, hepatic steatosis, and obesity, and whether treatment of ER stress and mitochondrial dysfunction enhances the efficacy of existing therapies that are impaired by metabolic syndrome (MS).

In summary, the following conclusions of this project can be drawn from the investigations of ER stress and mitochondrial dysfunction that have been found to occur in JFH-1 infected Huh7 cells:

1. The cellular uptake of glucose during HCV replication correlates with the upregulation of TXNIP transcription.

2. ER stress and the induction of the unfolded protein response (UPR) are evident in HCV SGR- and JFH-1 infected Huh7 cells, though inhibition of IRE-1α endoribonuclease activity appears to be effective in the suppression of TXNIP and downstream lipogenic gene transcription, and intracellular replicon replication in HCV SGR cells only.

3. Mitochondrial dysfunction is evident in both HCV SGR- and JFH-1 infected Huh7 cells and is likely to emanate from calcium store depletion following ER stress which contributes to the dysregulation of lipid metabolism in HCV gt2a infection models.

Bibliography

1. Hajarizadeh B, Grebely J, Dore GJ. Epidemiology and natural history of HCV infection. Nat Rev Gastroenterol Hepatol. 2013;10(9):553–62.

2. Farci P. Choo QL, Kuo G, Weiner AJ, Overby LR, Bradley DW, Houghton M. Isolation of a cDNA clone derived from a blood-borne non-A, non-B viral hepatitis genome [Science 1989;244:359-362]. J Hepatol. 2002;36(5):582–5.

3. Ashfaq UA, Javed T, Rehman S, Nawaz Z, Riazuddin S. An overview of HCV molecular biology, replication and immune responses. Virol J. 2011;8:161.

4. Trinks J, Gadano A, Argibay P. Evolving Trends in the Hepatitis C Virus Molecular Epidemiology Studies: From the Viral Sequences to the Human Genome. Epidemiol Res Int. 2012;2012:1–10.

5. Bartosch B. Hepatitis C virus and its complex interplay with hepatic glucose and lipid metabolism. J Hepatol. 2009;50(5):845–7.

6. Kelly DA. Hepatitis C infection after blood product transfusion. Arch Dis Child. 1996;75(5):363–5.

7. van de Laar TJW, van der Bij AK, Prins M, Bruisten SM, Brinkman K, Ruys TA, et al. Increase in HCV Incidence among Men Who Have Sex with Men in Amsterdam Most Likely Caused by Sexual Transmission. J Infect Dis. 2007;196(2):230–8.

8. Shi M, Lin X-D, Vasilakis N, Tian J-H, Li C-X, Chen L-J, et al. Divergent viruses discovered in arthropods and vertebrates revise the evolutionary history of the *Flaviviridae* and related viruses. J Virol. 2015;90(2):02036-15.

9. Huang YJS, Higgs S, Horne KM, Vanlandingham DL. Flavivirus-Mosquito interactions. Viruses. 2014;6(11):4703–30.

10. Kaito M, Ishida S, Tanaka H, Horiike S, Fujita N, Adachi Y, et al. Morphology of hepatitis C and hepatitis B virus particles as detected by immunogold electron microscopy. Med Mol Morphol. 2006;39(2):63–71.

11. Revie D, Salahuddin SZ. Human cell types important for hepatitis C virus replication in vivo and in vitro: old assertions and current evidence. Virol J. 2011;8(1):346.

12. Chang M, Williams O, Mittler J, Quintanilla A, Carithers RL, Perkins J, et al. Dynamics of hepatitis C virus replication in human liver. Am J Pathol. 2003;163(2):433–44.

13. Fletcher NF, McKeating JA. Hepatitis C virus and the brain. J Viral Hepat. 2012;19(5):301–6.

14. Popescu C-I, Riva L, Vlaicu O, Farhat R, Rouillé Y, Dubuisson J. Hepatitis C virus life cycle and lipid metabolism. Biology (Basel). 2014;3(4):892–921.

15. Dubuisson J, Cosset FL. Virology and cell biology of the hepatitis C virus life cycle - An update. J Hepatol. 2014;61(1):S3–13.

16. Ramanan V, Trehan K, Ong ML, Luna JM, Hoffmann HH, Espiritu C, et al. Viral genome imaging of hepatitis C virus to probe heterogeneous viral infection and responses to antiviral therapies. Virology. 2016;494:236–47.

17. Weiser BM, Tellinghuisen TL. Structural biology of the hepatitis C virus proteins. Drug Discov Today Technol. 2012;9(3).

18. Hundt J, Li Z, Liu Q. Post-translational modifications of hepatitis C viral proteins and their biological significance. World J Gastroenterol. 2013;19(47):8929–39.

19. Appel N, Schaller T, Penin F, Bartenschlager R. From Structure to Function : New Insights into Hepatitis C Virus RNA Replication. J Biol Chem. 2006;281(15):9833–6.

20. Paul D, Madan V, Bartenschlager R. Hepatitis C virus RNA replication and assembly: Living on the fat of the land. Cell Host Microbe. 2014;16(5):569–79.

21. Fraser CS, Doudna J a. Structural and mechanistic insights into hepatitis C viral translation initiation. Nat Rev Microbiol. 2007;5(1):29–38.

22. Khaliq S, Jahan S, Pervaiz A, Ali Ashfaq U, Hassan S. Down-regulation of IRES containing 5'UTR of HCV genotype 3a using siRNAs. Virol J. 2011;8(1):221.

23. Kikuchi K, Umehara T, Fukuda K, Kuno A, Hasegawa T, Nishikawa S. A hepatitis C virus (HCV) internal ribosome entry site (IRES) domain III-IV-targeted aptamer inhibits translation by binding to an apical loop of domain IIId. Nucleic Acids Res. 2005;33(2):683–92.

24. Shimoike T, McKenna SA, Lindhout DA, Puglisi JD. Translational insensitivity to potent activation of PKR by HCV IRES RNA. Antiviral Res. 2009;83(3):228–37.

25. Bradrick SS, Walters RW, Gromeier M. The hepatitis C virus 3'-untranslated region or a poly(A) tract promote efficient translation subsequent to the initiation phase. Nucleic Acids Res. 2006;34(4):1293–303.

26. Petrik J, Parker H, Alexander GJM. Human hepatic glyceraldehyde-3-phosphate dehydrogenase binds to the poly (U) tract of the 3' non-coding region of hepatitis C virus genomic RNA. J Gen Virol. 1999;80(1999):3109–13.

27. Bai Y, Zhou K, Doudna JA. Hepatitis C virus 3′UTR regulates viral translation through direct interactions with the host translation machinery. Nucleic Acids Res. 2013;41(16):7861–74.

28. Shetty S, Stefanovic S, Mihailescu MR. Hepatitis C virus RNA: Molecular switches mediated by long-range RNA-RNA interactions? Nucleic Acids Res. 2013;41(4):2526–40.

29. Tuplin A, Struthers M, Simmonds P, Evans DJ. A twist in the tail: SHAPE mapping of long-range interactions and structural rearrangements of RNA elements involved in HCV replication. Nucleic Acids Res. 2012;40(14):6908–21.

30. Marton S, Berzal-Herranz B, Garmendia E, Cueto FJ, Berzal-Herranz A. Anti-HCV RNA aptamers targeting the genomic cis-acting replication element. Pharmaceuticals. 2011;5(1):49–60.

31. Jones DM, McLauchlan J. Hepatitis C virus: Assembly and release of virus particles. J Biol Chem. 2010;285(30):22733–9.

32. Hüssy P, Langen H, Mous J, Jacobsen H. Hepatitis C virus core protein: carboxy-terminal boundaries of two processed species suggest cleavage by a signal peptide peptidase. Virology. 1996;224(1):93–104.

33. Ait-Goughoulte M, Hourioux C, Patient R, Trassard S, Brand D, Roingeard P. Core protein cleavage by signal peptide peptidase is required for hepatitis C virus-like particle assembly. J Gen Virol. 2006;87(4):855–60.

34. Boulant S, Montserret R, Hope RG, Ratinier M, Targett-Adams P, Lavergne JP, et al. Structural determinants that target the hepatitis C virus core protein to lipid droplets. J Biol Chem. 2006;281(31):22236–47.

35. Santolini E, Migliaccio G, Monica N La. Biosynthesis and Biochemical Properties of the Hepatitis C Virus Core Protein. J Virol. 1994;68(6):3631–41.

36. Tang X, Wagoner J, Negash A, Austin M, McLauchlan J, Hahn YS, et al. Functional characterization of core genes from patients with acute hepatitis C virus infection. J Infect Dis. 2010;201(6):912–22.

37. Shavinskaya A, Boulant S, Penin F, McLauchlan J, Bartenschlager R. The lipid droplet binding domain of hepatitis C virus core protein is a major determinant for efficient virus assembly. J Biol Chem. 2007;282(51):37158–69.

38. Hourioux C, Ait-Goughoulte M, Patient R, Fouquenet D, Arcanger-Doudet F, Brand D, et al. Core protein domains involved in hepatitis C virus-like particle assembly and budding at the endoplasmic reticulum membrane. Cell Microbiol. 2007;9(4):1014–27.

39. Matsumoto M, Hwang SB, Jeng K-S, Zhu N, Lai MMC. Homotypic Interaction and Multimerization of Hepatitis C Virus Core Protein. Virology. 1996;218(1):43–51.

40. Ren S, Pietschmann T, Kaehlcke K, Bartenschlager R, Yen TSB, Ott M. Targeting of Hepatitis C Virus Core Protein to Mitochondria through a Novel C-Terminal Localization Motif. J Virol. 2004;78(15):7958–68.

41. Falcón V, Acosta-Rivero N, Shibayama M, Chinea G, Gavilondo J V., De La Rosa MC, et al. HCV core protein localizes in the nuclei of nonparenchymal liver cells from chronically HCV-infected patients. Biochem Biophys Res Commun. 2005;329(4):1320–8.

42. Suzuki R, Sakamoto S, Tsutsumi T, Rikimaru A, Tanaka K, Shimoike T, et al. Molecular Determinants for Subcellular Localization of Hepatitis C Virus Core Protein. J Virol. 2005;79(2):1271–81.

43. Benali-Furet NL, Chami M, Houel L, De Giorgi F, Vernejoul F, Lagorce D, et al. Hepatitis C virus core triggers apoptosis in liver cells by inducing ER stress and ER calcium depletion. Oncogene. 2005;24(31):4921–33.

44. Filippin L, Magalhães PJ, Di Benedetto G, Colella M, Pozzan T. Stable interactions between mitochondria and endoplasmic reticulum allow rapid accumulation of calcium in a subpopulation of mitochondria. J Biol Chem. 2003;278(40):39224–34.

45. Piccoli C, Scrima R, Quarato G, D'Aprile A, Ripoli M, Lecce L, et al. Hepatitis C virus protein expression causes calcium-mediated mitochondrial bioenergetic dysfunction and nitro-oxidative stress. Hepatology. 2007;46(1):58–65.

46. Moriya K, Fujie H, Shintani Y, Yotsuyanagi H, Tsutsumi T, Ishibashi K, et al. The core protein of hepatitis C virus induces hepatocellular carcinoma in transgenic mice. Nat Med. 1998;4(9):1065–7.

47. Moriya K, Yotsuyanagi H, Shintani Y, Fujie H, Ishibashi K, Matsuura Y, et al. Hepatitis C virus core protein induces hepatic steatosis in transgenic mice. J Gen Virol. 1997;78 (Pt 7)(1997):1527–31.

48. Loizides-Mangold U, Clément S, Alfonso-Garcia A, Branche E, Conzelmann S, Parisot C, et al. HCV 3a core protein increases lipid droplet cholesteryl ester content via a mechanism dependent on sphingolipid biosynthesis. PLoS One. 2014;9(12):1–24.

49. Shi ST, Polyak SJ, Tu H, Taylor DR, Gretch DR, Lai MMC. Hepatitis C virus NS5A colocalizes with the core protein on lipid droplets and interacts with apolipoproteins. Virology. 2002;292(2):198–210.

50. Perlemuter G, Sabile A, Letteron P, Vona G, Topilco AA, Chretien Y, et al. Hepatitis C virus core protein inhibits microsomal triglyceride transfer protein activity and very low density lipoprotein secretion: a model of viral-related steatosis. FASEB J. 2002;16(2):185–94.

51. Hussain MM, Rava P, Walsh M, Rana M, Iqbal J. Multiple functions of microsomal triglyceride transfer protein. Nutr Metab (Lond). 2012;9(1):14.

52. Errington W, Wardell AD, McDonald S, Goldin RD, McGarvey MJ. Subcellular localisation of NS3 in HCV-infected hepatocytes. J Med Virol. 1999;59(4):456–62.

53. Maqbool MA, Imache MR, Higgs MR, Carmouse S, Pawlotsky J-M, Lerat H. Regulation of hepatitis C virus replication by nuclear translocation of nonstructural 5A protein and transcriptional activation of host genes. J Virol. 2013;87(10):5523–39.

54. Cerutti A, Maillard P, Minisini R, Vidalain PO, Roohvand F, Pecheur EI, et al. Identification of a functional, CRM-1-dependent nuclear export signal in hepatitis C virus core protein. PLoS One. 2011;6(10):e25854.

55. Levin A, Neufeldt CJ, Pang D, Wilson K, Loewen-Dobler D, Joyce MA, et al. Functional characterization of nuclear localization and export signals in hepatitis C virus proteins and their role in the membranous web. PLoS One. 2014;9(12):1–36.

56. Grakoui A, Wychowski C, Lin C, Feinstone SM, Rice CM. Expression and identification of hepatitis C virus polyprotein cleavage products. J Virol. 1993;67(3):1385–95.

57. Helle F, Vieyres G, Elkrief L, Popescu C-I, Wychowski C, Descamps V, et al. Role of N-linked glycans in the functions of hepatitis C virus envelope proteins incorporated into infectious virions. J Virol. 2010;84(22):11905–15.

58. Drummer HE, Maerz A, Poumbourios P. Cell surface expression of functional hepatitis C virus E1 and E2 glycoproteins. FEBS Lett. 2003;546(2–3):385–90.

59. Goffard A, Callens N, Bartosch B, Wychowski C. Role of N-Linked Glycans in the Functions of Hepatitis C Virus Envelope Glycoproteins. J Virol. 2005;79(13):8400–9.

60. Bartosch B, Vitelli A, Granier C, Goujon C, Dubuisson J, Pascale S, et al. Cell Entry of Hepatitis C Virus Requires a Set of Co-receptors that Include the CD81 Tetraspanin and the SR-B1 Scavenger Receptor. J Biol Chem. 2003;278(43):41624–30.

61. Meunier JC, Fournillier A, Choukhi A, Cahour A, Cocquerel L, Dubuisson J, et al. Analysis of the glycosylation sites of hepatitis C virus (HCV) glycoprotein E1 and the influence of E1 glycans on the formation of the HCV glycoprotein complex. J Gen Virol. 1999;80(4):887–96.

62. Takikawa S, Ishii K, Aizaki H, Suzuki T, Asakura H, Matsuura Y, et al. Cell fusion activity of hepatitis C virus envelope proteins. J Virol. 2000;74(11):5066–74.

63. Pérez-Berná AJ, Pabst G, Laggner P, Villalaín J. Biophysical characterization of the fusogenic region of HCV envelope glycoprotein E1. Biochim Biophys Acta - Biomembr. 2009;1788(10):2183–93.

64. Prentoe J, Verhoye L, Velázquez Moctezuma R, Buysschaert C, Farhoudi A, Wang R, et al. HVR1-mediated antibody evasion of highly infectious in vivo adapted HCV in humanised mice. Gut. 2015;65(12):1988–97.

65. Grassi G, Di Caprio G, Fimia GM, Ippolito G, Tripodi M, Alonzi T. Hepatitis C virus relies on lipoproteins for its life cycle. World J Gastroenterol. 2016;22(6):1953–65.

66. Nielsen SU, Bassendine MF, Burt AD, Martin C, Pumeechockchai W, Geoffrey L, et al. Association between Hepatitis C Virus and Very-Low-Density Lipoprotein (VLDL)/LDL Analyzed in Iodixanol Density Gradients Association between Hepatitis C Virus and Very-Low-Density Lipoprotein (VLDL)/LDL Analyzed in Iodixanol Density Gradients. J Virol. 2006;80:2418–2428.

67. Cocquerel L, Op de Beeck A, Lambot M, Roussel J, Delgrange D, Pillez A, et al. Topological changes in the transmembrane domains of hepatitis C virus envelope glycoproteins. EMBO J. 2002;21(12):2893–902.

68. Choukhi a, Ung S, Wychowski C, Dubuisson J. Involvement of endoplasmic reticulum chaperones in the folding of hepatitis C virus glycoproteins. J Virol. 1998;72(5):3851–8.

69. Chan S-W, Egan PA. Hepatitis C virus envelope proteins regulate CHOP via induction of the unfolded protein response. FASEB J. 2005;19(11):1510–2.

70. Atoom AM, Taylor NGA, Russell RS. The elusive function of the hepatitis C virus p7 protein. Virology. 2014;462–463(1):377–87.

71. Lin C, Lindenbach BD, Pragai BM, McCourt DW, Rice CM. Processing in the hepatitis C virus E2-NS2 region: identification of p7 and two distinct E2-specific products with different C termini. J Virol. 1994;68(8):5063–73.

72. Premkumar A, Wilson L, Ewart GD, Gage PW. Cation-selective ion channels formed by p7 of hepatitis C virus are blocked by hexamethylene amiloride. FEBS Lett. 2004;557(1–3):99–103.

73. Carrere-Kremer S, Montpellier-Pala C, Cocquerel L, Wychowski C, Penin F, Dubuisson J. Subcellular localization and topology of the p7 polypeptide of hepatitis C virus. J Virol. 2002;76(8):3720–30.

74. Griffin SDC, Harvey R, Clarke DS, Barclay WS, Harris M, Rowlands DJ. A conserved basic loop in hepatitis C virus p7 protein is required for amantadine-sensitive ion channel activity in mammalian cells but is dispensable for localization to mitochondria. J Gen Virol. 2004;85(2):451–61.

75. Wozniak AL, Griffin S, Rowlands D, Harris M, Yi M, Lemon SM, et al. Intracellular proton conductance of the hepatitis C virus p7 protein and its contribution to infectious virus production. PLoS Pathog. 2010;6(9):e1001087.

76. Boson B, Granio O, Bartenschlager R, Cosset F-L. A concerted action of hepatitis C virus P7 and nonstructural protein 2 regulates core localization at the endoplasmic reticulum and virus assembly. PLoS Pathog. 2011;7(7):e1002144.

77. Gentzsch J, Brohm C, Steinmann E, Friesland M, Menzel N, Vieyres G, et al. Hepatitis C Virus p7 is Critical for Capsid Assembly and Envelopment. PLoS Pathog. 2013;9(5):e1003355.

78. Bentham MJ, Foster TL, McCormick C, Griffin S. Mutations in hepatitis C virus p7 reduce both the egress and infectivity of assembled particles via impaired proton channel function. J Gen Virol. 2013;9:2236–48.

79. Jirasko V, Montserret R, Lee JY, Gouttenoire J, Moradpour D, Penin F, et al. Structural and functional studies of nonstructural protein 2 of the hepatitis C virus reveal its key role as organizer of virion assembly. PLoS Pathog. 2010;6(12):e1001233.

80. Santolini E, Pacini L, Fipaldini C, Migliaccio G, Monica N. The NS2 protein of hepatitis C virus is a transmembrane polypeptide. J Virol. 1995;69(12):7461–71.

81. Lorenz IC, Marcotrigiano J, Dentzer TG, Rice CM. Structure of the catalytic domain of the hepatitis C virus NS2-3 protease. Nature. 2006;442(7104):831–5.

82. Pallaoro M, Lahm A, Biasiol G, Brunetti M, Nardella C, Orsatti L, et al. Characterization of the Hepatitis C Virus NS2/3 Processing Reaction by Using a Purified Precursor Protein. J Virol. 2001;75(20):9939–46.

83. Welbourn S, Green R, Gamache I, Dandache S, Lohmann V, Bartenschlager R, et al. Hepatitis C virus NS2/3 processing is required for NS3 stability and viral RNA replication. J Biol Chem. 2005;280(33):29604–11.

84. Oem J-K, Jackel-Cram C, Li Y-P, Zhou Y, Zhong J, Shimano H, et al. Activation of sterol regulatory element-binding protein 1c and fatty acid synthase transcription by hepatitis C virus non-structural protein 2. J Gen Virol. 2008;89(Pt 5):1225–30.

85. Waris G, Felmlee DJ, Negro F, Siddiqui A. Hepatitis C virus induces proteolytic cleavage of sterol regulatory element binding proteins and stimulates their phosphorylation via oxidative stress. J Virol. 2007;81(15):8122–30.

86. Popescu CI, Callens N, Trinel D, Roingeard P, Moradpour D, Descamps V, et al. NS2 protein of hepatitis C virus interacts with structural and non-structural proteins towards virus assembly. PLoS Pathog. 2011;7(2):e1001278.

87. Anwar MI, Iqbal M, Yousef MS, Rahman M. Over-expression and characterization of NS3 and NS5A of hepatitis C virus genotype 3a. Microb Cell Fact. 2013;12:111.

88. Miller RH, Purcell RH. Hepatitis C virus shares amino acid sequence similarity with pestiviruses and flaviviruses as well as members of two plant virus supergroups. Proc Natl Acad Sci. 1990;87(6):2057–61.

89. Kyono K, Miyashiro M, Taguchi I. Characterization of ATPase Activity of a Hepatitis C Virus NS3 Helicase Domain, and Analysis Involving Mercuric Reagents. J Biochem. 2003;134(4):505–11.

90. Bartenschlager R, Ahlborn-Laake L, Mous J, Jacobsen H. Kinetic and structural analyses of hepatitis C virus polyprotein processing. J Virol. 1994;68(8):5045–55.

91. Fukuda K, Vishnuvardhan D, Sekiya S, Hwang J, Kakiuchi N, Taira K, et al. Isolation and characterization of RNA aptamers specific for the hepatitis C virus nonstructural protein 3 protease. Eur J Biochem. 2000;267(12):3685–94.

92. Love RA, Parge HE, Wickersham JA, Hostomsky Z, Habuka N, Moomaw EW, et al. The crystal structure of hepatitis C virus NS3 proteinase reveals a trypsin-like fold and a structural zinc binding site. Cell. 1996;87(2):331–42.

93. Shoji I, Suzuki T, Chieda S, Sato M, Harada T, Chiba T, et al. Proteolytic activity of NS3 serine proteinase of hepatitis C virus efficiently expressed inescherichia coli. Hepatology. 1995 Dec;22(6):1648–55.

94. Stempniak M, Hostomska Z, Nodes BR, Hostomsky Z. The Ns3 Proteinase Domain of Hepatitis-C Virus Is a Zinc- Containing Enzyme. J Virol. 1997;71(4):2881–6.

95. Barbato G, Cicero DO, Nardi MC, Steinkühler C, Cortese R, De Francesco R, et al. The solution structure of the N-terminal proteinase domain of the hepatitis C virus (HCV) NS3 protein provides new insights into its activation and catalytic mechanism. J Mol Biol. 1999;289(2):371–84.

96. da Silveira NJF, Arcuri H a, Bonalumi CE, de Souza FP, Mello IMVGC, Rahal P, et al. Molecular models of NS3 protease variants of the Hepatitis C virus. BMC Struct Biol. 2005;5:1.

97. Zhang C, Cai Z, Kim Y, Kumar R, Yuan F, Shi P, et al. Stimulation of Hepatitis C Virus (HCV) Nonstructural Protein 3 (NS3) Helicase Activity by the NS3 Protease Domain and by HCV RNA-Dependent RNA Polymerase. J Virol. 2005;3(14):8687–97.

98. Raney KD, Sharma SD, Moustafa IM, Cameron CE. Hepatitis C virus non-structural protein 3 (HCV NS3): A multifunctional antiviral target. J Biol Chem. 2010;285(30):22725–31.

99. Marks KM, Jacobson IM. The first wave: HCV NS3 protease inhibitors telaprevir and boceprevir. Antivir Ther. 2012;17:1119–31.

100. Nagpal N, Goyal S, Wahi D, Jain R, Jamal S, Singh A, et al. Molecular principles behind Boceprevir resistance due to mutations in hepatitis C NS3/4A protease. Gene. 2015;570(1):115–21.

101. Susser S, Vermehren J, Forestier N, Welker MW, Grigorian N, Füller C, et al. Analysis of long-term persistence of resistance mutations within the hepatitis C virus NS3 protease after treatment with telaprevir or boceprevir. J Clin Virol. 2011;52(4):321–7.

102. Kim JW, Seo MY, Shelat A, Kim CS, Kwon TW, Lu H, et al. Structurally Conserved Amino Acid W501 Is Required for RNA Helicase Activity but Is Not Essential for DNA Helicase Activity of Hepatitis C Virus NS3 Protein. J Virol. 2003;77(1):571–82.

103. Huang ZS, Wang CC, Wu HN. HCV NS3 protein helicase domain assists RNA structure conversion. FEBS Lett. 2010;584(11):2356–62.

104. Paolini C, De Francesco R, Gallinari P. Enzymatic properties of hepatitis C virus NS3-associated helicase. J Gen Virol. 2000;81(5):1335–45.

105. Serebrov V, Pyle AM. Periodic cycles of RNA unwinding and pausing by hepatitis C virus NS3 helicase. Nature. 2004;430(6998):476–80.

106. Pang PS, Jankowsky E, Planet PJ, Pyle AM. The hepatitis C viral NS3 protein is a processive DNA helicase with cofactor enhanced RNA unwinding. EMBO J. 2002;21(5):1168–76.

107. Ujino S, Yamaguchi S, Shimotohno K, Takaku H. Heat-shock protein 90 is essential for stabilization of the hepatitis C virus nonstructural protein NS3. J Biol Chem. 2009;284(11):6841–6.

108. Borowski P, Oehlmann K, Heiland M, Laufs R. Nonstructural protein 3 of hepatitis C virus blocks the distribution of the free catalytic subunit of cyclic AMP-dependent protein kinase. J Virol. 1997;71(4):2838–43.

109. Kalkeri G, Lin C, Gopilan J, Sloan K, Rijnbrand R, Kwong AD. Restoration of the activated Rig-I pathway in hepatitis C virus (HCV) replicon cells by HCV protease, polymerase, and NS5A inhibitors in vitro at clinically relevant concentrations. Antimicrob Agents Chemother. 2013;57(9):4417–26.

110. Dabral P, Khera L, Kaul R. Host proteins associated with Hepatitis C virus encoded NS4A. VirusDis. 2014;25(4):493–6.

111. Kohlway A, Pirakitikulr N, Barrera FN, Potapova O, Engelman DM, Pyle AM, et al. Hepatitis C virus RNA replication and virus particle assembly require specific dimerization of the NS4A protein transmembrane domain. J Virol. 2014;88(1):628–42.

112. Wölk B, Sansonno D, Kräusslich HG, Dammacco F, Rice CM, Blum HE, et al. Subcellular localization, stability, and trans-cleavage competence of the hepatitis C virus NS3-NS4A complex expressed in tetracycline-regulated cell lines. J Virol. 2000;74(5):2293–304.

113. Mottola G, Cardinali G, Ceccacci A, Trozzi C, Bartholomew L, Torrisi MR, et al. Hepatitis C virus nonstructural proteins are localized in a modified endoplasmic reticulum of cells expressing viral subgenomic replicons. Virology. 2002;293(1):31–43.

114. Satoh S, Tanji Y, Hijikata M, Kimura K, Shimotohno K. The N-terminal region of hepatitis C virus nonstructural protein 3 (NS3) is essential for stable complex formation with NS4A. J Virol. 1995;69:4255–60.

115. Shimizu Y, Yamaji K, Masuho Y, Yokota T, Inoue H, Sudo K, et al. Idetification of the sequence on NS4A required for enhanced cleavage of the NS5A/B site by hepatitis C virus NS3 protease. J Virol. 1996;70(1):127–32.

116. Failla C, Tomei L, De Francesco R. Both NS3 and NS4A are required for proteolytic processing of hepatitis C virus nonstructural proteins. J Virol. 1994;68(6):3753–60.

117. Tomei L, Failla C, Vitale RL, Bianchi E, De Francesco R. A central hydrophobic domain of the hepatitis C virus NS4A protein is necessary and sufficient for the activation of the NS3 protease. J Gen Virol. 1996;77(5):1065–70.

118. Lin C, Wu JW, Hsiao K, Su MS. The hepatitis C virus NS4A protein: interactions with the NS4B and NS5A proteins. J Virol. 1997;71(9):6465–71.

119. Tanaka T, Kuroda K, Ikeda M, Wakita T, Kato N, Makishima M. Hepatitis C virus NS4B targets lipid droplets through hydrophobic residues in the amphipathic helices. J Lipid Res. 2013;54(4):881–92.

120. Hügle T, Fehrmann F, Bieck E, Kohara M, Kräusslich HG, Rice CM, et al. The hepatitis C virus nonstructural protein 4B is an integral endoplasmic reticulum membrane protein. Virology. 2001;284(1):70–81.

121. Ashworth Briggs EL, Gomes RGB, Elhussein M, Collier W, Stuart Findlow I, Khalid S, et al. Interaction between the NS4B amphipathic helix, AH2, and charged lipid headgroups alters membrane morphology and AH2 oligomeric state - Implications for the Hepatitis C virus life cycle. Biochim Biophys Acta - Biomembr. 2015;1848(8):1671–7.

122. Gouttenoire J, Montserret R, Paul D, Castillo R, Meister S, Bartenschlager R, et al. Aminoterminal amphipathic α-helix AH1 of hepatitis C virus nonstructural protein 4B possesses a dual role in RNA replication and virus production. PLoS Pathog. 2014;10(10):e1004501.

123. Palomares-Jerez MF, Nemesio H, Franquelim HG, Castanho MARB, Villalaín J. N-Terminal AH2 segment of protein NS4B from hepatitis C virus. Binding to and interaction with model biomembranes. Biochim Biophys Acta - Biomembr. 2013;1828(8):1938–52.

124. Paul D, Romero-Brey I, Gouttenoire J, Stoitsova S, Krijnse-Locker J, Moradpour D, et al. NS4B self-interaction through conserved C-terminal elements is required for the establishment of functional hepatitis C virus replication complexes. J Virol. 2011;85(14):6963–76.

125. Gouttenoire J, Roingeard P, Penin F, Moradpour D. Amphipathic alpha-helix AH2 is a major determinant for the oligomerization of hepatitis C virus nonstructural protein 4B. J Virol. 2010;84(24):12529–37.

126. Blight KJ. Charged residues in hepatitis C virus NS4B are critical for multiple NS4B functions in RNA replication. J Virol. 2011;85(16):8158–71.

127. Palomares-Jerez F, Nemesio H, Villalaín J. The membrane spanning domains of protein NS4B from hepatitis C virus. Biochim Biophys Acta - Biomembr. 2012;1818(12):2958–66.

128. Kanwal N, Zaidi N us SS, Gomez MK. Non-structural protein NS4B: HCV replication web inducer. Asian Pacific J Trop Dis. 2012;2(6):497–501.

129. Li S, Yu X, Guo Y, Kong L. Interaction networks of hepatitis C virus NS4B: Implications for antiviral therapy. Cell Microbiol. 2012;14(7):994–1002.

130. Einav S, Elazar M, Danieli T, Jeffrey S, Glenn JS. A Nucleotide Binding Motif in Hepatitis C Virus (HCV) NS4B Mediates HCV RNA Replication A Nucleotide Binding Motif in Hepatitis C Virus (HCV) NS4B Mediates HCV RNA Replication. J Virol. 2004;78(20):11288–95.

131. Einav S, Sklan EH, Hyang MM, Gehrig E, Liu P, Hao Y, et al. The nucleotide binding motif of hepatitis C virus NS4B can mediate cellular transformation and tumor formation without Ha-ras co-transfection. Hepatology. 2008;47(3):827–35.

132. Einav S, Gerber D, Bryson PD, Sklan EH, Elazar M, Maerkl SJ, et al. Discovery of a hepatitis C target and its pharmacological inhibitors by microfluidic affinity analysis. Nat Biotechnol. 2008;26(9):1019–27.

133. Liefhebber JMP, Brandt BW, Broer R, Spaan WJM, van Leeuwen HC. Hepatitis C virus NS4B carboxy terminal domain is a membrane binding domain. Virol J. 2009;6:62.

134. Yu G-Y, Lee K-J, Gao L, Lai MMC. Palmitoylation and polymerization of hepatitis C virus NS4B protein. J Virol. 2006;80(12):6013–23.

135. Thompson AA, Zou A, Yan J, Duggal R, Hao W, Molina D, et al. Biochemical characterization of recombinant hepatitis C virus nonstructural protein 4B: evidence for ATP/GTP hydrolysis and adenylate kinase activity. Biochemistry. 2009;48(5):906–16.

136. Paul D, Bartenschlager R, McCormick C. The predominant species of nonstructural protein 4B in hepatitis C virus-replicating cells is not palmitoylated. J Gen Virol. 2015;96(7):1696–701.

137. Palomares-Jerez MF, Villalaín J. Membrane interaction of segment H1 ($NS4B_{H1}$) from hepatitis C virus non-structural protein 4B. Biochim Biophys Acta - Biomembr. 2011;1808(4):1219–29.

138. Guillén J, González-Álvarez A, Villalaín J. A membranotropic region in the C-terminal domain of Hepatitis C virus protein NS4B. Interaction with membranes. Biochim Biophys Acta - Biomembr. 2010;1798(3):327–37.

139. Koch JO, Bartenschlager R. Modulation of hepatitis C virus NS5A hyperphosphorylation by nonstructural proteins NS3, NS4A, and NS4B. J Virol. 1999;73(9):7138–46.

140. Nitta S, Sakamoto N, Nakagawa M, Kakinuma S, Mishima K, Kusano-Kitazume A, et al. Hepatitis C virus NS4B protein targets STING and abrogates RIG-I-mediated type I interferon-dependent innate immunity. Hepatology. 2013;57(1):46–58.

141. Nakhaei P, Hiscott J, Lin R. STING-ing the antiviral pathway. J Mol Cell Biol. 2010;2(3):110–2.

142. Gao L, Aizaki H, He J-W, Lai MMC. Interactions between viral nonstructural proteins and host protein hVAP-33 mediate the formation of hepatitis C virus RNA replication complex on lipid raft. J Virol. 2004;78(7):3480–8.

143. Wu MJ, Ke PY, Hsu JTA, Yeh CT, Horng JT. Reticulon 3 interacts with NS4B of the hepatitis C virus and negatively regulates viral replication by disrupting NS4B self-interaction. Cell Microbiol. 2014;16(11):1603–18.

144. Wan Q, Kuang E, Dong W, Zhou S, Xu H, Qi Y, et al. Reticulon 3 mediates Bcl-2 accumulation in mitochondria in response to endoplasmic reticulum stress. Apoptosis. 2007;12(2):319–28.

145. LeMay KL, Treadaway J, Angulo I, Tellinghuisen TL. A Hepatitis C Virus NS5A Phosphorylation Site That Regulates RNA Replication. J Virol. 2013;87(2):1255–60.

146. Sólyom Z, Ma P, Schwarten M, Bosco M, Polidori A, Durand G, et al. The disordered region of the HCV protein NS5A: Conformational dynamics, SH3 binding, and phosphorylation. Biophys J. 2015;109(7):1483–96.

147. Fridell R a, Qiu D, Valera L, Wang C, Rose RE, Gao M. Distinct functions of NS5A in hepatitis C virus RNA replication uncovered by studies with the NS5A inhibitor BMS-790052. J Virol. 2011;85(14):7312–20.

148. Tellinghuisen TL, Marcotrigiano J, Gorbalenya AE, Rice CM. The NS5A protein of hepatitis C virus is a zinc metalloprotein. J Biol Chem. 2004;279(47):48576–87.

149. Galli A, Scheel TKH, Prentoe JC, Mikkelsen LS, Gottwein JM, Bukh J. Analysis of hepatitis C virus core/NS5A protein co-localization using novel cell culture systems expressing core-NS2 and NS5A of genotypes 1-7. J Gen Virol. 2013;94:2221–35.

150. Camus G, Herker E, Modi AA, Haas JT, Ramage HR, Farese R V., et al. Diacylglycerol acyltransferase-1 localizes hepatitis C virus NS5A protein to lipid droplets and enhances NS5A interaction with the viral capsid core. J Biol Chem. 2013;288(14):9915–23.

151. Lin CC, Tsai P, Sun HY, Hsu MC, Lee JC, Wu IC, et al. Apolipoprotein J, a glucose-upregulated molecular chaperone, stabilizes core and NS5A to promote infectious hepatitis C virus virion production. J Hepatol. 2014;61(5):984–93.

152. Robinson LC, Marchant JS. Enhanced Ca2+ leak from ER Ca2+ stores induced by hepatitis C NS5A protein. Biochem Biophys Res Commun. 2009;368(3):593–9.

153. Kato K, Ogura T, Kishimoto A, Minegishi Y, Nakajima N, Miyazaki M, et al. Critical roles of AMP-activated protein kinase in constitutive tolerance of cancer cells to nutrient deprivation and tumor formation. Oncogene. 2002;21(39):6082–90.

154. Deng L, Shoji I, Ogawa W, Kaneda S, Soga T, Jiang D, et al. Hepatitis C virus infection promotes hepatic gluconeogenesis through an NS5A-mediated, FoxO1-dependent pathway. J Virol. 2011;85(17):8556–68.

155. Sheikh TI, Adam T, Qadri I. Upregulated hepatic expression of mitochondrial PEPCK triggers initial gluconeogenic reactions in the HCV-3 patients. Asian Pac J Trop Med. 2015;8(8):618–23.

156. He Y, Nakao H, Tan S-L, Polyak SJ, Neddermann P, Vijaysri S, et al. Subversion of cell signaling pathways by hepatitis C virus nonstructural 5A protein via interaction with Grb2 and P85 phosphatidylinositol 3-kinase. J Virol. 2002;76(18):9207–17.

157. Tan SL, Nakao H, He Y, Vijaysri S, Neddermann P, Jacobs BL, et al. NS5A, a nonstructural protein of hepatitis C virus, binds growth factor receptor-bound protein 2 adaptor protein in a Src homology 3 domain/ligand-dependent manner and perturbs mitogenic signaling. Proc Natl Acad Sci U S A. 1999;96(10):5533–8.

158. Zhao L-J, Hua X, He S-F, Ren H, Qi Z-T. Interferon alpha regulates MAPK and STAT1 pathways in human hepatoma cells. Virol J. 2011;8(1):157.

159. Gale MJ, Korth MJ, Tang NM, Tan S-L, Hopkins DA, Dever TE, et al. Evidence That Hepatitis C Virus Resistance to Interferon Is Mediated through Repression of the PKR Protein Kinase by the Nonstructural 5A Protein. Virology. 1997;230(2):217–27.

160. Choi HB, Kim YG, Oh JW. Biochemical properties of full-length hepatitis C virus RNA-dependent RNA polymerase expressed in insect cells. Exp Mol Med. 2003;35(6):475–85.

161. Lévêque VJ, Johnson RB, Parsons S, Ren J, Xie C, Zhang F, et al. Identification of a C-Terminal Regulatory Motif in Hepatitis C Virus RNA-Dependent RNA Polymerase : Structural and Biochemical Analysis Identification of a C-Terminal Regulatory Motif in Hepatitis C Virus RNA-Dependent RNA Polymerase : Structural and Biochemical Analysis. J Virol. 2003;77(16):9020–8.

162. Luo G, Hamatake RK, Mathis DM, Racela J, Rigat K, Lemm J, et al. De novo initiation of RNA synthesis by hepatitis C virus nonstructural protein 5B polymerase. J Virol. 2000;74(4):2017–22.

163. Powdrill MH, Tchesnokov EP, Kozak RA, Russell RS, Martin R, Svarovskaia ES, et al. Contribution of a mutational bias in hepatitis C virus replication to the genetic barrier in the development of drug resistance. Proc Natl Acad Sci U S A. 2011;108(51):20509–13.

164. Pugachev K V, Guirakhoo F, Ocran SW, Mitchell F, Parsons M, Penal C, et al. High fidelity of yellow fever virus RNA polymerase. J Virol. 2004;78(2):1032–8.

165. Ishido S, Fujita T, Hotta H. Complex formation of NS5B with NS3 and NS4A proteins of hepatitis C virus. Biochem Biophys Res Commun. 1998;244(1):35–40.

166. Shirota Y, Luo H, Qin W, Kaneko S, Yamashita T, Kobayashi K, et al. Hepatitis C virus (HCV) NS5A binds RNA-dependent RNA polymerase (RdRP) NS5B and modulates RNA-dependent RNA polymerase activity. J Biol Chem. 2002;277(13):11149–55.

167. Wang QM, Hockman MA, Staschke K, Johnson RB, Case KA, Lu J, et al. Oligomerization and cooperative RNA synthesis activity of hepatitis C virus RNA-dependent RNA polymerase. J Virol. 2002;76(8):3865–72.

168. Kyono K, Miyashiro M, Taguchi I. Human Eukaryotic Initiation Factor 4AII Associates with Hepatitis C Virus NS5B Protein in Vitro. Biochem Biophys Res Commun. 2002;292(3):659–66.

169. Kim SJ, Kim JH, Kim YG, Lim HS, Oh JW. Protein kinase C-related kinase 2 regulates hepatitis C virus RNA polymerase function by phosphorylation. J Biol Chem. 2004;279(48):50031–41.

170. Tu H, Gao L, Shi ST, Taylor DR, Yang T, Mircheff a K, et al. Hepatitis C virus RNA polymerase and NS5A complex with a SNARE-like protein. Virology. 1999;263(1):30–41.

171. Goh P-Y, Tan Y-J, Lim SP, Tan YH, Lim SG, Fuller-Pace F, et al. Cellular RNA helicase p68 relocalization and interaction with the hepatitis C virus (HCV) NS5B protein and the potential role of p68 in HCV RNA replication. J Virol. 2004;78(10):5288–98.

172. Shimakami T, Honda M, Kusakawa T, Murata T, Shimotohno K, Kaneko S, et al. Effect of hepatitis C virus (HCV) NS5B-nucleolin interaction on HCV replication with HCV subgenomic replicon. J Virol. 2006;80(7):3332–40.

173. Ashfaq UA, Khan SN, Nawaz Z, Riazuddin S. In-vitro model systems to study Hepatitis C Virus. Genet Vaccines Ther. 2011;9(1):7.

174. Bartosch B, Dubuisson J, Cosset F-L. Infectious Hepatitis C Virus Pseudo-particles Containing Functional E1–E2 Envelope Protein Complexes. J Exp Med. 2003;36331000(5):633–42.

175. Woerz I, Lohmann V, Bartenschlager R. Hepatitis C virus replicons: Dinosaurs still in business? J Viral Hepat. 2009;16(1):1–9.

176. Evans MJ, von Hahn T, Tscherne DM, Syder AJ, Panis M, Wölk B, et al. Claudin-1 is a hepatitis C virus co-receptor required for a late step in entry. Nature. 2007;446(7137):801–5.

177. Lohmann V. Replication of Subgenomic Hepatitis C Virus RNAs in a Hepatoma Cell Line. Science. 1999;285(5424):110–3.

178. Amako Y, Munakata T, Kohara M, Siddiqui A, Peers C, Harris M. Hepatitis C virus attenuates mitochondrial lipid β-oxidation by downregulating mitochondrial trifunctional-protein expression. J Virol. 2015;89(8):4092–101.

179. Molina S, Castet V, Pichard-Garcia L, Wychowski C, Meurs E, Pascussi JM, et al. Serum-derived hepatitis C virus infection of primary human hepatocytes is tetraspanin CD81 dependent. J Virol. 2008;82(1):569–74.

180. Podevin P, Carpentier A, Pne V, Aoudjehane L, Carrire M, Zadi S, et al. Production of infectious hepatitis C virus in primary cultures of human adult hepatocytes. Gastroenterology. 2010;139(4):1355–1364.e6.

181. Wakita T, Pietschmann T, Kato T, Date T, Miyamoto M, Zhao Z, et al. Production of infectious hepatitis C virus in tissue culture from a cloned viral genome. Nat Med. 2005;11(7):791–6.

182. Sumpter Jr. R, Loo YM, Foy E, Li K, Yoneyama M, Fujita T, et al. Regulating intracellular antiviral defense and permissiveness to hepatitis C virus RNA replication through a cellular RNA helicase, RIG-I. J Virol. 2005;79(5):2689–99.

183. Teimourpour R, Meshkat Z, Gholoubi A, Nomani H, Rostami S. Viral Load Analysis of Hepatitis C Virus in Huh7.5 Cell Culture System. Jundishapur J Microbiol. 2015;8(5):e19279.

184. Pietschmann T, Kaul A, Koutsoudakis G, Shavinskaya A, Kallis S, Steinmann E, et al. Construction and characterization of infectious intragenotypic and intergenotypic hepatitis C virus chimeras. Proc Natl Acad Sci U S A. 2006;103(19):7408–13.

185. Liu S, Xiao L, Nelson C, Hagedorn C. A Cell Culture Adapted HCV JFH1 Variant That Increases Viral Titers and Permits the Production of High Titer Infectious Chimeric Reporter Viruses. PLoS One. 2012;7(9):1–12.

186. Jiang J, Luo G. Cell culture-adaptive mutations promote viral protein-protein interactions and morphogenesis of infectious hepatitis C virus. J Virol. 2012;86(17):8987–97.

187. Bukh J, Pietschmann T, Lohmann V, Krieger N, Faulk K, Engle RE, et al. Mutations that permit efficient replication of hepatitis C virus RNA in Huh-7 cells prevent productive replication in chimpanzees. Proc Natl Acad Sci U S A. 2002;99(22):14416–21.

188. Saeed M, Andreo U, Chung H-Y, Espiritu C, Branch AD, Silva JM, et al. SEC14L2 enables pan-genotype HCV replication in cell culture. Nature. 2015;524(7566):471–5.

189. Zingg JM, Libinaki R, Meydani M, Azzi A. Modulation of phosphorylation of tocopherol and phosphatidylinositol by hTAP1/SEC14L2-mediated lipid exchange. PLoS One. 2014;9(7).

190. Wunschmann S, Medh JD, Klinzmann D, Schmidt WN, Stapleton JT. Characterization of hepatitis C virus (HCV) and HCV E2 interactions with CD81 and the low-density lipoprotein receptor. J Virol. 2000;74(21):10055–62.

191. Popescu C-I, Dubuisson J. Role of lipid metabolism in hepatitis C virus assembly and entry. Biol Cell. 2010;102(1):63–74.

192. Bishé B, Syed GH, Field SJ, Siddiqui A. Role of phosphatidylinositol 4-phosphate (PI4P) and its binding protein GOLPH3 in hepatitis C virus secretion. J Biol Chem. 2012;287(33):27637–47.

193. Mankouri J, Walter C, Stewart H, Bentham M, Park W, Heo W, et al. Release of Infectious Hepatitis C Virus from Huh7 Cells Occurs via a trans-Golgi Network-to-Endosome Pathway Independent of Very-Low-Density Lipoprotein Secretion. J Virol. 2016;90(16):7159-70.

194. Liu S, Yang W, Shen L, Turner JR, Coyne CB, Wang T. Tight Junction Proteins Claudin-1 and Occludin Control Hepatitis C Virus Entry and Are Downregulated during Infection To Prevent Superinfection. J Virol. 2009;83(4):2011–4.

195. Tong Y, Zhu Y, Xia X, Liu Y, Feng Y, Hua X, et al. Tupaia CD81, SR-BI, claudin-1, and occludin support hepatitis C virus infection. J Virol. 2011;85(6):2793–802.

196. Sainz B, Barretto N, Martin DN, Hiraga N, Imamura M, Hussain S, et al. Identification of the Niemann-Pick C1-like 1 cholesterol absorption receptor as a new hepatitis C virus entry factor. Nat Med. 2012;18(2):281–5.

197. Lupberger J, Felmlee DJ, Baumert TF. Cholesterol uptake and hepatitis C virus entry. J Hepatol. 2012;57(1):215–7.

198. Blanchard E, Belouzard S, Goueslain L, Wakita T, Dubuisson J, Wychowski C, et al. Hepatitis C virus entry depends on clathrin-mediated endocytosis. J Virol. 2006;80(14):6964–72.

199. Liu HM, Aizaki H, Machida K, Ou JHJ, Lai MMC. Hepatitis C virus translation preferentially depends on active RNA replication. PLoS One. 2012;7(8):e43600.

200. Fan Z, Yang QR, Twu JS, Sherker AH. Specific in vitro association between the hepatitis C viral genome and core protein. J Med Virol. 1999;59(2):131–4.

201. Eggert D, Rösch K, Reimer R, Herker E. Visualization and analysis of Hepatitis C Virus structural proteins at lipid droplets by super-resolution microscopy. PLoS One. 2014;9(7):e102511.

202. Huang H, Sun F, Owen DM, Li W, Chen Y, Gale M, et al. Hepatitis C virus production by human hepatocytes dependent on assembly and secretion of very low-density lipoproteins. Proc Natl Acad Sci U S A. 2007;104(14):5848–53.

203. Felmlee DJ, Hafirassou ML, Lefevre M, Baumert TF, Schuster C. Hepatitis C virus, cholesterol and lipoproteins - Impact for the viral life cycle and pathogenesis of liver disease. Viruses. 2013;5(5):1292–324.

204. Olofsson SO, Stillemark-Billton P, Asp L. Intracellular assembly of VLDL: Two major steps in separate cell compartments. Trends Cardiovasc Med. 2000;10(8):338–45.

205. Amako Y, Sarkeshik A, Hotta H, Yates J, Siddiqui A. Role of oxysterol binding protein in hepatitis C virus infection. J Virol. 2009;83(18):9237–46.

206. Wang H, Perry JW, Lauring AS, Neddermann P, De Francesco R, Tai AW. Oxysterol-binding protein is a phosphatidylinositol 4-kinase effector required for HCV replication membrane integrity and cholesterol trafficking. Gastroenterology. 2014;146(5).

207. Ariumi Y, Kuroki M, Maki M, Ikeda M, Dansako H, Wakita T, et al. The ESCRT system is required for hepatitis C virus production. PLoS One. 2011;6(1):e14517.

208. Diamond DL, Syder AJ, Jacobs JM, Sorensen CM, Walters KA, Proll SC, et al. Temporal proteome and lipidome profiles reveal hepatitis C virus-associated reprogramming of hepatocellular metabolism and bioenergetics. PLoS Pathog. 2010;6(1).

209. Weng L, Hirata Y, Arai M, Kohara M, Wakita T, Watashi K, et al. Sphingomyelin activates hepatitis C virus RNA polymerase in a genotype-specific manner. J Virol. 2010;84(22):11761–70.

210. Cho NJ, Lee C, Pang PS, Pham EA, Fram B, Nguyen K, et al. Phosphatidylinositol 4,5-bisphosphate is an HCV NS5A ligand and mediates replication of the viral genome. Gastroenterology. 2015;148(3):616–25.

211. Berger KL, Kelly SM, Jordan TX, Tartell MA, Randall G. Hepatitis C virus stimulates the phosphatidylinositol 4-kinase III alpha-dependent phosphatidylinositol 4-phosphate production that is essential for its replication. J Virol. 2011;85(17):8870–83.

212. Li H, Yang X, Yang G, Hong Z, Zhou L, Yin P, et al. Hepatitis C virus NS5A hijacks ARFGAP1 to maintain a phosphatidylinositol 4-phosphate-enriched microenvironment. J Virol. 2014;88(11):5956–66.

213. Zhang L, Hong Z, Lin W, Shao RX, Goto K, Hsu VW, et al. ARF1 and GBF1 generate a PI4P-Enriched environment supportive of hepatitis C virus replication. PLoS One. 2012;7(2):1–9.

214. Blackham S, Baillie A, Al-Hababi F, Remlinger K, You S, Hamatake R, et al. Gene expression profiling indicates the roles of host oxidative stress, apoptosis, lipid metabolism, and intracellular transport genes in the replication of hepatitis C virus. J Virol. 2010;84(10):5404–14.

215. Blackham S. Identification of Host Cell Factors Involved in the HCV Replication Cycle. Imperial College London; 2011.

216. Pamplona R. Membrane phospholipids, lipoxidative damage and molecular integrity: A causal role in aging and longevity. Biochim Biophys Acta - Bioenerg. 2008;1777(10):1249–62.

217. Hammond GR V., Fischer MJ, Anderson KE, Holdich J, Koteci A, Balla T, et al. PI4P and PI(4,5)P2 Are Essential But Independent Lipid Determinants of Membrane Identity. Science. 2012;337(6095):727–30.

218. Yin P, Hong Z, Yang X, Chung RT, Zhang L. A role for retromer in hepatitis C virus replication. Cell Mol Life Sci. 2015;73(4):869–81.

219. Bulankina A V., Deggerich A, Wenzel D, Mutenda K, Wittmann JG, Rudolph MG, et al. TIP47 functions in the biogenesis of lipid droplets. J Cell Biol. 2009;185(4):641–55.

220. Miyanari Y, Atsuzawa K, Usuda N, Watashi K, Hishiki T, Zayas M, et al. The lipid droplet is an important organelle for hepatitis C virus production. Nat Cell Biol. 2007;9(9):1089–97.

221. Felmlee DJ, Baumert TF. Hepatitis C virus co-opts innate immunity component for lipid droplet formation. J Hepatol. 2013;59(5):1118–20.

222. Li Q, Pène V, Krishnamurthy S, Cha H, Liang TJ. Hepatitis C virus infection activates an innate pathway involving IKK-α in lipogenesis and viral assembly. Nat Med. 2013;19(6):722–9.

223. Ogryzko V V., Schiltz RL, Russanova V, Howard BH, Nakatani Y. The transcriptional coactivators p300 and CBP are histone acetyltransferases. Cell. 1996;87(5):953–9.

224. Mogensen TH. Pathogen recognition and inflammatory signaling in innate immune defenses. Clin Microbiol Rev. 2009;22(2):240–73.

225. Yang DR, Zhu HZ. Hepatitis C virus and antiviral innate immunity: Who wins at tug-of-war? World J Gastroenterol. 2015;21(13):3786–800.

226. Yoneyama M, Kikuchi M, Natsukawa T, Shinobu N, Imaizumi T, Miyagishi M, et al. The RNA helicase RIG-I has an essential function in double-stranded RNA-induced innate antiviral responses. Nat Immunol. 2004;5(7):730–7.

227. Rehwinkel J, Reis e Sousa C. RIGorous detection: exposing virus through RNA sensing. Science. 2010;327(5963):284–6.

228. Saito T, Owen DM, Jiang F, Marcotrigiano J, Gale MJ. Innate immunity induced by composition-dependent RIG-I recognition of hepatitis C virus RNA. Nature. 2008;454(7203):523–7.

229. Uzri D, Gehrke L. Nucleotide sequences and modifications that determine RIG-I/RNA binding and signaling activities. J Virol. 2009;83(9):4174–84.

230. Eksioglu EA, Zhu H, Bayouth L, Bess J, Liu H yan, Nelson DR, et al. Characterization of HCV interactions with Toll-like receptors and RIG-I in liver cells. PLoS One. 2011;6(6).

231. Bellecave P, Sarasin-Filipowicz M, Sarasin-Filipowicz OD, Kennel A, Gouttenoire J, Meylan E, et al. Cleavage of mitochondrial antiviral signaling protein in the liver of patients with chronic hepatitis C correlates with a reduced activation of the endogenous interferon system. Hepatology. 2010;51(4):1127–36.

232. Loo Y-M, Owen DM, Li K, Erickson AK, Johnson CL, Fish PM, et al. Viral and therapeutic control of IFN-beta promoter stimulator 1 during hepatitis C virus infection. Proc Natl Acad Sci U S A. 2006;103(15):6001–6.

233. Baril M, Racine M-E, Penin F, Lamarre D. MAVS dimer is a crucial signaling component of innate immunity and the target of hepatitis C virus NS3/4A protease. J Virol. 2009;83(3):1299–311.

234. Inoue K, Tsukiyama-Kohara K, Matsuda C, Yoneyama M, Fujita T, Kuge S, et al. Impairment of interferon regulatory factor-3 activation by hepatitis C virus core protein basic amino acid region 1. Biochem Biophys Res Commun. 2012;428(4):494–9.

235. Seki E, Brenner DA. Toll-like receptors and adaptor molecules in liver disease: Update. Hepatology. 2008;48(1):322–35.

236. Wang N, Liang Y, Devaraj S, Wang J, Lemon SM, Li K. Toll-like receptor 3 mediates establishment of an antiviral state against hepatitis C virus in hepatoma cells. J Virol. 2009;83(19):9824–34.

237. Lester SN, Li K. Toll-like receptors in antiviral innate immunity. J Mol Biol. 2014;426(6):1246–64.

238. Arnaud N, Dabo S, Maillard P, Budkowska A, Kalliampakou KI, Mavromara P, et al. Hepatitis c virus controls interferon production through PKR activation. PLoS One. 2010;5(5).

239. Taylor DR, Tian B, Romano PR, Hinnebusch AG, Lai MM, Mathews MB. Hepatitis C virus envelope protein E2 does not inhibit PKR by simple competition with autophosphorylation sites in the RNA-binding domain. J Virol. 2001;75(3):1265–73.

240. Heim MH, Thimme R. Innate and adaptive immune responses in HCV infections. J Hepatol. 2014;61(1):S14–25.

241. Simmonds P, Holmes EC, Cha TA, Chan SW, McOmish F, Irvine B, et al. Classification of hepatitis C virus into six major genotypes and a series of subtypes by phylogenetic analysis of the NS-5 region. J Gen Virol. 1993;74(11):2391–9.

242. Echeverría N, Moratorio G, Cristina J, Moreno P. Hepatitis C virus genetic variability and evolution. World J Hepatol. 2015;7(6):831–45.

243. Messina JP, Humphreys I, Flaxman A, Brown A, Cooke GS, Pybus OG, et al. Global distribution and prevalence of hepatitis C virus genotypes. Hepatology. 2015;61(1):77–87.

244. Murphy DG, Sablon E, Chamberland J, Fournier E, Dandavino R, Tremblay CL. Hepatitis C virus genotype 7, a new genotype originating from Central Africa. J Clin Microbiol. 2015;53(3):967–72.

245. Cannon NA, Donlin MJ, Fan X, Aurora R, Tavis JE. Hepatitis C virus diversity and evolution in the full open-reading frame during antiviral therapy. PLoS One. 2008;3(5):1–12.

246. Mansky LM. Forward Mutation Rate of Human Immunodeficiency Virus Type 1 in a T Lymphoid Cell Line. AIDS Res Hum Retroviruses. 2009;12(4):307–14.

247. Sarwar MT, Kausar H, Ijaz B, Ahmad W, Ansar M, Sumrin A, et al. NS4A protein as a marker of HCV history suggests that different HCV genotypes originally evolved from genotype 1b. Virol J. 2011;8(1):317.

248. Moucari R, Asselah T, Cazals-Hatem D, Voitot H, Boyer N, Ripault MP, et al. Insulin Resistance in Chronic Hepatitis C: Association With Genotypes 1 and 4, Serum HCV RNA Level, and Liver Fibrosis. Gastroenterology. 2008;134(2):416–23.

249. Oliveira LP, Jesus RP, Boulhosa RS, Mendes CM, Lyra a C, Lyra LG. Metabolic syndrome in patients with chronic hepatitis C virus genotype 1 infection who do not have obesity or type 2 diabetes. Clin (Sao Paulo). 2012;67(3):219–23.

250. Poynard T, Ratziu V, McHutchison J, Manns M, Goodman Z, Zeuzem S, et al. Effect of treatment with peginterferon or interferon alfa-2b and ribavirin on steatosis in patients infected with hepatitis C. Hepatology. 2003;38(1):75–85.

251. Fehr M, Takanaga H. Evidence for High-Capacity Bidirectional Glucose Transport Across the Endoplasmic Reticulum Membrane By Genetically Encoded Fluorescence Resonance Energy Transfer Nanosensors. Mol Cell Biol. 2005;25(24):11102–12.

252. Antoine B, Lefrançois-Martinez AM, Le Guillou G, Leturque A, Vandewalle A, Kahn A. Role of the GLUT 2 glucose transporter in the response of the L-type pyruvate kinase gene to glucose in liver-derived cells. J Biol Chem. 1997;272(29):17937–43.

253. Bechmann LP, Hannivoort RA, Gerken G, Hotamisligil GS, Trauner M, Canbay A. The interaction of hepatic lipid and glucose metabolism in liver diseases. J Hepatol. 2012;56(4):952–64.

254. Kasai D, Adachi T, Deng L, Nagano-Fujii M, Sada K, Ikeda M, et al. HCV replication suppresses cellular glucose uptake through down-regulation of cell surface expression of glucose transporters. J Hepatol. 2009;50(5):883–94.

255. Roach PJ, Depaoli-Roach AA, Hurley TD, Tagliabracci VS. Glycogen and its metabolism: some new developments and old themes. Biochem J. 2012;441(3):763–87.

256. Seoane J, Gómez-Foix AM, O'Doherty RM, Gómez-Ara C, Newgard CB, Guinovart JJ. Glucose 6-phosphate produced by glucokinase, but not hexokinase I, promotes the activation of hepatic glycogen synthase. J Biol Chem. 1996;271(39):23756–60.

257. Han H-S, Kang G, Kim JS, Choi BH, Koo S-H. Regulation of glucose metabolism from a liver-centric perspective. Exp Mol Med. 2016;48(3):e218.

258. Díaz A, Martínez-Pons C, Fita I, Ferrer JC, Guinovart JJ. Processivity and subcellular localization of glycogen synthase depend on a non-catalytic high affinity glycogen-binding site. J Biol Chem. 2011;286(21):18505–14.

259. John S, Weiss JN, Ribalet B. Subcellular localization of hexokinases I and II directs the metabolic fate of glucose. PLoS One. 2011;6(3).

260. Bultot L, Guigas B, Von Wilamowitz-Moellendorff A, Maisin L, Vertommen D, Hussain N, et al. AMP-activated protein kinase phosphorylates and inactivates liver glycogen synthase. Biochem J. 2012;443(1):193–203.

261. Mankouri J, Tedbury PR, Gretton S, Hughes ME, Griffin SDC, Dallas ML, et al. Enhanced hepatitis C virus genome replication and lipid accumulation mediated by inhibition of AMP-activated protein kinase. Proc Natl Acad Sci U S A. 2010;107(25):11549–54.

262. Kim YM, Seo YH, Park CB, Yoon SH, Yoon G. Roles of GSK3 in metabolic shift toward abnormal anabolism in cell senescence. Ann N Y Acad Sci. 2010;1201:65–71.

263. Burwinkel B, Bakker HD, Herschkovitz E, Moses SW, Shin YS, Kilimann MW. Mutations in the liver glycogen phosphorylase gene (PYGL) underlying glycogenosis type VI. Am J Hum Genet. 1998;62(4):785–91.

264. Zmasek CM, Godzik A. Phylogenomic analysis of glycogen branching and debranching enzymatic duo. BMC Evol Biol. 2014;14(1):183.

265. Chu CA, Fujimoto Y, Igawa K, Grimsby J, Grippo JF, Magnuson M a, et al. Rapid translocation of hepatic glucokinase in response to intraduodenal glucose infusion and changes in plasma glucose and insulin in conscious rats. Am J Physiol Gastrointest Liver Physiol. 2004;286(4):G627-34.

266. Wolff M, Kauschke SG, Schmidt S, Heilker R. Activation and translocation of glucokinase in rat primary hepatocytes monitored by high content image analysis. J Biomol Screen. 2008;13(9):837–46.

267. Rizzo MA, Magnuson MA, Drain PF, Piston DW. A functional link between glucokinase binding to insulin granules and conformational alterations in response to glucose and insulin. J Biol Chem. 2002;277(37):34168–75.

268. Hirota K, Sakamaki JI, Ishida J, Shimamoto Y, Nishihara S, Kodama N, et al. A combination of HNF-4 and Foxo1 is required for reciprocal transcriptional regulation of glucokinase and glucose-6-phosphatase genes in response to fasting and feeding. J Biol Chem. 2008;283(47):32432–41.

269. Kim SY, Kim H Il, Kim TH, Im SS, Park SK, Lee IK, et al. SREBP-1c mediates the insulin-dependent hepatic glucokinase expression. J Biol Chem. 2004;279(29):30823–9.

270. Foretz M, Guichard C, Ferré P, Foufelle F. Sterol regulatory element binding protein-1c is a major mediator of insulin action on the hepatic expression of glucokinase and lipogenesis-related genes. Proc Natl Acad Sci U S A. 1999;96(22):12737–42.

271. Stoltzman C a, Peterson CW, Breen KT, Muoio DM, Billin AN, Ayer DE. Glucose sensing by MondoA:Mlx complexes: a role for hexokinases and direct regulation of thioredoxin-interacting protein expression. Proc Natl Acad Sci U S A. 2008;105(19):6912–7.

272. Pelicano H, Martin DS, Xu R-H, Huang P. Glycolysis inhibition for anticancer treatment. Oncogene. 2006;25(34):4633–46.

273. Shimizu T, Inoue K ichi, Hachiya H, Shibuya N, Shimoda M, Kubota K. Frequent alteration of the protein synthesis of enzymes for glucose metabolism in hepatocellular carcinomas. J Gastroenterol. 2014;49(9):1324–32.

274. DeBerardinis RJ, Mancuso A, Daikhin E, Nissim I, Yudkoff M, Wehrli S, et al. Beyond aerobic glycolysis: transformed cells can engage in glutamine metabolism that exceeds the requirement for protein and nucleotide synthesis. Proc Natl Acad Sci U S A. 2007;104(49):19345–50.

275. Ciou SC, Chou YT, Liu YL, Nieh YC, Lu JW, Huang SF, et al. Ribose-5-phosphate isomerase A regulates hepatocarcinogenesis via PP2A and ERK signaling. Int J Cancer. 2015;137(1):104–15.

276. Ripoli M, Aprile AD, Quarato G, Sarasin-filipowicz M, Scrima R, Cela O, et al. Hepatitis C Virus-Linked Mitochondrial Dysfunction Promotes Hypoxia-Inducible Factor 1α-Mediated Glycolytic Adaptation. 2010;84(1):647–60.

277. Vassilaki N, Kalliampakou KI, Kotta-Loizou I, Befani C, Liakos P, Simos G, et al. Low oxygen tension enhances hepatitis C virus replication. J Virol. 2013;87(5):2935–48.

278. Gray LR, Tompkins SC, Taylor EB. Regulation of pyruvate metabolism and human disease. Cell Mol Life Sci. 2014;71(14):2577–604.

279. Akram M. Citric Acid Cycle and Role of its Intermediates in Metabolism. Cell Biochem Biophys. 2014;68(3):475–8.

280. Nazaret C, Heiske M, Thurley K, Mazat JP. Mitochondrial energetic metabolism: A simplified model of TCA cycle with ATP production. J Theor Biol. 2009;258(3):455–64.

281. Owen OE, Kalhan SC, Hanson RW. The key role of anaplerosis and cataplerosis for citric acid cycle function. J Biol Chem. 2002;277(34):30409–12.

282. Khawaja Y, Karaman R. A Novel Mathematical Equation For Calculating The Number Of ATP Molecules Generated From Sugars In Cells. World J Pharm Res. 2015;4(4):303–12.

283. Bowtell JL, Marwood S, Bruce M, Constantin-teodosiu D, Greenhaff PL. Tricarboxylic Acid Cycle Intermadeate Pool Size: Functional Importance for Oxidative Metabolism in Exercising Human Skeletal Muscle. Sport Med. 2007;37(12):1071–88.

284. Houten SM, Wanders RJA. A general introduction to the biochemistry of mitochondrial fatty acid β-oxidation. J Inherit Metab Dis. 2010;33(5):469–77.

285. Schiff M, Miné M, Brivet M, Marsac C, Elmaleh-Bergés M, Evrard P, et al. Leigh's disease due to a new mutation in the PDHX gene. Ann Neurol. 2006;59(4):709–14.

286. Sheu KF, Calingasan NY, Lindsay JG, Gibson GE. Immunochemical characterization of the deficiency of the alpha-ketoglutarate dehydrogenase complex in thiamine-deficient rat brain. J Neurochem. 1998;70(3):1143–50.

287. Bourgeron T, Rustin P, Chretien D, Birch-Machin M, Bourgeois M, Viegas-Péquignot E, et al. Mutation of a nuclear succinate dehydrogenase gene results in mitochondrial respiratory chain deficiency. Nat Genet. 1995;11(2):144–9.

288. RH Behal, MS DeBuysere, B Demeler JHMO. Pyruvate Dehydrogenase Multienzyme Complex Characterization of Assembly Intermediates By Sedimentation Velocity Analysis. J Biol Chem. 1994;269(50):31372–7.

289. Karpusas M, Branchaud B, Remington SJ. Proposed mechanism for the condensation reaction of citrate synthase: 1.9-Å structure of the ternary complex with oxaloacetate and carboxymethyl coenzyme A. Biochemistry. 1990;29(9):2213–9.

290. Glusker JP. Mechanism of aconitase action deduced from crystallographic studies of its substrates. J Mol Biol. 1968;38(2):149–62.

291. Guffon N, Lopez-Mediavilla C, Dumoulin R, Mousson B, Godinot C, Carrier H, et al. 2-Ketoglutarate dehydrogenase deficiency, a rare cause of primary hyperlactataemia: Report of a new case. J Inherit Metab Dis. 1993;16(5):821–30.

292. Van Hove JLK, Saenz MS, Thomas JA, Gallagher RC, Lovell MA, Fenton LZ, et al. Succinyl-CoA ligase deficiency: a mitochondrial hepatoencephalomyopathy. Pediatr Res. 2010;68(2):159–64.

293. Mescam M, Vinnakota KC, Beard DA. Identification of the catalytic mechanism and estimation of kinetic parameters for fumarase. J Biol Chem. 2011;286(24):21100–9.

294. Dasika SK, Vinnakota KC, Beard DA. Determination of the catalytic mechanism for mitochondrial malate dehydrogenase. Biophys J. 2015;108(2):408–19.

295. Deniaud a, Sharaf el dein O, Maillier E, Poncet D, Kroemer G, Lemaire C, et al. Endoplasmic reticulum stress induces calcium-dependent permeability transition, mitochondrial outer membrane permeabilization and apoptosis. Oncogene. 2008;27(3):285–99.

296. Baumgartner HK, Gerasimenko J V., Thorne C, Ferdek P, Pozzan T, Tepikin A V., et al. Calcium elevation in mitochondria is the main Ca2+ requirement for mitochondrial permeability transition pore (mPTP) opening. J Biol Chem. 2009;284(31):20796–803.

297. Colombini M. A candidate for the permeability pathway of the outer mitochondrial membrane. Nature. 1979;279(5714):643–5.

298. Leung AWC, Varanyuwatana P, Halestrap AP. The mitochondrial phosphate carrier interacts with cyclophilin D and may play a key role in the permeability transition. J Biol Chem. 2008;283(39):26312–23.

299. Mallilankaraman K, Doonan P, Cárdenas C, Chandramoorthy HC, Müller M, Miller R, et al. MICU1 is an essential gatekeeper for mcu-mediated mitochondrial Ca 2+ uptake that regulates cell survival. Cell. 2012;151(3):630–44.

300. Pavlov E, Grigoriev SM, Dejean LM, Zweihorn CL, Mannella CA, Kinnally KW. The mitochondrial channel VDAC has a cation-selective open state. Biochim Biophys Acta - Bioenerg. 2005;1710(2–3):96–102.

301. Tan W, Colombini M. VDAC closure increases calcium ion flux. Biochim Biophys Acta - Biomembr. 2007;1768(10):2510–5.

302. Rostovtseva TK, Bezrukov SM. ATP transport through a single mitochondrial channel, VDAC, studied by current fluctuation analysis. Biophys J. 1998;74(5):2365–73.

303. Vergun O, Reynolds IJ. Distinct characteristics of Ca2+-induced depolarization of isolated brain and liver mitochondria. Biochim Biophys Acta - Bioenerg. 2005;1709(2):127–37.

304. Samanta K, Douglas S, Parekh AB. Mitochondrial calcium uniporter MCU supports cytoplasmic Ca2+ oscillations, store-operated Ca2+ entry and Ca2+-dependent gene expression in response to receptor stimulation. PLoS One. 2014;9(7):e101188.

305. Wan B, LaNoue KF, Cheung JY, Scaduto RC. Regulation of citric acid cycle by calcium. J Biol Chem. 1989;264(23):13430–9.

306. McCormack JG. Characterization of the effects of Ca2+ on the intramitochondrial Ca2+-sensitive enzymes from rat liver and within intact rat liver mitochondria. Biochem J. 1985;231(3):581–95.

307. Denton RM, Randle PJ, Martin BR. Stimulation by Calcium Ions of Pyruvate Dehydrogenase Phosphate Phosphatase. J Exp Biol. 1972;128:161–3.

308. Denton RM, Richards DA, Chin JG. Calcium ions and the regulation of NAD+-linked isocitrate dehydrogenase from the mitochondria of rat heart and other tissues. Biochem J. 1978;176(3):899–906.

309. Egnatchik RA, Leamy AK, Jacobson DA, Shiota M, Young JD. ER calcium release promotes mitochondrial dysfunction and hepatic cell lipotoxicity in response to palmitate overload. Mol Metab. 2014;3(5):544–53.

310. Görlach A, Bertram K, Hudecova S, Krizanova O. Calcium and ROS: A mutual interplay. Redox Biol. 2015;6:260–71.

311. Brault C, Lévy PL, Bartosch B. Hepatitis C virus-induced mitochondrial dysfunctions. Viruses. 2013;5(3):954–80.

312. Ivanov A V., Smirnova OA, Petrushanko IY, Ivanova ON, Karpenko IL, Alekseeva E, et al. HCV core protein uses multiple mechanisms to induce oxidative stress in human hepatoma huh7 cells. Viruses. 2015;7(6):2745–70.

313. Kong L, Li S, Huang M, Xiong Y, Zhang Q, Ye L, et al. The roles of endoplasmic reticulum overload response induced by HCV and NS4B protein in human hepatocyte viability and virus replication. PLoS One. 2015;10(4):1–15.

314. Nomura-Takigawa Y, Nagano-Fujii M, Deng L, Kitazawa S, Ishido S, Sada K, et al. Non-structural protein 4A of Hepatitis C virus accumulates on mitochondria and renders the cells prone to undergoing mitochondria-mediated apoptosis. J Gen Virol. 2006;87(7):1935–45.

315. Mbaya E, Oulès B, Caspersen C, Tacine R, Massinet H, Pennuto M, et al. Calcium signalling-dependent mitochondrial dysfunction and bioenergetics regulation in respiratory chain Complex II deficiency. Cell Death Differ. 2010;17(12):1855–66.

316. Satapati S, Kucejova B, Duarte JAG, Fletcher JA, Reynolds L, Sunny NE, et al. Mitochondrial metabolism mediates oxidative stress and inflammation in fatty liver. J Clin Invest. 2015;125(9):1–16.

317. Tapiero H, Mathé G, Couvreur P, Tew KD. II. Glutamine and glutamate. Biomed Pharmacother. 2002;56(9):446–57.

318. Watson JA, Lowenstein JM. Citrate and the Conversion of Carbohydrate into Fat. J Biol Chem. 1970;245:5993–6002.

319. Wang Q, Li S, Jiang L, Zhou Y, Li Z, Shao M, et al. Deficiency in hepatic ATP-citrate lyase affects VLDL-triglyceride mobilization and liver fatty acid composition in mice. J Lipid Res. 2010;51(9):2516–26.

320. Alberti KGMM, Zimmet P, Shaw J. The metabolic syndrome - A new worldwide definition. Lancet. 2005;366(9491):1059–62.

321. Aziz H, Gill U, Raza A, Gill ML. Metabolic syndrome is associated with poor treatment response to antiviral therapy in chronic hepatitis C genotype 3 patients. Eur J Gastroenterol Hepatol. 2014;26(5):538–43.

322. Eglit T, Rajasalu T, Lember M. Metabolic syndrome in Estonia: Prevalence and associations with insulin resistance. Int J Endocrinol. 2012;2012.

323. Chen T, Jia H, Li J, Chen X, Zhou H, Tian H. New onset diabetes mellitus after liver transplantation and hepatitis C virus infection: meta-analysis of clinical studies. Transpl Int. 2009;22(4):408–15.

324. Arase Y, Suzuki F, Suzuki Y, Akuta N, Kobayashi M, Kawamura Y, et al. Sustained virological response reduces incidence of onset of type 2 diabetes in chronic hepatitis C. Hepatology. 2009;49(3):739–44.

325. Vanni E, Abate ML, Gentilcore E, Hickman I, Gambino R, Cassader M, et al. Sites and mechanisms of insulin resistance in nonobese, nondiabetic patients with chronic hepatitis C. Hepatology. 2009;50(3):697–706.

326. Bose SK, Ray R. Hepatitis C virus infection and insulin resistance. World J Diabetes. 2014;5(1):52–8.

327. Aytug S, Reich D, Sapiro LE, Bernstein D, Begum N. Impaired IRS-1/PI3-Kinase Signaling in Patients with HCV: A Mechanism for Increased Prevalence of Type 2 Diabetes. Hepatology. 2003;38(6):1384–92.

328. Banerjee S, Saito K, Ait-Goughoulte M, Meyer K, Ray RB, Ray R. Hepatitis C virus core protein upregulates serine phosphorylation of insulin receptor substrate-1 and impairs the downstream akt/protein kinase B signaling pathway for insulin resistance. J Virol. 2008;82(6):2606–12.

329. Lowell B, Shulman G. Mitochondrial dysfunction and type 2 diabetes. Science. 2005;307(5708):384–7.

330. Zhang J, Gao Z, Yin J, Quon MJ, Ye J. S6K directly phosphorylates IRS-1 on Ser-270 to promote insulin resistance in response to TNF-α signaling through IKK2. J Biol Chem. 2008;283(51):35375–82.

331. Galic S, Hauser C, Kahn BB, Fawaz G, Neel BG, Tonks NK, et al. Coordinated Regulation of Insulin Signaling by the Protein Tyrosine Phosphatases PTP1B and TCPTP. Mol Cell Biol. 2005;25(2):819–29.

332. Galic S, Klingler-Hoffmann M, Fodero-Tavoletti MT, Puryer MA, Meng T-C, Tonks NK, et al. Regulation of insulin receptor signaling by the protein tyrosine phosphatase TCPTP. Mol Cell Biol. 2003;23(6):2096–108.

333. Vinciguerra M, Foti M. PTEN and SHIP2 phosphoinositide phosphatases as negative regulators of insulin signalling. Arch Physiol Biochem. 2006;112(2):89–104.

334. Bernsmeier C, Calabrese D, Heim MH, Duong HTF. Hepatitis C virus dysregulates glucose homeostasis by a dual mechanism involving induction of PGC1α and dephosphorylation of FoxO1. J Viral Hepat. 2014;21(1):9–18.

335. Rui L, Yuan M, Frantz D, Shoelson S, White MF. SOCS-1 and SOCS-3 block insulin signaling by ubiquitin-mediated degradation of IRS1 and IRS2. J Biol Chem. 2002;277(44):42394–8.

336. Kawaguchi T, Yoshida T, Harada M, Hisamoto T, Nagao Y, Ide T, et al. Hepatitis C virus down-regulates insulin receptor substrates 1 and 2 through up-regulation of suppressor of cytokine signaling 3. Am J Pathol. 2004;165(5):1499–508.

337. Korenaga M, Wang T, Li Y, Showalter LA, Chan T, Sun J, et al. Hepatitis C virus core protein inhibits mitochondrial electron transport and increases reactive oxygen species (ROS) production. J Biol Chem. 2005;280(45):37481–8.

338. Lenaz G, Fato R, Genova ML, Bergamini C, Bianchi C, Biondi A. Mitochondrial Complex I: Structural and functional aspects. Biochim Biophys Acta - Bioenerg. 2006;1757(9–10):1406–20.

339. Trounce I, Neill S, Wallace DC, Acad PN. Oxidative phosphorylation at the fin de siècle. Science. 1999;283(March):1488–94.

340. Miyamoto H, Moriishi K, Moriya K, Murata S, Tanaka K, Suzuki T, et al. Involvement of the PA28gamma-dependent pathway in insulin resistance induced by hepatitis C virus core protein. J Virol. 2007;81(4):1727–35.

341. Moriishi K, Shoji I, Mori Y, Suzuki R, Suzuki T, Kataoka C, et al. Involvement of PA28γ in the propagation of hepatitis C virus. Hepatology. 2010;52(2):411–20.

342. Negro F, Alaei M. Hepatitis C virus and type 2 diabetes. World J Gastroenterol. 2009;15(13):1537–47.

343. Shintani Y, Fujie H, Miyoshi H, Tsutsumi T, Tsukamoto K, Kimura S, et al. Hepatitis C Virus Infection and Diabetes: Direct Involvement of the Virus in the Development of Insulin Resistance. Gastroenterology. 2004;126(3):840–8.

344. Pazienza V, Vinciguerra M, Andriulli A, Mangia A. Hepatitis C virus core protein genotype 3a increases SOCS-7 expression through PPAR-γ in Huh-7 cells. J Gen Virol. 2010;91(7):1678–86.

345. Bose SK, Shrivastava S, Meyer K, Ray RB, Ray R. Hepatitis C virus activates the mTOR/S6K1 signaling pathway in inhibiting IRS-1 function for insulin resistance. J Virol. 2012;86(11):6315–22.

346. Hwang SJ, Luo JC, Chu CW, Lai CR, Lu CL, Tsay SH, et al. Hepatic steatosis in chronic hepatitis C virus infection: prevalence and clinical correlation. J Gastroenterol Hepatol. 2001;16(2):190–5.

347. Modaresi Esfeh J, Ansari-Gilani K. Steatosis and hepatitis C. Gastroenterol Rep. 2016;4(1):24–9.

348. Rubbia-Brandt L, Quadri R, Abid K, Giostra E, Malé PJ, Mentha G, et al. Hepatocyte steatosis is a cytopathic effect of hepatitis C virus genotype 3. J Hepatol. 2000;33(1):106–15.

349. Kumar D, Farrell GC, Fung C, George J. Hepatitis C virus genotype 3 is cytopathic to hepatocytes: Reversal of hepatic steatosis after sustained therapeutic response. Hepatology. 2002;36(5 II):1266–72.

350. Abid K, Pazienza V, De Gottardi A, Rubbia-Brandt L, Conne B, Pugnale P, et al. An in vitro model of hepatitis C virus genotype 3a-associated triglycerides accumulation. J Hepatol. 2005;42(5):744–51.

351. Domitrovich AM, Felmlee DJ, Siddiqui A. Hepatitis C virus nonstructural proteins inhibit apolipoprotein B100 secretion. J Biol Chem. 2005;280(48):39802–8.

352. Kliewer SA, Umesono K, Noonan DJ, Heyman RA, Evans RM. Convergence of 9-cis retinoic acid and peroxisome proliferator signalling pathways through heterodimer formation of their receptors. Nature. 1992;358(6389):771–4.

353. Heyman R a, Mangelsdorf DJ, Dyck J a, Stein RB, Eichele G, Evans RM, et al. 9-cis retinoic acid is a high affinity ligand for the retinoid X receptor. Cell. 1992;68(2):397–406.

354. Hashimoto T, Fujita T, Usuda N, Cook W, Qi C, Peters JM, et al. Peroxisomal and Mitochondrial Fatty Acid beta-Oxidation in Mice Nullizygous for Both Peroxisome Proliferator-activated Receptor alpha and Peroxisomal Fatty Acyl-CoA Oxidase. J Biol Chem. 1999;274(27):19228–36.

355. Cheng Y, Dharancy S, Malapel M, Desreumaux P. Hepatitis C virus infection down-regulates the expression of peroxisome proliferator-activated receptor alpha and carnitine palmitoyl acyl-CoA transferase 1A. World J Gastroenterol. 2005;11(48):7591–6.

356. Feld JJ, Hoofnagle JH. Mechanism of action of interferon and ribavirin in treatment of hepatitis C. Nature. 2005;436(7053):967–72.

357. Feld JJ, Nanda S, Huang Y, Chen W, Cam M, Pusek SN, et al. Hepatic gene expression during treatment with peginterferon and ribavirin: Identifying molecular pathways for treatment response. Hepatology. 2007;46(5):1548–63.

358. Leyssen P, Balzarini J, De Clercq E, Neyts J. The predominant mechanism by which ribavirin exerts its antiviral activity in vitro against flaviviruses and paramyxoviruses is mediated by inhibition of IMP dehydrogenase. J Virol. 2005;79(3):1943–7.

359. Maag D, Castro C, Hong Z, Cameron CE. Hepatitis C Virus RNA-dependent RNA Polymerase (NS5B) as a Mediator of the Antiviral Activity of Ribavirin. J Biol Chem. 2001;276(49):46094–8.

360. Haller O, Kochs G, Weber F. The interferon response circuit: Induction and suppression by pathogenic viruses. Virology. 2006;344(1):119–30.

361. Platanias LC. Mechanisms of type-I- and type-II-interferon-mediated signalling. Nat Rev Immunol. 2005;5(5):375–86.

362. Bender S, Reuter A, Eberle F, Einhorn E, Binder M, Bartenschlager R. Activation of Type I and III Interferon Response by Mitochondrial and Peroxisomal MAVS and Inhibition by Hepatitis C Virus. PLoS Pathog. 2015;11(11):1–30.

363. Guo J-T, Sohn J a, Zhu Q, Seeger C. Mechanism of the interferon alpha response against hepatitis C virus replicons. Virology. 2004;325(1):71–81.

364. Han J-Q, Barton DJ. Activation and evasion of the antiviral 2'-5' oligoadenylate synthetase/ribonuclease L pathway by hepatitis C virus mRNA. RNA. 2002;8(4):512–25.

365. Lurie Y, Rouzier-Panis R, Webster GJM, Dusheiko GM, Laughlin M, Jackson ML, et al. Optimal dosing frequency of pegylated interferon alfa-2b monotherapy for chronic hepatitis C virus infection. Clin Gastroenterol Hepatol. 2005;3(6):610–5.

366. Podobnik B, Helk B, Smilović V, Škrajnar, Fidler K, Jevševar S, et al. Conjugation of PolyPEG to Interferon Alpha Extends Serum Half-Life while Maintaining Low Viscosity of the Conjugate. Bioconjug Chem. 2015;26(3):452–9.

367. Manns MP, McHutchison JG, Gordon SC, Rustgi VK, Shiffman M, Reindollar R, et al. Peginterferon alfa-2b plus ribavirin compared with interferon alfa-2b plus ribavirin for initial treatment of chronic hepatitis C: a randomised trial. Lancet. 2001;358(9286):958–65.

368. Lusida MI, Nagano-Fujii M, Nidom CM, Soetjipto, Handajani R, Fujita T, et al. Correlation between mutations in the interferon sensitivity-determining region of NS5A protein and viral load of hepatitis C virus subtypes 1b, 1c, and 2a. J Clin Microbiol. 2001;39(11):3858–64.

369. Doyle SE, Schreckhise H, Khuu-Duong K, Henderson K, Rosler R, Storey H, et al. Interleukin-29 uses a type 1 interferon-like program to promote antiviral responses in human hepatocytes. Hepatology. 2006;44(4):896–906.

370. Dickensheets H, Sheikh F, Park O, Gao B, Donnelly RP. Interferon-lambda (IFN-λ) induces signal transduction and gene expression in human hepatocytes, but not in lymphocytes or monocytes. J Leukoc Biol. 2013;93(3):377–85.

371. Friborg J, Levine S, Chen C, Sheaffer AK, Chaniewski S, Voss S, et al. Combinations of lambda interferon with direct-acting antiviral agents are highly efficient in suppressing hepatitis c virus replication. Antimicrob Agents Chemother. 2013;57(3):1312–22.

372. Malcolm BA, Liu R, Lahser F, Agrawal S, Belanger B, Butkiewicz N, et al. SCH 503034, a mechanism-based inhibitor of hepatitis C virus NS3 protease, suppresses polyprotein maturation and enhances the antiviral activity of alpha interferon in replicon cells. Antimicrob Agents Chemother. 2006;50(3):1013–20.

373. Lin C, Kwong AD, Perni RB. Discovery and Development of VX-950, a Novel, Covalent, and Reversible Inhibitor of Hepatitis C Virus NS3.4A Serine Protease. Infect Disord -Drug Targets. 2006;6(April 2006):3–16.

374. Welsch C, Shimakami T, Hartmann C, Yang Y, Domingues FS, Lengauer T, et al. Peptidomimetic escape mechanisms arise via genetic diversity in the ligand-binding site of the hepatitis C Virus NS3/4A serine protease. Gastroenterology. 2012;142(3):654–63.

375. Lin TI, Lenz O, Fanning G, Verbinnen T, Delouvroy F, Scholliers A, et al. In vitro activity and preclinical profile of TMC435350, a potent hepatitis C virus protease inhibitory. Antimicrob Agents Chemother. 2009;53(4):1377–85.

376. Rosenquist Å, Samuelsson B, Johansson PO, Cummings MD, Lenz O, Raboisson P, et al. Discovery and development of simeprevir (TMC435), a HCV NS3/4A protease inhibitor. J Med Chem. 2014;57(5):1673–93.

377. Taieb V, Pacou M, Ho S, Pettré S, Van Sanden S, Pisini M, et al. A network meta-analysis to compare simeprevir with boceprevir and telaprevir in combination with peginterferon-α and ribavirin in patients infected with genotype 1 Hepatitis C virus. J Med Econ. 2015;18(10):787–96.

378. Ogawa E, Furusyo N, Dohmen K, Kajiwara E, Kawano A, Nomura H, et al. Effectiveness of triple therapy with simeprevir for chronic hepatitis C genotype 1b patients with prior telaprevir failure. J Viral Hepat. 2015;22(12):992–1001.

379. Gao M, Nettles RE, Belema M, Snyder LB, Nguyen VN, Fridell RA, et al. Chemical genetics strategy identifies an HCV NS5A inhibitor with a potent clinical effect. Nature. 2010;465(7294):96–100.

380. Zanaga LP, Miotto N, Mendes LC, Stucchi RSB, Vigani AG. Treatment of hepatitis C virus genotype 3 infection with direct-acting antiviral agents. Brazilian J Med Biol Res. 2016 Oct 24;49(11):e5504.

381. Nettles JH, Stanton RA, Broyde J, Amblard F, Zhang H, Zhou L, et al. Asymmetric binding to NS5A by daclatasvir (BMS-790052) and analogs suggests two novel modes of HCV inhibition. J Med Chem. 2014;57(23):10031–43.

382. Targett-Adams P, Graham EJS, Middleton J, Palmer A, Shaw SM, Lavender H, et al. Small molecules targeting hepatitis C virus-encoded NS5A cause subcellular redistribution of their target: insights into compound modes of action. J Virol. 2011;85(13):6353–68.

383. Qi H, Olson CA, Wu NC, Ke R, Loverdo C, Chu V, et al. A Quantitative High-Resolution Genetic Profile Rapidly Identifies Sequence Determinants of Hepatitis C Viral Fitness and Drug Sensitivity. PLoS Pathog. 2014;10(4).

384. Nitta S, Asahina Y, Matsuda M, Yamada N, Sugiyama R, Masaki T, et al. Effects of Resistance-Associated NS5A Mutations in Hepatitis C Virus on Viral Production and Susceptibility to Antiviral Reagents. Sci Rep. 2016;6:34652.

385. Murakami E, Tolstykh T, Bao H, Niu C, Micolochick Steuer HM, Bao D, et al. Mechanism of activation of PSI-7851 and its diastereoisomer PSI-7977. J Biol Chem. 2010;285(45):34337–47.

386. Sofia MJ, Bao D, Chang W, Du J, Nagarathnam D, Rachakonda S, et al. Discovery of a luoro-2′-β- C -methyluridine Nucleotide Prodrug (PSI-7977) for the treatment of hepatitis C virus. J Med Chem. 2010;53(19):7202–18.

387. Lawitz EJ, Dvory-Sobol H, Doehle BP, Worth AS, McNally J, Brainard DM, et al. Clinical resistance to velpatasvir (GS-5816), a novel pan-genotypic inhibitor of the hepatitis C virus NS5A protein. Antimicrob Agents Chemother. 2016;60(9):5368–78.

388. Feld JJ, Jacobson IM, Asselah T, Ruane PJ, Gruener N, Abergel A, et al. Sofosbuvir and Velpatasvir for HCV Genotype 1, 2, 4, 5, and 6 Infection. N Engl J Med. 2015;373(27):2599–607.

389. Zeuzem S, Dusheiko GM, Salupere R, Mangia A, Flisiak R, Hyland RH, et al. Sofosbuvir and Ribavirin in HCV Genotypes 2 and 3. N Engl J Med. 2014;370:1993-2001.

390. Mangia A, Piazzolla V. Overall efficacy and safety results of sofosbuvir-based therapies in Phase II and III studies. Dig Liver Dis. 2014;46(S5):S179–85.

391. Costantino A, Spada E, Equestre M, Bruni R, Tritarelli E, Coppola N, et al. Naturally occurring mutations associated with resistance to HCV NS5B polymerase and NS3 protease inhibitors in treatment-naïve patients with chronic hepatitis C. Virol J. 2015;12:186.

392. Camilloni C, Sahakyan AB, Holliday MJ, Isern NG, Zhang F, Eisenmesser EZ, et al. Cyclophilin A catalyzes proline isomerization by an electrostatic handle mechanism. Proc Natl Acad Sci U S A. 2014;111(28):10203–8.

393. Chatterji U, Bobardt M, Selvarajah S, Yang F, Tang H, Sakamoto N, et al. The isomerase active site of cyclophilin A is critical for hepatitis C virus replication. J Biol Chem. 2009;284(25):16998–7005.

394. Smith T, Ferreira L, Hebert C, Norris K, Sauk J. Hsp47 and Cyclophilin B Traverse the Endoplasmic Reticulum with Procollagen into Pre-Golgi Intermediate Vesicles: A Role For Hsp47 And Cyclophilin B in The Export of Procollagen From The Endoplasmic Reticulum. J Biol Chem. 1995;270(4):18323–8.

395. Laker RC, Taddeo EP, Akhtar YN, Zhang M, Hoehn KL, Yan Z. The Mitochondrial Permeability Transition Pore Regulator Cyclophilin D Exhibits Tissue-Specific Control of Metabolic Homeostasis. PLoS One. 2016;11(12):e0167910.

396. Nguyen TT, Stevens M V., Kohr M, Steenbergen C, Sack MN, Murphy E. Cysteine 203 of Cyclophilin D Is Critical for Cyclophilin D Activation of the Mitochondrial Permeability Transition Pore. J Biol Chem. 2011;286(46):40184–92.

397. Colgan J, Asmal M, Yu B, Luban J. Cyclophilin A-deficient mice are resistant to immunosuppression by cyclosporine. J Immunol. 2005;174(10):6030–8.

398. Beals CR, Clipstone N a, Ho SN, Crabtree GR. Nuclear localization of NF-ATc by a intramolecular interaction. Genes Dev. 1997;4:824–34.

399. Sun S, Guo M, Zhang JB, Ha A, Yokoyama KK, Chiu RH. Cyclophilin a (CypA) interacts with NF-κB subunit, p65/RelA, and contributes to NF-κB activation signaling. PLoS One. 2014;9(8):e96211.

400. Nakagawa M, Sakamoto N, Tanabe Y, Koyama T, Itsui Y, Takeda Y, et al. Suppression of hepatitis C virus replication by cyclosporin A is mediated by blockade of cyclophilins. Gastroenterology. 2005;129(3):1031–41.

401. Coelmont L, Hanoulle X, Chatterji U, Berger C, Snoeck J, Bobardt M, et al. DEB025 (Alisporivir) inhibits hepatitis c virus replication by preventing a cyclophilin a induced Cis-trans isomerisation in domain ii of NS5A. PLoS One. 2010;5(10):e13687.

402. Zhong Z, Li X, Yamashina S, von Frankenberg M, Enomoto N, Ikejima K, et al. Cyclosporin A causes a hypermetabolic state and hypoxia in the liver: prevention by dietary glycine. J Pharmacol Exp Ther. 2001;299(3):858–65.

403. Quarato G, D'Aprile A, Gavillet B, Vuagniaux G, Moradpour D, Capitanio N, et al. The cyclophilin inhibitor alisporivir prevents hepatitis C virus-mediated mitochondrial dysfunction. Hepatology. 2012;55(5):1333–43.

404. Flisiak R, Feinman S V., Jablkowski M, Horban A, Kryczka W, Pawlowska M, et al. The cyclophilin inhibitor debio 025 combined with PEG IFNα2a significantly reduces viral load in treatment-naïve hepatitis C patients. Hepatology. 2009;49(5):1460–8.

405. Mullany LE, Herrick JS, Wolff RK, Slattery ML. MicroRNA Seed Region Length Impact on Target Messenger RNA Expression and Survival in Colorectal Cancer. PLoS One. 2016;11(4):e0154177.

406. Lee Y, Kim M, Han J, Yeom K-H, Lee S, Baek SH, et al. MicroRNA genes are transcribed by RNA polymerase II. Embo J. 2004;23(20):4051–60.

407. Yi R, Qin Y, Macara IG, Cullen BR. Exportin-5 mediates the nuclear export of pre-microRNAs and short hairpin RNAs. Genes Dev. 2003;17(24):3011–6.

408. Lee Y, Ahn C, Han J, Choi H, Kim J, Yim J, et al. The nuclear RNase III Drosha initiates microRNA processing. Nature. 2003;425(6956):415–9.

409. Denli AM, Tops BBJ, Plasterk RH a, Ketting RF, Hannon GJ. Processing of primary microRNAs by the Microprocessor complex. Nature. 2004;432(7014):231–5.

410. Han J, Lee Y, Yeom K, Kim Y, Jin H, Kim VN. The Drosha – DGCR8 complex in primary microRNA processing. Genes Dev. 2004;3016–27.

411. Dueck A, Ziegler C, Eichner A, Berezikov E, Meister G. MicroRNAs associated with the different human Argonaute proteins. Nucleic Acids Res. 2012;40(19):9850–62.

412. Janas MM, Wang B, Harris AS, Aguiar M, Shaffer JM, Subrahmanyam Y V, et al. Alternative RISC assembly: binding and repression of microRNA-mRNA duplexes by human Ago proteins. RNA. 2012;18(11):2041–55.

413. Miyoshi K, Okada TN, Siomi H, Siomi MC. Characterization of the miRNA-RISC loading complex and miRNA-RISC formed in the Drosophila miRNA pathway. RNA. 2009;15(7):1282–91.

414. Martin HC, Wani S, Steptoe AL, Krishnan K, Nones K, Nourbakhsh E, et al. Imperfect centered miRNA binding sites are common and can mediate repression of target mRNAs. Genome Biol. 2014;15(3):R51.

415. Humphreys DT, Westman BJ, Martin DIK, Preiss T. MicroRNAs control translation initiation by inhibiting eukaryotic initiation factor 4E/cap and poly(A) tail function. Proc Natl Acad Sci U S A. 2005;102(47):16961–6.

416. Gatfield D, Martelot G Le, Vejnar CE, Gerlach D, Schaad O, Oresic M, et al. Integration of microRNA miR-122 in hepatic circadian gene expression. Genes Dev. 2009;23(11):1313–26.

417. Nakao K, Miyaaki H, Ichikawa T. Antitumor function of microRNA-122 against hepatocellular carcinoma. J Gastroenterol. 2014;49(4):589–93.

418. Abu-Elheiga L, Brinkley WR, Zhong L, Chirala SS, Woldegiorgis G, Wakil SJ. The subcellular localization of acetyl-CoA carboxylase 2. Proc Natl Acad Sci U S A. 2000;97(4):1444–9.

419. Esau C, Davis S, Murray SF, Yu XX, Pandey SK, Pear M, et al. miR-122 regulation of lipid metabolism revealed by in vivo antisense targeting. Cell Metab. 2006;3(2):87–98.

420. Xu H, He JH, Xiao ZD, Zhang QQ, Chen YQ, Zhou H, et al. Liver-enriched transcription factors regulate microRNA-122 that targets CUTL1 during liver development. Hepatology. 2010;52(4):1431–42.

421. Thibault PA, Huys A, Amador-Cañizares Y, Gailius JE, Pinel DE, Wilson JA. Regulation of Hepatitis C Virus Genome Replication by Xrn1 and MicroRNA-122 Binding to Individual Sites in the 5' Untranslated Region. J Virol. 2015;89(12):6294–311.

422. Li Y, Masaki T, Yamane D, McGivern DR, Lemon SM. Competing and noncompeting activities of miR-122 and the 5' exonuclease Xrn1 in regulation of hepatitis C virus replication. Proc Natl Acad Sci U S A. 2013;110(5):1881–6.

423. Ottosen S, Parsley TB, Yang L, Zeh K, Van Doorn LJ, Van Der Veer E, et al. In Vitro antiviral activity and preclinical and clinical resistance profile of miravirsen, a novel anti-hepatitis C virus therapeutic targeting the human factor miR-122. Antimicrob Agents Chemother. 2015;59(1):599–608.

424. Gebert LFR, Rebhan MAE, Crivelli SEM, Denzler R, Stoffel M, Hall J. Miravirsen (SPC3649) can inhibit the biogenesis of miR-122. Nucleic Acids Res. 2014;42(1):609–21.

425. Hoke GD, Draper K, Freier SM, Gonzalez C, Driver VB, Zounes MC, et al. Effects of phosphorothioate capping on antivense oligonucleotide stability, hybridization and antiviral efficacy versus herpes simplex virus infection. Nucleic Acids Res. 1991;19(20):5743–8.

426. Iversen P, Zhu S, Meyer A, Zon G. Cellular Uptake and Subcellular Distribution of Phosphorothioate Oligonucleotides into Cultured Cells. Antisense Res Dev. 1992;2(3):211–22.

427. Kurreck J, Wyszko E, Gillen C, Erdmann V a. Design of antisense oligonucleotides stabilized by locked nucleic acids. Nucleic Acids Res. 2002;30(9):1911–8.

428. Van Der Ree MH, Van Der Meer AJ, De Bruijne J, Maan R, Van Vliet A, Welzel TM, et al. Long-term safety and efficacy of microRNA-targeted therapy in chronic hepatitis C patients. Antiviral Res. 2014;111:53–9.

429. Van Der Ree MH, Van Der Meer AJ, Van Nuenen AC, De Bruijne J, Ottosen S, Janssen HL, et al. Miravirsen dosing in chronic hepatitis C patients results in decreased microRNA-122 levels without affecting other microRNAs in plasma. Aliment Pharmacol Ther. 2016;43(1):102–13.

430. Reesink HW, Janssen HLA, Zeuzem S, Lawitz E, Rodriguez-Torres M, Patel K, et al. 58 Final Results - randomized, double-blind, placebo-controlled safety, anti-viral proof-of-concept study of miravirsen, an oligonucleotide targeting miR-122, in treatment-naive patients with genotype 1 chronic HCV infection. J Hepatol. 2012 Mar 1;56:S26.

431. Zeisel MB, Crouchet E, Baumert TF, Schuster C. Host-targeting agents to prevent and cure hepatitis C virus infection. Viruses. 2015;7(11):5659–85.

432. Gibson G. Microarray analysis: Genome-scale hypothesis scanning. PLoS Biol. 2003;1(1):28–9.

433. Wu JM, Skill NJ, Maluccio MA. Evidence of aberrant lipid metabolism in hepatitis C and hepatocellular carcinoma. HPB. 2010;12(9):625–36.

434. Asayama K, Sandhir R, Sheikh FG, Hayashibe H, Nakane T, Singh I. Increased peroxisomal fatty acid beta-oxidation and enhanced expression of peroxisome proliferator-activated receptor-alpha in diabetic rat liver. Mol Cell Biochem. 1999;194(1–2):227–34.

435. Patwari P, Higgins LJ, Chutkow WA, Yoshioka J, Lee RT. The interaction of thioredoxin with Txnip: Evidence for formation of a mixed disulfide by disulfide exchange. J Biol Chem. 2006;281(31):21884–91.

436. Jung H, Kim MJ, Kim DO, Kim WS, Yoon SJ, Park YJ, et al. TXNIP maintains the hematopoietic cell pool by switching the function of p53 under oxidative stress. Cell Metab. 2013;18(1):75–85.

437. Sans CL, Satterwhite DJ, Stoltzman CA, Breen KT, Ayer DE. MondoA-Mlx heterodimers are candidate sensors of cellular energy status: mitochondrial localization and direct regulation of glycolysis. Mol Cell Biol. 2006;26(13):4863–71.

438. Dentin R, Denechaud PD, Benhamed F, Girard J, Postic C. Hepatic gene regulation by glucose and polyunsaturated fatty acids: a role for ChREBP. J Nutr. 2006;136(5):1145–9.

439. Kim GS, Jung JE, Narasimhan P, Sakata H, Chan PH. Induction of thioredoxin-interacting protein is mediated by oxidative stress, calcium, and glucose after brain injury in mice. Neurobiol Dis. 2012;46(2):440–9.

440. Saxena G, Chen J, Shalev A. Intracellular shuttling and mitochondrial function of thioredoxin-interacting protein. J Biol Chem. 2010;285(6):3997–4005.

441. Chen J, Cha-Molstad H, Szabo A, Shalev A. Diabetes induces and calcium channel blockers prevent cardiac expression of proapoptotic thioredoxin-interacting protein. Am J Physiol Endocrinol Metab. 2009;296(5):E1133-9.

442. Xu G, Chen J, Jing G, Shalev A. Preventing β-cell loss and diabetes with calcium channel blockers. Diabetes. 2012;61(4):848–56.

443. Yu FX, Chai TF, He H, Hagen T, Luo Y. Thioredoxin-interacting protein (Txnip) gene expression: Sensing oxidative phosphorylation status and glycolytic rate. J Biol Chem. 2010;285(33):25822–30.

444. Lerner AG, Upton JP, Praveen PVK, Ghosh R, Nakagawa Y, Igbaria A, et al. IRE1α induces thioredoxin-interacting protein to activate the NLRP3 inflammasome and promote programmed cell death under irremediable ER stress. Cell Metab. 2012;16(2):250–64.

445. Li J, Ni M, Lee B, Barron E, Hinton D, Lee A. The unfolded protein response regulator GRP78/Bip is required for ER integrity and stress-induced autophagy in mammalian cells. Cell Death Differ. 2009;15(9):1460–71.

446. Tong JJ, Liu J, Bertos NR, Yang X-J. Identification of HDAC10, a novel class II human histone deacetylase containing a leucine-rich domain. Nucleic Acids Res. 2002;30(5):1114–23.

447. Lee JH, Jeong EG, Choi MC, Kim SH, Park JH, Song SH, et al. Inhibition of histone deacetylase 10 induces thioredoxin-interacting protein and causes accumulation of reactive oxygen species in SNU-620 human gastric cancer cells. Mol Cells. 2010;30(2):107–12.

448. Cha-Molstad H, Saxena G, Chen J, Shalev A. Glucose-stimulated expression of Txnip is mediated by carbohydrate response element-binding protein, p300, and histone H4 acetylation in pancreatic beta cells. J Biol Chem. 2009;284(25):16898–905.

449. Liu JH, Liu DF, Wang NN, Lin HL, Mei X. Possible role for the thioredoxin system in the protective effects of probucol in the pancreatic islets of diabetic rats. Clin Exp Pharmacol Physiol. 2011;38(8):528–33.

450. Patwari P, Chutkow WA, Cummings K, Verstraeten VLRM, Lammerding J, Schreiter ER, et al. Thioredoxin-independent regulation of metabolism by the α-arrestin proteins. J Biol Chem. 2009;284(37):24996–5003.

451. Chutkow WA, Patwari P, Yoshioka J, Lee RT. Thioredoxin-interacting protein (Txnip) is a critical regulator of hepatic glucose production. J Biol Chem. 2008;283(4):2397–406.

452. Oroz J, Barrera-Vilarmau S, Alfonso C, Rivas G, De Alba E. ASC pyrin domain self-associates and binds NLRP3 protein using equivalent binding interfaces. J Biol Chem. 2016;291(37):19487–501.

453. Zhou R, Tardivel A, Thorens B, Choi I, Tschopp J. Thioredoxin-interacting protein links oxidative stress to inflammasome activation. Nat Immunol. 2010;11(2):136–40.

454. Burdette D, Haskett A, Presser L, McRae S, Iqbal J, Waris G. Hepatitis C virus activates interleukin-1β via caspase-1-inflammasome complex. J Gen Virol. 2012;93(2):235–46.

455. Zhou R, Yazdi A, Menu P, Tschopp J. A role for mitochondria in NLRP3 inflammasome activation. Nature. 2011;469(7329):221–5.

456. Shrivastava S, Mukherjee A, Ray R, Ray RB. Hepatitis C virus induces interleukin-1beta (IL-1beta)/IL-18 in circulatory and resident liver macrophages. J Virol. 2013;87(22):12284–90.

457. McRae S, Iqbal J, Sarkar-Dutta M, Lane S, Nagaraj A, Ali N, et al. The hepatitis C virus-induced NLRP3 inflammasome activates the sterol regulatory element-binding protein (SREBP) and regulates lipid metabolism. J Biol Chem. 2016;291(7):3254–67.

458. Negash AA, Ramos HJ, Crochet N, Lau DTY, Doehle B, Papic N, et al. IL-1β Production through the NLRP3 Inflammasome by Hepatic Macrophages Links Hepatitis C Virus Infection with Liver Inflammation and Disease. PLoS Pathog. 2013;9(4):1–13.

459. Amemiya-Kudo M, Shimano H, Hasty AH, Yahagi N, Yoshikawa T, Matsuzaka T, et al. Transcriptional activities of nuclear SREBP-1a, -1c, and -2 to different target promoters of lipogenic and cholesterogenic genes. J Lipid Res. 2002;43(8):1220–35.

460. Schmittgen TD, Livak KJ. Analyzing real-time PCR data by the comparative CT method. Nat Protoc. 2008;3(6):1101–8.

461. Baillie AJ. Cellular and Viral Determinants for Hepatitis C Virus Replication. Imperial College London; 2010.

462. Yi M. Hepatitis C Virus: Propagation, Quantification, and Storage. Curr Protoc Microbiol. 2010 Nov;Chapter 15:Unit-15D.1.

463. Griffiths EJ, Stern MD, Silverman HS. Measurement of mitochondrial calcium in single living cardiomyocytes by selective removal of cytosolic indo 1. Am J Physiol - Cell Physiol. 1997 Jul 1;273(1):C37 LP-C44.

464. Santos JH, Mandavilli BS, Houten B Van. Measuring Oxidative mtDNA Damage and Repair Using Quantitative PCR. Methods Mol Biol. 2002;197:159–76.

465. Deutsch MJ, Schriever SC, Roscher AA, Ensenauer R. Digital image analysis approach for lipid droplet size quantitation of Oil Red O-stained cultured cells. Anal Biochem. 2014;445(1):87–9.

466. Kumari S, Lecker DN, Khan A. Interaction of iodine species with glycogen at high concentrations of iodine. J Polym Sci Part A Polym Chem. 1997;35(5):927–31.

467. Kapadia SB, Chisari F V. Hepatitis C virus RNA replication is regulated by host geranylgeranylation and fatty acids. Proc Natl Acad Sci U S A. 2005;102(7):2561–6.

468. Tsukahara R, Haniu H, Matsuda Y, Tsukahara T. Heart-type fatty-acid-binding protein (FABP3) is a lysophosphatidic acid-binding protein in human coronary artery endothelial cells. FEBS Open Bio. 2014;4:947–51.

469. Gaits F, Fourcade O, Le Balle F, Gueguen G, Gaigé B, Gassama-Diagne A, et al. Lysophosphatidic acid as a phospholipid mediator: Pathways of synthesis. FEBS Lett. 1997;410(1):54–8.

470. Zhou Y, Abidi P, Kim A, Chen W, Huang TT, Kraemer FB, et al. Transcriptional activation of hepatic ACSL3 and ACSL5 by oncostatin M reduces hypertriglyceridemia through enhanced β-oxidation. Arterioscler Thromb Vasc Biol. 2007;27(10):2198–205.

471. Kassan A, Herms A, Fernández-Vidal A, Bosch M, Schieber NL, Reddy BJN, et al. Acyl-CoA synthetase 3 promotes lipid droplet biogenesis in ER microdomains. J Cell Biol. 2013;203(6):985–1001.

472. De La Cadena SG, Hernández-Fonseca K, Camacho-Arroyo I, Massieu L. Glucose deprivation induces reticulum stress by the PERK pathway and caspase-7- and calpain-mediated caspase-12 activation. Apoptosis. 2014;19(3):414–27.

473. Zeiger W, Ito D, Swetlik C, Oh-Hora M, Villereal ML, Thinakaran G. Stanniocalcin 2 is a negative modulator of store-operated calcium entry. Mol Cell Biol. 2011;31(18):3710–22.

474. Bertolotti A, Zhang Y, Hendershot LM, Harding HP, Ron D. Dynamic interaction of BiP and ER stress transducers in the unfolded-protein response. Nat Cell Biol. 2000;2(6):326–32.

475. Shen J, Chen X, Hendershot L, Prywes R. ER stress regulation of ATF6 localization by dissociation of BiP/GRP78 binding and unmasking of golgi localization signals. Dev Cell. 2002;3(1):99–111.

476. Ouyang YB, Xu LJ, Emery JF, Lee AS, Giffard RG. Overexpressing GRP78 influences Ca2+ handling and function of mitochondria in astrocytes after ischemia-like stress. Mitochondrion. 2011;11(2):279–86.

477. Li H, Zhu X, Fang F, Jiang D, Tang L. Down-regulation of GRP78 enhances apoptosis via CHOP pathway in retinal ischemia-reperfusion injury. Neurosci Lett. 2014;575:68–73.

478. Denton RM, McCormack JG, Edgell NJ. Role of calcium ions in the regulation of intramitochondrial metabolism. Effects of Na+, Mg2+ and ruthenium red on the Ca2+-stimulated oxidation of oxoglutarate and on pyruvate dehydrogenase activity in intact rat heart mitochondria. Biochem J. 1980;190(1):107–17.

479. Huang H-L, Hsing H-W, Lai T-C, Chen Y-W, Lee T-R, Chan H-T, et al. Trypsin-induced proteome alteration during cell subculture in mammalian cells. J Biomed Sci. 2010;17:36.

480. Ainbinder A, Boncompagni S, Protasi F, Dirksen RT. Role of Mitofusin-2 in mitochondrial localization and calcium uptake in skeletal muscle. Cell Calcium. 2015;57(1):14–24.

481. Ott M, Robertson JD, Gogvadze V, Zhivotovsky B, Orrenius S. Cytochrome c release from mitochondria proceeds by a two-step process. Proc Natl Acad Sci U S A. 2002;99(3):1259–63.

482. Peng T-I, Jou M-J. Oxidative stress caused by mitochondrial calcium overload. Ann N Y Acad Sci. 2010;1201:183–8.

483. Shokolenko I, Venediktova N, Bochkareva a, Wilson GL, Alexeyev MF. Oxidative stress induces degradation of mitochondrial DNA. Nucleic Acids Res. 2009;37(8):2539–48.

484. Bäuerle J, Laguno M, Mauss S, Mallolas J, Murillas J, Miquel R, et al. Mitochondrial DNA depletion in liver tissue of patients infected with hepatitis C virus: Contributing effect of HIV infection? HIV Med. 2005;6(2):135–9.

485. Hansen AB, Griner NB, Anderson JP, Kujoth GC, Prolla TA, Loeb LA, et al. Mitochondrial DNA integrity is not dependent on DNA polymerase-β activity. DNA Repair (Amst). 2006;5(1):71–9.

486. Gincel D, Shoshan-Barmatz V. Glutamate interacts with VDAC and modulates opening of the mitochondrial permeability transition pore. J Bioenerg Biomembr. 2004;36(2):179–86.

487. Krippeit-Drews P, Düfer M, Drews G. Parallel oscillations of intracellular calcium activity and mitochondrial membrane potential in mouse pancreatic B-cells. Biochem Biophys Res Commun. 2000;267(1):179–83.

488. Kaufman RJ, Malhotra JD. Calcium trafficking integrates endoplasmic reticulum function with mitochondrial bioenergetics. Biochim Biophys Acta - Mol Cell Res. 2014;1843(10):2233–9.

489. Scaduto RC, Grotyohann LW. Measurement of mitochondrial membrane potential using fluorescent rhodamine derivatives. Biophys J. 1999;76:469–77.

490. To MS, Aromataris EC, Castro J, Roberts ML, Barritt GJ, Rychkov GY. Mitochondrial uncoupler FCCP activates proton conductance but does not block store-operated Ca2+ current in liver cells. Arch Biochem Biophys. 2010;495(2):152–8.

491. Chen J, Fontes G, Saxena G, Poitout V, Shalev A. Lack of TXNIP Protects Against Mitochondria-Mediated Apoptosis but Not Against Fatty Acid-Induced ER Stress-Mediated β-Cell Death. Diabetes. 2010;59(February):440–7.

492. Ma L, Tsatsos NG, Towle HC. Direct role of ChREBP·Mlx in regulating hepatic glucose-responsive genes. J Biol Chem. 2005;280(12):12019–27.

493. Chen JLY, Merl D, Peterson CW, Wu J, Liu PY, Yin H, et al. Lactic acidosis triggers starvation response with paradoxical induction of TXNIP through MondoA. PLoS Genet. 2010;6(9).

494. Jonckheere AI, Smeitink JAM, Rodenburg RJT. Mitochondrial ATP synthase: Architecture, function and pathology. J Inherit Metab Dis. 2012;35(2):211–25.

495. Stock D, Leslie AG, Walker JE. Molecular architecture of the rotary motor in ATP synthase. Science. 1999;286(5445):1700–5.

496. Andrews B, Carroll J, Ding S, Fearnley IM, Walker JE. Assembly factors for the membrane arm of human complex I. Proc Natl Acad Sci U S A. 2013;110(47):18934–9.

497. Wei MC, Zong WX, Cheng EH, Lindsten T, Panoutsakopoulou V, Ross AJ, et al. Proapoptotic BAX and BAK: a requisite gateway to mitochondrial dysfunction and death. Science. 2001;292(5517):727–30.

498. Farah BL, Sinha RA, Wu Y, Singh BK, Lim A, Hirayama M, et al. Hepatic mitochondrial dysfunction is a feature of Glycogen Storage Disease Type Ia (GSDIa). Sci Rep. 2017;7:44408.

499. Ozaki Y, Takeda T, Akanishi N, Hakuno F, Toyoshima Y, Takahashi S-I, et al. Insulin injection restored increased insulin receptor substrate (IRS)-2 protein during short-term protein restriction but did not affect reduced insulin-like growth factor (IGF)-I mRNA or increased triglyceride accumulation in the liver of rats. Biosci Biotechnol Biochem. 2014;78(1):130–8.

500. Aharoni-Simon M, Hann-Obercyger M, Pen S, Madar Z, Tirosh O. Fatty liver is associated with impaired activity of PPARγ-coactivator 1α (PGC1α) and mitochondrial biogenesis in mice. Lab Invest. 2011;91(7):1018–28.

501. Rizzatti V, Boschi F, Pedrotti M, Zoico E, Sbarbati A, Zamboni M. Lipid droplets characterization in adipocyte differentiated 3T3-L1 cells: Size and optical density distribution. Eur J Histochem. 2013;57(3):159–62.

502. Boulant S, Douglas MW, Moody L, Budkowska A, Targett-Adams P, McLauchlan J. Hepatitis C virus core protein induces lipid droplet redistribution in a microtubule- and dynein-dependent manner. Traffic. 2008;9(8):1268–82.

503. Han D, Antunes F, Canali R, Rettori D, Cadenas E. Voltage-dependent anion channels control the release of the superoxide anion from mitochondria to cytosol. J Biol Chem. 2003;278(8):5557–63.

504. Okado-Matsumoto A, Fridovich I. Subcellular distribution of superoxide dismutases (SOD) in rat liver. Cu,Zn-SOD in mitochondria. J Biol Chem. 2001;276(42):38388–93.

505. Thai M, Graham NA, Braas D, Nehil M, Komisopoulou E, Kurdistani SK, et al. Adenovirus E4ORF1-induced MYC activation promotes host cell anabolic glucose metabolism and virus replication. Cell Metab. 2014;19(4):694–701.

506. Zhang X, Zhang J-H, Chen X-Y, Hu Q-H, Wang M-X, Jin R, et al. Reactive Oxygen Species-Induced TXNIP Drives Fructose-Mediated Hepatic Inflammation and Lipid Accumulation Through NLRP3 Inflammasome Activation. Antioxid Redox Signal. 2015;22(10):848–70.

507. Ding B, Parmigiani A, Divakaruni AS, Archer K, Murphy AN, Budanov A V. Sestrin2 is induced by glucose starvation via the unfolded protein response and protects cells from non-canonical necroptotic cell death. Sci Rep. 2016;6(22538):1–14.

508. Wang M, Wey S, Zhang Y, Ye R, Lee AS. Role of the unfolded protein response regulator GRP78/BiP in development, cancer, and neurological disorders. Antioxid Redox Signal. 2009;11(9):2307–16.

509. Wang L, Perera BGK, Hari SB, Bhhatarai B, Backes BJ, Seeliger MA, et al. Divergent allosteric control of the IRE1α endoribonuclease using kinase inhibitors. Nat Chem Biol. 2012;8(12):982–9.

510. Uemura A, Oku M, Mori K, Yoshida H. Unconventional splicing of XBP1 mRNA occurs in the cytoplasm during the mammalian unfolded protein response. J Cell Sci. 2009;122(Pt 16):2877–86.

511. Ghosh R, Wang L, Wang ES, Perera BGK, Igbaria A, Morita S, et al. Allosteric inhibition of the IRE1α RNase preserves cell viability and function during endoplasmic reticulum stress. Cell. 2014;158(3):534–48.

512. Kanyada Koysombat. Imperial College. Effect of a Thioredoxin Interacting Protein Regulator on Hepatitis C Virus Replication. 2014.

513. Saxena G, Chen J, Shalev A. Intracellular shuttling and mitochondrial function of thioredoxin-interacting protein. J Biol Chem. 2010;285(6):3997–4005.

514. Cheung EC, Ludwig RL, Vousden KH. Mitochondrial localization of TIGAR under hypoxia stimulates HK2 and lowers ROS and cell death. Proc Natl Acad Sci U S A. 2012;109(50):20491–6.

515. Uzbekov R, Roingeard P. Nuclear lipid droplets identified by electron microscopy of serial sections. BMC Res Notes. 2013;6(1):386.

516. Kaadige MR, Looper RE, Kamalanaadhan S, Ayer DE. Glutamine-dependent anapleurosis dictates glucose uptake and cell growth by regulating MondoA transcriptional activity. Proc Natl Acad Sci. 2009;106(35):14878–83.

517. Brisac C, Téoulé F, Autret A, Pelletier I, Colbère-Garapin F, Brenner C, et al. Calcium flux between the endoplasmic reticulum and mitochondrion contributes to poliovirus-induced apoptosis. J Virol. 2010;84(23):12226–35.

518. Lee SJ, Zhang J, Choi AM, Kim HP. Mitochondrial dysfunction induces formation of lipid droplets as a generalized response to stress. Oxid Med Cell Longev. 2013;2013:327167.

519. Sena L, Chandel N. Physiological roles of mitochondrial reactive oxygen species. Mol Cell. 2012;48(2):158–67.

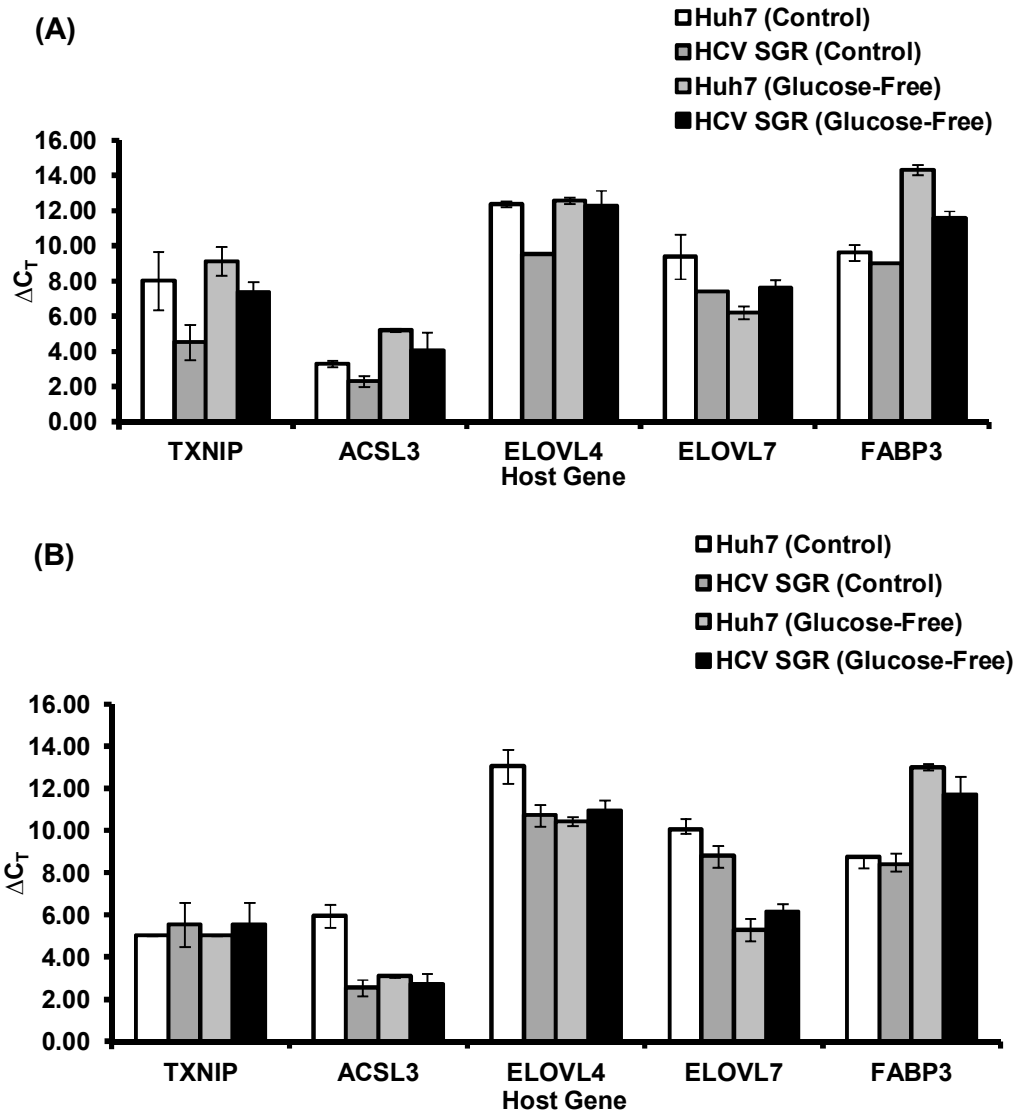
520. Tikunov A, Johnson CB, Pediaditakis P, Markevich N, Jeffrey M, Lemasters JJ, et al. Closure of VDAC Causes Oxidative Stress and Accelerates the Ca2+-induced Mitochondrial Permeability Transition in Rat Liver Mitochondria. Arch Biochem Biophys. 2011;495(2):174–81.

521. Bartlett DW, Davis ME. Insights into the kinetics of siRNA-mediated gene silencing from live-cell and live-animal bioluminescent imaging. Nucleic Acids Res. 2006;34(1):322–33.

Appendix

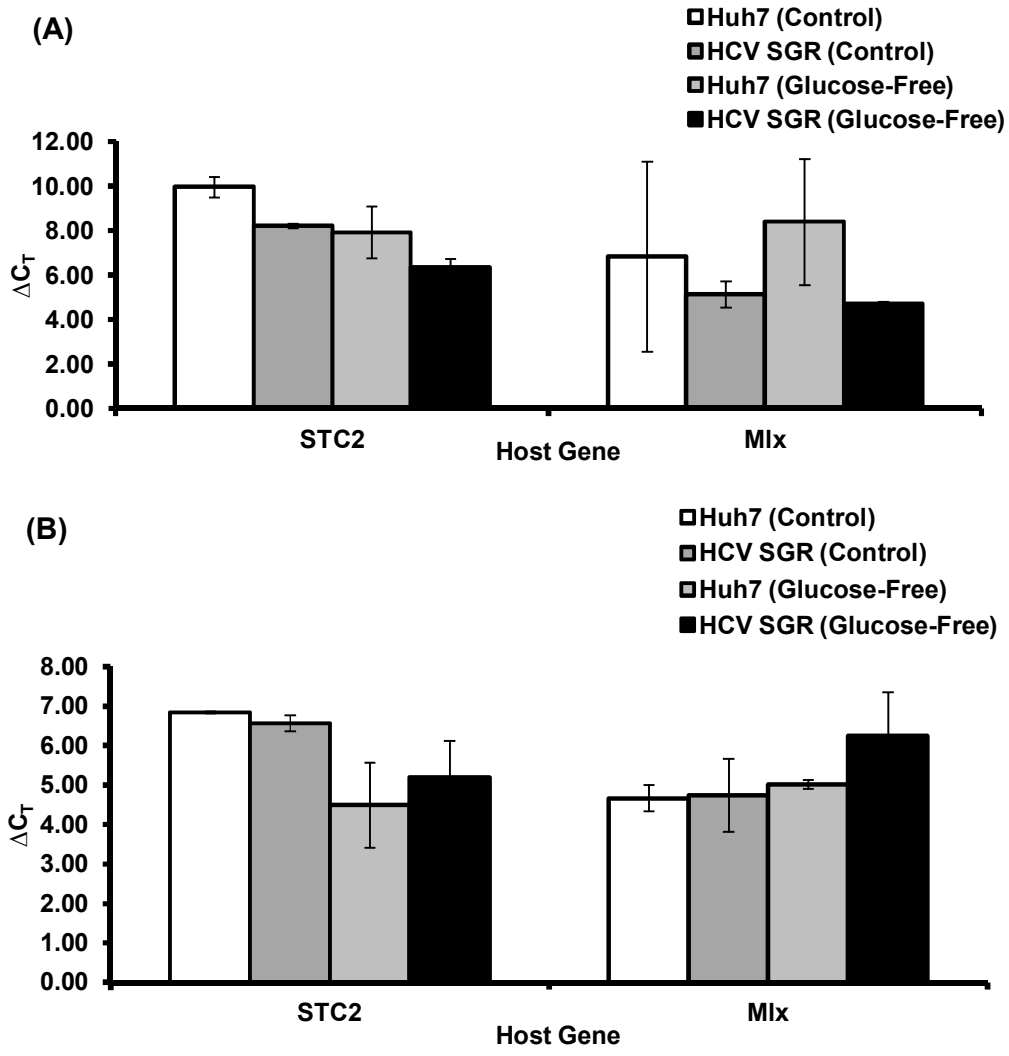
Appendix A1 – ΔC_T Graphs for qRT-PCR Data (Chapter 3)

A1.1. – ΔC_T for Lipogenic gene transcription in HCV SGR cells +/- glucose [25 mM] (24, 48 Hours)



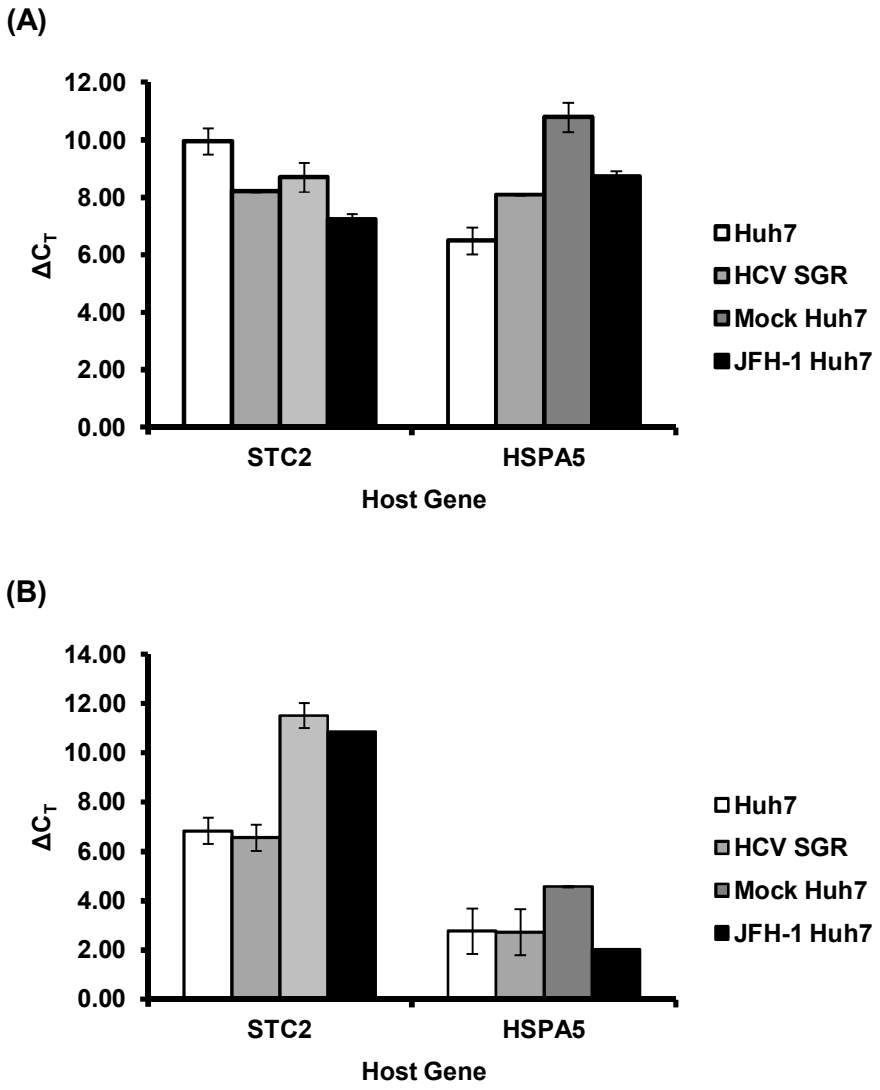
A1.1. represents the difference in raw cycle threshold values (ΔC_T) between genes of interest (GOI) and an internal control (GAPDH) in Huh7 cells compared to HCV SGR cells cultured under both control (glucose-rich) and glucose free conditions. **(A)**: ΔC_T values at 24 hours post-seeding. **(B)**: ΔC_T values at 48 hours post-seeding. Data shown are averages of triplicate measurements from a single experiment with error bars representing standard deviation (SD). Relative fold changes in gene transcription ($\Delta\Delta C_T$) are shown in **Figure 18 (A, B)**.

A1.2. – ΔC_T for STC2 and Mlx transcripton in HCV SGR cells +/- glucose [25 mM] (24, 48 Hours)



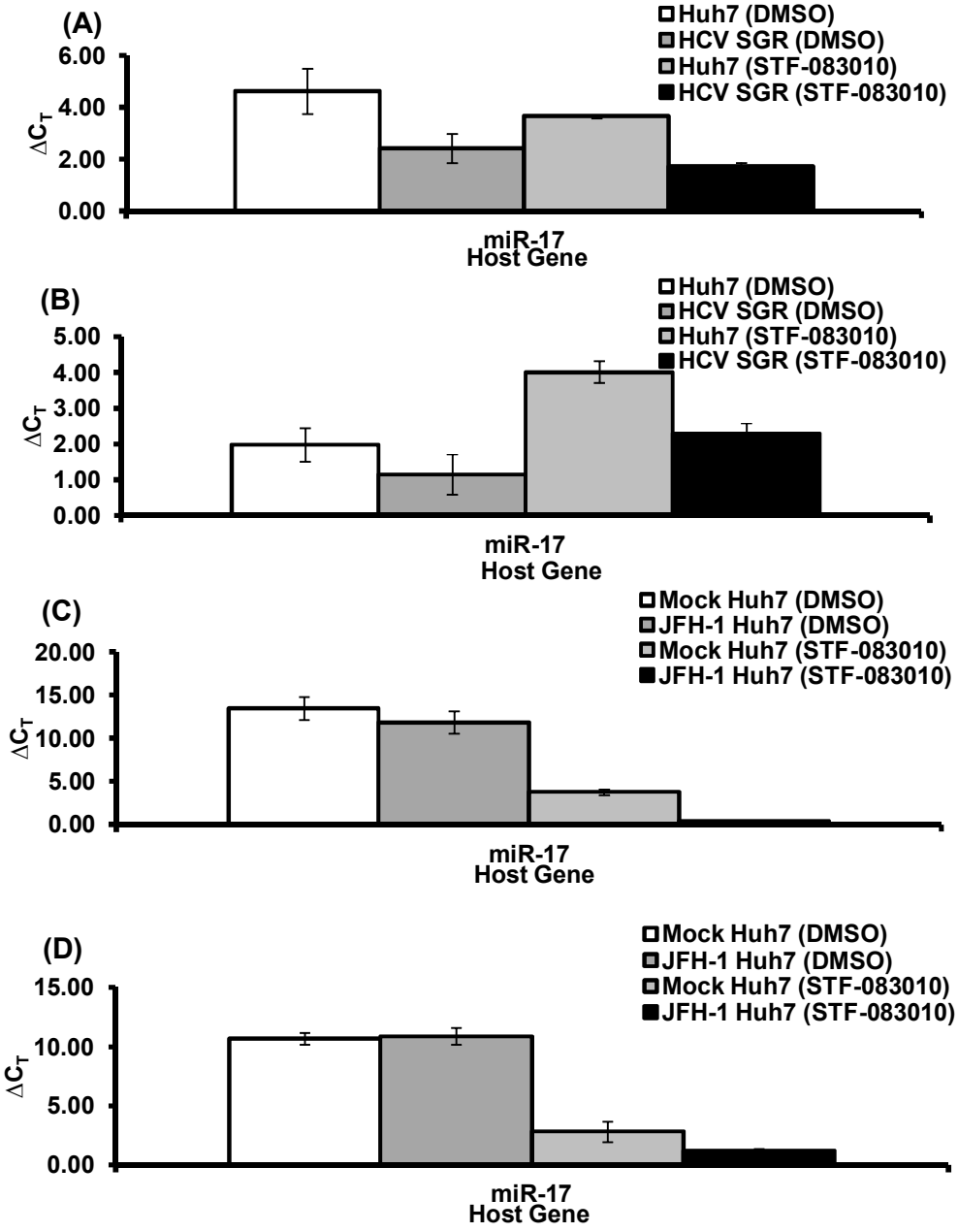
A1.2. represents the difference in raw cycle threshold values (ΔC_T) between genes of interest (GOI) and an internal control (GAPDH) in Huh7 cells compared to HCV SGR cells cultured under both control (glucose-rich) and glucose free conditions. **(A)**: ΔC_T values at 24 hours post-seeding. **(B)**: ΔC_T values at 48 hours post-seeding. Data shown are averages of triplicate measurements from a single experiment with error bars representing standard deviation (SD). Relative fold changes in gene transcription ($\Delta\Delta C_T$) are shown in **Figure 19 (A, B)**.

A1.3. - ΔC_T for STC2 and HSPA5 transcripton in HCV gt2a infection models (24, 48 hours)



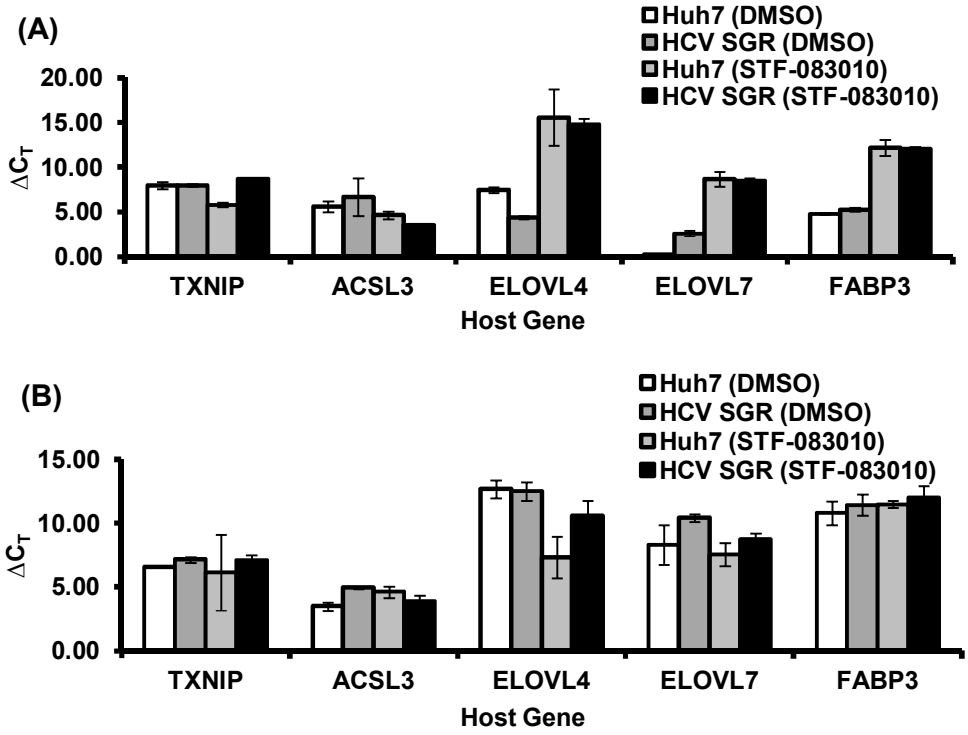
A1.3. represents the difference in raw cycle threshold values (ΔC_T) between genes of interest (GOI) and an internal control (GAPDH) at 24- and 48 hours in Huh7 cells compared to HCV SGR cells (post-seeding), and mock infected controls relative to JFH-1 infected Huh7 cells (post-infection). **(A)**: ΔC_T values at 24 hours post-seeding. **(B)**: ΔC_T values at 48 hours. Data shown are averages of triplicate measurements from a single experiment with error bars representing standard deviation (SD). Relative fold changes in gene transcription ($\Delta\Delta C_T$) are shown in **Figure 23 (A, B)**.

A1.4. - ΔC_T for miR-17 expression levels in HCV gt2a infection models treated with STF-083010 (24, 48 hours)



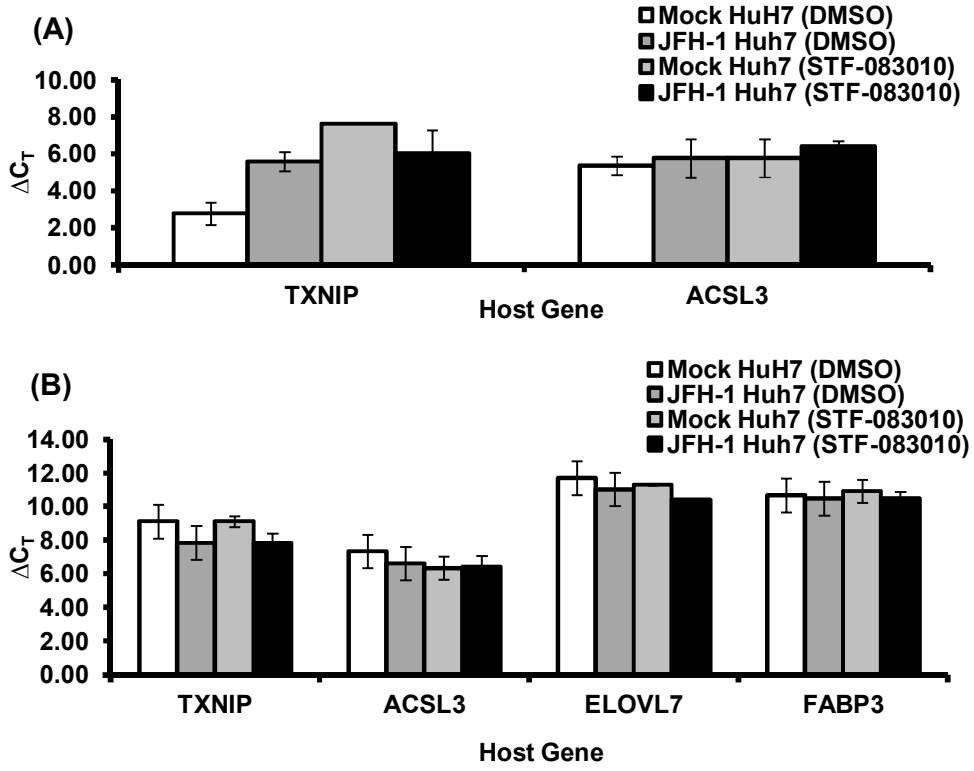
A1.4. represents the difference in raw cycle threshold values (ΔC_T) between miR-17 and an internal control (U6) in Huh7 cells compared to HCV SGR cells, and mock infected controls relative to JFH-1 infected Huh7 cells treated with STF-083010 or DMSO. **(A)**: ΔC_T values at 24 hours post-seeding. **(B)**: ΔC_T values at 48 hours post-seeding. **(C)**: ΔC_T values at 24 hours post-infection. **(D)**: ΔC_T values at 48 hours post-infection. Data shown are averages of triplicate measurements from a single experiment with error bars representing standard deviation (SD). Relative fold changes in gene transcription ($\Delta\Delta C_T$) are shown in **Figure 25 (A, B)**.

A1.5. - ΔC_T for Lipogenic gene transcription in HCV SGR cells treated with STF-083010 (24, 48 Hours)



A1.5. represents the difference in raw cycle threshold values (ΔC_T) between genes of interest (GOI) and an internal control (GAPDH) in Huh7 cells compared to HCV SGR cells treated with STF-083010 or DMSO. **(A)**: ΔC_T values at 24 hours post-seeding. **(B)**: ΔC_T values at 48 hours post-seeding. Data shown are averages of triplicate measurements from a single experiment with error bars representing standard deviation (SD). Relative fold changes in gene transcription ($\Delta\Delta C_T$) are shown in **Figure 26 (A, B)**.

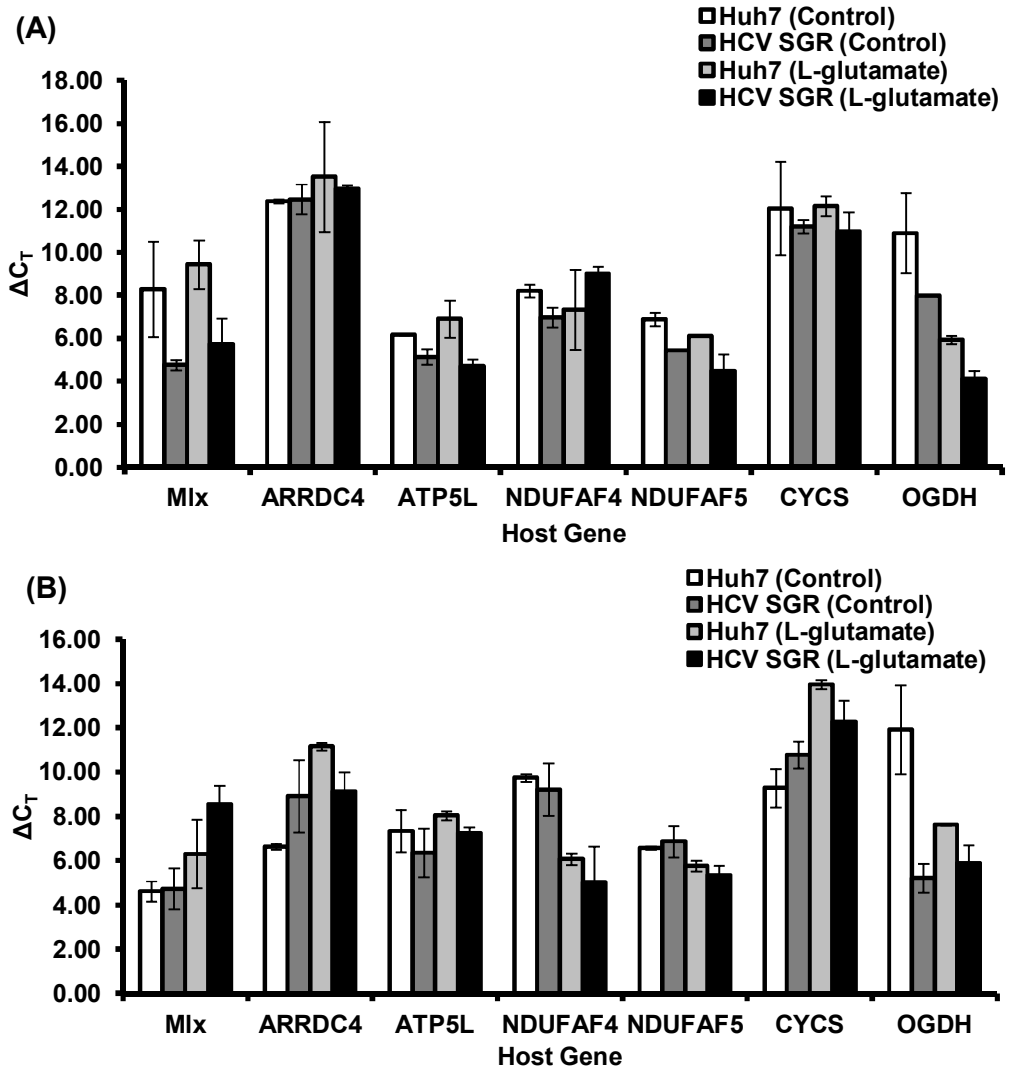
A1.6 - ΔC_T for Lipogenic gene transcription in JFH-1 infected Huh7 cells treated with STF-083010 (24, 48 Hours)



A1.6. represents the difference in raw cycle threshold values (ΔC_T) between genes of interest (GOI) and an internal control (GAPDH) in mock- and JFH-1 infected Huh7 cells treated with STF-083010 or DMSO. **(A)**: ΔC_T values at 24 hours post-infection. **N.B**: ELOVL7 and FABP3 are not transcriptionally induced in either mock- or JFH-1 infected Huh7 cells under both DMSO and STF-083010 treatments at 24 hours post-infection. **(B)**: ΔC_T values at 48 hours post-infection. Data shown are averages of triplicate measurements from a single experiment with error bars representing standard deviation (SD). Relative fold changes in gene transcription ($\Delta\Delta C_T$) are shown in **Figure 27 (A, B)**.

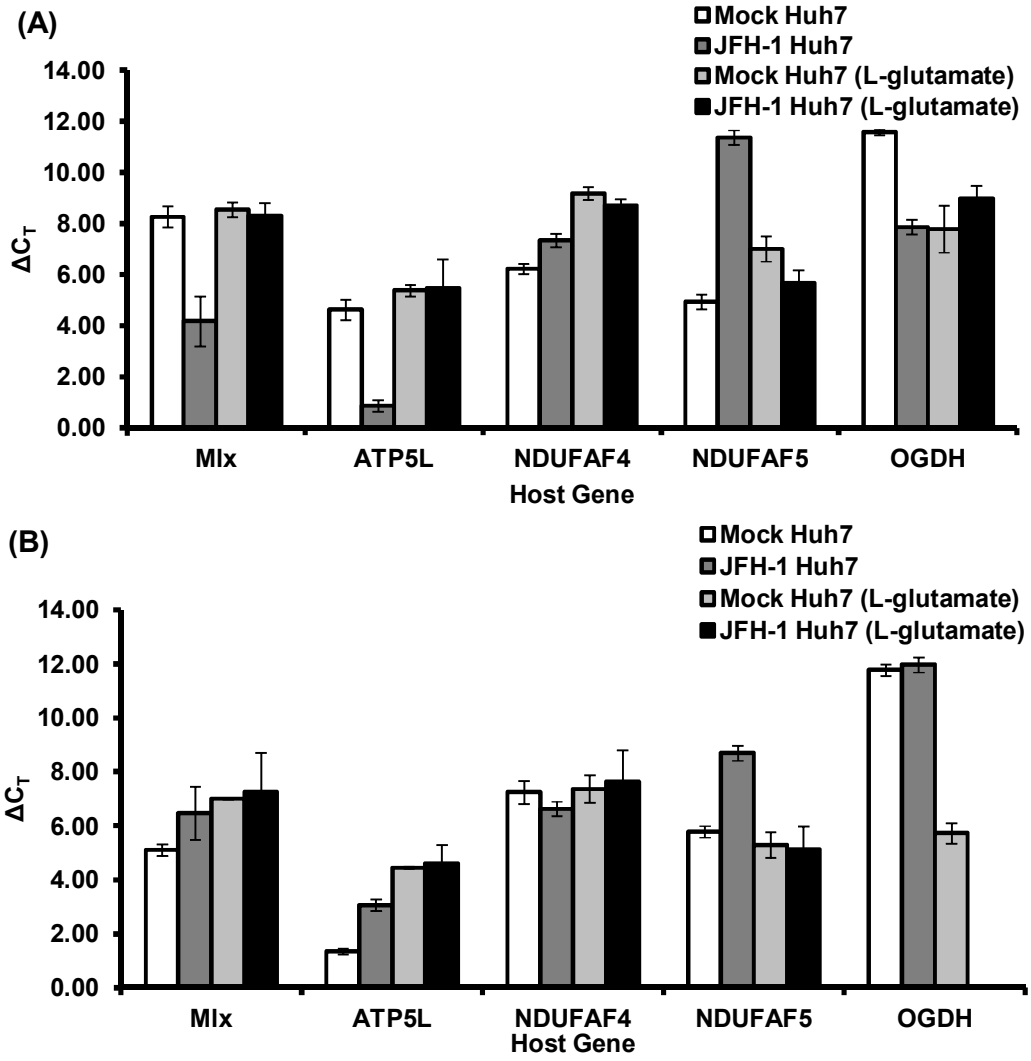
Appendix A2 – ΔC_T Graphs for qRT-PCR Data (Chapter 4)

A2.1. – ΔC_T for Oxidative Phosphorylation gene transcription in Huh7 and HCV SGR cells +/- L-glutamate (24, 48 hours)



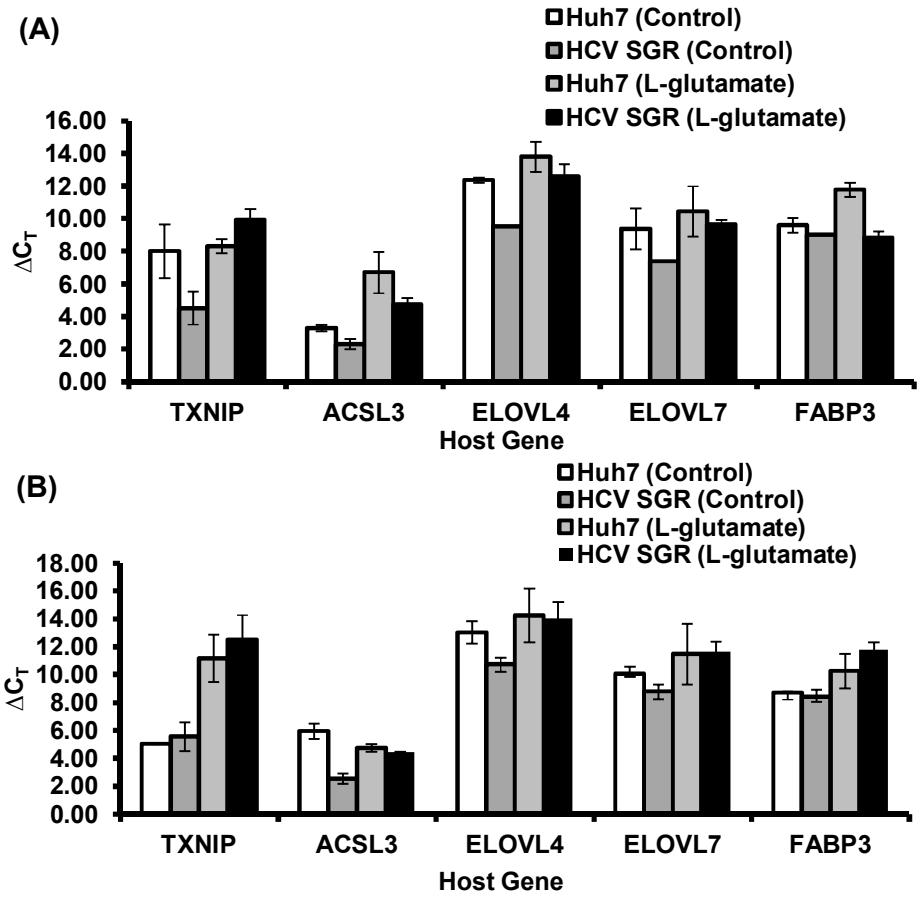
A2.1. represents the difference in raw cycle threshold values (ΔC_T) between genes of interest (GOI) and an internal control (GAPDH) in Huh7 cells compared to HCV SGR cells under control conditions or treated with L-glutamate. **(A)**: ΔC_T values at 24 hours post-seeding. **(B)**: ΔC_T values at 48 hours post-seeding. Data shown are averages of triplicate measurements from a single experiment with error bars representing standard deviation (SD). Relative fold changes in gene transcription ($\Delta\Delta C_T$) are shown in **Figure 40 (A, B)**.

A2.2. – ΔC_T for Oxidative phosphorylation gene transcription in Mock- and JFH-1 infected Huh7 cells (MOI – 7.5) +/- L-glutamate (24, 48 hours)



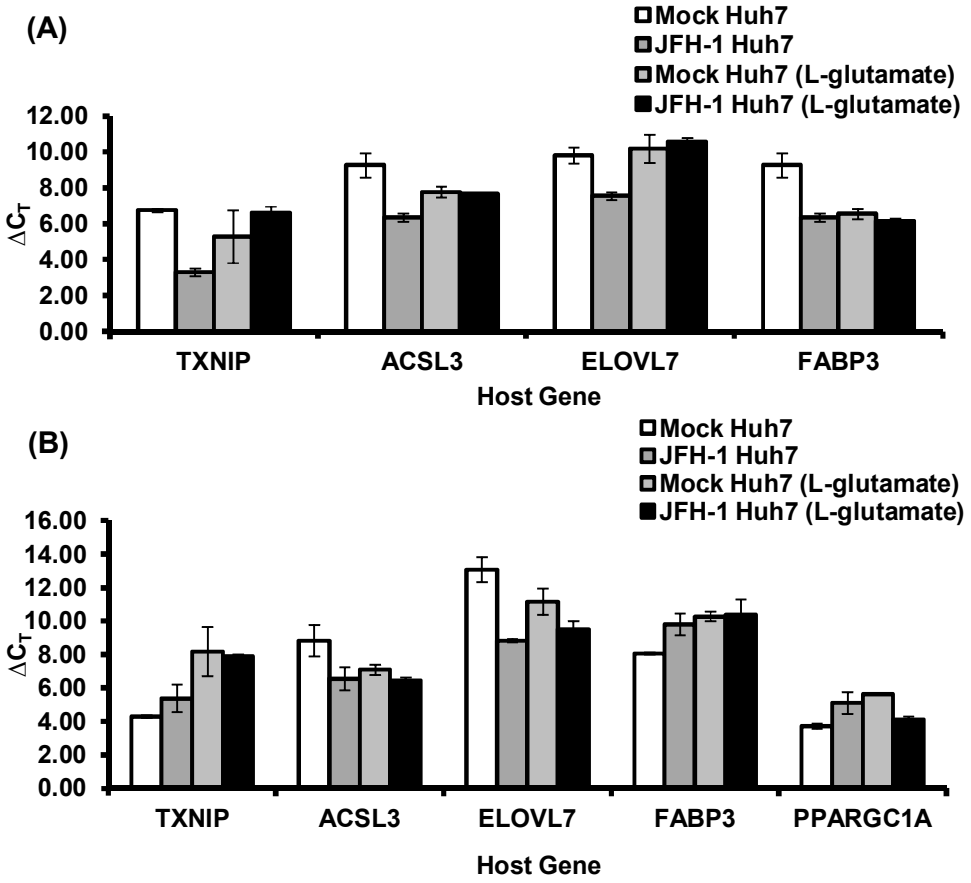
A2.2. represents the difference in raw cycle threshold values (ΔC_T) between genes of interest (GOI) and an internal control (GAPDH) in mock- and JFH-1 infected Huh7 cells under control conditions or treated with L-glutamate. **(A)**: ΔC_T values at 24 hours post-infection. **(B)**: ΔC_T values at 48 hours post-infection. Data shown are averages of triplicate measurements from a single experiment with error bars representing standard deviation (SD). Relative fold changes in gene transcription ($\Delta\Delta C_T$) are shown in **Figure 41 (A, B)**.

A2.3. – ΔC_T for Lipogenic gene transcription in Huh7 and HCV SGR cells +/- L-glutamate (24, 48 hours)



A2.3. represents the difference in raw cycle threshold values (ΔC_T) between genes of interest (GOI) and an internal control (GAPDH) in Huh7 cells compared to HCV SGR cells under control conditions or treated with L-glutamate. **(A)**: ΔC_T values at 24 hours post-seeding. **(B)**: ΔC_T values at 48 hours post-seeding. Data shown are averages of triplicate measurements from a single experiment with error bars representing standard deviation (SD). Relative fold changes in gene transcription ($\Delta\Delta C_T$) are shown in **Figure 44 (A, B)**.

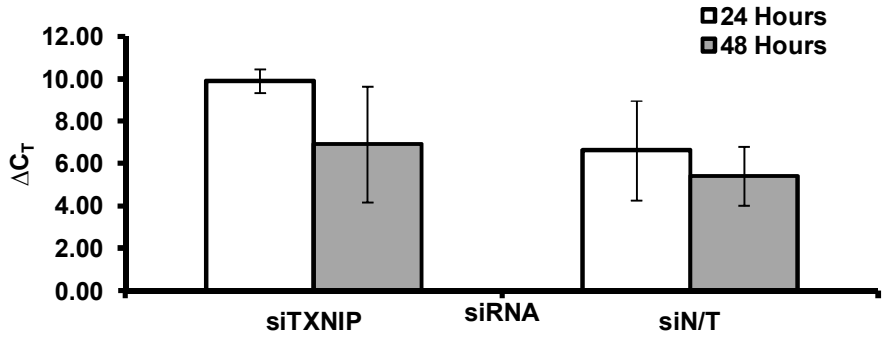
A2.4. - ΔC_T for Lipogenic gene transcription in Mock- and JFH-1 infected Huh7 cells (MOI – 7.5) +/- L-glutamate (24, 48 hours)



A2.4. represents the difference in raw cycle threshold values (ΔC_T) between genes of interest (GOI) and an internal control (GAPDH) in mock- and JFH-1 infected Huh7 cells under control conditions or treated with L-glutamate. **(A)**: ΔC_T values at 24 hours post-infection. **(B)**: ΔC_T values at 48 hours post-infection. Data shown are averages of triplicate measurements from a single experiment with error bars representing standard deviation (SD). Relative fold changes in gene transcription ($\Delta\Delta C_T$) are shown in **Figure 45 (A, B)**.

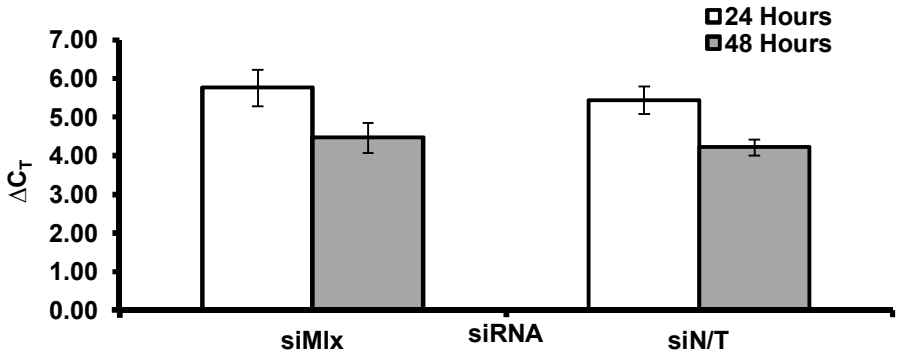
Appendix A3 – ΔCT Graphs for qRT-PCR Data (Chapter 5)

A3.1. – ΔC_T for TXNIP transcription in HCV SGR cells transfected with siRNA targeting TXNIP (siTXNIP) (24, 48 Hours)



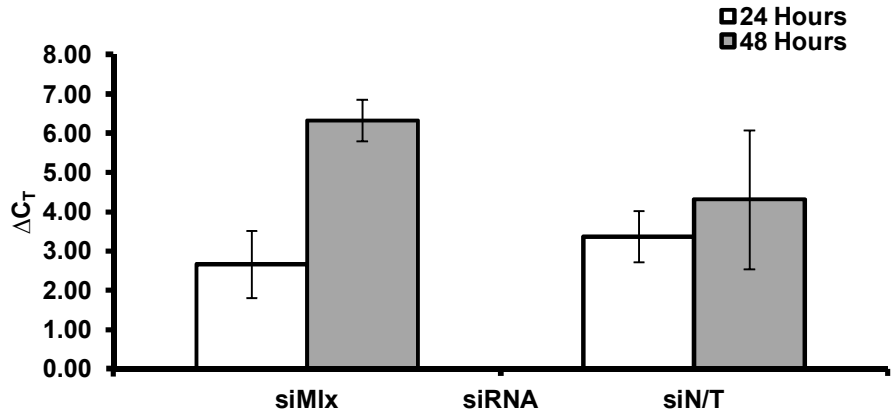
A3.1. represents the difference in raw cycle threshold values (ΔC_T) between Thioredoxin-interacting protein (TXNIP) and an internal control (GAPDH) in HCV SGR cells transfected with either targeting (siTXNIP) or non-targeting (siN/T) siRNA at 24- and 48 hours post-transfection. Data shown are averages of triplicate measurements from a single experiment with error bars representing standard deviation (SD). Relative fold changes in gene transcription ($\Delta\Delta C_T$) are shown in **Figure 60**.

A3.2. – ΔC_T for Mlx transcription in HCV SGR cells transfected with siRNA targeting Mlx (siMlx) (24, 48 Hours)



A3.2. represents the difference in raw cycle threshold values (ΔC_T) between Max-like protein (Mlx) and an internal control (GAPDH) in HCV SGR cells transfected with either targeting (siMlx) or non-targeting (siN/T) siRNA at 24- and 48 hours post-transfection. Data shown are averages of triplicate measurements from a single experiment with error bars representing standard deviation (SD). Relative fold changes in gene transcription ($\Delta\Delta C_T$) are shown in **Figure 62**.

A3.3. – ΔC_T for TXNIP transcription in HCV SGR cells transfected with siRNA targeting Mlx (siMlx) (24, 48 Hours)



A3.3. represents the difference in raw cycle threshold values (ΔC_T) between Thioredoxin-interacting protein (TXNIP) and an internal control (GAPDH) in HCV SGR cells transfected with either targeting (siMlx) or non-targeting (siN/T) siRNA at 24- and 48 hours post-transfection. Data shown are averages of triplicate measurements from a single experiment with error bars representing standard deviation (SD). Relative fold changes in gene transcription ($\Delta\Delta C_T$) are shown in **Figure 63**.